Univerzita Karlova v Praze

1. lékařská fakulta

Anatomický ústav

Studijní program: Vývojová biologie

Studijní obor: Biomedicína

MUDr. Jiří Beneš, Jr.

Vývojové mechanismy arytmií – úloha konexinů v arytmogenezi

Developmental mechanisms of arrhythmias - role of connexins in arrhythmogenesis

Typ závěrečné práce: Disertační

Vedoucí závěrečné práce: Prof. MUDr. David Sedmera, DSc.

Praha 2013

Prohlášení:

Prohlašuji, že jsem závěrečnou práci zpracoval samostatně a že jsem uvedl všechny použité informační zdroje. Současně dávám svolení k tomu, aby tato závěrečná práce byla archivována v Ústavu vědeckých informací 1. lékařské fakulty Univerzity Karlovy v Praze a zde užívána ke studijním účelům, za předpokladu, že každý, kdo tuto práci použije pro svou přednáškovou nebo publikační aktivitu, se zavazuje, že bude tento zdroj informací řádně citovat.

Souhlasím se zpřístupněním elektronické verze mé práce v Digitálním repozitáři Univerzity Karlovy v Praze (http://repozitar.cuni.cz). Práce je zpřístupněna pouze v rámci Univerzity Karlovy v Praze.

Souhlasím – ~~Nesouhlasím~~*****

V Praze 6.4. 2013

Jiří Beneš

Podpis

*** Nehodící se škrtnete**

Identifikační záznam

BENEŠ, Jr., Jiří. *Vývojové mechanismy arytmií – úloha konexinů v arytmogenezi [Developmental mechanisms of arrhythmias - role of connexins in arrhythmogenesis]*. Praha, 2013. Počet stran …, počet příloh ... Disertační práce. Univerzita Karlova v Praze, 1. lékařská fakulta, Anatomický ústav. Vedoucí práce Sedmera, David.

Abstrakt:

Cíle: Hlavním cílem této práce je prohloubení znalostí o vlastnostech konexinů při arytmogenezi. Práce se zabývá hlavně rolí konexinu 40 (Cx40) při embryonálním vývoji srdce u myší a změnami v distribuci konexinu 43 (Cx43) při objemovém srdečním selhání u potkanů.
Metody: Vliv Cx40 na vývoj srdce byl studován na transgenním kmenu myší GFP:Cx40 s použití metody optického mapování. Oběhové selhání bylo zkoumáno na potkanech s provedeným aortokaválním zkratem. Morfologické změny v srdcích byly zkoumány na histologických řezech za použití imunofluorescenčních metod.
Výsledky: V síních je Cx40 během vývoje nutný zejména v počátečních fázích, od 12,5 embryonálního dne postupně zastupuje jeho funkci Cx43. Absence Cx40 vede ke zpomalení vedení a ke vzniku ektopických pacemakerů. V komorách vede absence Cx40 v převodním systému k insuficienci vedení přes pravé Tawarovo raménko a dochází postupně k blokádě. U potkanů s oběhovým srdečním selháním byla prokázána excentrická hypertrofie (definovaná jak makroskopicky tak mikroskopicky) bez přítomnosti výraznější fibrózy. Hlavní potenciální arytmogenní změnou je snížení množství a defosforylace Cx43.
Shrnutí: Práce komplexně popisuje vliv absence Cx40 na vývoj převodního systému srdečního během kardiogeneze a morfologicky hodnotí dopad oběhového přetížení na myokard komor a na vznik potencionálního arytmogenního substrátu.

Klíčová slova: *connexin40, connexin43*, optické mapování, hypertrofie srdce, srdeční selhání, arytmogeneze, myš, potkan

Abstract:

Objective: The aim of this study is an improvement of our knowledge concerning the role of connexins in arrhythmogenesis. The main focus is on the role of *connexin40* (Cx40) in heart development in mice and changes in *connexin43* expression in volume overload heart failure rat model.
Methods: The influence of Cx40 on heart develoment was studied on transgenic mouse Cx40:GFP model using the method of optical mapping. Volume overload heart failure was examined in the rats with aortocaval shunt. Morphological changes in hearts were examined using imunofluorescence microscopical techniques.
Results: In the atria, Cx40 is important especially during the early stages. Cx43 can partially substitute its function from 12.5 embryonic day on. Cx40 deficiency leads to decreased conduction velocity and ectopic sites of activation. Absence of Cx40 in ventricular conduction system leads to the development of right bunde branch block. Volume overload in rats leads to excentric hypertrofy and later to heart failure. We described morphological as well as microscopical changes in failing hearts. Without the presence of fibrosis, the main arrhythmogenic substrate we found was reduced amount of Cx43 and its dephosphorylation.
Conclusions: This study decribes in detail the impact of Cx40 deficiency on the development of cardiac condution system during cardiogenesis and evaluates the changes during volume overload heart failure that can function as arrhytmogenic substrate.

Key words: *connexin40*, *connexin43*, optical mapping, cardiac hypertrophy, heart failure, arrhythmogenesis, mouse, rat

Grantová podpora

Práce shrnutá v této disertaci byla podpořena granty MSMT VZ 0021620806, GACR 13 -12412S, 304/08/0615, 1M0538.

Poděkování

Na prvním místě bych rád poděkoval prof. D. Sedmerovi, svému školiteli, za obětavé vedení a za neskonalou trpělivost a toleranci. Vděčím mu za celou řadu velmi cenných rad a připomínek, bez kterých by tato práce nikdy nemohla vzniknout.

Nemalou zásluhu na mé práci mají i ostatní spolupracovníci jak z laboratoře prof. M. Grima (kterému též patří můj hluboký vděk a obdiv) na Anatomickém ústavu 1. lékařské fakulty, tak z pracovišť Akademie Věd. Jmenovitě děkuji kolegyni Mgr. B. Šaňkové, se kterou jsme velkou část zde uvedených dat získávali společně, E. Kluzákové, Mgr. A. Kvasilové, M. Jindrákové a M. Pleschnerové, které velmi pečlivě a kvalitně pomohly s přípravou histologických vzorků, Ing. E. Krejčí, PhD za genetickou analýzu a Jarmile Svatůňkové za pomoc s analýzou optického mapování.

Dále bych chtěl poděkovat za spolupráci doc. V. Melenovskému a jeho laboratoři z IKEMu a M. Campione a G. Ammirabile z University v Padově.

Použité zkratky:

AV	atrioventrikulární
AVF	arteriovenous fistula (tepeno-žilní spojka)
Cx	connexin
DMSO	dimethylsulfoxid
ED	embryonical day, embryonální den
GFP	green fluorescence protein (zelený fluorescenční protein)
IKEM	Institut klinické a experimentální medicíny
PIR	primary interventricular ring
SA	sinoatriální
SD	směrodatná odchylka
WGA	wheat germ aglutinin
WT	wild type, geneticky neupravená myš

Obsah

1. Shrnutí

Ve své práci jsem se zaměřil na zkoumání mechanismů, které vedou ke vzniku srdečních arytmií, a to zejména na změny v expresi, lokalizaci a fosforylaci konexinů.

Na modelu Cx40 deficitních myší jsem popsal změny v šíření vzruchu v síních a změny v pacemakerové aktivitě. Zjistil jsem, že při chybění Cx40 v atriích dochází k výraznému zpomalení vedení vzruchu a k častému vzniku ektopické pacemakerové aktivity v síních. Rozumět dokonale úloze Cx40 v síních je velice důležité zejména pro jeho možnou roli při atriální fibrilaci, což je nejčastější klinicky významnější arytmie vůbec.

Popsal jsem změny ve vývoji komorového převodního systému při deficitu Cx40, z nichž nejnápadnější byl pomalu se rozvíjející blok pravého raménka Tawarova, který koreloval s morfologickou stavbou raménka a jeho postupným zmenšováním během vývoje. Vliv přítomnosti Cx40 na vývoj ramének převodního systému poukazuje na důležitý vztah mezi morfologickými a elektrofyziologickými faktory, které podmiňují šíření signálu srdcem.

A konečně na modelu srdečního selhání u potkanů jsem popsal v terénu morfologicky definované excentrické hypertrofie změny v expresi a fosforylaci Cx43, které se ukazují jako jeden z klíčových mechanismů vzniku arytmií v hypertrofických srdcích bez přítomnosti myokardiální fibrózy.

Summary

The main objective of my PhD work was to uncover some of the mechanisms that are responsible for cardiac arrhythmias, especially expression, localization and phosphorylation of connexins.

Using a Cx40 deficient mouse model I described changes in atrial impulse propagation and pacemaker activity. I found out that a lack of Cx40 in the atria leads to a significant decrease of conduction velocity and to ectopic pacemaker activity in the atria. Discovering the precise function of Cx40 is important for its potential role in the pathogenesis of atrial fibrillation- the most common clinically relevant arrhythmia in humans.

I also described the changes in development of bundle branches in Cx40 deficient mice, especially slow onset of right bunde branch block in correlation with its morphological thining during organogenesis. This shows an important correlation between morphological and funcional factors of impulse propagation in the heart.

Finally, I described changes in Cx43 expression and phosphorylation in a rat model of volume overload heart failure. These changes are one of the most important pathophysiological mechanisms underlying arrhytmogenesis in hypertrophied hearts without myocardial fibrosis.

2. Úvod

Srdeční choroby jsou v rozvinutých zemích stále nejčastější příčinou mortality populace. Arytmie k této úmrtnosti nemalou měrou přispívají, mají však též druhý aspekt. Maligní arytmie jsou nejčastější příčinou náhlé srdeční smrti, která často nastává u mladých a dříve zdravých jedinců (často s neodhalenou genetickou či morfologickou vadou). Hluboké a komplexní pochopení mechanismů arytmogeneze je klíčové pro diagnostiku, prevenci a terapii takovýchto arytmií.

Ve své práci jsem se snažil prohloubit znalosti lékařské vědy o vlastnosti a potenciální roli konexinů v arytmogenezi na zvířecích modelech a o jejich vliv na embryonální vývoj srdce.

Používal jsem dva zvířecí modely. Prvním byly geneticky upravené myši s deficitem Cx40, u nichž jsem zkoumal dopad této absence na vznik a šíření vzruchu v komorách a v síních během embryogeneze pomocí speciální elektrofyziologické metody optického mapování. Druhým modelem byli potkani, kterým byla operativně vytvořena komunikace mezi břišní aortou a dolní dutou žilou, čímž vznikl arteriovenózní zkrat, objemové přetížení a postupné rozvinutí srdečního selhávání a posléze selhání. Na tomto modelu jsem popsal morfologii změn při vznikajícícm srdečním selhání a pak jsem se zaměřil na možné faktory, které u těchto potkanů mohou vyvolávat (často maligní) arytmie.

2.1 Hypotézy

1.) Cx40 je hlavním konexinem v síních a předpokládal jsem tedy největší dopad jeho deficitu na šíření vzruchu právě zde.

2.) Je také nejrychleji vedoucím konexinem (viz. 3.2), dá se tedy předpokládat, že hlavním dopadem bude zpomalení vedení vzruchu. V pozdějších fázích vývoje se vyskytuje též v raménkách převodního systému, kde lze tedy očekávat změny ve vedení.

3.) Při objemovém srdečním selhání u potkanů jsem předpokládal vznik excentrické hypertrofie komor, jak byla popsána v literatuře, a v takto změněném myokardu se dá předpokládat řada patologických změn. Zaměřil jsem se na hlavní mechanismy, které by za tohoto stavu mohly být přítomny a mohly by vést ke vzniku arytmií. Předpokládal jsem změny zejména v distribuci „gap junctions“ v myokardu a jejich lokalizace na kardiomyocytu, změny fosforylace Cx43 a jeho množství.

3. Přehled problematiky disertační práce

Tato kapitola nabízí teoretický základ k mé práci. Zabývá se anatomií převodního systému srdečního, mikroanatomií buněčných spojení typu „gap junctions“, obecnými patofyziologickými mechanismy vzniku arytmií a mechanismy srdečného selhání.

3.1 Funkční anatomie převodního systému srdečního

Srdce vyšších obratlovců má vyvinutý vlastní autonomní systém tvorby a šíření elektrických impulzů svalovinou a vegetativní nervový systém srdeční činnost pouze moduluje.

Převodní systém srdeční (Obr.1) tvoří sinoatriální (SA) uzel, atrioventrikulární (AV) uzel, Hisův atrioventrikulární svazek, Tawarova raménka a Purkyňova vlákna. Největší pozornost v této kapitole věnuji SA uzlu, neboť má pro mou práci největší význam.

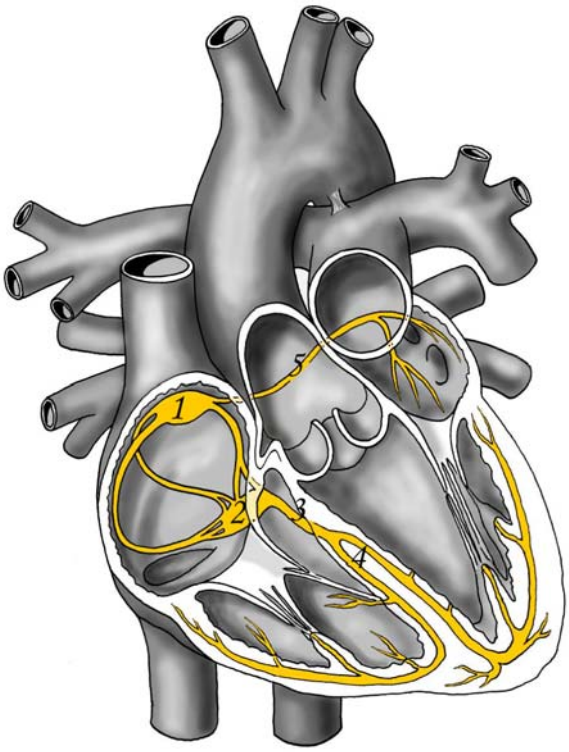

Obrázek 1 **Anatomie převodního systému srdečního;** 1 – SA uzel; 2 – AV uzel; 3 – Hisův svazek; 4 – Tawarova raménka; 5 – Bachmannův interatriální svazek

(zdroj: archiv Anatomického ústavu 1.LF UK, nakreslil Jan Kacvinský)

3.1.1 Sinoatriální uzel

Místo, v němž činnost srdeční vzniká, se nazývá „pacemaker“, a fyziologicky ho představuje SA uzel. Je to anatomicky relativně složitá struktura tvaru dlouhé slzy, u které můžeme popsat hlavu, která se nachází ve stěně pravé síně subendokardiálně v oblasti ústí horní duté žíly. a ocas, který se

táhne dále do *crista terminalis* (Anderson, 1979). V uzlu rozeznáváme centrální a periferní oblasti, které se od sebe liší skladbou „gap junctions“, iontových kanálů a tedy i elektrofyziologickými vodivými vlastnostmi (Lei et al., 2007). Pro funkci uzlu je též důležitá okrajová oblast přechodu tkáně SA uzlu do myokardu síně, která je typicky prstovitě uspořádaná. Předpokládá se, že toto uspořádání hraje důležitou roli při šíření vzruchu (Liu et al., 2007).

Pacemakerová aktivita je umožněna díky souhře několika specifických iontových kanálů na membráně buněk SA uzlu. Patří mezi ně sodíkový kanál SCN5A a kalciové kanály RYR2 a CASQ2 (Park and Fishman, 2011). Pro automaticitu je nejdůležitějším iontovým kanálem Na^+/K^+ kanál HCN4 (Accili et al., 2002). Tento kanál vytváří tzv. „funny current“, otevírá se totiž netradičně během hyperpolarizace membrány, čímž vyvolá opět depolarizaci a celý proces začne znovu – je tedy zodpovědný za automaticitu vzniku vzruchu v srdci. Je tedy dobrým molekulárním markrem pacemakerové aktivity (Moosmang et al., 2001).

Z dalších významných molekul přítomných v SA uzlu je třeba zmínit gap junction proteiny Cx45 a Cx30,2 (viz. 3.2.4) (Gros et al., 2004).

Přítomnost HCN4 mRNA je v buňkách vznikajícího myšího myokardu detekovatelná již velmi záhy – od 7,5ED; osmý den je patrná distribuce symetricky v kaudálních částech srdeční trubice a postupně dochází k asymetrické lokalizaci do oblasti SA uzlu v pravé síni (Garcia-Frigola et al., 2003). Kromě oblasti SA uzlu můžeme kanály HCN4 vidět též v oblasti ústí pulmonálních žil (patrné i dále na obr. 7 v oblasti levé síně), což jistě stojí za všimnutí, zejména vzhledem k častému původu fibrilace síní právě v této oblasti.

Embryonální mechanismy podmiňující vznik SA uzlu jsou z velké části stále neznámé. Nicméně je známo, že důležitou roli při vývoji SA uzlu hraje transkripční faktor Tbx3 (Hoogaars et al. 2007), transkripční faktor Pitx2 (zodpovědný za pravo/levou osu těla) (Ammirabile et al., 2011) a transkripční faktor Nkx2-5 (Mommersteeg et al., 2007).

3.1.2 Atrioventrikulární uzel a komorový převodní systém

Z SA uzlu se šíří vzruch síněmi až do oblasti atrioventrikulárního (AV) uzlu, který leží před ústím sinus coronarius do pravé síně. V tomto místě je vzruch výrazně zpomalen, aby měly komory během své diastoly dostatek času na naplnění (také reguluje eventuální přenos rychle následujících impulsů při patologii síní). Myokard síní a komor je totiž v tomto místě elektricky izolován

fibrózní tkání srdečního skeletu (zejména fibrózními prstenci cípatých chlopní) a Hisův svazek, což je struktura tvořená speciálně přeměněnými kardiomyocyty pokračující z AV uzlu, je (fyziologicky) jediným místem jejich komunikace (Kolditz et al., 2007).
Hisův svazek se záhy rozdělí na dvě Tawarova raménka – menší a tenčí pravé raménko a na široké levé. Raménka se posléze větví v trabekulách komor na Purkyňova vlákna. Vlákna převodního systému se nacházejí převážně subendokardiálně (v části myokardu sousedícím s intraluminální výstelkou srdce).

3.1.3 Historické souvislosti objevu převodního systému srdečního

Převodní systém srdeční byl objeven ve zcela opačném pořadí, než v jakém funguje (Eliška, 2006).
Jako první byla morfologicky popsána vlákna v komorách ovcí J. E. Purkyněm v roce 1845. Purkyně tato vlákna zpočátku považoval za chrupavčitou tkáň, což později zavrhl (Purkyně, 1845). Až po několika letech, v roce 1852, popsal funkci těchto vláken švýcarský fyziolog Rudolf Kölliker a nazval je Purkyňova vlákna.
Druhou objevenou částí převodního systému byl svazek mezi síněmi a komorami, který objevil internista Wilhelm His Jr. v roce 1893. Na něj navazoval objev AV uzlu, který publikoval ve své knize Sunao Tawara (Tawara, 1906).
Posledním objeveným prvkem byl potom SA uzel objevený až o rok později Keithem a Flackem (Keith and Flack, 1907).

3.1.4 Vývoj převodního systému

Původ buněk převodního systému byl dlouhou dobu předmětem bádání. Původně se předpokládalo, že vznikají z buněk neurální lišty (Gorza et al., 1988), později se však pomocí retrovirových studií potvrdilo, že progenitory buněk převodního systému pocházejí ze základů embryonálního srdce (Gourdie et al., 1995).

Studie zabývající se vývojem převodního systému srdečního byly prováděny zejména na kuřatech a na potkanech. U obou druhů je v zásadních bodech vývoj převodního systému podobný. Na počátku vývoje srdce je vytvořena primitivní trubice, ve které se šíří vzruch pomalu izotropicky od venózního konce k arteriálnímu, zatím bez přispění převodního systému (Kamino et al., 1991). Později dochází k zakroucení srdeční trubice a v tomto stádiu srdeční kličky, kdy dochází stále

k šíření signálu jednoduše od počátku ke konci, můžeme již rozlišit rychleji a pomaleji vedoucí oblasti (Arguello et al., 1986). Významným krokem ve vývoji vedení vzruchu je trabekularizace myokardu. V trabekulách dochází k rychlejšímu vedení a vytváří se zde podklad pro pozdější His-Purkyňův systém (Reckova et al., 2003; Sedmera et al., 1998). Později se začíná vytvářet mezikomorové septum a když je septace dokončena, definitivně se mění aktivace z dřívější „od baze k hrotu“ na konečnou aktivaci „od hrotu k bazi“, která je úzce spjata s vytvořením Tawarových ramének (Chuck et al., 1997). Před dokončením septace komor probíhá aktivace z podkovovité struktury zvané primární prstenec („primary interventricular ring“ - PIR), kterou tvoří tkáně po obvodu atrioventrikulárního kanálu (Wessels et al., 1992; Sankova et al., 2012).

3.2 Konexiny

Konexiny jsou transmembránové proteiny (Obr. 2) tvořené čtyřmi transmembránovými α-šroubovicemi, dvěma extracelulárními kličkami (které tvoří základ pozdějšího mezibuněčného spoje), jednou intracelulární kličkou a dvěma konci; C-terminální konec je různě dlouhý a určuje jednotlivé druhy konexinů (Unger et al., 1999). V lidském geonomu bylo identifikováno 21 konexinových genů, u myší pak pouze 20 (Sohl et al., 2004). Jejich označení je odvozeno od molekulové hmotnosti a každý konexin má jinou distribuci v buňkách organismu a jiné biofyzikální vlastnosti (Willecke et al., 2002). Jednotlivé konexiny polymerizují do hexamerní struktury, které se říká konexon. Ten je pak samotným buněčným kanálem (vlastně polovičním, neboli hemi-kanálem, jdoucím pouze přes jednu buněčnou membránu) (Goodenough et al., 1996).

Hlavní úlohou konexinů je mezibuněčná komunikace. Jsou součástí buněčných spojení typu „gap junctions“, které spojují dvě přilehlé buněčné membrány (Obr. 2, Herve et al., 2007) a umožňují prostup iontům, malým metabolitům, druhým poslům a jiným molekulám (menším než 1kDa). Konexony se navíc samostatně účastní některých procesů buněčné signalizace (Goodenough et al., 2003).

Vytváření „gap junctions“ z konexinových monomerů je považováno za složitý proces. (Musil a Goodenough, 1993, 1996). Konexiny oligomerizují do hemikanálu (konexonu) a poté jsou přesunuty na plasmatickou membránu, kde interagují s konexonem z protilehlé buňky. Během

toho dochází ke shlukování kanálů do funkční organely – „gap junctions“. Celý proces je ovlivňován mnoha faktory (např. napětím, pH, fosforylací) (Saez et al., 2003).

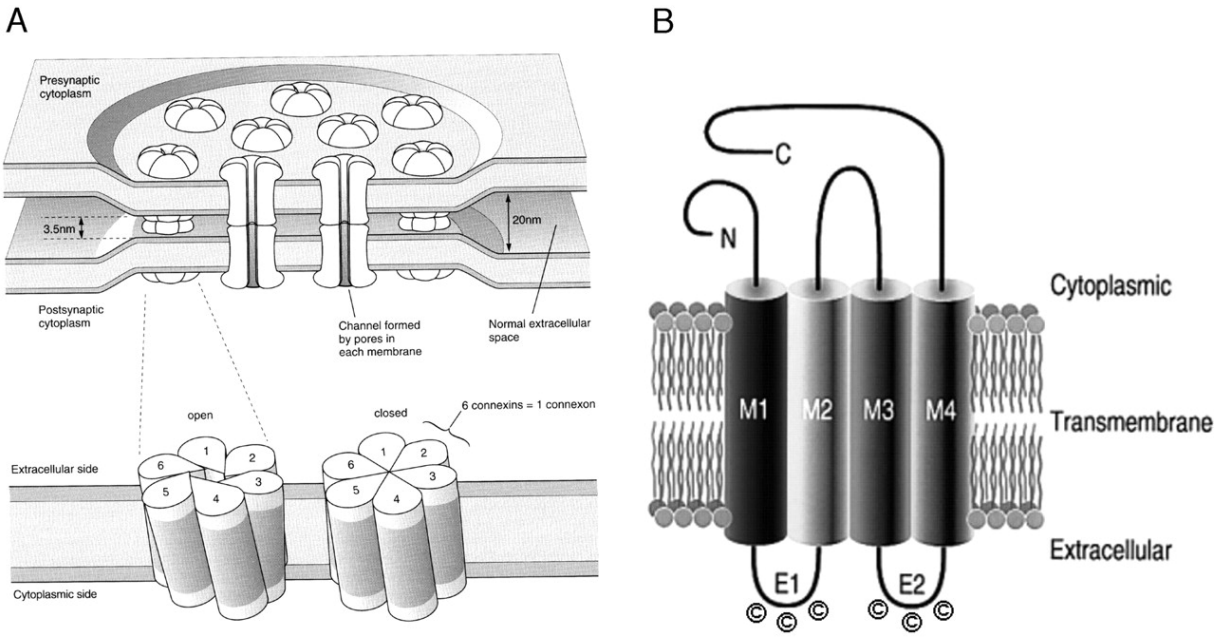

Obrázek 2 **Schéma konexinů a vytvoření gap junction**; na obrázku A je vidět formování buněčného spoje typu gap junction vytvářeného spojováním jednotlivých konexonů; na obrázku B je vidět molekulární struktura jednoho transmembránového konexinu (zdroj Söhl et al., 2004).

Vzhledem k tomu, že změny v distribuci a geometrii gap junction byly pozorovány u řady lidských nemocí (ischemické choroby srdeční, hypertrofické kardiomyopatie, srdečního selhání, ale také např. u temporální epilepsie), začal se v posledních letech podrobněji zkoumat mechanismus interakce connexinů s cytoskeletem, s molekulami signální transdukce a s jinými buněčnými spojeními (Giepmans et al., 2004). Hlavní molekulou, které se v této souvislosti věnuje nejvíce pozornosti, je membránově asociovaná guanylátkinasa ZO-1 (Zonula Occludens-1), které je mimo jiné zodpovědná za polarizaci buněk (Anderson et al., 1996; Hunter et al., 2005).

V kardiomyocytech savců byla potvrzena exprese pěti konexinů – Cx30, Cx30,2, Cx40, Cx43 a Cx45 (v následujícím textu jsou seřazeny podle jejich významu pro myokard). Jejich role v šíření vzruchu srdečním svalem (a v embryonálním vývoji) byla částečně objasněna studiemi na transgenních myších (Gros et al., 2004; Verheule et al., 2013).

3.2.1 Cx43

Cx43 je hlavním konexinem savčích srdcí. U myší je Cx43 kódován genem *Gja1* a je exprimován všemi kardiomyocyty s výjimkou buněk většiny částí převodního systému srdečního (SA a AV uzlu, Hisova svazku a prox. částí Tawarových ramének) (Boyett et al., 2006).

Cx43 je během embryonálního vývoje u myší detekován od 13ED jak v komorách, tak v předsíních (van Kempen et al., 1991), zpočátku v malém množství a postupně je ve výrazném nadbytku (Coppen et al., 2003). Jeho význam byl prokázán zejména při vývoji výtokové části srdce (Eckardt et al., 2006).

Exprese Cx43 je potlačovaná transkripčními faktory Tbx18 (determinující SA uzel), Tbx2 a Tbx3 (podílející se na diferenciaci AV uzlu) (Bakker et al., 2008, Kappor et al., 2011).

Vztah snížení Cx43 a zvýšené náchylnosti k arytmiím byl popsán u řady srdečních patologií, například u infarktu myokardu či u srdeční hypertrofie (Saffitz et al., 1999). Mechanismus uzavření „gap junctions" spojů (tzv. uncoupling) při srdeční ischemii pomáhá srdečnímu svalu při uzdravení (de Mello et al., 1969), což ovšem vede k častým arytmiím v období reperfúze (15-60 minut po ischemii) (Wit and Peters, 2012).

3.2.1.1 Cx43 na myších modelech

Vztah mezi expresí Cx43 a šířením impulsu myokardem byl zkoumán na geneticky modifikovaných myších.

Ztráta Cx43 v srdci během vývoje vede k srdečním abnormalitám a je neslučitelná s postnatálním životem (Eckardt et al., 2006). $Cx43^{-/-}$ myši umírají krátce po porodu na respirační selhání způsobené obstrukcí výtokové části pravé komory (Reaume et al., 1995). Tento defekt je způsoben již záhy během embryogeneze, kdy nepřítomnost Cx43 vede k abnormální aktivaci p53, což způsobí apoptózu kmenových buněk, které by měly migrovat do srdce (Francis and Lo, 2006).

U Cx43 deficientních heterozygotů (množství srdečního Cx43 bylo sníženo zhruba na polovinu) byly popsány rozporuplné výsledky. Někteří autoři uvádějí, že rychlost šíření se snížila o 23% - 44% (Eloff et al., 2001), jiní neobjevili abnormality žádné (Morley et al., 1999).

Při použití podmíněné delece Cx43 pouze v buňkách myokardu (při snížení množství Cx43 v kardiomyocytech o 95%) docházelo u myší k náhlé srdeční smrti do 2 měsíců života. U těchto srdcí bylo popsáno snížení longitudinální a transversální rychlosti šíření vzruchu o 42% a 56%. U zvířat byly pozorovány komorové arytmie (Gutstein et al, 2001).

Jiná studie použila k odstranění Cx43 myší mutanty, u nichž se Cx43 kódující sekvence odstranila po podání 4-hydroxytamoxifenu (čímž se odstranily eventuální vývojové kompenzační mechanismy hrající roli u předchozích studií). Zjistilo se, že až při snížení množství Cx43 v buňkách o 70% - 95% dojde ke snížení rychlosti vedení, zvýšení nehomogenity šíření impulsu a vyššímu výskytu arytmií (van Rijen et al, 2004).

3.2.1.2 Fosforylace Cx43

Cx43 je fosfoprotein, který může být fosforylován řadou kináz (Kwak et al., 1996) a defosforylován protein fosfatázami – např. PP1 a PP2A (Duthe et al., 2001). Nejčastější místa fosforylace jsou serinové zbytky na C-konci.

Zatímco fosforylace Cx43 může mít na kanály „gap junctions" různé dopady (Bowling et al., 2001), defosforylace prokazatelně potlačuje mezibuněčnou komunikaci pomocí „gap junctions" (Duthe et al., 2001). Změny ve fosforylaci Cx43 byly popsány u řady patologických stavů srdce, zejména při srdeční ischémii (Uzzaman et al., 2000; Emdad et al., 2001), ale též u stavů srdečního selhání (Ai et al., 2005; Benes Jr. et al., 2011). Zpomalení vedení v důsledku snížené fosforylace Cx43 může přispívat k arytmogenezi při těchto stavech a modulace fosforylace Cx43 je možným terapeutickým cílem při pátrání po nových antiarytmických lécích. Skupina Roberta Gourdieho popsala nedávno zpomalení patologických změn v okolí infarktové zóny po podání látky αCT1 (peptid podobný C-konci Cx43) (O´Quinn et al., 2011).

3.2.2 Cx40

U myší je Cx40 kódován genem *Gja5* a je exprimován zejména v kardiomyocytech síní myší i lidí (u potkanů nebyl v síních Cx40 objeven), v buňkách převodního systému komor a v centrálních částech AV uzlu. Cx40 se nenachází v pracovním myokardu komor dospělců ani v SA uzlu (Verheijck et al., 2001).

Hlavními transkripčními faktory, které potlačují expresi Cx40, jsou Tbx2 a Tbx3 (Hoogaars et al., 2004). Inaktivace Tbx2 vede k vytvoření Cx40 pozitivní akcesorní dráhy a k ventrikulární preexcitaci (Aanhaanen et al., 2011). Expresi Cx40 naopak zesilují transkripční faktory Nkx2-5, Tbx5 a T3-LacZ (Harris et al., 2006; Pikard et al., 2005).

3.2.2.1 Cx40 na myších modelech

Myší knock-out pro Cx40 byl původně vytvořen dvěma skupinami (Kirchhof et al., 1998; Simon et al. 1998). V obou případech byly myši životaschopné, což znamená, že funkce Cx40 je zastupitelná nějakým jiným konexinem. Tento myší model byl oběma skupinami (a později i jinými) velmi dobře popsán. U dospělých jedinců byla zjištěna prodloužená doba aktivace síní (na EKG jde o vlnu P) i komor (na podkladě rozšířeného QRS komplexu) a porucha AV vedení (Bevilacqua et al., 2000). Při stimulacích síní byla u těchto myší popsána vyšší incidence supraventrikulárních tachyarytmií (Hagendorff et al., 1999).

Rozsáhlou elektrofyziologickou studii u dospělých jedinců provedli též Verheule et al. (1999). Zjistili, že rychlost šíření vzruchu komorami není u Cx40 deficitních myší výrazněji změněna, zatímco rychlost šíření vzruchu v síních byla snížena o 30% (u heterozygotů nepozorovali výraznější změny). Navíc na EKG křivkách pozorovali změny QRS komplexů, které se dají interpretovat jako blokáda pravého Tawarova raménka. Poruchu vedení v pravém raménku u dospělých jedinců bez Cx40 potvrdili později též van Rijen et al. (2001).

Další skupina, která se podrobně zabývala studiem Cx40, je skupina Gregory Morleyho (Tamaddon et al., 2000; Leaf et al., 2008). Jejich práce je zajímavá zejména tím, že též používají metodu optického mapování (viz 4.1). Uvedli, že jak částečná (u heterozygotů), tak úplná ztráta Cx40 vede k nehomogenní vodivosti myokardu síní. U embryonálních stádií pozorovali v síních vznik ektopických pacemakerů (viz 7.2.2).

Kromě myokardu je Cx40 přítomen též v endotelu tepen a má zde též vztah k ateroskleróze (Kwak et al., 2002; Chadjichristos et al., 2010). U Cx40 deficitních myší byla v této souvislosti popsána sekundární arteriální hypertenze způsobená změnami tepen v ledvinách (de Wit et al., 2003).

3.2.2.2 Cx40 během myší embryogeneze

Přítomnost malých množství mRNA pro Cx40 je patrna již v 8,5ED; až do 14,5ED je distribuce Cx40 stejná v síních i v komorách (v levé komoře se objevuje dříve než v pravé). Po 14. dnu však dochází k výraznému úbytku Cx40 v komorách, zatímco v síních přetrvává (Delorme et al., 1997). U dospělých jedinců je pak omezen pouze na síně a na komorový převodní systém srdeční (Gros et al., 1996).

Role Cx40 při kardiogenezi jako takové je víceméně neznámá. Je však zřejmé, že deficit Cx40 je spojen s častějšími závažnými vrozenými srdečními vadami (Gu et al., 2003).

3.2.3 Cx45

Cx45 je u myší kódován genem *Gjc1*. Je prvním konexinem, který se začne vyskytovat ve vyvíjejícím se myokardu. V časných stádiích vývoje (do 9,5ED) se nachází ve všech částech myokardu, časem však dochází k jeho omezení pouze na oblasti převodního systému (včetně SA uzlu) a na nejperifernější oblasti mezikomorové přepážky (Gros et al., 2005). Delece *Gjc1* vede k prenatálnímu úmrtí plodu ve stádiu 10ED, což poukazuje na fakt, že přítomnost Cx45 je nutná pro normální kardiogenezi (Gros et al., 2004). Bez Cx45 dochází k poruše epitelo-mesenchymální transformace, která je v srdci nutná pro tvorbu endokardových poštářků a k septaci (Kumai et al., 2000).

U dospělých je Cx45 hlavním konexinem v SA uzlu, který jinak zcela postrádá Cx40 i Cx43 (Verheijck et al., 2001). Studie na podmíněném knock-outu Cx45 postnatálně ukázaly, že defekt v expresi Cx45 neovlivní srdeční frekvenci, což předpokládá, že se sám o sobě nepodílí na pacemakerové aktivitě (Frank et al., 2012).

3.2.4 Cx30

Jde o protein tvořící relativně rychle vodící kanál a u myší se nachází zejména v SA uzlu (Gros et al., 2010). Cx30 deficitní myši mají asi o 9% vyšší srdeční frekvenci než kontroly a tato vyšší frekvence je přítomna i po blokaci autonomní inervace, což ukazuje, že Cx30 nějakým způsobem ovlivňuje pacemakerovou aktivitu (Gros et al., 2010).

3.2.5 Cx30.2

Cx30.2 je kódován genem *Gjc3* a vyskytuje se zejména v SA a AV uzlu (a v menších množstvích též v Hisové svazku a v proximálních částech Tawarových ramének). Jeho hlavní funkcí je zpomalení propagace impulsu v oblasti AV uzlu, což ovlivňuje počet impulsů převedených z atrií na komory (Kreuzberg et al., 2006).

3.2.6 Konexiny v myokardu a jejich role v arytmogenezi

Na rozdíl od svalu kosterního není srdeční svalovina tvořena syncytii uspořádanými do svalových vláken. Je tvořena krátkými buňkami, kardiomyocyty, které jsou spojeny v oblastech tzv. interkalárních disků. Mezibuněčné spoje umožňují četná spojení „gap junctions“, která zprostředkovávají rozsáhlou výměnu látek mezi buňkami (proto se svalovina myokardu někdy označuje jako tzv. „funkční syntitium“). Důležitou roli v šíření vzruchu hraje prostorové uspořádání jednotlivých „gap junctions“. Velmi se liší například v myokardu komor a síní (Saffitz et al., 1994). Kardiomyocyt v komorách (měřeno u psů v oblasti subendokardu) je napojen interkalárními disky průměrně na 11-12 jiných buněk, z nichž polovina je orientovaná bokem („side-to-side“) a polovina koncem („end-to-end“). Naproti tomu v síních (v oblasti crista terminalis pravé síně, u psů) je většina kardiomycytů spojená „end-to-end“. Snížené množství „gap junctions“ bylo prokazatelně spojené se zpomalením vedení vzruchu myokardem (Peters et al., 1997). Kromě sníženého množství „gap junctions“ však bude hrát v arytmogenezi velkou roli i distribuce a poměr jednotlivých end-to-end a side-to-side spojení (Gourdie et al., 1996).

Strukturální změny (remodelace) patří k základní odpovědi srdeční tkáně na poškození či nemoc. Změny v srdeční mikrostruktuře vedou k výrazným funkčním změnám. Ačkoli strukturální remodelace jistě slouží důležitým účelům adaptace na vyvolávající patologický stav, je zřejmé, že také nemalou měrou přispívá k morbiditě a mortalitě pacientů se srdečním onemocněním. Klasickým příkladem těchto maladaptivních procesů je vznik anatomického podkladu (substrátu) komorových arytmií. Tyto substráty vznikají vlivem strukturálních změn v odpovědi na běžné srdeční nemoci jako je infarkt myokardu nebo arteriální hypertenze. V obou případech jsou změny v myokardu zpočátku prospěšné – vazivová jizva po transmurálním infarktu zabraňuje ruptuře stěny a hypertrofie kardiomyocytů umožní srdci lépe snášet zvýšenou tlakovou zátěž. Nicméně obě tyto změny současně mění elektrické vlastnosti srdeční tkáně a tím zvyšují riziko vzniku vážných arytmií. Zpomalování vedení či blokace jsou nečastějším podkladem reentry fenoménu (Obr 3).

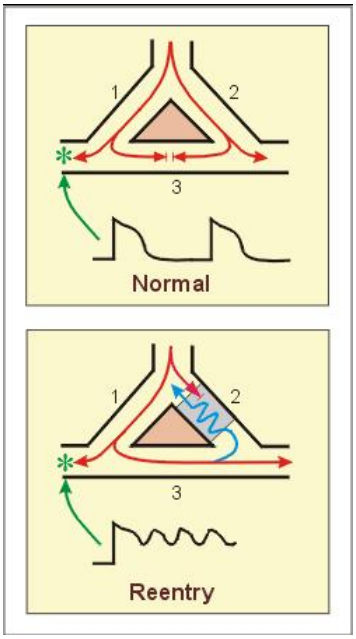

Obrázek 3 **Reentry fenomén**

Pokud se vzruch šíří dvěma částmi myokardu, které mají obdobné vodící vlastnosti (jako na horním obrázku, 1 a 2), dochází v případě střetu k rovnoměrnému šíření. Pokud existuje část svaloviny s porušenou vodivostí (vede pomaleji – dolní obrázek, 2), rychleji vedoucí vzruch se může obracet a dostávat se do oblastí pomaleji vedoucího myokardu z druhé strany (reentry).
(Zdroj: http://www.cvphysiology.com)

Ten nejčastěji vzniká v životaschopném, nicméně pozměněném, myokardu v okrajích infarktových jizev (Dillon et al., 1988). Řada elektrofyziologických vlastností této tkáně (jako klidový membránový potenciál či vznik akčního potenciálu) se po nějaké době vrací téměř k původním hodnotám. I přesto však si tyto oblasti zachovávají svou arytmogenicitu (Boyden et al., 1988). Mezi nejdůležitější patofyziologické mechanismy, které jsou za tento fakt zodpovědné, patří změny v přenosu látek mezi kardiomyocyty pomocí „gap junctions".

Vzhledem k tomu, že u lidských patologií můžeme těžko předpokládat úplnou ztrátu Cx40, asi nejlepším modelem pro korelaci se situací u pacientů jsou heterozygotní jedinci. Např. u heterozygotní delece Cx40 u dospělých myší bylo popsáno zpomalené vedení v levé síni (Leaf, 2008). Vzhledem k tomu, že častým místem vzniku atriální fibrilace je oblast ústí plicních žil v levé síni, jsou změny vedení v této oblasti velmi důležitým arytmogenním činitelem.

Jiným mechanismem vzniku arytmií v poškozených srdcích může být spuštěná aktivita (tzv. „triggered aktivity"), která nevzniká na podkladě fenoménu reentry, nýbrž nestabilitou membránového potenciálu srdečních buněk, které se opakovaně depolarizují a repolarizují. Tento mechanismus se vyskytuje často u neischemických poruch srdečního rytmu a je spojen zejména s poruchami iontových kanálů (Pogwizd et al., 2004).

3.3 Základní patofyziologie srdečního selhání

Srdeční selhání je stav, kdy srdce nestačí plnit svou funkci při přečerpávání krve. Velmi hrubě a orientačně lze srdeční selhání rozdělit na selhávání z tlakového přetížení (např. při arteriální hypertenzi) a na selhávání z objemového přetížení (např. při aortální regurgitaci).

Zvýšení objemu krve, které musí srdce přečerpat, svalovinu zatěžuje a postupně dochází k rozšíření (dilataci) a následné (excentrické) hypertrofii jednotlivých oddílů srdečních (Ford et al., 1976). Nejen rozšíření stěny, ale též zvětšení celého objemu srdečního oddílu tím slouží jako kompenzační mechanismus a srdce se tím adaptuje na nastalou situaci (Grossmann et al., 1975). V tomto stádiu je srdeční selhání kompenzované a tento stav se dá spíše vhodněji označit jako srdeční selhávání. Nicméně po určitě době dochází k dekompenzaci a rozvíjí se již plně srdeční selhání (Hood et al., 1968). Mezi nejčastější patologické stavy, které k tomuto stavu vedou, patří u lidí chlopenní vady (nedomykavost chlopní) a arteriovenózní ztraty (např. uměle vytvářené shunty u dlouhodobě hemodialyzovaných pacientů pro snadnější přístup do cévního řečiště).

Srdeční selhání (nezávisle na druhu a etiologii) představuje výrazné riziko vzniku život ohrožujících komorových tachyarytmií (Artham et al., 2009) a je jedním z největších rizikových faktorů náhlé srdeční smrti (Haider et al., 1998).

Zlepšující se lékařská péče a relativně stagnující (či klesající) porodnost v rozvinutých zemích způsobuje postupné stárnutí naší populace. Tento fakt spolu se útlumem fyzické aktivity vede k častějšímu výskytu srdečních patologií vedoucích postupně až k srdečnímu selhání. Například úmrtnost na infarkty myokardu s rozvojem katetrizačních technik v posledním desetiletí velmi výrazně poklesla a téměř každý pacient po infarktu v co nejkratší době podstoupí katetrizační zákrok a uzávěr je mu rekanalizován. Zlepšením terapie akutních stavů (tento fakt nepostihuje pouze kardiologii, jde o celomedicínský problém) přibývá pacientů s chronickými obtížemi, a proto se dnes stále více a více kardiaků postupně dostává do fáze srdečního selhávání.

3.3.1 Změny konexinů při srdečním selhání

Proces hypertrofie je dynamický děj, při němž dochází k velkým změnám k genové expresi a ve struktuře jak kardiomyocytů tak intersticia. Rychlost vedení je v hypertrofických komorách zpočátku zvýšená, časem dochází k jejímu poklesu (Winterton et al., 1994). V souvislosti s těmito

změnami bylo prokázáno, že u pacientů s chronickými myokardiálními poruchami (jako je ischemická kardiomyopatie či aortální stenóza), dochází ke snížení exprese Cx43 (Peters et al., 1993). Remodelace gap junction byla velmi úzce spjata s rozvojem reentry arytmií u pacientů po zhojených infarktech myokardu (Peters et al., 1997). Po obvodu infarktových jizev byly popsány oblasti fibrózy, přestavby a redistribuce „gap junctions“, což přispívá ke zpomalení a k blokům vedení vzruchu (Takamatsu et al., 2008). V oblastech myokardu sousedícím s jizvou bylo prokázáno snížení mezibuněčných spojů, snížení celkových napojení jedné buňky na okolní a redistribuce „gap junctions“ na strany buněk (Luke et al., 1991).

Šíření vzruchu zdravým myokardem probíhá ve směru dlouhé osy kardiomyocytu, což umožňuje rychlé a přímé šíření vzruchu. Oproti tomu např. komorová tachykardie je typicky způsobena tím, že se signál šíří myokardem transversálně. Koncová spojení v oblasti interkalárních disků jsou přerušena a signál musí kličkovat myokardem dokud nenarazí na porefrakterní tkáň a neiniciuje další impuls (De Bakker et al., 1993).

Podobné změny byly popsány též u neischemických chronických srdečních patologií (Uzzaman et al., 2000).

4 Metodika

4.1 Zvířata

Všechny experimenty byly prováděny v souladu s §11 vyhlášky č.207/2004 Sb. o ochraně, chovu a využití pokusných zvířat a byly schváleny Odbornou komisí pro práci s pokusnými zvířaty 1.LF UK a IKEM. Zvířata byla držena ve větrané místnosti s dvanáctihodinovým cyklem světlo/tma a byla krmena ad libitum.

4.1.1 Myši Cx40:GFP

Kmen transgenních knock-in myší vyvinula ve své laboratoři Lucille Miquerol pro studium morfologie převodního systému (Miquerol et al., 2004). Alela GFP v místě genu pro Cx40 umožňuje u heterozygotů fluorescenční vizualizaci míst, kde je exprimován Cx40 (tedy zejména převodní systém srdeční). V homozygotním stavu lze daný model užít jako model Cx40 deficitních myší (absence molekuly Cx40 u homozygotů potvrzena pomocí metod molekulární biologie). Myši byly připouštěny přes noc a při ranním nálezu zátky, byl tento čas považován za stádium 0,5ED. Myši byly pravidelně váženy a březí samice byly v daném požadovaném stádiu (9,5ED – 18,5ED) usmrceny cervikální dislokací, embrya byla rychle disekována a uložena do studeného Tyrodova pufru.

4.1.2 Potkani s objemovým srdečním selháním

Pro zkoumání vlivu objemového srdečního selhání na arytmogenezi (viz. Kapitola 6) byly použiti samci rodu Wistar vážící 300-350g. U potkanů byl proveden arteriovenózní zkrat (viz dále) a data byla hodnocena ve dvou intervalech po provedení zkratu – po 11 týdnech (ve stádiu počínajícího srdečního selhání) a po 21 týdnech (ve stádiu pokročilého srdečního selhání). Asi 13% zvířat uhynulo do sedmi dnů po provedeném zkratu, dalších 5% potom do ukončení projektu. Tato zvířata byla vyloučena ze studie.

Mezi základní vnější příznaky vznikajícího srdečního selhání patřila letargie, obtížné dýchání, cyanóza a naježení chlupů. Tyto příznaky se po 21 týdnech po operaci vyskytovaly až u 80% zvířat.

Jako kontroly byly užiti potkani, kteří prošli stejnou operací, bez finálního provedení zkratu („sham“).

4.1.3 Aortokavální zkrat

Pro vyvolání oběhového přetížení u potkanů se operativně provedl aortokavální zkrat (Obr. 4) dle metody popsané Garciou a Dieboltem (Garcia et al., 1990). Potkani byli uspáni intraabdominální aplikací ketaminu a midazolamu, proveden řez ve střední čáře a z přístupu do levého srůstového pole byla v retroperitoneu obnažena aorta a dolní dutá žíla. Do aorty byla opatrně vbodnuta jehla 1,2 mm a poté z lumen bylo bodnuto do dolní duté žíly, čímž se vytvořila komunikace. Aorta byla nad bodnutím zaklipována, jehla odstraněna a na místo vpichu bylo aplikováno akrylamidové lepidlo. Po třech minutách byl klip odstraněn a zkrat prokázán pulsací dolní duté žíly. Tím byla vytvořena spojka mezi tepenným a žilním systémem (AVF – arteriovenous fistula).

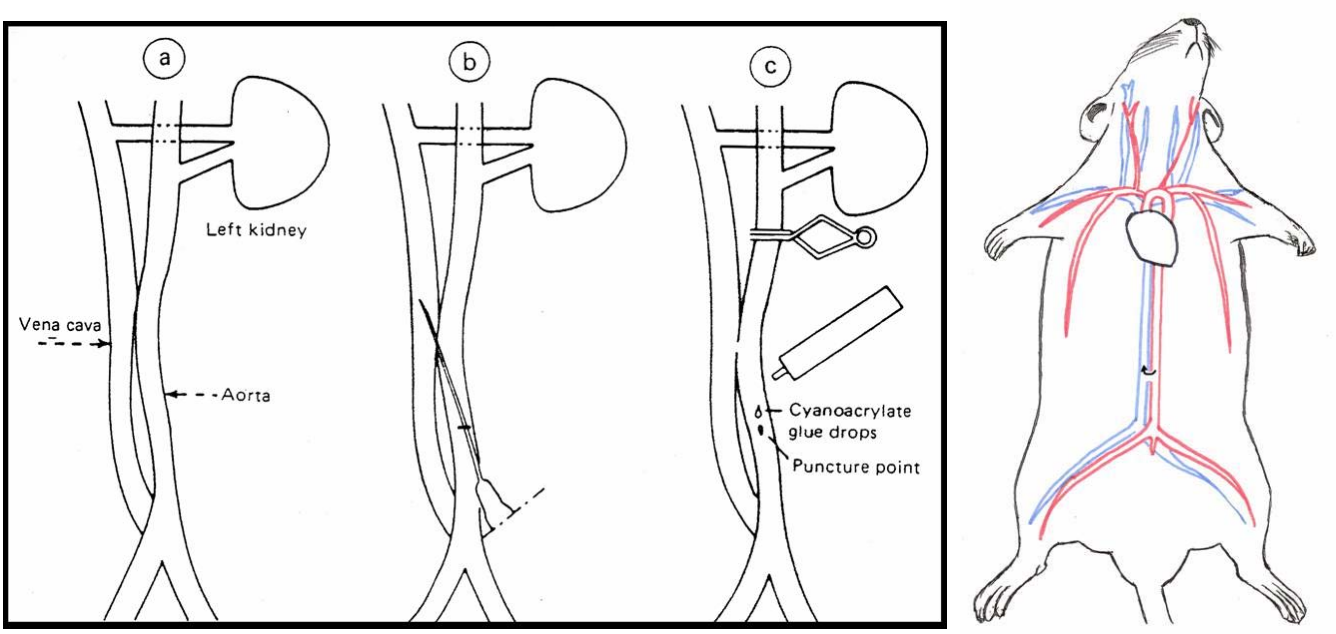

Obrázek 4 **Schéma provedení aortokaválního zkratu**

(zdroj: Garcia, 1990)

4.2 Optické mapování

Optické mapování (Obr. 5) je specializovaná elektrofyziologická mikroskopická metoda, která využívá schopnosti látky di-4-ANEPPS reagovat na změny membránového potenciálu buněk změnou intenzity fluorescence (Kamino et al., 1981).

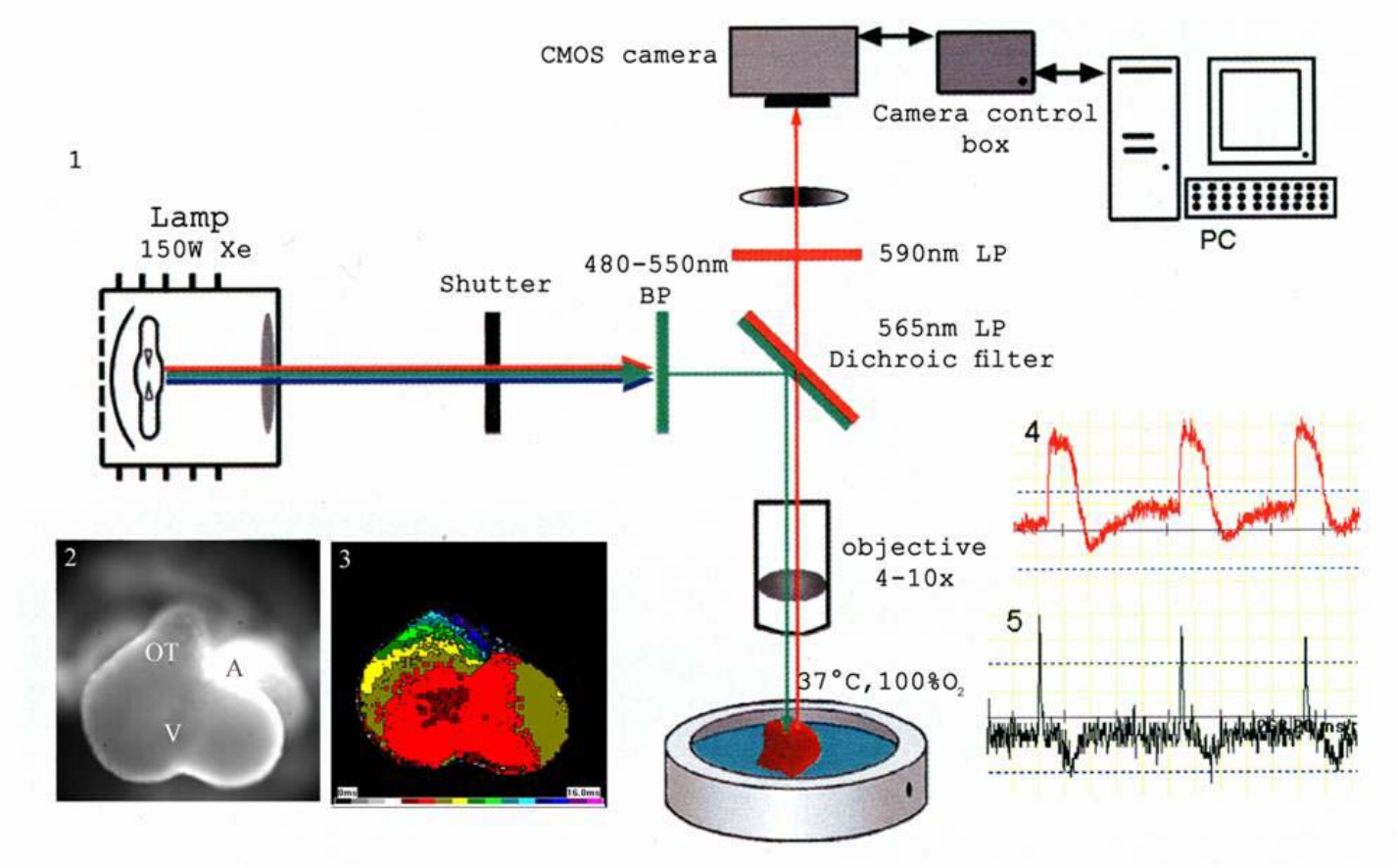

***Obrázek 5* Schéma optického mapování**
1 – mikroskop s vysokorychlostní CMOS kamerou, xenonovou lampou, filtry a s explantovaným srdcem v komůrce; 2 – obraz myšího embryonálního srdce při pohledu mikroskopem; 3 – optická mapa isochron komorové aktivace; 4 – záznam intensity fluorescence v čase z jednoho pixelu obrázku (hodnoty jsou invertovány, aby se křivka více blížila elektricky zaznamenému akčnímu potenciálu); 5 – první derivace tohoto záznamu, jejíž maximum $(dP/dt)_{max}$ je považováno za čas aktivace.
(zdroj: Sedmera et al., 2005)

Po usmrcení samice cervikální dislokací a explantaci dělohy byla pod disekčním mikroskopem z jednotlivých embryí vyjmuta srdce s dorzální částí hrudní stěny a byla vložena do chladného roztoku di-4-ANEPPS (předem připraveném v roztoku DMSO v koncentraci 1,25g/l) v Tyrodově pufru, obvykle v poměru 1:25 (celkové množství se lišilo dle stádia embryonálního vývoje) a byla zde inkubována 5-10 minut (opět v závislosti na stádiu vývoje). Obarvená srdce byla vložena do tkáňové komůrky se silikonovým dnem, ve které byl Tyrodův pufr (o teplotě 37°C a se stálým

probubláváním 100% kyslíkem), a zde bylo srdce pomocí miniaturních špendlíků pod disekčním mikroskopem připevněné za ponechání části hrudní stěny. Při zkoumání šíření signálu v síních bylo ještě nutné mikrochirurgicky odstřihnout výtokovou část srdce (konotrunkus).

Kvůli odstranění eventuálních artefaktů způsobených přílišnými pohyby srdce při kontrakci aplikujeme blebbistatin, což je látka, která vazbou na aktin blokuje vazbu s myosinem, čímž zabraňuje kontrakci, aniž by interferovala s přenosem akčního potenciálu na membráně (Biermann et al., 1998; Fedorov et al., 2007). Malé množství blebbistatinu aplikujeme buď do tkáňové komůrky nebo spolu s di-4-ANEPPS přímo do inkubace.

Tkáňovou komůrku jsme umístili pod mikroskop, kde jsme obarvenou tkáň osvítili světlem z xenonové lampy procházejícím přes filtr, který propouští světlo o vlnových délkách 480-550 nm. Toto zelené světlo vyvolá červenou fluorescenci, jejíž pokles, vlivem obarvení barvivem di-4-ANEPPS, odpovídá akčnímu potenciálu na povrchu srdce (Witkowski et al., 1997). To je snímáno vysokorychlostní digitální kamerou MiCAM ULTIMA L.

Pořízená data jsou analyzována programem BV_Analyzer – potlačí se šum pomocí digitální filtrace a provede se derivace získaných dat, díky níž se nám zobrazí části záznamu s největší změnou intenzity fluorescence v čase jako jednotlivé hroty, které odpovídají aktivaci v jednotlivých pixelech obrázku (Obr. 4). Z toho lze získat jak videa šíření vzruchu, tak aktivační mapy (viz Kapitola 5).

4.3 Mikroskopické metody

Pro posuzování morfologie srdeční tkáně jak potkanů se srdečním selháním (viz Kapitola 6), tak Cx40 deficitních myší (viz Kapitola 5) jsme používali konfokální mikroskop Leica SPE a světelný mikroskop Olympus BX51.

Vzorky tkáně byly fixovány 4% paraformaldehydem v PBS a napuštěny sacharózou. Poté byly zality do média Tissue-Tek a pomocí tekutého dusíku rychle zmraženy. Bločky byly krájeny na kryotomu a poté obarveny klasickými postupy – první řez obarven hematoxylin-eosinem a následné řezy poté pikrosiriusovou červení (kolagen), Sudanovou černí (lipidy) nebo specifickou protilátkou.

Použité protilátky – α-actinin, *connexin43, phosphoconnexin43*, HCN4.

Déle byl použit Hoechst 33342 k dobarvení jader a WGA:Alexa488 na obarvení membrán.

4.4 Analýza dat

Snímky pořízené konfokálním mikroskopem jsem analyzoval pomocí Adobe Photoshopu a programu ImageJ.

Pro měření šíře kardiomyocytů bylo nutné barvení pomocí WGA, které zobrazilo membrány. Měřili jsem deset šířek z jednoho řezu. Aby bylo jisté, že buňka je zobrazena ve svém největším průměru, hledali jsem buňky s přítomností jádra na řezu.

Pro měření délky kardiomyocytů jsme využívali imunofluorescenčně značený Cx43, který dobře zobrazil oblasti interkalárních disků.

Na hodnocení množství jsme využívali poměr plochy zeleného fluorescenčního signálu (reprezentující autofluorescenci cytoplasmy kardiomyocytů) a červeného signálu (protilátka proti Cx43). Nálezy byly korelovány s metodou western blotu.Distribuci Cx43 jsme měřili podobným způsobem jako množství, ale před analýzou plochy dané červeným signálem jsme odstranili z obrázku signál Cx43 z interkalárních disků. Tím zůstal pouze Cx43 přítomný na buněčné membráně laterálně či v cytoplasmě.

Statistickou analýzu jsme prováděli dle standardních postupů nepárovaným t-testem a výsledky byly shledány statisticky významnými při hodnotě $p<0,05$.

5. Výsledky I.

Vliv deficitu Cx40 na aktivaci síní a komor během embryonálního vývoje u myší

Následující kapitola shrnuje výsledky z rozsáhlé studie myšího modelu Cx40/GFP myší, kdy jsme v naší laboratoři pomocí optického mapování definovali základní aktivační vzory pozorované na embryonálních srdcích v různých fázích vývoje a korigovali je s morfologicko-embryologickými poznatky a následně zjišťovali, jak se liší obrazy aktivace u myší s částečným či úplným deficitem Cx40 (Sankova et al., 2012; Benes et al., under revision).

5.1 Aktivace síní a porovnání vlivu deficitu Cx40 ve stádiu 12,5ED

Měření a posuzování šíření aktivace v síních naráží na značné anatomické překážky, neboť síně jsou výrazně prostorově členité anatomické struktury a získávat vhodný dvourozměrný obraz v jedné rovině zaostření je problematické. Je jistě možné jejich tvar mechanicky uzpůsobit podobně to v některých studiích udělala skupina Gregory Morleyho (Leaf et al., 2008), avšak tato manipulace přináší řadu artefaktů, změněných podmínek pro šíření vzruchu a je spojena s traumatizací stěny, která mění podmínky vodivosti.

Proto jsme pro základní analýzu aktivace síní zvolili stádium 12,5ED, neboť v tomto stádiu nejsou ještě atria tolik členitá a po odstranění výtokové části srdce lze bez obtíží vizualizovat oblast SA uzlu i síní.

5.1.1 Druhy aktivace 12,5ED

Typické aktivační mapy u jednotlivých genotypů jsou zobrazené na Obr. 6. U wild type myší (WT) (n=19) jsme pozorovali zcela jednotné druhy aktivace – z oblasti paramediálně vpravo, tedy z oblasti základů SA uzlu (Liu et al., 2007). Odtud se pak šíří signál na obě strany, nejdříve aktivuje pravou a posléze levou síň. Průměrná celková doba aktivace obou síní byla 7 ms.

U heterozygotů ($Cx40^{+/-}$) (n=12) byl způsob aktivace obdobný jako u WT. Průměrná doba aktivace byla však signifikantně prodloužena, činila 9 ms.

U srdcí Cx40 deficitních ($Cx40^{-/-}$) jsme pozorovali dva druhy aktivace síní. Pouze v 6 případech (z 18) docházelo k typické aktivaci, jakou jsme pozorovali u WT. U zbytku srdcí docházelo k aktivaci z ektopického místa, které se nacházelo více laterálně v pravé síni. Doba aktivace komor byla 19 ms, v případě aktivace z oblasti SA uzlu a 28 ms v případě aktivace ektopické. Rozdíly mezi výsledky byly statisticky významné ($p<0,05$).

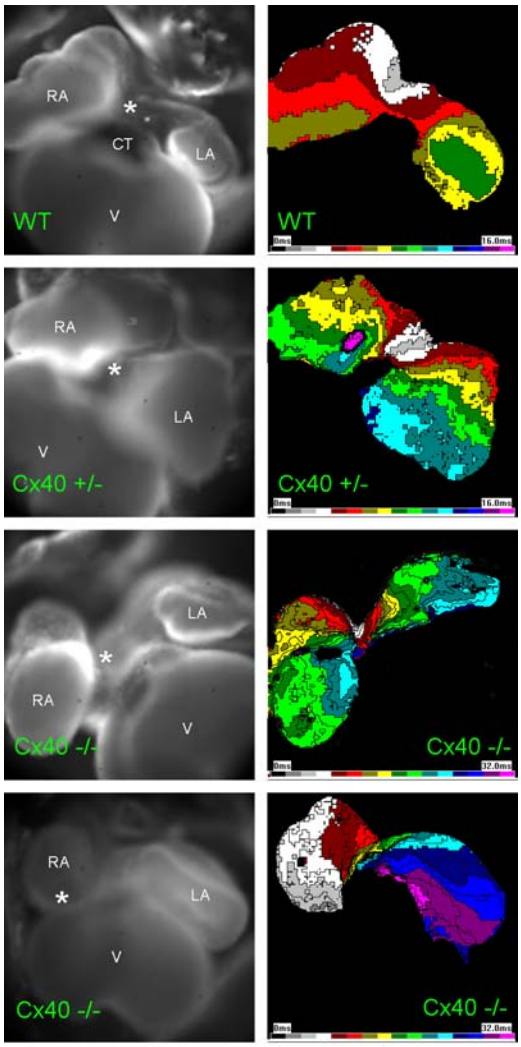

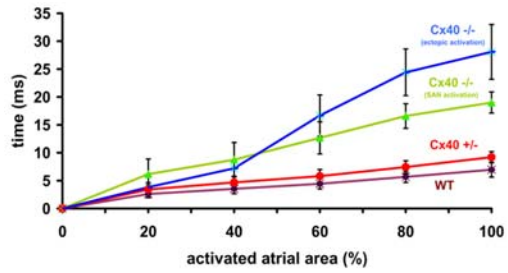

***Obrázek 6* Nejčastější způsoby aktivace síní u jednotlivých genotypů v období 12,5ED**

RA – pravá síň; LA – levá síň; CT – odstřižený výtokový trakt; V – komory; hvězdička – místo první aktivace

V levém sloupci jsou mikroskopické obrazy srdcí k daným optickým mapám, které jsou v sloupci pravém. Místo první aktivace je šedé a poté se šíří podle daných barevných izochron. U WT a heterozygotů odpovídá jedna barva na škále 1 ms, u Cx40 deficitních myší odpovídá jedna barva 2 ms.

Graf níže zobrazuje jednotlivé doby aktivace u daných genotypu pro 12,5ED a 14,5ED.

(zdroj: Benes et al, under revision)

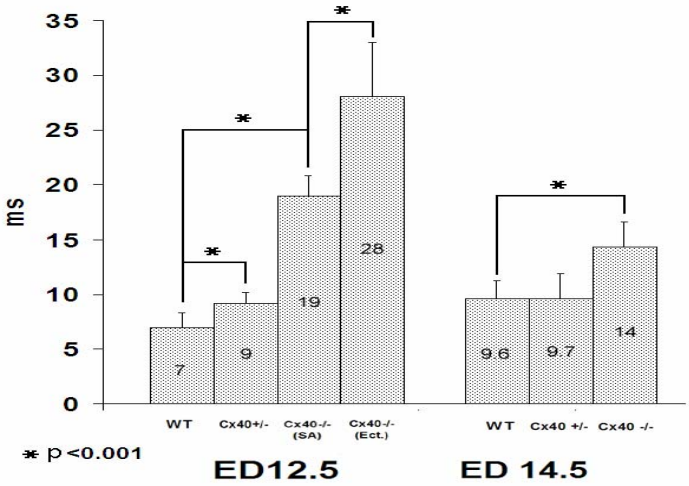

5.1.2 Srdeční frekvence na 12,5ED

Frekvence síní byla relativně uniformní, pokud docházelo k aktivaci z oblasti SA uzlu. U WT byla 96 aktivací/min; u $Cx40^{+/-}$ pak 92 aktivací/min a u $Cx40^{-/-}$ 85 aktivací/min (SD se u všech genotypů pohybovalo mezi hodnotami 25-29). Tyto vysledky poukazují na fakt, že množství Cx40 neovlivňuje srdeční frekvenci. Výrazné rozdíly ve frekvenci byly však u srdcí s ektopickou aktivací, kde byl průměr 116 aktivací/min, nicméně směrodatná odchylka 52,6 poukazuje na značnou variabilitu.

5.1.3 Zhodnocení situace na stádiu 14,5ED

V tomto stádiu již atria výrazně prominují vpřed a hodnocení dorzálních partií síní je problematické (viz výše). I přesto jsme se pokoušeli zhodnotit aspoň orientačně situaci i na tomto pozdějším stádiu vývoje.

Průměrná doba aktivace u WT (n=5) byla 9,5 ms, u Cx40 heterozygotů (n=9) 9,7 ms a u Cx40 deficitních myší (n=11) byla vyšší – 14 ms (viz. graf na Obr 6). Stejně jako na předchozím stádiu i zde byla patrná ektopická aktivace u některých srdcí.

5.1.4 Pátrání po místu ektopické aktivity

Vzhledem k relativně identickému místu ektopické aktivity, pozorované v oblasti pravé síně, jsem se rozhodli prozkoumat, zda toto ektopické místo nemá nějaký morfologický podklad. Prozkoumali jsme histologickou strukturu řady srdcí $Cx40^{-/-}$ (na stádiu 12,5ED, 14,5ED i dospělců) nabarvených anti-HCN4 protilátkou a nenalezli žádné HCN4 pozitivní buňky v oblasti pravého ouška ani nikde jinde mimo oblast vznikajícího SA uzlu (Obr. 7)

5.1.5 Shrnutí

1. Přítomnost Cx40 přímo ovlivňuje rychlost šíření vzruchu v síních a pokud chybí, je šíření výrazně zpomalené (doba aktivace prodloužená).
2. U Cx40 deficitních myší jsme u 2/3 případů pozorovali ektopickou aktivaci síní a doba této aktivace byla výrazně prodloužená.
3. Množství Cx40 neovlivňuje frekvenci srdeční činnosti; při ektopické aktivaci jsou srdeční frekvence značně nehomogenní.
4. V pravé síni jsme neobjevily HCN4 pozitivní buňky mimo oblasti SA uzlu.

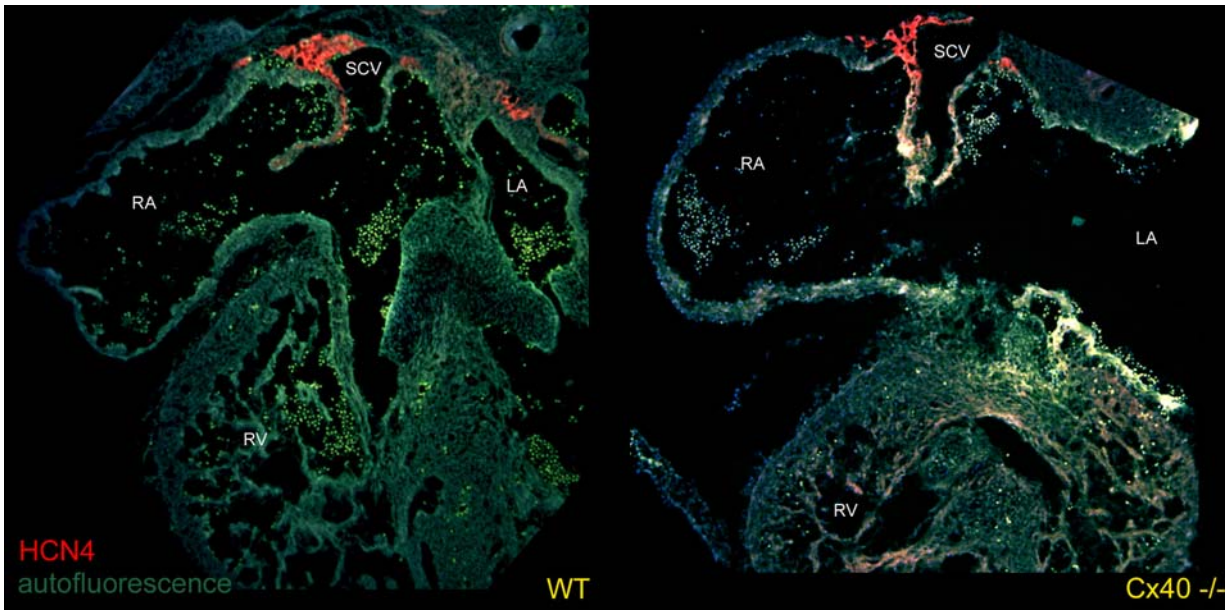

Obrázek 7 **Histologické zobrazení embryonálních srdcí na stádiu 12,5ED**
Vlevo – kontrola; Vpravo – Cx40-/-; červené buňky – HCN4 pozitivní buňky SA uzlu; RA – pravá síň; LA – levá síň; RV – pravá komora; SCV – horní dutá žíla
(zdroj: Benes et al., under revision)

5.2 Normální vývoj komorového převodního systému u myší

Předtím, než jsme začali zkoumat vliv Cx40 na vedení vzruchu v komorách, bylo nejprve potřeba podrobně popsat, jaké druhy aktivace vidíme u WT během jednotlivých fází kardiogeneze. Podobné studie byly provedeny i v minulosti (Rentschler et al., 2001) na relativně malém množství vzorků. Proto jsme v naší laboratoři provedli rozsáhlou studii pomocí optického mapování na myších (Sankova et al., 2012).

5.2.1 Vedení v časných fázích vývoje

Pomocí optického mapování jsme byli schopni získat informace o šíření vzruchu až od 9,5ED. V dřívějších stádiích byla vyvíjející se srdce příliš náchylná k toxicitě di-4-ANEPPS a nedostali jsme dostatečný signál (resp. srdce *in vitro* často nejevila spontánní aktivitu vůbec).

Ve vznikající komoře pozorujeme T3-LacZ pozitivní prstenec v okolí budoucího interventrikulárního septa (Obr. 8) – tzv. primární interventrikulární prstenec („primary interventricular ring“, PIR). Tato struktura v komorách poté slouží k šíření vzruchu před vývojem

Tawarových ramének. Od 10,5ED pozorujeme v komorách expresi Cx40 v trabekulách a postupný vývoj Tawarových ramének.

Na mapách z optického mapování vidíme v těchto stádiích dva druhy aktivace (Obr.9). První je vznik aktivace v oblasti levé komory a druhý typ aktivace je z oblasti mezikomorové, tedy z místa PIR. Signál u této cirkulární struktury může šířit oběma směry, což ovlivňuje místo vzniku první aktivace.

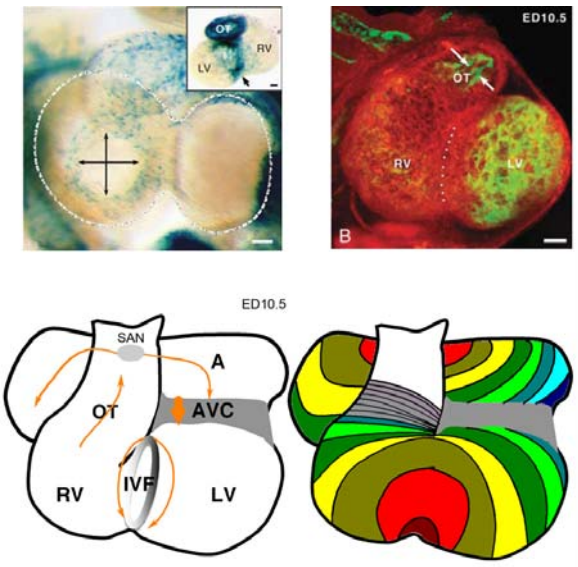

Obrázek 8 **Primární interventrikulární prstenec**

Obrázek vlevo nahoře – exprese T3-LacZ na whole-mount srdcích na 10ED, jasně zřetelná prstencovitá struktura mezi komorami (boční pohled).
Obrázek vpravo nahoře – exprese Cx40 (zelená) v myším srdci na 12,5ED
Obrázky dole – schéma a optická mapa typická pro šíření vzruchu z PIR

5.2.2 Vedení v pozdějších fázích vývoje

Pozdější fáze vývoje byly již dříve popsány i jinými skupinami (Renschler et al., 2001). Tyto studie byly prováděny na malém množství embryí a přisuzovaly obvykle každému stádiu specifický druh aktivace. Z našich dat vyplývá, že celá situace je značně složitější a k aktivaci dochází postupným přechodem z primitivnějších vzorů na vyspělejší.

Aktivace pomocí PIR je postupně nahrazována aktivací cestou Tawarových ramének a poslední stádium, na kterém PIR pozorujeme, je 12,5ED (Obr. 9). První raménko, které začne fungovat, je zpravidla to pravé, posléze se přidá i levé a od stádia 14,5ED je převážná část srdcí aktivována již oběma raménky, což se projeví typickým obrazem dvou míst aktivace (Obr. 10). Toto je již dospělý typ, který pozorujeme i postnatálně.

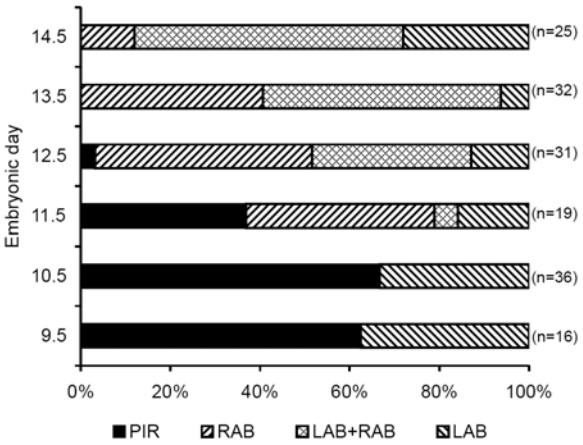

***Obrázek 9* Zastoupení jednotlivých druhů komorové aktivace u myších embryií;** RAB – aktivace zprava; LAB – aktivace zleva (right and left apical breakthrought)
(zdroj: Sankova et al., 2012)

5.3 Vliv deficitu Cx40 na vývoj převodního systému u myší

Na časných stádiích vývoje neměl deficit Cx40 výraznější dopad na vznik a šíření signálu po komorách. Hlavními strukturami, které byly nedostatkem Cx40 postiženy, byla přirozeně Tawarova raménka, v nichž hraje tento konexin klíčovou úlohu. Proto jsme se zaměřili na zhodnocení funkčnosti jednotlivých ramének během vývoje. Ta byla reprezentována aktivací z oblasti levé resp. pravé komory. Zajímali jsme se o stádia 12,5ED a výše, neboť právě v této době dochází k jejich nejmarkantnějšímu vývoji.

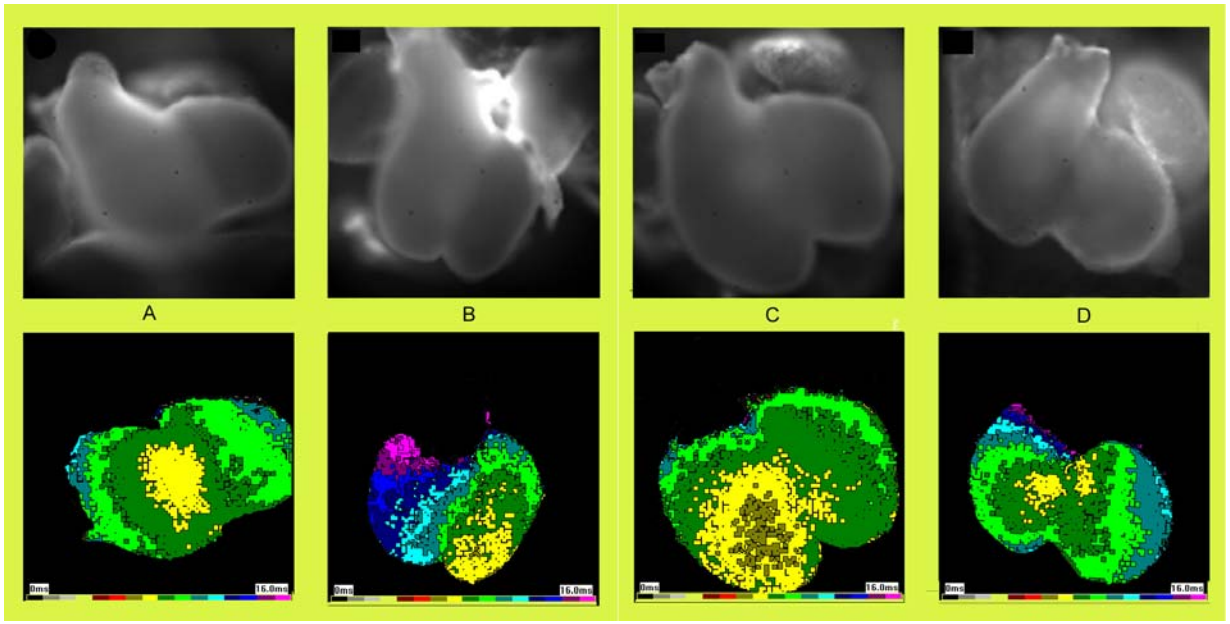

***Obrázek 10* Nejčastější druhy aktivace komor ve stádiu 12,5ED (bez ohledu na genotyp)**
A aktivace cestou PIR; B – aktivace cestou levého raménka; C – aktivace cestou pravého raménka; D – aktivace cestou obou ramének

5.3.1 Funkce levého Tawarova raménka během vývoje

Funkčnost ramének u jednotlivých genotypů během vývoje je graficky znázorněna na obrázku 11. Na 12,5ED je převažujícím typem aktivace zprava. Levé raménko je u všech genotypů funkční asi v 40 - 60% zkoumaných srdcí. U Cx40 deficitních je tento poměr sice nižší, rozdíly výsledků však nejsou statisticky významné.

Zajímavá situace nastává ve stádiu 14,5ED, kdy vidíme zřejmé (a statisticky významné) snížení funkčních levých ramének u Cx40 deficitních myší, kdy u nich toto raménko nacházíme funkční u 54% srdcí, zatímco u WT je funkční v 93%.

Situace se ovšem v dalších stádiích již normalizuje a jak na 16,5ED tak na 18,5ED je levé raménko funkční ve 100% případů u všech genotypů.

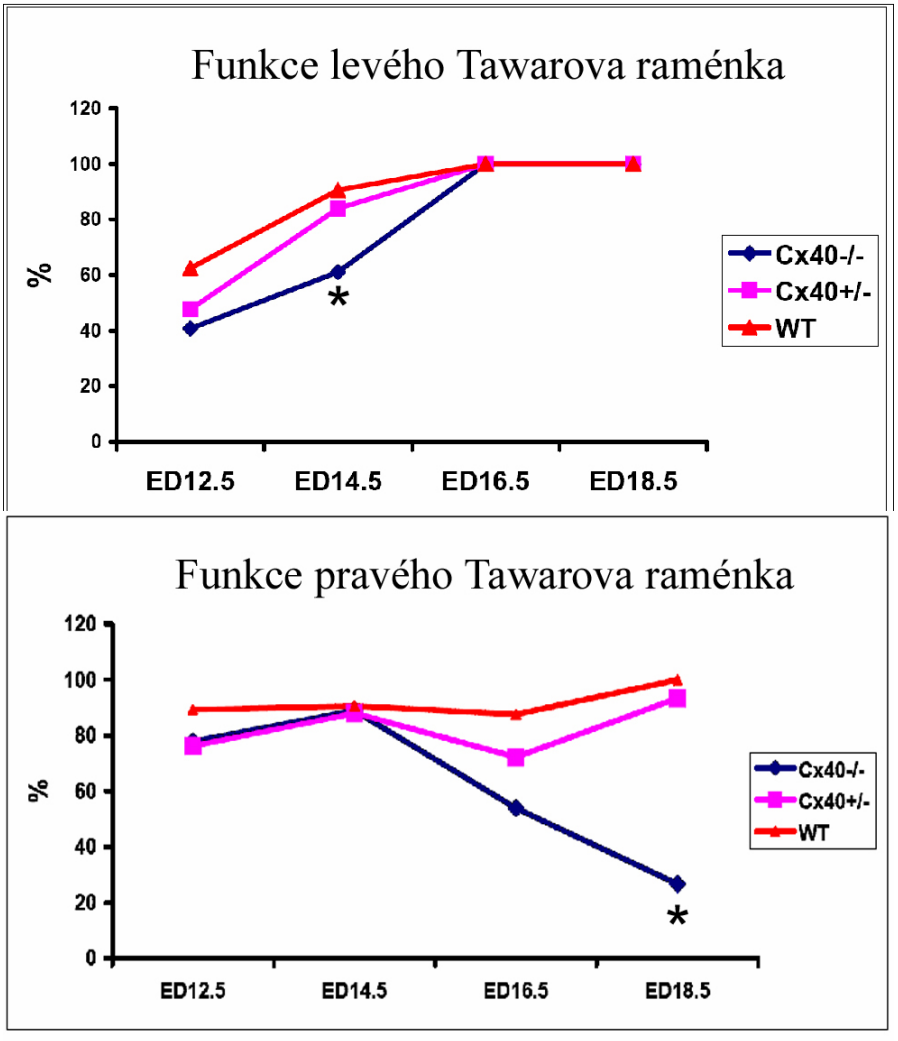

***Obrázek 11* Funkčnost jednotlivých ramének během vývoje**
Hvězdička označuje statisticky významné rozdíly**.** Počty jednotlivých mapovaných srdcí (n) pro daná stádia u sledovaných genotypů se pohybovaly mezi 15-36 (u kontrol mezi 8-30).
(Zdroj: Sankova et al., 2012)

5.3.2 Funkce pravého Tawarova raménka během vývoje

Dynamika funkčnosti pravého raménka je značně odlišná od levého. U všech genotypů je na 12,5ED i na 14,5ED pravé raménko funkční zhruba v 80% případů. U WT a $Cx40^{+/-}$ zárodků dochází poté k postupnému vzestupu až do 100%, zatímco u Cx40 deficitních jedinců dochází k prudkému poklesu a na stádiu 18,5ED je aktivace zprava přítomna pouze u 27% srdcí. Podobný blok pravého Tawarova raménka byl popisován dříve v literatuře u dospělých myší s deficitem Cx40 (Verheule et al., 1999).

U heterozygotů je ve většině případů naznačen mírný pokles funkčnosti (přechodný fenotyp).

5.3.3 Doba aktivace komor

Podobně jako u síní se naskýtá otázka, zda je u Cx40 deficitních srdcí delší doba aktivace.

Rozdíly v časech aktivace u WT a heterozygotů byly pouze malé a statisticky nevýznamné. U Cx40 deficitních srdcí docházelo k prodloužení aktivačních časů, které však bylo patrné a statisticky významné až v pozdějších stádiích vývoje. Na 18,5ED byla průměrná doba aktivace komor u WT 5,2 ms a u Cx40-/- 7,5 ms ($p<0,05$). Je zřejmé, že rozdíl zde není natolik výrazný jako v síních.

5.3.4 Shrnutí

1. Funkce levého raménka je deficitem Cx40 ovlivněna méně výrazně, dochází pouze k nižšímu zastoupení funkčních levých ramének na stádiu 14,5ED a později je stav již normální.
2. Funkce pravého raménka je zpočátku vývoje normální a později vlivem deficitu Cx40 rapidně klesá.
3. Deficit Cx40 mírně prodlužuje aktivační čas komor v pozdějších stádiích vývoje.

6. Výsledky II.

Arytmogenní substrát a morfologické změny u potkaního modelu objemového srdečního selhání

Druhou studií je model objemového srdečního selhání u potkanů. Na tomto modelu pracuje skupina doc. MUDr. Melenovského v IKEMu a zajímá se mj. o změny v metabolismu lipidů při vyvolaném srdečním selhání (Melenovsky et al., 2011). Ve své studii jsem se zajímal zejména o morfologické změny, které oběhové přetížení přineslo, a o potenciální patofyziologický podklad arytmií, které byly při srdečním selhání pozorovány jak u tohoto modelu, tak u pacientů v klinické praxi. Práce byly publikovány (Benes, Jr. et al., 2011; Melenovsky et al., 2011) a máme v plánu pokračovat s výzkumem i na pozdějších stádiích selhání.

6.1 Makroskopické a mikroskopické morfologické změny

K posouzení celkových změn v organismu byly zváženy u potkanů všechny vnitřní orgány s maximální pozorností zaměřenou na srdce. Hypertrofie srdeční se dá nejlépe vyjádřit pomocí poměru váhy srdce ku váze těla (HBWR – heart to body weight ratio), které bylo v obou stádiích selhávání u AVF potkanů zhruba dvojnásobné (přesné hodnoty viz přiložený článek). U srdcí byly výrazně zesílené stěny a to vždy výrazněji v pravé komoře (stěna pravé komory po 11 týdnech o 58% silnější a po 21 týdnech o 146% silnější než kontroly; stěna levé komory v těchto stádiích o 33% a o 83%). Tento fakt poukazuje na vznikající kompenzatorní excentrickou hypertrofii myokardu.

Z ostatních orgánů byl výrazný nárůst váhy pozorován zejména u plic, což souvisí s retencí tekutiny danou městnáním krve při selhávání levé komory.

Na skenech z konfokálního mikroskopu jsme měřili změny ve velikosti buněk (Obr. 12). Jak se dá předpokládat, kardiomyocyty se při popisované excentrické hypertrofii jak prodloužily, tak zesílily, a to výrazněji opět v pravé komoře a více ve střední vrstvě stěny (v midmyokardu) než ve vnitřní vrstvě svaloviny stěny (v subendokardu).

6.2 Arytmogenní substrát v komorách selhávajících srdcí

Z hlediska vzniku arytmií jsme se zajímali zejména o množství, distribuci a fosforylaci Cx43 a o přítomnost fibrotických změn v myokardu.

Obrázek 12
Obraz morfologických změn v myokardu u selhávajících srdcí 11.týdnů po operaci (AVF) a kontrol (Sham)
Modře – jádra
Červeně – v horní dvou řádcích actinin, v dolních Cx43
Zeleně – v horních dvou řádcích membrány a vazivová tkáň, v dolních autofluorescence cytoplasmy
(Zdroj: Benes et al., 2011)

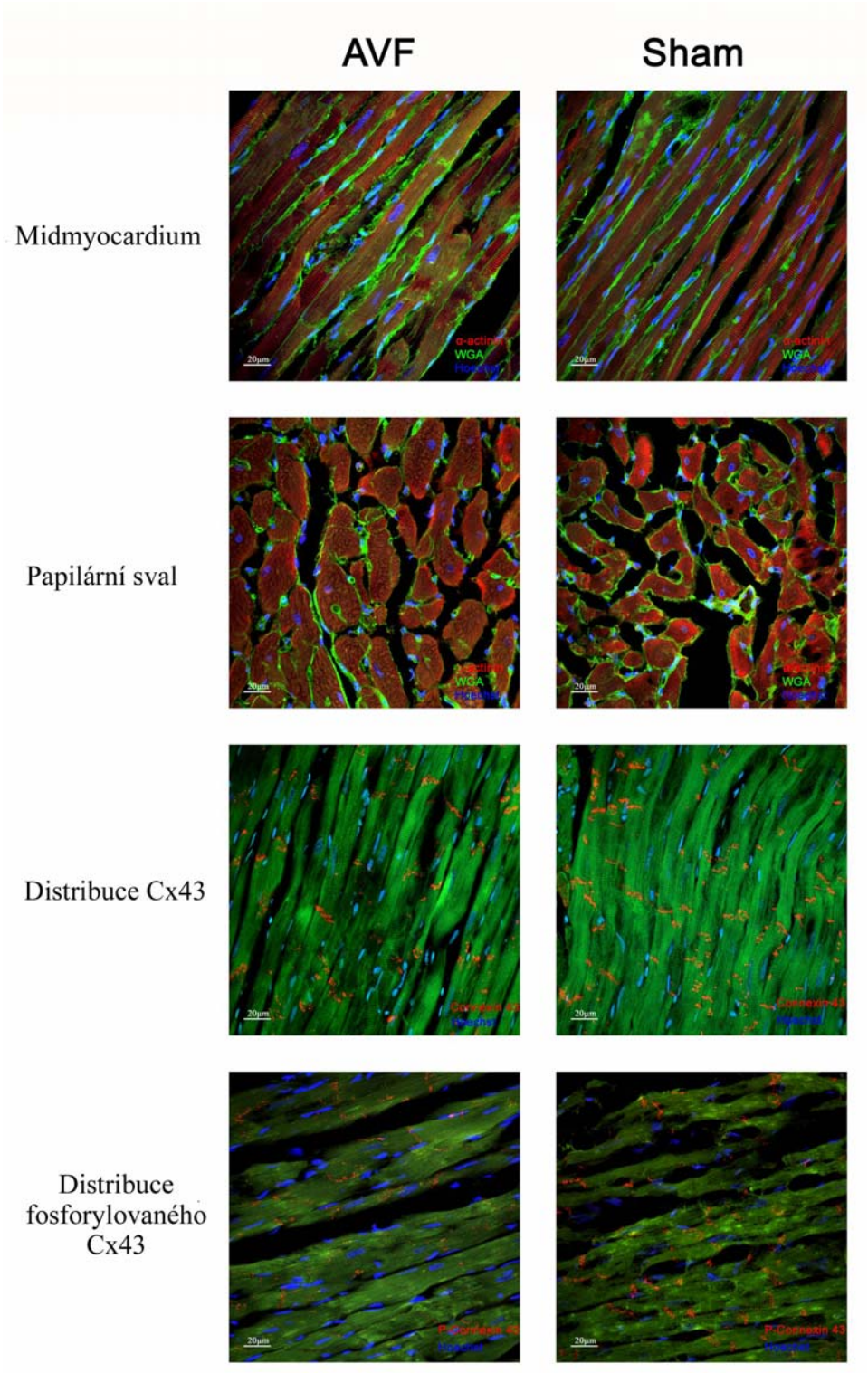

Komorovou fibrózu jsme hodnotili na konfokálních skenech poměrem plochy zeleného kanálu (charakterizující barvení pomocí WGA, tedy vazivo a membrány) vůči červenému kanálu, který reprezentoval cytoplasmu buněk (při barvení pomocí fluorescenční Ig proti alfa-actininu). Poté jsme nález potvrdili klasickým barvením picrosiriusovou červení. Výsledek byl vyjádřen jako poměr plochy zeleného signálu ku ploše tkáně. U AVF potkanů 21 dní po operaci byla 26%, u kontrol 28,6%.

Distribuci a množství Cx43 a fosforylované formy Cx43 jsme hodnotili též z konfokálních skenů (viz Obr. 12) na řezech barvených specifickými protilátkami. Výsledky jsme poté ještě ověřovali pomocí Western blottingu.

Celkové množství Cx43 nebylo při hodnocení z histologických řezů u AVF srdcí výrazněji sníženo. Western blotting prokázal snížení asi na 60% (což by vzhledem k abundanci Cx43 nemělo mít výraznější funkční dopad). Mnohem důležitější pro arytmogenezi je však lokalizace „gap junctions“. Kromě oblasti interkalárních disků se Cx43 může též vyskytovat na laterálních stranách kardiomyocytů nebo v cytoplasmě (viz 3.2.1). Nicméně ani v tomto jsme neobjevili na daných řezech rozdíl. Poměr Cx43 umístěného v interkalárních discích ku celkovému Cx43 v buňkách byl u AVF 33,7% a u kontrol 35,5%.

Hlavním parametrem, který vykazoval změnu, byla fosforylace. Měřili jsme množství fosforylovaného Cx43 v levé komoře v obou stádiích srdečního selhání a zjistili jsem, že v období 11 týdnů po operaci nedocházelo ještě k poklesu fosforylovaného Cx43, ale 21 týdnů po operaci se již projevil pokles množství fosforylovaného Cx43 zhruba na 50% (tento údaj potvrdil též Western blotting).

7. Diskuze a závěry

7.1 Vliv Cx40 na šíření vzruchu v síních

Role Cx40 v arytmogenezi byla popsána již mnoha skupinami (Dupont et al., 2001; Polontchouk et al., 2001; Hauer et al., 2006). I přesto stále není přesná úloha Cx40 zcela objasněná.

Ve své studii jsem popsal pomocí metody optického mapování způsob šíření vzruchu v atriích u myší na embryonálním stádiu 12,5ED (a orientačně jsem vyhodnotil též situaci na 14,5ED). Výsledky mé studie přinesly následující závěry.

7.1.1. Rychlost vedení vzruchu

Nedostatek Cx40 v embryonálních síních přímo ovlivňuje rychlost šíření vzruchu myokardiální tkání. Tento fakt sám o sobě překvapivý není, neboť Cx40 je převažujícím konexinem v síních a je rychle vedoucím kanálem. Fakt, že k šíření dochází (byť zpomaleně) i v Cx40 deficitních atriích ukazuje, že chybějící funkci Cx40 je schopen zastat jiný protein, zejména Cx43. Podle studie Delorme et al. (Delorme et al., 1997) je exprese Cx43 v myších atriích patrná od 12,5ED. Z našich dat vyplývá, že zpomalení vedení při absenci Cx40 je na 12,5ED mnohem výraznější než na 14,5ED (aktivační čas na tomto stádiu je u $Cx40^{-/-}$ pouze cca o 30% delší oproti více než trojnásobnému zvýšení na 12,5ED, viz obr. 6). Postupné zastoupení funkce chybějícího Cx40 postupně vzrůstajícím množstvím konexinu 43 by tento fakt vcelku dobře vysvětlovalo. Navíc naše současné výzkumy tohoto modelu na stádiu 10,5ED ukazují, že zde je dopad absence Cx40 ještě větší než na 12,5ED.

7.2.2 Ektopická místa aktivace

Až 2/3 ze zkoumaných $Cx40^{-/-}$ srdcí vykazovaly ektopické místo první aktivace v síních. Toto místo bylo u všech srdcí, která jsme zmapovali, umístěno v oblasti pravé síně a jejího ouška. Vzhledem k tomu, že ektopické místo jevilo takovouto uniformitu, přemýšleli jsem o možném ektopickém vzniku srdečního pacemakeru. Na histologických řezech (Obr. 7) deseti $Cx40^{-/-}$ srdcí na stádiu 12,5ED jsme nenašli v pravé síni žádné HCN4 pozitivní kardiomyocyty, které by mohly přispívat k potenciální tkáňové automacii. Nález lze tak vysvětlit buď funkční poruchou (u níž je však takováto jednotnost ne zcela přesvědčivá) nebo abnormálním šířením signálu z SA uzlu. Vzhledem k tomu, že v uzlu samotném se Cx40 nenachází, musí docházet k hlavním změnám

v oblasti obklopující uzel, kde poté vzniká blok vedení, podobně jak byl popsán v literatuře v králičích srdcích (Sano et al., 1965; Boyett et al., 1999). Vzruch by poté odcházel z SA uzlu jinou cestou, tzv. „abnormal exit site“ (Fedorov et al., 2009). Proti této teorii svědčí fakt, že frekvence srdcí s ektopickým místem aktivity byly obvykle vyšší než při aktivaci z SA uzlu (která naopak byla relativně uniformní v rámci genotypů). Dá se proto předpokládat, že opravdu vzniká funkční místo ektopické aktivity v pravé síni, které začne vytvářet rychlejší rytmus, čímž znemožní funkci pomalejšímu SA uzlu (jde vlastně o jakési síňové extrasystoly).
Rozsáhlou studii zabývající se Cx40 deficitními myšmi provedla slupina Gregory Morleyho (Leaf et al., 2008). Zabývali se řadou stádií a mimo jiné popsali též změny během embryonálního vývoje, resp. na stádiích 13,5ED a 15,5ED. V mnohém se jejich data shodují s našimi , avšak s jednou důležitou diskrepancí. Též pozorovali u Cx40-/- srdcí vznik ektopických aktivací v síních, avšak na mnoha rozličných místech. Tato odlišnost má jistě řadu možných vysvětlení. Leaf et al. (Leaf et al., 2008) používali odlišný protokol pro optické mapování a techniku přípravy a umístění srdce (zejména mechanické přizpůsobování tvaru síní). Odlišná stádia vývoje a odlišný genetický podklad myší jistě též sehráli svou roli.

7.2.3 Doba aktivace síní z ektopického místa

Pokud docházelo k šíření aktivace z ektopického místa, doba šíření po atriích byla ještě více prodloužena než při pouhé absenci Cx40 při šíření z SA uzlu. Tento fakt poukazuje na přítomnost jistých preferenčních cest šíření vzruchu v síních, které vedou od SA uzlu a urychlují průběh aktivace. Jedním z těchto svazků je například interatriální svazek Bachmannův, který byl již dříve popsán u kuřete (Sedmera et al., 2006).

Verheule et al. popsal ve své studii řadu elektrofyziologických změn u Cx40 deficitních dospělých myší (Verheule, 1999). Mimo jiné objevil prodlouženou vlnu P (která odpovídá aktivaci síní) a pokles rychlosti vedení vzruchu o 30%, což odpovídá našim výsledkům na stádiu 14,5ED. Navíc při stimulaci síní elektrodou vyvolával u myší síňové tachyarytmie až u 50% zkoumaných Cx40-/- mutant. Toto dokazuje, že takového zpomalení vedení by mohlo být též u lidí podkladem pro vznik arytmií při poruchách distribuce Cx40.

7.2 Vliv Cx40 na vývoj funkce komorového převodního systému

Vzhledem k převažující lokalizaci Cx40 v trabekulách komor a posléze v Tawarových raménkách, hlavní změny při deficitu Cx40 jsme očekávali ve změnách aktivací v jednotlivých fázích vývoje. Struktura PIR neobsahuje Cx40, a proto jsme nepředpokládali (a ani nenacházeli) výraznější změny v aktivaci na časných stádiích. V pozdějších obdobích embryonálního vývoje jsme však našli změny výrazné.

7.2.1 Blokáda pravého raménka Tawarova

Nejzajímavějším nálezem byl postupně vznikající blok pravého Tawarova raménka, jak je vidět na obr 11. Změny EKG tohoto druhu popsalo už dříve na dospělých myších několik vědeckých skupin (Verheule et al, 1999; Tamaddon et al., 2000). Důvod, proč je pravé raménko zpočátku u většiny Cx40-/- srdcí funkční a posléze dochází k jeho blokádě, je třeba hledat v morfologické stavbě vznikajícího pravého raménka. Na obr. 13 je patrné, že struktura raménka je zpočátku relativně objemná a široká a s postupujícím růstem srdce dochází ke ztenčování až do konečné fáze, kdy pravé raménko Tawarovo tvoří pouze nevelké množství vláken převodního systému. Předpokládáme tedy, že v počátcích vývoje ramének převodního systému je pro funkci rozhodující morfologické struktura (v tomto případě velikost), která dostatečně nahrazuje absenci rychle vedoucího Cx40. S postupem času, kdy dochází k ztenčování této struktury, stává se závislejší na přítomnosti rychle vedoucích kanálů, které v případě Cx40-/- srdcí přítomny nejsou a tudíž zde dochází k blokádě.

7.2.2 Snížení funkce levého raménka Tawarova ve 14,5ED

Statisticky významný pokles funkčnosti levého Tawarova raménka na 14,5ED připisujeme spíše než morfologii (jak tomu bylo vpravo) samotnému deficitu Cx40. Ten je v komorách ve větším množství detekovatelný až od 14,5ED dále. Otázka přítomnosti a funkčnosti Tawarových ramének na stádiu 12,5ED je silně diskutabilní. Cx43 je zde detekovatelný až o den později. Tato diskrepance nejspíš způsobuje pokles patrný v grafu na obr 11. Na 14,5ED je nepřítomnost Cx40 v levém raménku částečně kompenzována morfologií, nicméně jak je vidět, pokles funkčnosti tu patrný je. O den později nastoupí exprese Cx43, který dostatečně zastoupí v objemném levém raménku funkci Cx40.

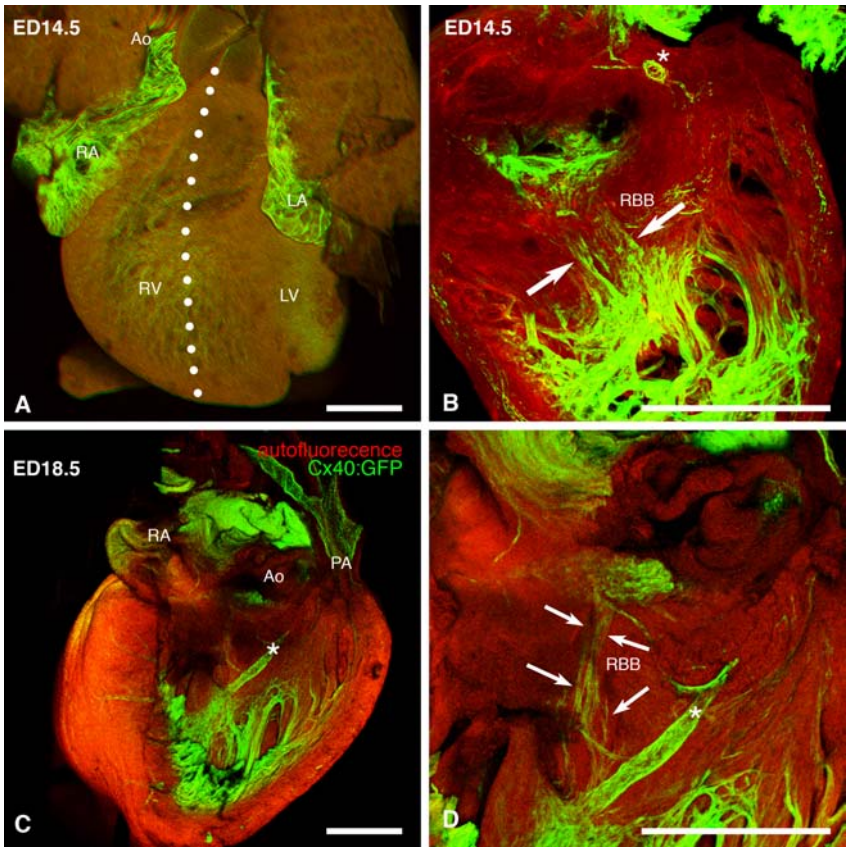

Obrázek 13 **Morfologie pravého raménka Tawarova** (RBB) na 14,5ED a na 18,5ED; šipky definují průběh raménka; hvězdička – septální tepna; RV a LV – pravá a levá komora; měřítko – 500µm *(Zdroj: Sankova et al., 2012)*

7.3 Arytmogenní substrát při objemovém srdečním selhání

U velké řady srdečních patologií (např. angina pectoris, hypertrofie komory při hypertenzi) je jedním z hlavních arytmogenních činitelů srdeční fibróza. V myokardu se nacházejí oblasti (větší či menší) fibrotické tkáně, které vytvářejí blokády vodivosti a jsou příčinou reentry fenoménů. V našem modelu objemového srdečního selhání jsme však fibrózu neprokázali, a přesto byly u potkanů pozorovány časté arytmie. Důvodů hledat na těchto srdcích arytmogenní potenciál bylo však více. Podobné stavy objemového přetížení myokardu prokazatelně spojeny se život ohrožujícími komorovými tachyarytmiemi byly popsány v literatuře (von Olshausen et al., 1983). Zvýšené riziko náhlé srdeční smrti bylo popsáno i u symptomatických pacientů s objemovým přetížením daným mitrální regurgitací (Grigioni et al., 1999).

Vzhledem k absenci výraznějších fibrotických změn v selhávajících srdcích jsme se zaměřili na jiné potenciální zdroje arytmií. Věnovali jsme se zejména změnám v distribuci, množství a

fosforylaci Cx43 v srdci. Kromě změn v Cx43 však mohou přicházet jako možné zdroje poruch rytmu v úvahu též např. změny v iontových kanálech, které se často výrazně podílejí na patogenezi arytmií (Shah et al., 2005).

Většina změn v distribuci a množství Cx43 v myokardu selhávajících potkanů nebyla významná a výsledky korespondovaly s některými obdobnými studiemi provedenými v minulosti (u několika studií docházelo ve výsledcích k diskrepancím vlivem odlišných metod výzkumu – viz diskuse v přiloženém článku) (Burstein et al., 2009; Dupont et al., 2001; Emdad et al., 2001).

Jako možný arytmogenní substrát jsme objevili výrazně sníženou fosforylaci Cx43 ve stádiu dekompenzovaného srdečního selhání (21 týdnů po vytvoření zkratu). Tyto změny jsou v souladu s výsledky jiných skupin zabývajících se srdečním selháním a arytmiemi (Ai et al., 2005). Ovlivnění fosforylace Cx43 při srdečních patologiích se tímto jeví jako dobrá potenciální cesta k farmakologické profylaxi arytmií, jak potvrdila již skupina Roberta Gourdieho (O´Quinn et al., 2011).

8. Literatura

Aanhaanen WT, Boukens BJ, Sizarov A, Wakker V, de Gier-de Vries C, van Ginneken AC, Moorman AF, Coronel R, and Christoffels VM. Defective Tbx2-dependent patterning of the atrioventricular canal myocardium causes accessory pathway formation in mice. *J Clin Invest* 121: 534-544.

Accili EA, Proenza C, Baruscotti M, and DiFrancesco D. From funny current to HCN channels: 20 years of excitation. *News Physiol Sci* 17: 32-37, 2002.

Ai X and Pogwizd SM. Connexin 43 downregulation and dephosphorylation in nonischemic heart failure is associated with enhanced colocalized protein phosphatase type 2A. *Circ Res* 96: 54-63, 2005.

Ammirabile G, Tessari A, Pignataro V, Szumska D, Sutera Sardo F, Benes J, Jr., Balistreri M, Bhattacharya S, Sedmera D, and Campione M. Pitx2 confers left morphological, molecular, and functional identity to the sinus venosus myocardium. *Cardiovasc Res* 93: 291-301.

Anderson JM. Cell signalling: MAGUK magic. *Curr Biol* 6: 382-384, 1996.

Anderson KR, Ho SY, and Anderson RH. Location and vascular supply of sinus node in human heart. *Br Heart J* 41: 28-32, 1979.

Arguello C, Alanis J, Pantoja O, and Valenzuela B. Electrophysiological and ultrastructural study of the atrioventricular canal during the development of the chick embryo. *J Mol Cell Cardiol* 18: 499-510, 1986.

Artham SM, Lavie CJ, Milani RV, Patel DA, Verma A, and Ventura HO. Clinical impact of left ventricular hypertrophy and implications for regression. *Prog Cardiovasc Dis* 52: 153-167, 2009.

Bakker ML, Boukens BJ, Mommersteeg MT, Brons JF, Wakker V, Moorman AF, and Christoffels VM. Transcription factor Tbx3 is required for the specification of the atrioventricular conduction system. *Circ Res* 102: 1340-1349, 2008.

Bevilacqua LM, Simon AM, Maguire CT, Gehrmann J, Wakimoto H, Paul DL, and Berul CI. A targeted disruption in connexin40 leads to distinct atrioventricular conduction defects. *J Interv Card Electrophysiol* 4: 459-467, 2000.

Biermann M, Rubart M, Moreno A, Wu J, Josiah-Durant A, and Zipes DP. Differential effects of cytochalasin D and 2,3 butanedione monoxime on isometric twitch force and transmembrane action potential in isolated ventricular muscle: implications for optical measurements of cardiac repolarization. *J Cardiovasc Electrophysiol* 9: 1348-1357, 1998

Bowling N, Huang X, Sandusky GE, Fouts RL, Mintze K, Esterman M, Allen PD, Maddi R, McCall E, and Vlahos CJ. Protein kinase C-alpha and -epsilon modulate connexin-43 phosphorylation in human heart. *J Mol Cell Cardiol* 33: 789-798, 2001.

Boyden PA, Gardner PI, and Wit AL. Action potentials of cardiac muscle in healing infarcts: response to norepinephrine and caffeine. *J Mol Cell Cardiol* 20: 525-537, 1988.

Boyett MR, Honjo H, Yamamoto M, Nikmaram MR, Niwa R, and Kodama I. Downward gradient in action potential duration along conduction path in and around the sinoatrial node. *Am J Physiol* 276: H686-698, 1999.

Boyett MR, Inada S, Yoo S, Li J, Liu J, Tellez J, Greener ID, Honjo H, Billeter R, Lei M, Zhang H, Efimov IR, and Dobrzynski H. Connexins in the sinoatrial and atrioventricular nodes. *Adv Cardiol* 42: 175-197, 2006.

Burstein B, Comtois P, Michael G, Nishida K, Villeneuve L, Yeh YH, and Nattel S. Changes in connexin expression and the atrial fibrillation substrate in congestive heart failure. *Circ Res* 105: 1213-1222, 2009.

Coppen SR, Kaba RA, Halliday D, Dupont E, Skepper JN, Elneil S, and Severs NJ. Comparison of connexin expression patterns in the developing mouse heart and human foetal heart. *Mol Cell Biochem* 242: 121-127, 2003.

de Bakker JM, van Capelle FJ, Janse MJ, Tasseron S, Vermeulen JT, de Jonge N, and Lahpor JR. Slow conduction in the infarcted human heart. 'Zigzag' course of activation. Circulation 88: 915-926, 1993.

de Mello WC, Motta GE, and Chapeau M. A study on the healing-over of myocardial cells of toads. *Circ Res* 24: 475-487, 1969.

de Wit C, Roos F, Bolz SS, and Pohl U. Lack of vascular connexin 40 is associated with hypertension and irregular arteriolar vasomotion. *Physiol Genomics* 13: 169-177, 2003.

Delorme B, Dahl E, Jarry-Guichard T, Briand JP, Willecke K, Gros D, and Theveniau-Ruissy M. Expression pattern of connexin gene products at the early developmental stages of the mouse cardiovascular system. *Circ Res* 81: 423-437, 1997.

Dillon SM, Allessie MA, Ursell PC, and Wit AL. Influences of anisotropic tissue structure on reentrant circuits in the epicardial border zone of subacute canine infarcts. *Circ Res* 63: 182-206, 1988.

Dupont E, Ko Y, Rothery S, Coppen SR, Baghai M, Haw M, and Severs NJ. The gap-junctional protein connexin40 is elevated in patients susceptible to postoperative atrial fibrillation. *Circulation* 103: 842-849, 2001.

Dupont E, Matsushita T, Kaba RA, Vozzi C, Coppen SR, Khan N, Kaprielian R, Yacoub MH, and Severs NJ. Altered connexin expression in human congestive heart failure. *J Mol Cell Cardiol* 33: 359-371, 2001.

Duthe F, Plaisance I, Sarrouilhe D, and Herve JC. Endogenous protein phosphatase 1 runs down gap junctional communication of rat ventricular myocytes. *Am J Physiol Cell Physiol* 281: C1648-1656, 2001.

Eckardt D, Kirchhoff S, Kim JS, Degen J, Theis M, Ott T, Wiesmann F, Doevendans PA, Lamers WH, de Bakker JM, van Rijen HV, Schneider MD, and Willecke K. Cardiomyocyte-restricted deletion of connexin43 during mouse development. *J Mol Cell Cardiol* 41: 963-971, 2006.

Eliška O. Purkyňova vlákna převodního systému srdce – historie a současnost Purkyňových objevů. *Časopis lékařů českých 145*, 2006

Eloff BC, Lerner DL, Yamada KA, Schuessler RB, Saffitz JE, and Rosenbaum DS. High resolution optical mapping reveals conduction slowing in connexin43 deficient mice. *Cardiovasc Res* 51: 681-690, 2001.

Emdad L, Uzzaman M, Takagishi Y, Honjo H, Uchida T, Severs NJ, Kodama I, and Murata Y. Gap junction remodeling in hypertrophied left ventricles of aortic-banded rats: prevention by angiotensin II type 1 receptor blockade. *J Mol Cell Cardiol* 33: 219-231, 2001.

Emdad L, Uzzaman M, Takagishi Y, Honjo H, Uchida T, Severs NJ, Kodama I, and Murata Y. Gap junction remodeling in hypertrophied left ventricles of aortic-banded rats: prevention by angiotensin II type 1 receptor blockade. *J Mol Cell Cardiol* 33: 219-231, 2001.

Fedorov VV, Lozinsky IT, Sosunov EA, Anyukhovsky EP, Rosen MR, Balke CW, and Efimov IR. Application of blebbistatin as an excitation-contraction uncoupler for electrophysiologic study of rat and rabbit hearts. *Heart Rhythm* 4: 619-626, 2007.

Fedorov VV, Schuessler RB, Hemphill M, Ambrosi CM, Chang R, Voloshina AS, Brown K, Hucker WJ, and Efimov IR. Structural and functional evidence for discrete exit pathways that connect the canine sinoatrial node and atria. Circ Res 104: 915-923, 2009.

Ford LE. Heart size. Circ Res 39: 297-303, 1976.

Francis RJ and Lo CW. Primordial germ cell deficiency in the connexin 43 knockout mouse arises from apoptosis associated with abnormal p53 activation. *Development* 133: 3451-3460, 2006.

Frank M, Wirth A, Andrie RP, Kreuzberg MM, Dobrowolski R, Seifert G, Offermanns S, Nickenig G, Willecke K, and Schrickel JW. Connexin45 provides optimal atrioventricular nodal conduction in the adult mouse heart. *Circ Res* 111: 1528-1538.

Garcia-Frigola C, Shi Y, and Evans SM. Expression of the hyperpolarization-activated cyclic nucleotide-gated cation channel HCN4 during mouse heart development. *Gene Expr Patterns* 3: 777-783, 2003.

Giepmans BN. Gap junctions and connexin-interacting proteins. *Cardiovasc Res* 62: 233-245, 2004.

Goodenough DA and Paul DL. Beyond the gap: functions of unpaired connexon channels. *Nat Rev Mol Cell Biol* 4: 285-294, 2003.

Goodenough DA, Goliger JA, and Paul DL. Connexins, connexons, and intercellular communication. *Annu Rev Biochem* 65: 475-502, 1996.

Gorza L, Schiaffino S, and Vitadello M. Heart conduction system: a neural crest derivative? *Brain Res* 457: 360-366, 1988.

Gourdie RG, Mima T, Thompson RP, and Mikawa T. Terminal diversification of the myocyte lineage generates Purkinje fibers of the cardiac conduction system. *Development* 121: 1423-1431, 1995.

Grigioni F, Enriquez-Sarano M, Ling LH, Bailey KR, Seward JB, Tajik AJ, and Frye RL. Sudden death in mitral regurgitation due to flail leaflet. *J Am Coll Cardiol* 34: 2078-2085, 1999.

Gros D, Alcoléa S, Dupays L, Meysen S, Miquerol L, Théveniau-Ruissy M et al. Connexins in cardiac development: expression, role, and transcriptional kontrol. In: Winterhagen E ed. Gap Junctions in Development and Diseases. Berlin, Heidelberg: Springer-Verlag; 2005. p29-55

Gros D, Dupays L, Alcolea S, Meysen S, Miquerol L, and Theveniau-Ruissy M. Genetically modified mice: tools to decode the functions of connexins in the heart-new models for cardiovascular research. *Cardiovasc Res* 62: 299-308, 2004.

Gros D, Dupays L, Alcolea S, Meysen S, Miquerol L, and Theveniau-Ruissy M. Genetically modified mice: tools to decode the functions of connexins in the heart-new models for cardiovascular research. *Cardiovasc Res* 62: 299-308, 2004.

Gros D, Theveniau-Ruissy M, Bernard M, Calmels T, Kober F, Sohl G, Willecke K, Nargeot J, Jongsma HJ, and Mangoni ME. Connexin 30 is expressed in the mouse sino-atrial node and modulates heart rate. *Cardiovasc Res* 85: 45-55, 2010

Gros DB and Jongsma HJ. Connexins in mammalian heart function. *Bioessays* 18: 719-730, 1996.

Grossman W, Jones D, and McLaurin LP. Wall stress and patterns of hypertrophy in the human left ventricle. *J Clin Invest* 56: 56-64, 1975.

Gu H, Smith FC, Taffet SM, and Delmar M. High incidence of cardiac malformations in connexin40-deficient mice. *Circ Res* 93: 201-206, 2003.

Gutstein DE, Morley GE, Tamaddon H, Vaidya D, Schneider MD, Chen J, Chien KR, Stuhlmann H, and Fishman GI. Conduction slowing and sudden arrhythmic death in mice with cardiac-restricted inactivation of connexin43. *Circ Res* 88: 333-339, 2001.

Hagendorff A, Schumacher B, Kirchhoff S, Luderitz B, and Willecke K. Conduction disturbances and increased atrial vulnerability in Connexin40-deficient mice analyzed by transesophageal stimulation. *Circulation* 99: 1508-1515, 1999.

Haider AW, Larson MG, Benjamin EJ, and Levy D. Increased left ventricular mass and hypertrophy are associated with increased risk for sudden death. *J Am Coll Cardiol* 32: 1454-1459, 1998.

Harris BS, Spruill L, Edmonson AM, Rackley MS, Benson DW, O'Brien TX, and Gourdie RG. Differentiation of cardiac Purkinje fibers requires precise spatiotemporal regulation of Nkx2-5 expression. *Dev Dyn* 235: 38-49, 2006.

Hauer RN, Groenewegen WA, Firouzi M, Ramanna H, and Jongsma HJ. Cx40 polymorphism in human atrial fibrillation. *Adv Cardiol* 42: 284-291, 2006.

Herve JC. Gap junction channels: from protein genes to diseases. *Prog Biophys Mol Biol* 94: 1-4, 2007.

His W Jr. Die Thätigkeit des embryonalen Herzen und deren Bedeutung für die Lehre von der Herzbewegung beim Erwachsenen. *Arebeiten aus der med. Klinik zu Leipzig*, 1893

Hood WP, Jr., Rackley CE, and Rolett EL. Wall stress in the normal and hypertrophied human left ventricle. *Am J Cardiol* 22: 550-558, 1968.

Hoogaars WM, Engel A, Brons JF, Verkerk AO, de Lange FJ, Wong LY, Bakker ML, Clout DE, Wakker V, Barnett P, Ravesloot JH, Moorman AF, Verheijck EE, and Christoffels VM. Tbx3 controls the sinoatrial node gene program and imposes pacemaker function on the atria. *Genes Dev* 21: 1098-1112, 2007.

Hoogaars WM, Tessari A, Moorman AF, de Boer PA, Hagoort J, Soufan AT, Campione M, and Christoffels VM. The transcriptional repressor Tbx3 delineates the developing central conduction system of the heart. *Cardiovasc Res* 62: 489-499, 2004.

Hunter AW, Barker RJ, Zhu C, and Gourdie RG. Zonula occludens-1 alters connexin43 gap junction size and organization by influencing channel accretion. *Mol Biol Cell* 16: 5686-5698, 2005.

Chadjichristos CE, Scheckenbach KE, van Veen TA, Richani Sarieddine MZ, de Wit C, Yang Z, Roth I, Bacchetta M, Viswambharan H, Foglia B, Dudez T, van Kempen MJ, Coenjaerts FE, Miquerol L, Deutsch U, Jongsma HJ, Chanson M, and Kwak BR. Endothelial-specific deletion of connexin40 promotes atherosclerosis by increasing CD73-dependent leukocyte adhesion. *Circulation* 121: 123-131.

Chuck ET, Freeman DM, Watanabe M, and Rosenbaum DS. Changing activation sequence in the embryonic chick heart. Implications for the development of the His-Purkinje system. *Circ Res* 81: 470-476, 1997.

Kamino K, Hirota A, and Fujii S. Localization of pacemaking activity in early embryonic heart monitored using voltage-sensitive dye. *Nature* 290: 595-597, 1981.

Kamino K. Optical approaches to ontogeny of electrical activity and related functional organization during early heart development. *Physiol Rev* 71: 53-91, 1991.

Kapoor N, Galang G, Marban E, and Cho HC. Transcriptional suppression of connexin43 by TBX18 undermines cell-cell electrical coupling in postnatal cardiomyocytes. *J Biol Chem* 286: 14073-14079.

Keith A, Flack M. The for mand nature of the muscular connections between primary divisions of the vertebrate heart. *J. Anat. Physiol., 41,* 1907

Kirchhoff S, Nelles E, Hagendorff A, Kruger O, Traub O, and Willecke K. Reduced cardiac conduction velocity and predisposition to arrhythmias in connexin40-deficient mice. *Curr Biol* 8: 299-302, 1998.

Kolditz DP, Wijffels MC, Blom NA, van der Laarse A, Markwald RR, Schalij MJ, and Gittenberger-de Groot AC. Persistence of functional atrioventricular accessory pathways in postseptated embryonic avian hearts: implications for morphogenesis and functional maturation of the cardiac conduction system. Circulation 115: 17-26, 2007.

Kreuzberg MM, Willecke K, and Bukauskas FF. Connexin-mediated cardiac impulse propagation: connexin 30.2 slows atrioventricular conduction in mouse heart. *Trends Cardiovasc Med* 16: 266-272, 2006.

Kwak BR and Jongsma HJ. Regulation of cardiac gap junction channel permeability and conductance by several phosphorylating conditions. *Mol Cell Biochem* 157: 93-99, 1996.

Kwak BR, Mulhaupt F, Veillard N, Gros DB, and Mach F. Altered pattern of vascular connexin expression in atherosclerotic plaques. *Arterioscler Thromb Vasc Biol* 22: 225-230, 2002.

Leaf DE, Feig JE, Vasquez C, Riva PL, Yu C, Lader JM, Kontogeorgis A, Baron EL, Peters NS, Fisher EA, Gutstein DE, and Morley GE. Connexin40 imparts conduction heterogeneity to atrial tissue. *Circ Res* 103: 1001-1008, 2008.

Lei M, Zhang H, Grace AA, and Huang CL. SCN5A and sinoatrial node pacemaker function. *Cardiovasc Res* 74: 356-365, 2007.

Liu J, Dobrzynski H, Yanni J, Boyett MR, and Lei M. Organisation of the mouse sinoatrial node: structure and expression of HCN channels. *Cardiovasc Res* 73: 729-738, 2007.

Luke RA and Saffitz JE. Remodeling of ventricular conduction pathways in healed canine infarct border zones. J Clin Invest 87: 1594-1602, 1991.

Melenovsky V, Benes J, Skaroupkova P, Sedmera D, Strnad H, Kolar M, Vlcek C, Petrak J, Benes J, Jr., Papousek F, Oliyarnyk O, Kazdova L, and Cervenka L. Metabolic characterization of volume overload heart failure due to aorto-caval fistula in rats. *Mol Cell Biochem* 354: 83-96.

Miquerol L, Meysen S, Mangoni M, Bois P, van Rijen HV, Abran P, Jongsma H, Nargeot J, and Gros D. Architectural and functional asymmetry of the His-Purkinje system of the murine heart. *Cardiovasc Res* 63: 77-86, 2004.

Mommersteeg MT, Hoogaars WM, Prall OW, de Gier-de Vries C, Wiese C, Clout DE, Papaioannou VE, Brown NA, Harvey RP, Moorman AF, and Christoffels VM. Molecular pathway for the localized formation of the sinoatrial node. *Circ Res* 100: 354-362, 2007.

Moosmang S, Stieber J, Zong X, Biel M, Hofmann F, and Ludwig A. Cellular expression and functional characterization of four hyperpolarization-activated pacemaker channels in cardiac and neuronal tissues. *Eur J Biochem* 268: 1646-1652, 2001.

Morley GE, Vaidya D, Samie FH, Lo C, Delmar M, and Jalife J. Characterization of conduction in the ventricles of normal and heterozygous Cx43 knockout mice using optical mapping. *J Cardiovasc Electrophysiol* 10: 1361-1375, 1999.

Musil LS and Goodenough DA. Biochemical analysis of connexin43 intracellular transport, phosphorylation, and assembly into gap junctional plaques. *J Cell Biol* 115: 1357-1374, 1991.

Musil LS and Goodenough DA. Multisubunit assembly of an integral plasma membrane channel protein, gap junction connexin43, occurs after exit from the ER. *Cell* 74: 1065-1077, 1993.

O'Quinn MP, Palatinus JA, Harris BS, Hewett KW, and Gourdie RG. A peptide mimetic of the connexin43 carboxyl terminus reduces gap junction remodeling and induced arrhythmia following ventricular injury. *Circ Res* 108: 704-715.

Park DS and Fishman GI. The cardiac conduction system. *Circulation* 123: 904-915.

Peters NS, Coromilas J, Severs NJ, and Wit AL. Disturbed connexin43 gap junction distribution correlates with the location of reentrant circuits in the epicardial border zone of healing canine infarcts that cause ventricular tachycardia. *Circulation* 95: 988-996, 1997.

Peters NS, Green CR, Poole-Wilson PA, and Severs NJ. Reduced content of connexin43 gap junctions in ventricular myocardium from hypertrophied and ischemic human hearts. Circulation 88: 864-875, 1993.

Pizard A, Burgon PG, Paul DL, Bruneau BG, Seidman CE, and Seidman JG. Connexin 40, a target of transcription factor Tbx5, patterns wrist, digits, and sternum. *Mol Cell Biol* 25: 5073-5083, 2005.

Pogwizd SM and Bers DM. Cellular basis of triggered arrhythmias in heart failure. Trends Cardiovasc Med 14: 61-66, 2004.

Polontchouk L, Haefliger JA, Ebelt B, Schaefer T, Stuhlmann D, Mehlhorn U, Kuhn-Regnier F, De Vivie ER, and Dhein S. Effects of chronic atrial fibrillation on gap junction distribution in human and rat atria. *J Am Coll Cardiol* 38: 883-891, 2001.

Reckova M, Rosengarten C, deAlmeida A, Stanley CP, Wessels A, Gourdie RG, Thompson RP, and Sedmera D. Hemodynamics is a key epigenetic factor in development of the cardiac conduction system. *Circ Res* 93: 77-85, 2003.

Rentschler S, Vaidya DM, Tamaddon H, Degenhardt K, Sassoon D, Morley GE, Jalife J, and Fishman GI. Visualization and functional characterization of the developing murine cardiac conduction system. *Development* 128: 1785-1792, 2001.

Saez JC, Berthoud VM, Branes MC, Martinez AD, and Beyer EC. Plasma membrane channels formed by connexins: their regulation and functions. *Physiol Rev* 83: 1359-1400, 2003.

Saffitz JE, Kanter HL, Green KG, Tolley TK, and Beyer EC. Tissue-specific determinants of anisotropic conduction velocity in canine atrial and ventricular myocardium. *Circ Res* 74: 1065-1070, 1994.

Saffitz JE, Schuessler RB, and Yamada KA. Mechanisms of remodeling of gap junction distributions and the development of anatomic substrates of arrhythmias. *Cardiovasc Res* 42: 309-317, 1999.

Sankova B, Benes J, Jr., Krejci E, Dupays L, Theveniau-Ruissy M, Miquerol L, and Sedmera D. The effect of connexin40 deficiency on ventricular conduction system function during development. *Cardiovasc Res* 95: 469-479.

Sano T and Yamagishi S. Spread Of Excitation From The Sinus Node. *Circ Res* 16: 423-430, 1965.

Sedmera D, Pexieder T, Hu N, and Clark EB. A quantitative study of the ventricular myoarchitecture in the stage 21-29 chick embryo following decreased loading. *Eur J Morphol* 36: 105-119, 1998.

Sedmera D, Wessels A, Trusk TC, Thompson RP, Hewett KW, and Gourdie RG. Changes in activation sequence of embryonic chick atria correlate with developing myocardial architecture. *Am J Physiol Heart Circ Physiol* 291: H1646-1652, 2006.

Sedmera D, Reckova M, Rosengarten C, Torres MI, Gourdie RG, and Thompson RP. Optical mapping of electrical activation in the developing heart. *Microsc Microanal* 11: 209-215, 2005.

Sepp R, Severs NJ, and Gourdie RG. Altered patterns of cardiac intercellular junction distribution in hypertrophic cardiomyopathy. *Heart* 76: 412-417, 1996.

Shah M, Akar FG, and Tomaselli GF. Molecular basis of arrhythmias. *Circulation* 112: 2517-2529, 2005.

Simon AM, Goodenough DA, and Paul DL. Mice lacking connexin40 have cardiac conduction abnormalities characteristic of atrioventricular block and bundle branch block. *Curr Biol* 8: 295-298, 1998.

Sohl G and Willecke K. Gap junctions and the connexin protein family. *Cardiovasc Res* 62: 228-232, 2004.

Tamaddon HS, Vaidya D, Simon AM, Paul DL, Jalife J, and Morley GE. High-resolution optical mapping of the right bundle branch in connexin40 knockout mice reveals slow conduction in the specialized conduction system. *Circ Res* 87: 929-936, 2000.

Tawara S. Das Reizleitungssystem des Säugetierherzen. Eine anatomish-histologishe studie über das Atrioventricularbündel und die Purkinjeschen Fäden. *Jena, Verlag v. Gustav Fischer*, 1906

Takamatsu T. Arrhythmogenic substrates in myocardial infarct. Pathol Int 58: 533-543, 2008.

Unger VM, Kumar NM, Gilula NB, and Yeager M. Three-dimensional structure of a recombinant gap junction membrane channel. *Science* 283: 1176-1180, 1999.

Uzzaman M, Honjo H, Takagishi Y, Emdad L, Magee AI, Severs NJ, and Kodama I. Remodeling of gap junctional coupling in hypertrophied right ventricles of rats with monocrotaline-induced pulmonary hypertension. *Circ Res* 86: 871-878, 2000.

van Kempen MJ, Fromaget C, Gros D, Moorman AF, and Lamers WH. Spatial distribution of connexin43, the major cardiac gap junction protein, in the developing and adult rat heart. *Circ Res* 68: 1638-1651, 1991.

van Rijen HV, Eckardt D, Degen J, Theis M, Ott T, Willecke K, Jongsma HJ, Opthof T, and de Bakker JM. Slow conduction and enhanced anisotropy increase the propensity for ventricular tachyarrhythmias in adult mice with induced deletion of connexin43. *Circulation* 109: 1048-1055, 2004.

van Rijen HV, van Veen TA, van Kempen MJ, Wilms-Schopman FJ, Potse M, Krueger O, Willecke K, Opthof T, Jongsma HJ, and de Bakker JM. Impaired conduction in the bundle branches of mouse hearts lacking the gap junction protein connexin40. *Circulation* 103: 1591-1598, 2001.

Verheijck EE, van Kempen MJ, Veereschild M, Lurvink J, Jongsma HJ, and Bouman LN. Electrophysiological features of the mouse sinoatrial node in relation to connexin distribution. *Cardiovasc Res* 52: 40-50, 2001.

Verheule S, van Batenburg CA, Coenjaerts FE, Kirchhoff S, Willecke K, and Jongsma HJ. Cardiac conduction abnormalities in mice lacking the gap junction protein connexin40. *J Cardiovasc Electrophysiol* 10: 1380-1389, 1999.

Verheule S and Kaese S. Connexin diversity in the heart: insights from transgenic mouse models. Front Pharmacol 4: 81.

von Olshausen K, Schwarz F, Apfelbach J, Rohrig N, Kramer B, and Kubler W. Determinants of the incidence and severity of ventricular arrhythmias in aortic valve disease. *Am J Cardiol* 51: 1103-1109, 1983.

Wessels A, Vermeulen JL, Verbeek FJ, Viragh S, Kalman F, Lamers WH, and Moorman AF. Spatial distribution of "tissue-specific" antigens in the developing human heart and skeletal muscle. III. An immunohistochemical analysis of the distribution of the neural tissue antigen G1N2 in the embryonic heart; implications for the development of the atrioventricular conduction system. *Anat Rec* 232: 97-111, 1992.

Willecke K, Eiberger J, Degen J, Eckardt D, Romualdi A, Guldenagel M, Deutsch U, and Sohl G. Structural and functional diversity of connexin genes in the mouse and human genome. *Biol Chem* 383: 725-737, 2002.

Winterton SJ, Turner MA, O'Gorman DJ, Flores NA, and Sheridan DJ. Hypertrophy causes delayed conduction in human and guinea pig myocardium: accentuation during ischaemic perfusion. Cardiovasc Res 28: 47-54, 1994.

Witkowski FX, Clark RB, Larsen TS, Melnikov A, and Giles WR. Voltage-sensitive dye recordings of electrophysiological activation in a Langendorff-perfused mouse heart. *Can J Cardiol* 13: 1077-1082, 1997.

Witt AL, and Peters NS. The role of gap junction in the arrhytmias of ischemia and infarction. *Heart Rhythm* 9, 308-311, 2012

9. Seznam publikací autora a jeho podíl na práci

Články přímo související s prací:

1. Myocardial morphological characteristics and proarrhythmic substrate in the rat model of heart failure due to chronic volume overload.; **Benes J Jr**, Melenovsky V, Skaroupkova P, Pospisilova J, Petrak J, Cervenka L, Sedmera D. Anat Rec (Hoboken). **2011** Jan;294(1):102-11.
IF: 1,473
Podíl J.B. na práci: konfokální mikroskopie, analýza takto získaných dat, zpracování dat do podoby článku

2. The effect of connexin40 deficiency on ventricular conduction system function during development. Sankova B, **Benes J Jr,** Krejci E, Dupays L, Theveniau-Ruissy M, Miquerol L, Sedmera D. Cardiovasc Res. **2012** Sep 1;95(4):469-79. Epub 2012 Jun 27.
IF: 6,064
Podíl J.B. na práci: optické mapování a zpracování dat z Cx40 deficitních myší

3. The role of connexin40 in developing atrial conduction
Benes J, Jr., Ammirabile G, Sankova B, Campione M, Krejci E, Kvasilova A, Sedmera D
(in revision)
Podíl J.B. na práci: optické mapování, analýza a zpracování dat do podoby článku

Ostatní publikace autora:

4. Metabolic characterization of volume overload heart failure due to aorto-caval fistula in rats. Melenovsky V, Benes J, Skaroupkova P, Sedmera D, Strnad H, Kolar M, Vlcek C, Petrak J, **Benes J Jr**, Papousek F, Oliyarnyk O, Kazdova L, Cervenka L. Mol Cell Biochem. **2011** Aug;354(1-2):83-96.
IF: 2,057
Podíl J.B. na práci: morfologická analýza modelu srdečního selhání

5. Pitx2 confers left morphological, molecular, and functional identity to the sinus venosus myocardium. Ammirabile G, Tessari A, Pignataro V, Szumska D, Sutera Sardo F, **Benes J Jr,** Balistreri M, Bhattacharya S, Sedmera D, Campione M. Cardiovasc Res. **2012** Feb 1;93(2):291-301. Epub 2011 Nov 23.
IF: 6,064
Podíl J.B. na práci: spolupráce a pomoc s optickým mapováním

10. Publikace autora

Myocardial Morphological Characteristics and Proarrhythmic Substrate in the Rat Model of Heart Failure Due to Chronic Volume Overload

JIRI BENES JR.,[1,2,3]* VOJTECH MELENOVSKY,[4,5] PETRA SKAROUPKOVA,[5,6] JANA POSPISILOVA,[7] JIRI PETRAK,[7] LUDEK CERVENKA,[5,6] AND DAVID SEDMERA[1,2]

[1]Charles University in Prague, First Faculty of Medicine, Institute of Anatomy, U nemocnice 3, 12800 Prague 2, Czech Republic

[2]Institute of Physiology, Department of Cardiovascular Morphogenesis, Academy of Sciences of the Czech Republic, Videnska 1083, 14220 Prague 4, Czech Republic

[3]Department of Radiology of the First Faculty of Medicine and General Teaching Hospital, Charles University in Prague, First Faculty of Medicine, U Nemocnice 2, Prague 2, Czech Republic

[4]Department of Cardiology, Institute of Clinical and Experimental Medicine-IKEM, Videnska 1958/9, 14021 Prague 4, Czech Republic

[5]Center for Cardiovascular Research, Institute of Clinical and Experimental Medicine-IKEM, Videnska 1958/9, 14021 Prague 4, Czech Republic

[6]Center of Experimental Medicine, Institute of Clinical and Experimental Medicine-IKEM, Videnska 1958/9, 14021 Prague 4, Czech Republic

[7]Charles University in Prague, First Faculty of Medicine, Institute of Pathological Physiology, U nemocnice 5, 12800 Prague 2, Czech Republic

ABSTRACT

Chronic volume overload leads to cardiac hypertrophy and later to heart failure (HF), which are both associated with increased risk of cardiac arrhythmias. The goal of this study was to describe changes in myocardial morphology and to characterize arrhythmogenic substrate in rat model of developing HF due to volume overload. An arteriovenous fistula (AVF) was created in male Wistar rats between the inferior vena cava and abdominal aorta using needle technique. Myocardial morphology, tissue fibrosis, and connexin43 distribution, localization and phosphorylation were examined using confocal microscopy and Western blotting in the stage of compensated hypertrophy (11 weeks), and decompensated HF (21 weeks). Heart to body weight (BW) ratio was 89% and 133% higher in AVF rats at 11 and 21 weeks, respectively. At 21 weeks but not 11 weeks, AVF rats had pulmonary congestion (increased lung to BW ratio) indicating presence of decompensated HF. The myocytes in left ventricular midmyocardium were significantly thicker (+8% and +45%) and longer (+88% and +97%). Despite extensive hypertrophy, there was no excessive fibrosis in the AVF ventricles. Distribution and localization of connexin43 were similar between groups, but its phosphorylation was significantly lower in AVF hearts at 21st week, but not 11th week, suggesting that HF,

Grant sponsor: Ministry of Education, Youth and Sports; Grant numbers: VZ 0021620806, 1M0510, 1M0538, LC06044 and 1M6798582302; Grant sponsor: Academy of Sciences of the Czech Republic; Grant number: AV0Z50110509; Grant sponsor: Grant Agency of the Czech Republic; Grant numbers: 304/08/0615 and 305/09/1390; Grant sponsor: Ministry of Health of the Czech Republic; Grant numbers: MZO-00023001 and NS10497-3/2009.

*Correspondence to: Jiri Benes Jr., Institute of Anatomy, U nemocnice 3, 12800, Prague 2, Czech Republic.
E-mail: jiri.benes2@lf1.cuni.cz

Received 15 January 2010; Accepted 9 September 2010
DOI 10.1002/ar.21280
Published online 2 November 2010 in Wiley Online Library (wileyonlinelibrary.com).

rather than hypertrophy contributes to the connexin43 hypophosphorylation. In conclusion, volume overload leads to extensive eccentric hypertrophy, but not to myocardial fibrosis. Increased vulnerability to arrhythmia in this HF model is possibly related to gap junction remodeling with hypophosphorylation of connexin43. Anat Rec, 294:102–111, 2011. © 2010 Wiley-Liss, Inc.

Key words: cardiac hypertrophy; heart failure; connexin43; rat

The increase in volume loading of the heart due to valve insufficiency or arteriovenous fistula (AVF) causes dilation of cardiac chambers and cardiac hypertrophy (Ford, 1976). It is believed that this process is due to cardiomyocyte elongation and hypertrophy that compensate volume overload and normalize wall stress (Grossman et al., 1975). Despite cardiac output being often increased (such as in the case of chronic arteriovenous fistula–AVF), substantial part of stroke volume is shunted or recirculated and is not contributing to systemic perfusion. Diminished systemic perfusion leads to redistribution of cardiac output and neurohumoral activation. When compensatory mechanisms become inadequate, overt heart failure (HF) develops (Hood et al., 1968) in a way similar to other models of LV hypertrophy-HF transition (Hatt et al., 1979; Legault et al., 1990; Ruzicka et al., 1993; Ryan et al., 2007).

Regardless its etiology, cardiac hypertrophy is associated with increased incidence of potentially life-threatening ventricular arrhythmias (Artham et al., 2009) and is one of the strongest risk factors for sudden cardiac death (Haider et al., 1998). The mechanisms of arrhythmias in eccentric hypertrophy due to volume overload are known less than in cardiac hypertrophy due to pressure overload or chronic myocardial infarction. Arrhythmogenesis is often linked to increased electrical heterogeneity of myocardial tissue and slowed impulse conduction (Shah et al., 2005). The involved mechanisms consist of myocardial fibrosis, changes in cell and tissue architecture, membrane excitability, and alterations of gap-junctional coupling (Libby et al., 2008). Gap junctions are required for electrical impulse propagation and synchronous contraction in the healthy heart and their alterations might contribute to abnormal conduction and thus be a substrate for arrhythmia (von Olshausen et al., 1983; Kligfield et al., 1987; Kostin et al., 2003; Wiegerinck et al., 2008). The main protein forming gap junctions in rat ventricular myocardium is connexin43 (Sohl and Willecke, 2004). Changes in amount and in localization of connexin43 have been reported in the diseased myocardium (Severs et al., 2004). Some of the previous studies demonstrated a reduction in connexin43 levels in left ventricles of transplant patients with end-stage HF (Dupont et al., 2001). Lateralization of connexin43 from intercalated discs to lateral membrane of myocytes occurs in experimentally induced hypertrophy of right and left ventricle of the rat (Uzzaman et al., 2000; Emdad et al., 2001). Apart from alterations in connexin43 levels, the dephosphorylation of connexin43 was described during several pathological states, including myocardial ischemia (Beardslee et al., 2000; Burstein et al., 2009). Taking all this into an account, new antiarrhythmic drugs targeting function of gap junctions are developed, with rotigaptide, a selective gap junction modifier, as an example (Haugan et al., 2006).

In our study, HF in rats was induced by AVF. Similar volume overload HF models were created also by other groups in dogs (Legault et al., 1990) and rats (Hatt et al., 1979; Ruzicka et al., 1993; Ryan et al., 2007). However, no previous study characterized cardiac morphology at two distinct phases of HF development. The main purpose of this study was thus to provide morphological characteristics of the AVF experimental rat HF model induced by volume overload with a focus on abnormalities in myocardial tissue potentially contributing to arrhythmogenesis, such as fibrosis and connexin43 distribution.

MATERIAL AND METHODS

Animals

The rats were kept in air-conditioned animal facility on a 12-hr/12-hr light/dark cycle. Throughout the experiments the rats were fed a normal salt, normal protein diet (0.45% NaCl, 19−21% protein) produced by SEMED (Prague, Czech Republic) and had free access to tap water. The rats were weighted weekly. Studies were made according to Animal Protection Law of the Czech Republic (311/1997) and were approved by the Ethic Committee of the Institute of Clinical and Experimental Medicine (Prague, Czech Republic).

Male Wistar rats weighting 300−350 g were used for this study and the changes were evaluated in two intervals following the experimental procedure, after 11 and 21 weeks. Some of the animals died after the surgery, this early mortality ($\leq$7 days) occurred mostly within the first 48 hr and was about 13%. Another 5% of animals with AVF died prior to the end of experiment. All animals that died during the course of experiment were excluded from the study. Some of the animals showed milder signs of incipient HF (lethargy, difficult breathing, cyanosis, piloerection), 65% after 11 weeks and 80% after 21 weeks of volume overload. During hemodynamic measurements of LV intraventricular pressure with 2F Millar catheter (data not shown), we observed in ACF rats frequent nonsustained polytopic ventricular ectopy. Approximately in 10% of ACF rats, these manipulations led to sustained ventricular tachycardia degenerating into ventricular fibrillation (VF). In contrast, no complex ectopy or VF was observed in control rats. For quantitative analysis we used seven AVF rats that were sacrificed 11 weeks after the surgery (plus six sham-operated controls at this time point) and seven AVF rats sacrificed

TABLE 1. Changes in weight of internal organs of AVF and Sham-operated rats

Changes at the organ level								
	11 weeks				21 weeks			
Weight (g)	AVF (n = 7)	Sham (n = 6)	Difference	Statistics (t = test)	AVF (n = 7)	Sham (n = 8)	Difference	Statistic s (t-test)
Body	482 ± 33	465 ± 17	+ 3.5%	$P = 0.289$	500 ± 43	487 ± 42	+ 2.6%	P= 0 .597
Heart	2.52 ± 0.32	1.29 ± 0.09	+ 95.7%	$\mathbf{P = 1 \times 10^{-6}}$	2.52 ± 0.34	1.05 ± 0.08	+ 140%	$\mathbf{P = 6 \times 10^{-7}}$
Ventricles	2.05 ± 0.29	1.04 ± 0.08	+ 96.2%	$\mathbf{P = 6 \times 10^{-6}}$	2.02 ± 0.27	0.91 ± 0.06	+ 123%	$\mathbf{P = 7 \times 10^{-7}}$
Atria	0.47 ± 0.10	0.24 ± 0.05	+ 94%	$\mathbf{P = 3 \times 10^{-6}}$	0.49 ± 0.14	0.14 ± 0.02	+ 246%	$\mathbf{P = 1 \times 10^{-4}}$
Lungs	2.07 ± 0.32	1.64 ± 0.19	+ 26.2%	$\mathbf{P = 0.014}$	2.7 ± 0.56	1.68 ± 0.27	+ 61.3%	$\mathbf{P = 0.002}$
Liver	15.30 ± 2.80	15.02 ± 1.67	+ 1.8%	$P = 0.838$	15.88 ± 2.65	14.25 ± 1.10	+ 11.4%	$P = 0.189$
Kidneys	1.34 ± 0.12	1.44 ± 0.11	−7.1%	$P = 0.226$	1.24 ± 0.10	1.27 ± 0.10	−2.25%	$P = 0.481$
HBWR	5.23 ± 0.54	2.77 ± 0.17	+ 88.9%	$\mathbf{P = 4 \times 10^{-7}}$	5.02 ± 0.51	2.16 ± 0.11	+ 133%	$\mathbf{P = 4 \times 10^{-8}}$

HBWR, heart to body weight ratio.
Data are presented as mean ± SD.

21 weeks after the surgery (plus eight sham-operated controls).

Aortocaval Shunt

Aortocaval fistula was created by the method described by Garcia and Diebold (1990). On the day of surgery, anesthesia was induced by intraperitoneal application of ketamine and midazolam. The abdomen was opened through a midline section, intestines moved upwards and the aorta and inferior vena cava were exposed in the retroperitoneum. Using 1.2 mm needle (Becton-Dickinson), the abdominal aorta was pierced into inferior vena cava between renal artery and bifurcation. The needle was removed after clamping the aorta above and applying acrylamide tissue glue to the puncture site. After 3 min, the clamp was removed and the functionality of the shunt was verified by pulsation of the inferior vena cava. Sham-operated rats underwent the same procedure without needle puncture.

Since the fistula have spontaneously closed in some operated animals, only rats with visually-verified fistula patency at the termination and heart to body weight (BW) ratio over 4 g/kg were used for quantitative morphological evaluation.

Morphological Examination

At 11 and 21 weeks after AVF procedure, rats were anesthetized with intraperitoneal phenobarbital application, sacrificed by exsanguination and their organs were weighted. Beating heart was excised and the coronary tree was immediately orthogradely perfused with 10 mL ice-cold St. Thomas cardioplegia solution. The hearts were fixed in 4% paraformaldehyde in phosphate buffer saline (PBS) and ran through ascending series of saccharose prior to embedding into Tissue-Tek. The blocks were cut on cryomicrotome at 12 μm thickness.

Guide series were stained by hematoxylin-eosin with alcian blue using usual techniques. Sister sections were stained by the following primary antibodies: cardiac α-actinin (monoclonal mouse antibody, Sigma, Clone EA-53, #A7811, 1:500), connexin43 (polyclonal rabbit antibody, Sigma, #C6219, 1:200), and phosphoconnexin43 (polyclonal rabbit antibody, Cell Signaling Technology, #3511, 1:100).

The staining was performed in dark humid chamber. On Day 1, the sections were blocked in normal goat serum (1:20) and in 1% bovine serum albumin in (PBS) for 20 min. Primary antibody was then applied overnight. On Day 2, the sections were washed in three changes of PBS, and species-appropriate secondary antibody conjugated with Rhodamine Red (Jackson Immuno Research) was applied for 4 hr in the dark. After washing in PBS again was applied solution of wheat germ agglutinin (WGA) conjugated with Alexa 488 (1:50, Invitrogen, #W11261) followed by three washes in PBS. WGA is a lectin, which binds to basal membranes and extracellular matrix and thus can be indirectly used also for detection of fibrosis. Finally, the nuclei were counterstained with Hoechst 33258 (1:100,000 diluted in 0.1% Triton-X in distilled water, Sigma-Aldrich, #86140-5). In the end, the sections were washed with distilled water and dehydrated in ascending series of ethanol (70%−100%), cleared in xylene, and mounted in Depex medium.

Western Blotting

Left ventricle samples from AVF and sham-operated animals (pools of six hearts per group) were pulverized under liquid nitrogen and extracted in NHT buffer (140 mM NaCl, 10 mM HEPES, 1.5% Triton X-100, pH 7.4) containing Phosphatase Inhibitor Cocktail 1 (Sigma-Aldrich, Czech Republic). Samples (40 μg) were combined with SDS loading buffer containing DTT, boiled for 5 min and resolved by SDS-PAGE on precast 4%−15% gradient minigels (Bio-Rad, CA) in Tris-Glycine buffer. Electrophoresis was performed in quadruplicate at constant voltage for 30 min at 45 V per gel, and then at 90 V per gel until the dye front reached the gel bottom. Proteins were then transferred to 0.45 μm PVDF membranes (Millipore, MA) in semi-dry blotter (Hoeffer, Canada) at 0.8 mA/cm^2 of membrane for 80 min. Membranes were incubated with blocking buffer containing PBS and 0.1% TWEEN 20 for 2 hr. As primary antibodies, rabbit anti-connexin (1:6,000, Sigma-Aldrich) and anti-phospho-connexin (1:1,000, Cell Signaling Technology) antibodies were used. After thorough washing in blocking buffer, secondary horseradish peroxidase-conjugated goat anti-rabbit antibody (1:16,000, Sigma-Aldrich) was applied for 1 hr. After washing, signal was detected using Western Blotting Luminol Reagent (Santa Cruz

Biotechnology, CA) and membranes were exposed to X-ray films (Kodak, Czech Republic). Membranes were scanned on GS-800 calibrated densitometer (Bio-RAD) and the signal was quantified by the Quantity One software (Bio-Rad).

Quantitative Evaluation and Statistical Analysis

The quantitative analysis is based upon numbers of animals indicated in Tables 1 and 2. In total, 14 AVF and 14 sham hearts were analyzed.

Image acquisition was performed on Leica SPE confocal microscope (immunofluorescence) and Olympus BX51 microscope with DP70 CCD camera (transmitted light). Six optical sections per each sample spaced by one micron were projected using maximum intensity algorithm. The images were analyzed using standard imaging software (Adobe Photoshop, ImageJ).

Myocyte width in midmyocardium and subendocardium was evaluated on sections stained with anti α-actinin antibody and WGA. Cell length and differences in connexin43 levels and distribution was evaluated on anti-connexin43 staining with WGA. For evaluation of phosphorylated connexin43 changes, we used specific phosphorylated connexin43 antibody. Fibrosis was evaluated using WGA staining and confirmed by Picrosirius Red staining examined in polarized light.

The cell width and length in midmyocardium was measured by averaging 10 cell transverse diameters from each confocal image. Cell width in papillary muscle was calculated from cross sectional areas of myocytes, assuming circular geometry, using also 10 cells from each image. To avoid underestimation, only cells in which nucleus was present were measured.

The distribution and localization of connexin43 and phosphorylated connexin43 was measured by comparing red channel (representing connexin43 or phosphorylated connexin43) and green channel (representing myocyte cytoplasmic autofluorescence) of confocal images using threshold and area measurements in ImageJ. The same procedure was used for evaluation of fibrosis on WGA pictures.

All data are presented as a mean ± SD. Differences between groups were statistically analyzed by unpaired Student's two-tailed t-test. Differences were considered statistically significant at a value of $P < 0.05$.

RESULTS

Organ Changes After AVF

We measured BW, weight of the whole heart, ventricles, and atria separately as well as weight of some other organs (lungs, liver, kidneys) on both sampling intervals. Changes in the whole animal BW were not significant (Table 1). The heart weight was considerably increased (by 96% after 11 weeks and by 140% after 21 weeks of volume overload). The contribution of individual chambers to total heart weight increase was also evaluated. In addition to heart weight increase, the changes can be better expressed by heart to BW ratio. This ratio was significantly increased at both stages, clearly demonstrating cardiac hypertrophy.

Concerning the other organs, the lungs were significantly heavier (by 26% after 11 weeks and by 61% after

TABLE 2. Quantification of cellular changes in the heart of AVF rats with heart failure

Changes in the heart	After 11 weeks				After 21 weeks			
	AVF (n = 7)	Sham (n = 6)	Difference	Statistics files *t*-test)	AVF (n = 7)	Sham (n = 8)	Difference	Statistics (*t*-test)
Wall thickness (mm)								
Left ventricle	29.99 ± 5.87	22.56 ± 3.00	+ 33%	$\boldsymbol{P = 0.020}$	46.02 ± 5.61	25.05 ± 1.53	+ 83.7%	$\boldsymbol{P = 3 \times 10^{-6}}$
Right ventricle	15.51 ± 1.76	9.81 ± 1.30	+ 58.1%	$\boldsymbol{P = 3 \times 10^{-4}}$	30.05 ± 4.44	12.23 ± 1.96	+ 146%	$\boldsymbol{P = 3 \times 10^{-6}}$
Myocyte size (Mm)								
Width in LV midmyocardium	11.03 ± 0.77	10.18 ± 0.82	+ 8.3%	$P = 0.083$	14.20 ± 2.62	9.78 ± 1.02	+ 45.1%	$\boldsymbol{P = 0.003}$
Width in LV papillary muscle	29.65 ± 4.57	24.96 ± 2.42	+ 18.8%	$P = 0.064$	28.87 ± 4.41	26.15 ± 3.52	+ 22.5%	$P = 0.249$
Length in LV midmyocardium	117.43 ± 8.07	62.26 ± 6.78	+ 88.6%	$\boldsymbol{P = 2 \times 10^{-7}}$	115.83 ± 14.97	58.77 ± 1.84	+ 97.0%	$\boldsymbol{P = 0.013}$
Width in RV midmyocardium	14.39 ± 0.86	10.14 ± 0.25	+ 42.0%	$\boldsymbol{P = 0.001}$	13.94 ± 1.71	10.43 ± 0.80	+ 33.6%	$\boldsymbol{P = 0.001}$
Length in RV midmyocardium	114.73 ± 6.92	85.73 ± 3.01	+ 33.8%	$\boldsymbol{P = 7 \times 10^{-5}}$	116.41 ± 5.26	89.65 ± 4.51	+ 29.8%	$\boldsymbol{P = 2 \times 10^{-4}}$

Data are presented as mean ± SD.

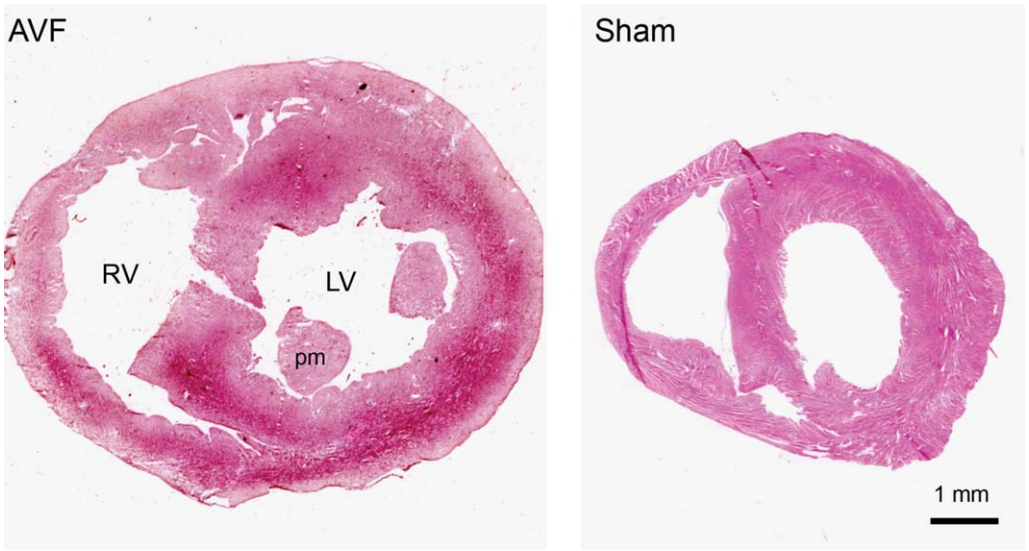

Fig. 1. Hematoxylin-eosin staining of frozen sections of AVF and sham-operated rat hearts. Note gross increase in heart size. LV, left ventricle, pm, papillary muscle, RV, right ventricle.

21 weeks of volume overload) which corresponds to development of HF and to congestion in the pulmonary circulation. Weight of liver and kidneys was not significantly changed.

Ventricular fibrosis was also evaluated from WGA confocal images and no significant changes were found. The ratio of green channel area (WGA staining, thus showing membranes and fibrotic tissues around myocytes) to area of all tissues on the section in AVF was 25.98% ± 6.27; and in controls 28.62% ± 3.87 ($P = 0.39$). This data was obtained from the hearts with decompensated HF (21 weeks after surgery), and confirmed by Picrosirius Red staining that showed likewise no differences between AVF and sham ventricles (data not shown).

Cellular Changes in the Ventricles

For understanding of morphological changes in the heart, we measured free wall thickness of the left and right ventricle (Fig. 1) and myocyte dimensions in the left ventricular myocardium (Table 2).

Both ventricles showed hypertrophy (Fig. 2) and its extent increased with time of volume overload, which can be clearly seen by the dynamics of wall thickness increase in both ventricles (Table 2). Right ventricle was more affected by volume overload from aortocaval shunt than the left ventricle (after 21 weeks of volume overload the left ventricle wall thickness increased by 84% vs. 146% for the right ventricle).

The thickness and the length of myocytes were measured on confocal images in midmyocardial layer of both ventricles and in the papillary muscle of the left ventricle. The hypertrophy in the midmyocardial layer was more extensive than in the subendocardium. The cells in the papillary muscles also underwent hypertrophy (Fig. 2) but the increase was smaller (by 19% after 11 weeks and by 23% after 21 weeks of volume overload, P = NS). The cell thickness in midmyocardial layer increased significantly (by 8% and 45%, respectively) in both ventricles with developing ventricular hypertrophy. Cell length in midmyocardium increased in both stages by 90% in the left ventricle and by 30% in the right ventricle, which indicates dilation of the ventricles (Table 2).

Connexin43 Expression

Using immunofluorescence staining and confocal microscopy imaging, we have qualitatively assessed total amount of connexin43 in myocytes, evaluated the distribution of connexin within the cells as well as the differences in phosphorylated isoform of connexin43. The measurements were performed in left ventricular myocardium 21 weeks after aortocaval fistula creation.

We found no notable difference in total amount of connexin43 per cell (Fig. 3). A small decrease could be seen in connexin43 levels during volume overload. The localization of connexin43 in the cell is an important determinant of possible arrhythmogenesis. We measured percentage of connexin43 in intercalated discs from the total amount of connexin43 in the cell (which can be localized also on the sides of cells and in the cytoplasm). We found no significant difference between AVF and sham-operated rats. AVF rats had 33.7% of connexin43 florescence situated in intercalated discs, sham-operated rats had 35.5% of connexin43 in the discs ($P = 0.8$).

Phosphorylation of connexin43 is important for functionality of this protein in gap junctions. We thus evaluated the amount of phosphorylated connexin43 in left ventricular myocardium on both stages and found that there was no apparent decrease in phosphorylated isoform of connexin43 in AVF group in the stage of compensated cardiac hypertrophy (11 weeks after creating the fistula). At the stage of decompensated HF (21 weeks after creating the fistula), however, the decrease in expression of the phosphorylated isoform was notable (Fig. 3).

The amount of total and phosphorylated connexin43 were quantified by western blotting on pools of 6 AVF

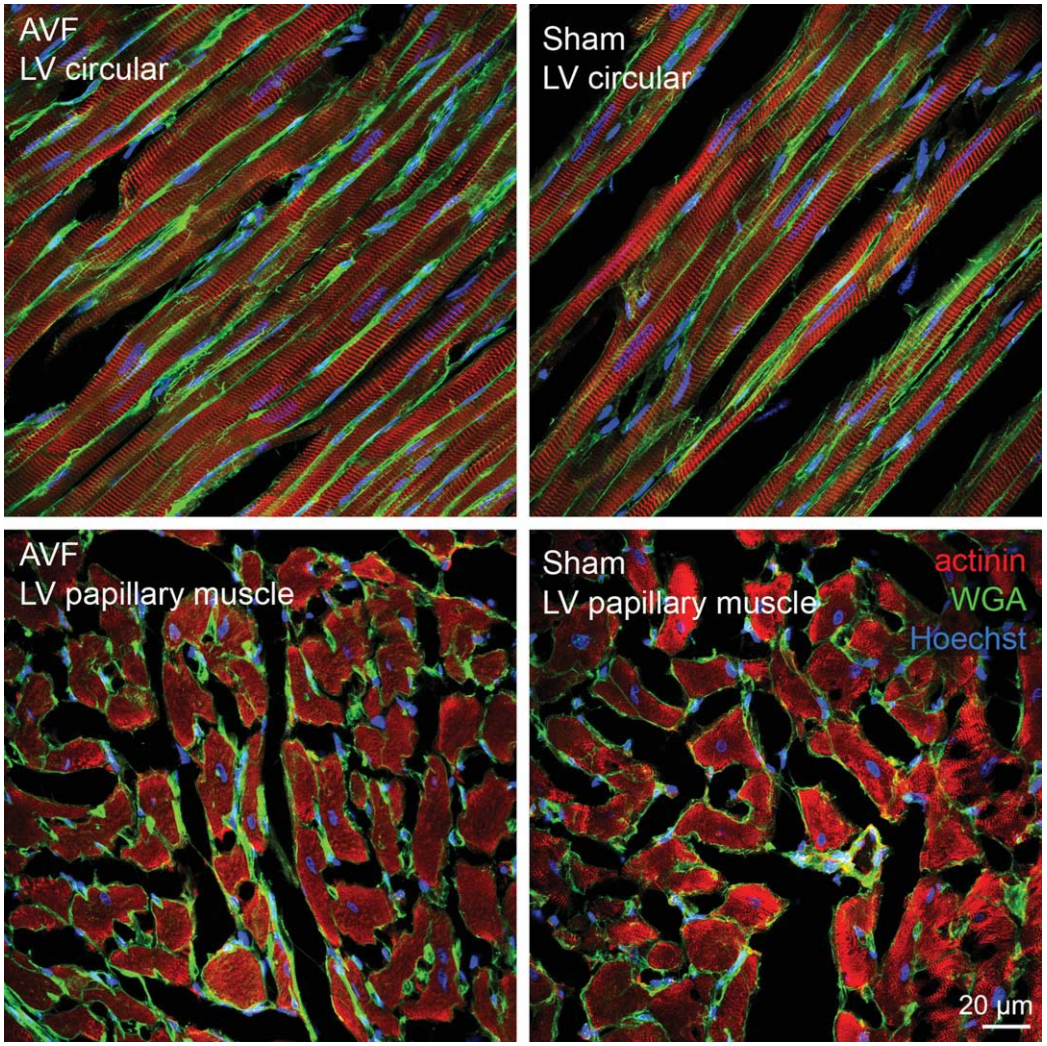

Fig. 2. Confocal micrographs of left ventricular midmyocardium (upper panels) and cross sections through papillary muscles of left ventricle (lower panels). Note increase in transverse myocyte diameter in the AVF hearts. For values of myocyte width please see Table 2. There is no increase in fibrosis (WGA, green staining).

and 6 sham samples at 21 weeks. There was over 60% decrease in both isoforms (Fig. 4).

DISCUSSION

Aortocaval fistula results in volume overload, which induces cardiac dilation and hypertrophy. Over time, this leads to HF and increased mortality. In our study, rats at 21 weeks demonstrated not only hypertrophy, but also decompensated HF phenotype with increased normalized weight of lungs and HF symptoms. In the failing rats, there was an increased heart weight, heart to BW ratio, and thickness of ventricular walls. The hypertrophy was present already after 11 weeks and the heart weight did not change with the time of volume overload, which shows that hypertrophy as a compensatory mechanism evolving early after creation of AVF. However, this compensated state became decompensated over time, resulting in development of congestive HF, as was demonstrated by increasing lung weight. The dynamic nature of changes during development of HF was best exemplified by increased heart to BW ratio, which was increased by almost 90% at 11 weeks but by more than 130% at 21 weeks in comparison with aged-matched sham controls (Table 1). Since the total weight of the animals did not change significantly, other organs have to shrink; this indicates increased catabolic state characteristic of HF and documented in a separate functional and metabolic study (Benes et al., submitted) by decreased fat reserves. At present, we are evaluating chronic changes in animals that have been in HF for 1 year to extend the longitudinal aspect of this study and to see the combined effects of HF and ageing. Cardiac dilation and hypertrophy were confirmed by increased size of cardiomyocytes, which were enlarged in both longitudinal and transverse diameters. Cardiomyocytes in

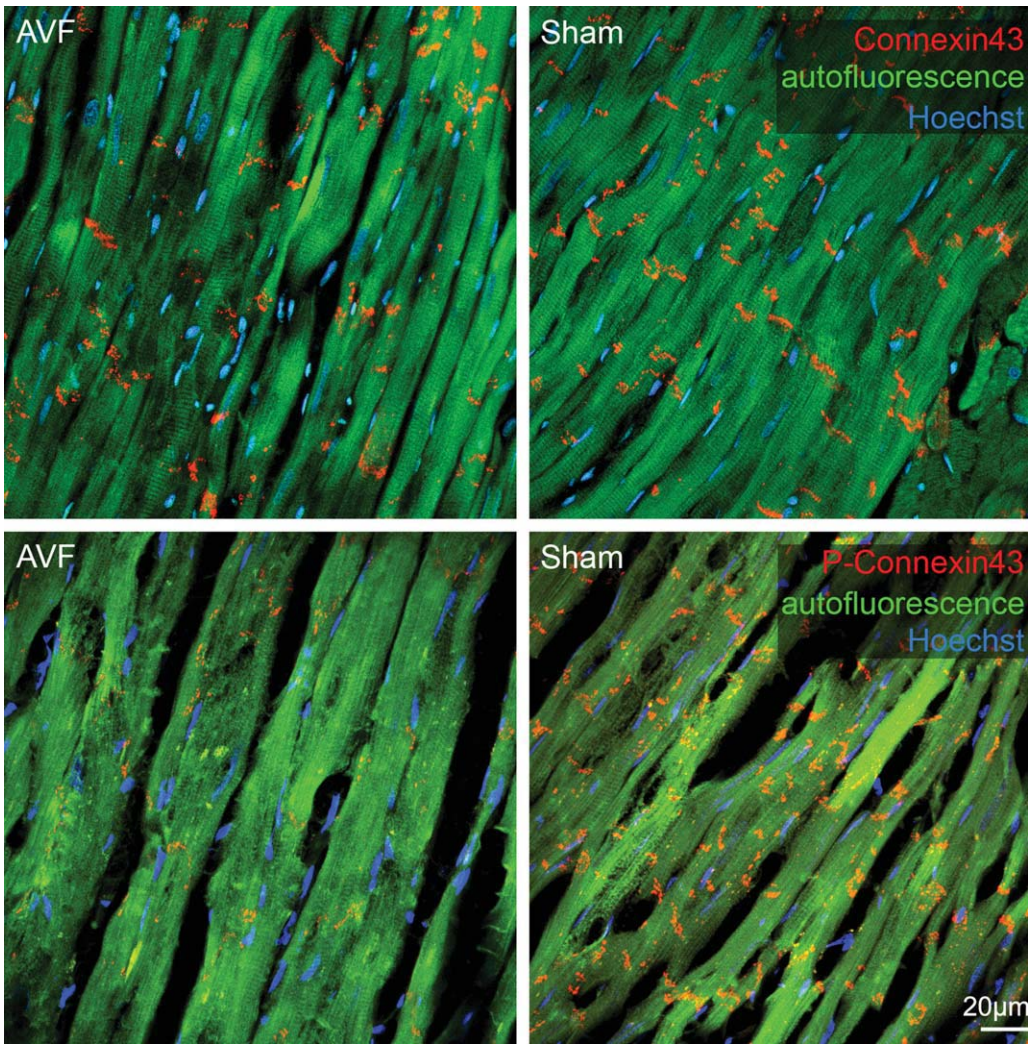

Fig. 3. Distribution and phosphorylation of connexin43 in left ventricular myocardium. Upper panels show confocal images of connexin43 distribution. Lower panels show confocal images of phosphoconnexin43 localization in left ventricular myocardium.

midmyocardium were more affected than those in papillary muscles. This is in contrast with asymmetric cellular hypertrophy in pressure overload model (Campbell et al., 1989), where most pronounced hypertrophy was found in the subendocardial layers. The interesting discrepancy between continued increase in ventricular wall thickness that could not be explained by increased myocyte dimensions, especially in the right ventricle (Table 2) suggests, in the notable absence of fibrosis, that there could be activation of myocyte (or resident stem cells) proliferation, that was recognized previously in decompensated HF in humans (Kajstura et al., 1998).

AVF model of volume overload induced HF had been described before. However, no previous study described these changes in decompensated HF stage. The principal new findings of our study include distinction between compensated (11 weeks) and decompensated (21 weeks) stage of HF, complete morphological evaluation of possible arrhythmogenic substrates (cell size and shape, connexin expression and distribution, fibrosis) and providing links between these findings and ventricular arrhythmias (Fig. 5). Our data thus provide solid morphological grounds for ongoing functional, metabolic and pharmacological studies in this model. Ruzicka et al. used this model for describing renin-angiotensin system and effects of angiotensin converting enzyme inhibitors in situation of volume overload (Ruzicka et al., 1993). Ryan et al. described remodeling process induced by bradykinin (Ryan et al., 2007). Study of Hatt et al. (1979) is closest to our morphological approach. Hatt et al. measured cells in failing hearts and our study generally corresponds with their findings. Their sampling intervals were 1 and 6 months, so it is not possible to compare exactly our findings with theirs. In their study, the hearts of rats with volume overload increased their weight by 81% after 6 month (compare to our increase by 140% after 21 weeks). They also measured cell width in midwall and in subendocardium and described greater increase in cell width in subendocardium than in midwall, which is in contrast to our data. Generally, the

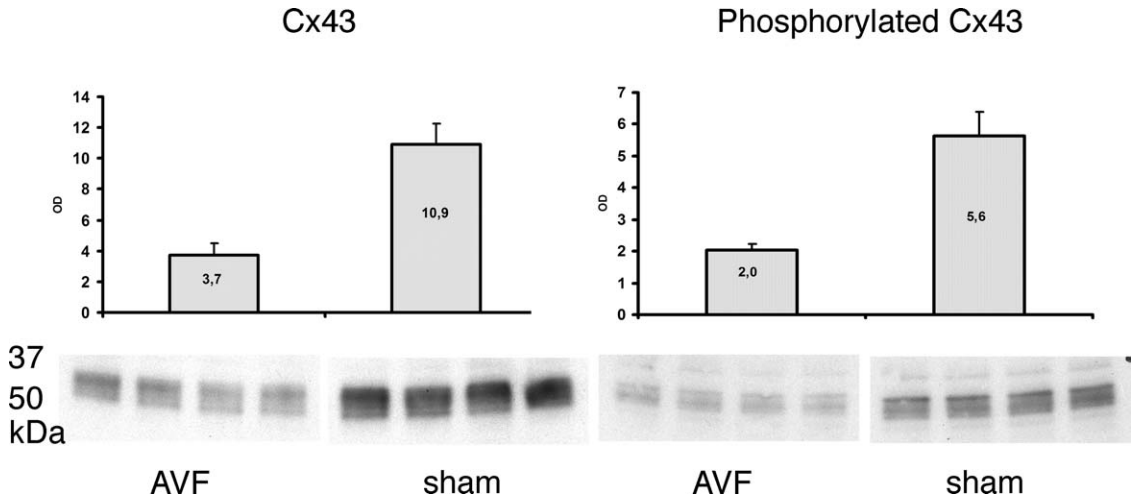

Fig. 4. Western blot on a pool of 6 + 6 samples performed in quadruplicate shows over 60% decrease in both total and phosphorylated connexin43 in the AVF hearts 21 weeks after shunt creation. Values are mean ± SD.

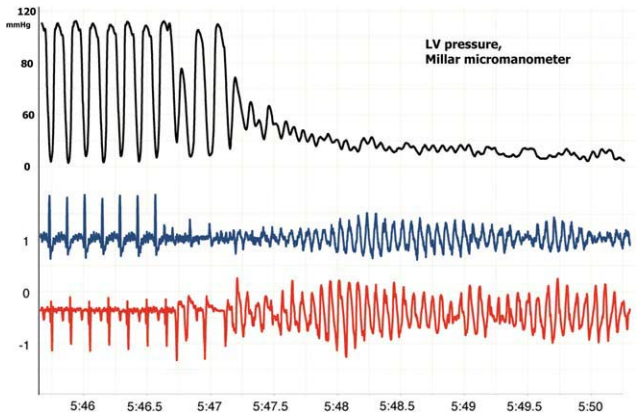

Fig. 5. ECG tracing (2 leads, bottom) and the left ventricular pressure tracing (2F Millar catheter) from a rat with AVF. Several ectopic beats degenerate into fast polymorphic ventricular tachycardia and later to ventricular fibrillation with immediate collapse of the circulation, visible in the pressure channel.

changes they described in the group of rats 6 month after performing the fistula were much milder than our findings. The possible reason for this is that they used female rats and there is known strong gender difference in cardiac response to volume overload—females are far less prone to eccentric remodeling and to the development of HF symptoms (Gardner et al., 2009). Since the methodology of fistula creation was not described in detail in that study, it is also possible that their method of fistula creation may have differed (e.g., different diameter of the needle, no exclusion of animals where AVF closed spontaneously). The reason for different findings in subendocardial myocyte width changes can be explained by the fact that we measured width in papillary muscle from transversal sections through the cells while Hatt et al. measured cells in myocardial wall in transversal sections.

Hypertrophic or failing rat or human hearts have bigger predisposition to develop severe ventricular arrhythmias (von Olshausen et al., 1983; Kligfield et al., 1987). Increased risk of sudden, presumably arrhythmic death was found even in asymptomatic subjects with left ventricular volume overload due to mitral regurgitation (Grigioni et al., 1999). Similarly, we observed increased excitability of hypertrophied AVF hearts, characterized by high frequency of ventricular ectopic beats and bursts of ventricular tachycardia, particularly during intraventricular measurements of pressure using Millar catheter (our unpublished observations). In several AVF animals, this ectopy even degenerated into lethal ventricular fibrillation, which is exceedingly rare in normal rat hearts (Fig. 5). In previous study that examined long-term survival of rats with AVF, 27% of all animals died without preceding HF symptoms (Brower and Janicki 2001), suggesting that arrhythmic sudden cardiac death occurs in substantial proportion of animals with AVF-induced chronic volume overload. Since no excessive collagen accumulation was found in the ventricular myocardium, we suggest that other arrhythmogenic mechanisms than fibrosis might be involved. In our study, we focused on connexin43 changes. Changes in connexin43 can lead to slowing of conduction velocity in ventricular wall, which may create a substrate for re-entry phenomenon (Libby et al., 2008). The main changes described in previous studies were changes in expression, localization, and phosphorylation (Severs et al., 2004). This is not, however, the only possible mechanism. Other contributing factors can be changes in ion channel expression, which can also substantially contribute to arrhythmogenesis (Shah et al., 2005).

In a partial contrast with previous studies of connexin43 changes in HF (Dupont et al., 2001; Emdad et al., 2001; Uzzaman et al., 2000), we found only mild difference in total connexin43 levels by immunohistochemistry (but there was over 60% reduction by Western blot), and the changes in localization were also insignificant. Possible reason for this discrepancy can be differences in HF models or methods used. Dupont et al. described the changes in humans and used Northern blot for quantification, detecting thus mRNA levels

(Dupont et al., 2001). Emdad et al. described HF in rats induced by pressure overload from aortic banding and they used enzymatic separation of myocytes to measure connexin43 levels by immunohistochemistry (Emdad et al., 2001). Recent study of Burstein et al. described changes in dog HF atria and they found also no difference in the amount of connexin43, which corresponds to our immunohistochemistry data (Burstein et al., 2009). Study of Goldfine et al. describes connexin43 changes in volume overload HF model. They found decrease in connexin43 levels in acute state of volume overload HF but when compensatory hypertrophy developed, the amount of connexin43 seemed to normalize (Goldfine et al., 1999). In any case, the absolute levels of connexin43 have to be decreased over 50% to induce significant physiological phenotype per se, as indicated by apparent normality of connexin43 heterozygous mice as well as ventricular arrhythmias leading to sudden cardiac death observed in myocardium-restricted null animals (Gutstein et al., 2001). In this respect, the 60% decreased in total amount of connexin43 found in our Western blot seems biologically sufficiently significant to form (together with changes in cell shape) a proarrhythmogenic substrate, as ventricular arrhythmias were recorded in ~10% of our HF animals.

Phosphorylation of connexin43 can influence conductance, assembly and degradation of gap junctions (Lampe and Lau, 2004; Laird, 2005; Solan and Lampe, 2005). Recent work suggests an important role of connexin43 phosphorylation in HF (Akar et al., 2004; Ai and Pogwizd, 2005). We found greatly decreased phosphorylation of connexin43 in the stage of decompensated HF (21 weeks after operation). The phosphorylation of connexin43 at the earlier stage, when congestive HF was not yet developed (11 weeks after operation), was also slightly decreased but without statistical significance. Thus, our data suggest that the HF and not the hypertrophy itself contribute to the hypophosphorylation. Targeting the phosphorylation status of connexin43 using specific drugs in patients with HF can be a method to prevent development of fatal ventricular arrhythmias.

ACKNOWLEDGMENTS

We would like to express our sincere thanks to Ms. Eva Kluzakova and Ms. Marie Jindrakova for their excellent technical assistance. D. Sedmera is a recipient of the Purkinje Fellowship from the Academy of Sciences of the Czech Republic.

LITERATURE CITED

Ai X, Pogwizd SM. 2005. Connexin 43 downregulation and dephosphorylation in nonischemic heart failure is associated with enhanced colocalized protein phosphatase type 2A. Circ Res 96: 54–63.

Akar FG, Spragg DD, Tunin RS, Kass DA, Tomaselli GF. 2004. Mechanisms underlying conduction slowing and arrhythmogenesis in nonischemic dilated cardiomyopathy. Circ Res 95:717–725.

Artham SM, Lavie CJ, Milani RV, Patel DA, Verma A, Ventura HO. 2009. Clinical impact of left ventricular hypertrophy and implications for regression. Prog Cardiovasc Dis 52:153–167.

Beardslee MA, Lerner DL, Tadros PN, Laing JG, Beyer EC, Yamada KA, Kleber AG, Schuessler RB, Saffitz JE. 2000. Dephosphorylation and intracellular redistribution of ventricular connexin43 during electrical uncoupling induced by ischemia. Circ Res 87:656–662.

Brower GL, Janicki JS. 2001. Contribution of ventricular remodeling to pathogenesis of heart failure in rats. Am J Physiol Heart Circ Physiol 280:H674–H683.

Burstein B, Comtois P, Michael G, Nishida K, Villeneuve L, Yeh YH, Nattel S. 2009. Changes in connexin expression and the atrial fibrillation substrate in congestive heart failure. Circ Res 105:1213–1222.

Campbell SE, Rakusan K, Gerdes AM. 1989. Change in cardiac myocyte size distribution in aortic-constricted neonatal rats. Basic Res Cardiol 84:247–258.

Dupont E, Matsushita T, Kaba RA, Vozzi C, Coppen SR, Khan N, Kaprielian R, Yacoub MH, Severs NJ. 2001. Altered connexin expression in human congestive heart failure. J Mol Cell Cardiol 33:359–371.

Emdad L, Uzzaman M, Takagishi Y, Honjo H, Uchida T, Severs NJ, Kodama I, Murata Y. 2001. Gap junction remodeling in hypertrophied left ventricles of aortic-banded rats: prevention by angiotensin II type 1 receptor blockade. J Mol Cell Cardiol 33:219–231.

Ford LE. 1976. Heart size. Circ Res 39:297–303.

Garcia R, Diebold S. 1990. Simple, rapid, and effective method of producing aortocaval shunts in the rat. Cardiovasc Res 24:430–432.

Gardner JD, Murray DB, Voloshenyuk TG, Brower GL, Bradley JM, Janicki JS. 2010. Estrogen Attenuates Chronic Volume Overload Induced Structural and Functional Remodeling in Male Rat Hearts. Am J Physiol Heart Circ Physiol 298:H497–H504.

Goldfine SM, Walcott B, Brink PR, Magid NM, Borer JS. 1999. Myocardial connexin43 expression in left ventricular hypertrophy resulting from aortic regurgitation. Cardiovasc Pathol 8:1–6.

Grigioni F, Enriquez-Sarano M, Ling LH, Bailey KR, Seward JB, Tajik AJ, Frye RL. 1999. Sudden death in mitral regurgitation due to flail leaflet. J Am Coll Cardiol 34:2078–2085.

Grossman W, Jones D, McLaurin LP. 1975. Wall stress and patterns of hypertrophy in the human left ventricle. J Clin Invest 56:56–64.

Gutstein DE, Morley GE, Tamaddon H, Vaidya D, Schneider MD, Chen J, Chien KR, Stuhlmann H, Fishman GI. 2001. Conduction slowing and sudden arrhythmic death in mice with cardiac-restricted inactivation of connexin43. Circ Res 88:333–339.

Haider AW, Larson MG, Benjamin EJ, Levy D. 1998. Increased left ventricular mass and hypertrophy are associated with increased risk for sudden death. J Am Coll Cardiol 32:1454–1459.

Hatt PY, Rakusan K, Gastineau P, Laplace M. 1979. Morphometry and ultrastructure of heart hypertrophy induced by chronic volume overload (aorto-caval fistula in the rat). J Mol Cell Cardiol 11:989–998.

Haugan K, Miyamoto T, Takeishi Y, Kubota I, Nakayama J, Shimojo H, Hirose M. 2006. Rotigaptide (ZP123) improves atrial conduction slowing in chronic volume overload-induced dilated atria. Basic Clin Pharmacol Toxicol 99:71–79.

Hood WP, Jr., Rackley CE, Rolett EL. 1968. Wall stress in the normal and hypertrophied human left ventricle. Am J Cardiol 22:550–558.

Kajstura J, Leri A, Finato N, Di Loreto C, Beltrami CA, Anversa P. 1998. Myocyte proliferation in end-stage cardiac failure in humans. Proc Natl Acad Sci U S A 95:8801–8805.

Kligfield P, Hochreiter C, Niles N, Devereux RB, Borer JS. 1987. Relation of sudden death in pure mitral regurgitation, with and without mitral valve prolapse, to repetitive ventricular arrhythmias and right and left ventricular ejection fractions. Am J Cardiol 60:397–399.

Kostin S, Rieger M, Dammer S, Hein S, Richter M, Klovekorn WP, Bauer EP, Schaper J. 2003. Gap junction remodeling and altered connexin43 expression in the failing human heart. Mol Cell Biochem 242:135–144.

Laird DW. 2005. Connexin phosphorylation as a regulatory event linked to gap junction internalization and degradation. Biochim Biophys Acta 1711:172–182.

Lampe PD, Lau AF. 2004. The effects of connexin phosphorylation on gap junctional communication. Int J Biochem Cell Biol 36:1171–1186.

Legault F, Rouleau JL, Juneau C, Rose C, Rakusan K. 1990. Functional and morphological characteristics of compensated and decompensated cardiac hypertrophy in dogs with chronic infrarenal aorto-caval fistulas. Circ Res 66:846–859.

Libby P, Bonow RO, Mann DL, Zipes DP, Braunwald E, editors. 2008. Braunwald's Heart Disease, 8th ed. Philadelphia: Elsevier.

Ruzicka M, Yuan B, Harmsen E, Leenen FH. 1993. The renin-angiotensin system and volume overload-induced cardiac hypertrophy in rats. Effects of angiotensin converting enzyme inhibitor versus angiotensin II receptor blocker. Circulation 87:921–930.

Ryan TD, Rothstein EC, Aban I, Tallaj JA, Husain A, Lucchesi PA, Dell'Italia LJ. 2007. Left ventricular eccentric remodeling and matrix loss are mediated by bradykinin and precede cardiomyocyte elongation in rats with volume overload. J Am Coll Cardiol 49:811–821.

Severs NJ, Coppen SR, Dupont E, Yeh HI, Ko YS, Matsushita T. 2004. Gap junction alterations in human cardiac disease. Cardiovasc Res 62:368–377.

Shah M, Akar FG, Tomaselli GF. 2005. Molecular basis of arrhythmias. Circulation 112:2517–2529.

Sohl G, Willecke K. 2004. Gap junctions and the connexin protein family. Cardiovasc Res 62:228–232.

Solan JL, Lampe PD. 2005. Connexin phosphorylation as a regulatory event linked to gap junction channel assembly. Biochim Biophys Acta 1711:154–163.

Uzzaman M, Honjo H, Takagishi Y, Emdad L, Magee AI, Severs NJ, Kodama I. 2000. Remodeling of gap junctional coupling in hypertrophied right ventricles of rats with monocrotaline-induced pulmonary hypertension. Circ Res 86:871–878.

von Olshausen K, Schwarz F, Apfelbach J, Rohrig N, Kramer B, Kubler W. 1983. Determinants of the incidence and severity of ventricular arrhythmias in aortic valve disease. Am J Cardiol 51:1103–1109.

Wiegerinck RF, van Veen TA, Belterman CN, Schumacher CA, Noorman M, de Bakker JM, Coronel R. 2008. Transmural dispersion of refractoriness and conduction velocity is associated with heterogeneously reduced connexin43 in a rabbit model of heart failure. Heart Rhythm 5:1178–1185.

Cardiovascular Research (2012) **95**, 469–479
doi:10.1093/cvr/cvs210

The effect of connexin40 deficiency on ventricular conduction system function during development

Barbora Sankova[1,2†], Jiri Benes Jr[1,2†], Eliska Krejci[1,2], Laurent Dupays[3], Magali Theveniau-Ruissy[4], Lucile Miquerol[4], and David Sedmera[1,2*]

[1]Department of Cardiovascular Morphogenesis, Institute of Physiology, Academy of Sciences of the Czech Republic, Videnska 1083, 14220 Prague, Czech Republic; [2]First Faculty of Medicine, Institute of Anatomy, Charles University in Prague, Prague, Czech Republic; [3]Division of Developmental Biology, MRC National Institute for Medical Research, Mill Hill, London, UK; and [4]Developmental Biology Institute of Marseilles-Luminy (IBDML), CNRS UMR7288 Aix-Marseille Université, Campus de Luminy, Marseille, France

Received 29 November 2011; revised 19 June 2012; accepted 21 June 2012; online publish-ahead-of-print 27 June 2012

Time for primary review: 16 days

Aims The aim of this study was to characterize ventricular activation patterns in normal and connexin40-deficient mice in order to dissect the role of connexin40 in developing the conduction system.

Methods and results We performed optical mapping of epicardial activation between ED9.5–18.5 and analysed ventricular activation patterns and times of left ventricular activation. Mouse embryos deficient for connexin40 were compared with normal and heterozygous littermates. Morphology of the primary interventricular ring (PIR) was delineated with the help of T3-LacZ transgene. Four major types of ventricular activation patterns characterized by primary breakthrough in different parts of the heart were detected during development: PIR, left ventricular apex, right ventricular apex, and dual right and left ventricular apices. Activation through PIR was frequently present at the early stages until ED12.5. From ED14.5, the majority of hearts showed dual left and right apical breakthrough, suggesting functionality of both bundle branches. Connexin40-deficient embryos showed initially a delay in left bundle branch function, but the right bundle branch block, previously described in the adults, was not detected in ED14.5 embryos and appeared only gradually with 80% penetrance at ED18.5.

Conclusion The switch of function from the early PIR conduction pathway to the mature apex to base activation is dependent upon upregulation of connexin40 expression in the ventricular trabeculae. The early function of right bundle branch does not depend on connexin40. Quantitative analysis of normal mouse embryonic ventricular conduction patterns will be useful for interpretation of effects of mutations affecting the function of the cardiac conduction system.

Keywords Mouse embryo • Right bundle branch block • Left bundle branch • Optical mapping

1. Introduction

The mouse is a popular genetic model for human diseases, including those of the cardiovascular system. Some of these involve the normal function of the cardiac conduction system. Despite its morphology being well characterized down to the molecular level, a comprehensive quantitative study of conduction system function is not available.

Extensive studies in the chick embryo[1–4] have shown that the hallmark of ventricular conduction system function is the shift of ventricular activation to a pattern originating from the apex, rather than the base of the heart. Before this shift, the activation pattern utilizes a preferential pathway along forming the interventricular septum known as the primary interventricular ring (PIR).[5] The term 'primary ring' was first used by Wessels *et al.*;[6] the PIR represents only the ventricular part of this structure described in preseptated mouse and human hearts. It connects proximally to the ring-shaped atrioventricular canal, which acts as a delay generator prior to differentiation of the atrioventricular node. During further morphogenesis, rightward expansion of the atrioventricular canal that creates the inflow to the right ventricle results in opening of the PIR, transforming it into a horseshoe-shaped structure.[5] In the chick, the mature activation pattern is already observed during chamber formation, but becomes fully established only after ventricular septation. In contrast, studies in the embryonic mouse[7,8] and rabbit[9] suggested that apex-to-base activation is present from the onset of chamber formation in mammals. Our data from embryonic rats,[10] however, have

† B.S. and J.B. contributed equally to this manuscript.

* Corresponding author. Tel: +420 296 442 561; fax: +420 241 062 488, Email: dsedmera@biomed.cas.cz

shown rather diffuse epicardial breakthrough at early stages as well as a base-to-apex preferential conduction pathway along the forming interventricular septum. Since all the mammalian studies are based on a rather small number of analysed hearts, we felt that a systematic, quantitative overview of mouse embryonic activation patterns was due, and would likely uncover similar variability, as did our earlier chicken studies.

Conduction through the cardiac tissue is determined by the tissue geometry (cell size and shape, intercellular connections, and amount and distribution of connective tissue) as well as by ion channels expression and type together with the polarity of the intercellular junctions. One important determinant of conduction velocity and anisotropy is the expression and the distribution of gap junction (gj) proteins—connexins. Five major connexins (Cx) are expressed in the mouse heart in dynamic spatiotemporal patterns. Cx45 (gja7) is expressed at low levels throughout the myocardium and is enriched in the slow-conducting nodes and the extended cardiac conduction system.[11,12] Its deletion results in early lethality and conduction block. The recently identified Cx30.2 (gjd3) is also characteristic of the slowly conducting areas.[13] Cx30 (gjb6) is specifically expressed in a part of the sinoatrial node, and modulates the intrinsic heart rate.[14] Cx43 (gja1) is the main connexin of the working chamber myocardium, and its deficiency results in slower conduction and a propensity for arrhythmias.[15–17] Cx40 (gja5) is expressed in the mouse embryo in the fast-conducting atrial myocardium and ventricular chamber myocardium; there, it becomes gradually restricted to the entire trabecular network and subsequently to the bundle branches and the Purkinje fibre network.[18–20] Cx40 deficiency causes embryonic and atrial conduction anomalies[21] and slower conduction with right bundle branch block in the ventricular conduction system.[22–25] However, the functional importance of Cx40 in the developing conduction system has not been studied.

The first aim of this study was thus to characterize the major ventricular activation patterns during mouse development and correlate them with cardiac morphogenesis and conduction system formation. The second goal was to assess the effects of a lack of Cx40, considered to be a robust marker of the ventricular conduction system, on conduction system function during development.

2. Methods

2.1 Animals

All the animal experiments were performed in accordance with the Czech law governing animal care and experimentation, and were approved by the institutional committee. The investigation conforms to the European Directive 2010/63/EU of the European Parliament. The Cx40:GFP knock-in mice were described previously.[18] They were maintained in a homozygous state and crossed with the Swiss strain. The breeding pairs set up to obtain the desired embryonic genotypes (wild type, heterozygous, and homozygous) were caged overnight and the noon of the day when plug was discovered was considered embryonic day (ED) 0.5. Time-pregnant females (ED9.5–18.5) were killed by cervical dislocation and the embryos rapidly dissected in cold Tyrodes-HEPES solution (pH 7.4). In total, 397 embryos were analysed, with a minimum of two litters and 10 embryos per genotype per stage.

2.2 Optical mapping

The embryos were first decapitated, and the hearts together with the adjacent posterior thoracic wall were isolated and stained with voltage-sensitive dye di-4-ANEPPS for 5–15 min (depending on the stage) in preparation for optical mapping exactly as described recently.[5] The only difference was the addition of blebbistatin[26,27] into the staining solution for the hearts at ED16.5 and 18.5 to shorten the equilibration period in warm oxygenated Tyrodes during which the hearts became frequently arrhythmic. Analysis of recordings resulting in the generation of spatiotemporal epicardial activation maps was performed using the BV_Analyzer software bundled with the Ultima L camera as described previously.[28,29] In-depth discussion of the limitations of this approach as well as arrhythmias encountered in the embryonic hearts can be found in the Supplementary material online.

2.3 Data analysis and statistics

Ventricular activation patterns were interpreted in conjunction with morphology as discussed previously, and categorized accordingly. The differences in the frequency of the individual patterns[2] were analysed using Person's Chi-square test in Microsoft Excel, and *P*-values below 0.05 were considered significant. The differences in the continuous variable (ventricular activation times) were compared using unpaired two-tailed Student's *t*-test. The data are presented as mean ± SD.

2.4 Morphological evaluation

For the morphogenesis of the mouse ventricular conduction system, we used previously published data by Viragh and Challice,[30–32] Rentschler *et al.*,[7,8] and our own studies.[18,33] The PIR theory is supported by additional studies in humans,[6,34] chicks,[3] and rats;[10] for its visualization in the mouse, we used the T3 transgene and X-gal staining as described.[35] A 22 kb fragment of the Cx40 genomic domain was cloned and sequenced. The cloned region comprised a non-coding region with 4 kb upstream of the first non-coding exon (exon 1) plus the 18 kb intron. This fragment was engineered upstream of the nls-LacZ reporter gene, replacing the coding exon 2, and used to generate a transgenic mouse line. In addition, we analysed the extent of *Cx*40 expression by whole-mount epifluorescence and confocal microscopy.[36] For further morphological analysis, the hearts were fixed in 4% paraformaldehyde for 1 h and processed for standard paraffin histology. Serial sections were alternatively stained with haematoxylin–eosin, anti-alpha smooth muscle actin (Sigma) or anti-beta galactosidase (cappel-MP Biomedicals), and anti-TBX3 (E-20, Santa-Cruz) antibodies using standard procedures.[18] 3D images of whole-mount immunofluorescence were acquired with a two-photon microscope (Zeiss MP7) and images were treated with the Volocity software.

3. Results

3.1 Conduction at early developmental stages

The earliest time point when we were able to obtain reproducible recordings from stable hearts was ED9.5. The younger hearts showed either no spontaneous activity or complete atrioventricular block after staining, and this was not alleviated even if they were stained by the generally less toxic calcium indicator rhod-2. The embryonic heart at ED9.5 had a primitive right ventricle, less developed than the left ventricle, and *Cx*40 was expressed only in the atria, the left ventricular chamber, and the endocardium of the outflow tract (*Figure 1A*). From ED10.5, *Cx*40 expression was observed in the trabeculae of the right ventricle (*Figure 1B* and *C*). *Cx*40 was absent in the PIR tissues; these could be visualized at this stage with the T3-lacZ transgene whose expression marked a ring around the interventricular foramen (*Figure 1D–F*) best visible from the lateral view. At mid-gestation, the T3-lacZ reporter gene is expressed in the

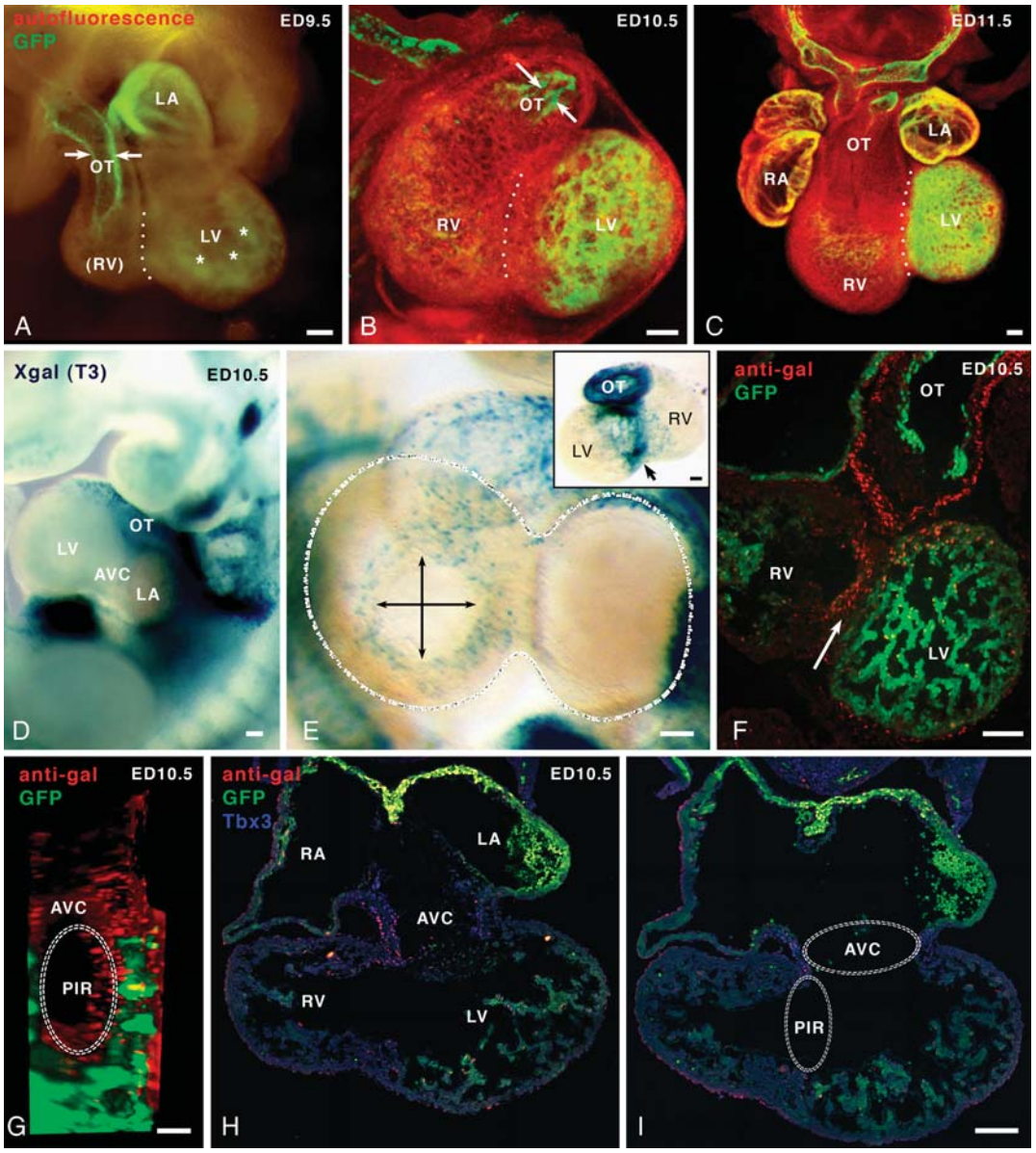

Figure 1 The morphology of the ventricular conduction system in the developing mouse heart. (*A*) *Cx*40 expression visualized by *Cx40:GFP* fluorescence at ED9.5 is found in the atria, the (left) ventricular trabeculae (asterisks), and the outflow tract endocardium (arrows). (*B*) At ED10.5, the expression is more prominent in the left ventricle, although some staining is visible in the right ventricular trabeculae as well as the outflow tract endocardium. (*C*) This pattern is similar at ED11.5, where a rich network of the pectinate muscles could be seen in both atrial appendages. White dots indicate the position of the PIR, devoid of Cx40, corresponding externally to forming interventricular groove. (*A*, *B*, *C*) Tissue autofluorescence in the red channel, in green GFP fluorescence. (*D*) T3-LacZ expression detected in whole-mount staining of an ED10.5 heart in a left lateral view and in a dorso-ventral view of the heart. The transgene is expressed in the branchial arches, the outflow tract, and the dorsal region of the atria. In addition, the transgene detects the primitive ring present as a circle at the ventricular level (*E*, higher magnification, double-sided arrows). Insert shows the same heart-posterior view in transmitted light after isolation from the embryo confirming the heavy staining in the PIR between the left and the right ventricle (arrow) and the outflow tract. (*F*) Nuclear expression of the beta galactosidase (red) is detected by immunohistochemistry on a section of an ED10.5 heart in the PIR tissues (arrow), which are devoid of Cx40 (green, detected by GFP fluorescence), as well as in the outflow tract myocardium. (*G*) Two-photon whole-mount immunoconfocal reconstruction of the PIR at ED10.5 from the lateral view. T3 transgene expression dominant in the endocardium and the epicardium is visualized in red with an antibody against beta-galactosidase, in green channel GFP (Cx40) also detected by immunohistochemistry. For more detail, see Supplementary material online, *Movie S1*. (*H*) A frontal section at ED10.5 of a T3 *Cx40:GFP* heart to illustrate the transgene expression in the atrioventricular canal and the PIR (red); in blue is the Tbx3 immunostaining. (*I*) A more posterior section of the same heart with the outlines of the PIR and the AVC, connecting at the inner curvature. Scale bars 100 μm. AVC, atrioventricular canal; Ao, aorta; LA, left atrium; LV, left ventricle; OT, outflow tract; PIR, primary interventricular ring; Pu, pulmonary trunk; RA, right atrium; RV, right ventricle.

Table 1 The frequency of epicardial activation patterns during development in *Cx40:GFP* heterozygotes

ED	PIR	LAB	RAB	LAB+RAB
9.5	10 (63%)	6 (37%)	0	0
10.5	24 (67%)	12 (33%)	0	0
11.5	7 (37%)	3 (16%)	8 (42%)	1 (5%)
12.5	1 (3%)	4 (13%)	15 (48%)	11 (36%)
13.5	0	2 (6%)	13 (41%)	17 (53%)
14.5	0	7 (28%)	3 (12%)	15 (60%)

The frequency of ventricular activation by the PIR declines between ED9.5 and 12.5, being replaced by the apex to base activation pattern. The presence of both left and right apical breakthrough was the most common pattern at ED14.5. The same frequency of ventricular activation patterns (with minor deviations) was also seen in wild types of several different backgrounds (data not shown).
PIR, primary interventricular ring; RAB, right apical breakthrough; LAB, left apical breakthrough.

myocytes of the atria and the atrio-ventricular conduction system as indicated by the Tbx3 co-staining but not in the ventricular myocardium (GFP-positive; *Figure 1H* and *I*). The three-dimensional image of the PIR (T3-lacZ-positive) demonstrated its connection to the atrioventricular ring and the *Cx*40-positive ventricular trabeculae (*Figure 1G–I*), and this can be best appreciated in the Supplementary material online, *Movie S1*. These results confirm the existence of a specific ring of cardiomyocytes (PIR) joining the atrioventricular conduction system to the conductive ventricular trabeculae.

At early developmental stages (ED9.5–10.5, *Table 1*), we observed two activation patterns using optical mapping: the first one from the primitive (left) ventricular apex, and the other, more frequent, originating from the forming interventricular (bulboventricular) groove (*Figure 2*). The electrical impulse was generated at the site of the forming sinoatrial node and spread bilaterally to both atria. From the atrioventricular canal, the electrical impulse was transmitted to the ventricles along the junction of the atrioventricular canal and the PIR (*Figure 2*). As the PIR is a circular structure, the electrical

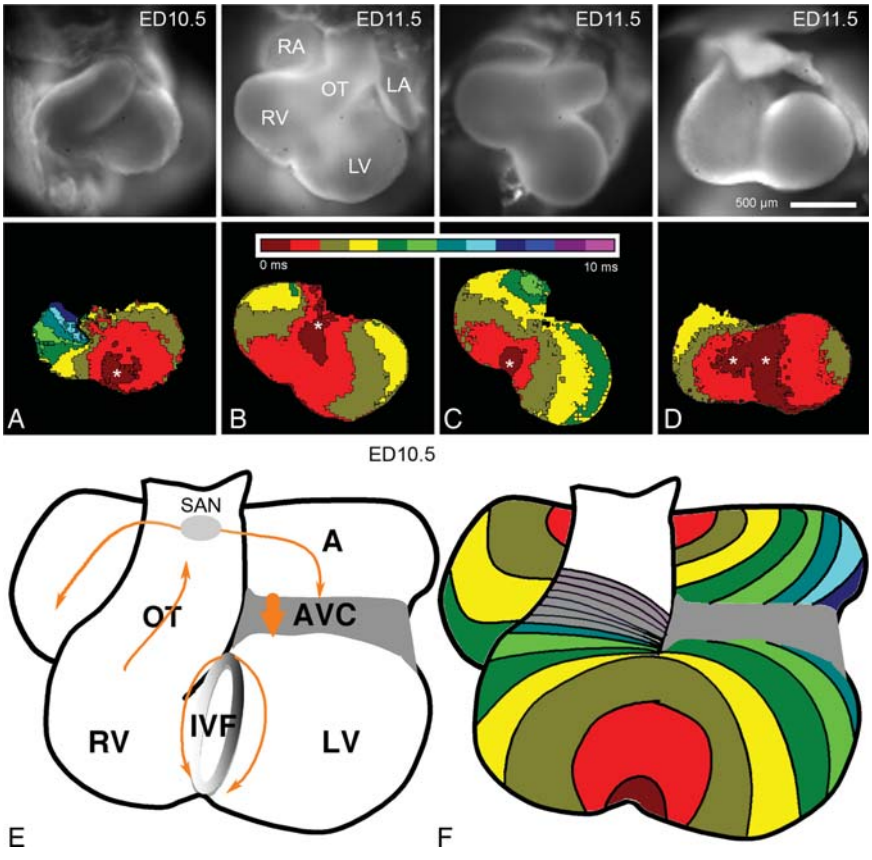

Figure 2 Examples of transitional activation patterns in early embryonic hearts. All examples are from *Cx40:GFP* heterozygous embryos; each colour band corresponds to a 1 ms time interval, and an asterisk indicates the first epicardial breakthrough site. (*A*) A single left-sided breakthrough (asterisk) at ED10.5. (*B*) The PIR type of activation at ED11.5, starting from the atrioventricular junction ventrally. (*C*) The same pattern, but using the posterior pathway, resulting in the first activation apparent ventrally in the interventricular groove between the right and left ventricular apices, was observed in a littermate of (*B*). (*D*) Transition between the ring-type and the apex-to-base activation patterns resulting in two distinct activation foci was also observed at ED11.5. (*E*) A diagram showing an ED10.5 heart and the spread of electrical impulse marked by orange arrows. (*F*) A typical epicardial activation map of an ED10.5 heart (depicted in *E*) obtained by merging atrial and ventricular activation maps. Electrical impulse is generated in the site of the sinoatrial node (SAN) and spreads laterally (atrial activation time 8 ms). The atrioventricular canal is not visualized on activation maps due to overlap with the atria, and the delay generated there is 180 ms. In this example, the ventricles are activated along the dorsal preferential activation pathway of the PIR. The outflow tract is another slowly conducting region (not coloured, isochronal intervals 1 ms). AVC, atrioventricular canal; IVF, interventricular foramen; LA, left atrium; LV, left ventricle; OT, outflow tract; RA, right atrium; RV, right ventricle.

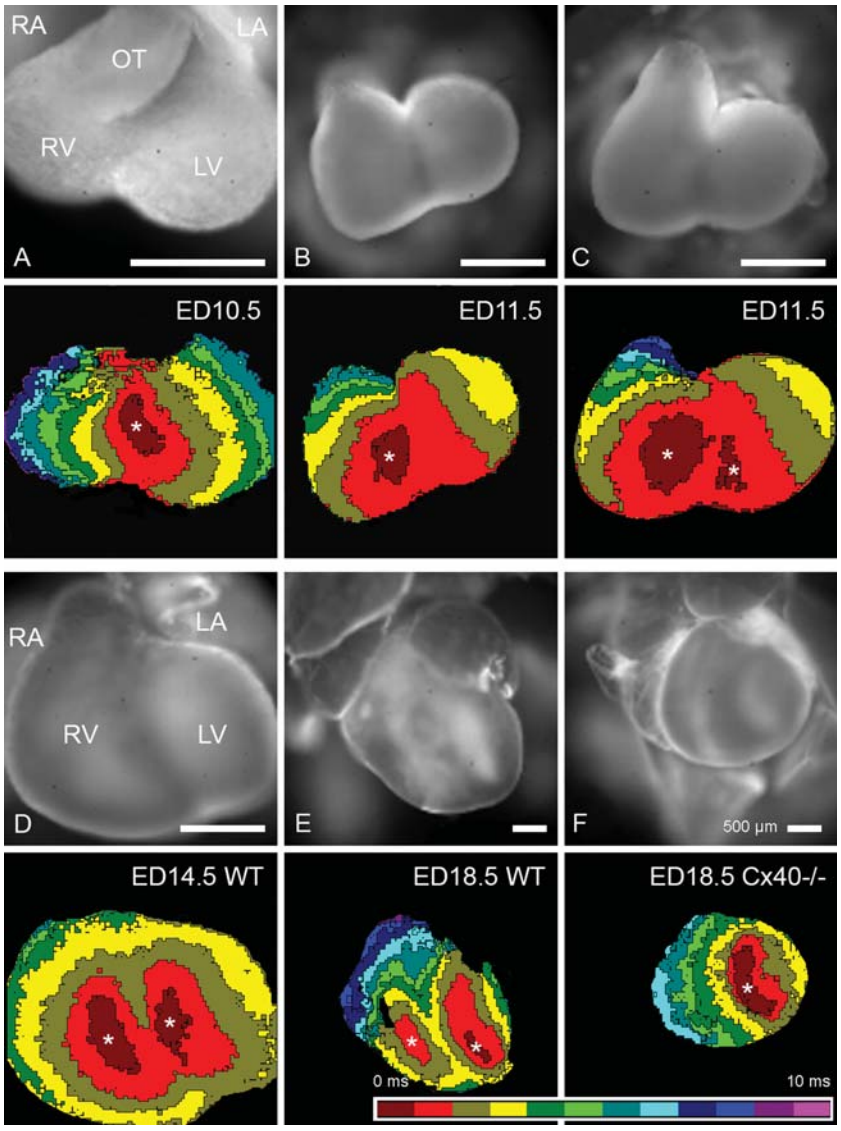

Figure 3 Typical examples of ventricular activation patterns observed in the developing mouse heart. (*A*) PIR-type activation at ED10.5. (*B*) Right-sided apical breakthrough at ED11.5. (*C*) Dual left- and right-sided breakthrough at ED11.5. All examples are from *Cx40:GFP* heterozygous animals. (*D*) Typical dual left- and right-sided apical breakthrough at ED14.5 in the wild type, interpreted as an evidence of the function of the right and left bundle branch. (*E*) The same pattern is also the most common one in the wild type at ED18.5. (*F*) A typical single (left) apical breakthrough in a *Cx*40-null heart, interpreted as right bundle block. The coloured isochrones are in 1 ms intervals and the white asterisk marks the first site of activation. The scale bars in all panels are 500 μm.

impulse travels into the ventricles along its ventral (*Figure 2B*) or dorsal aspect. The latter case was manifested as ventricular activation initiating between the apices of the ventricles (*Figure 2C*).

3.2 Conduction at later developmental stages

From ED11.5, four basic patterns of conduction, consistent with previous data from literature,[7,8] were detected (*Figure 3A–C*). Until ED12.5, the ventricles were activated through the PIR using a preferential pathway along the forming interventricular septum. The frequency of this pattern, initially present in the majority of hearts (*Table 1*), gradually decreased. Several transitional patterns were observed at ED10.5–ED11.5 (*Figure 2D*), until clear apex-to-base activation was observed, originating initially and more frequently from the right side. This right-sided breakthrough, first present at ED11.5, was observed in nearly all hearts from ED14.5, at which stage it could be related to the functionality of the right bundle branch. In addition, a second breakthrough near the left ventricular apex was observed from ED11.5. Unlike at earlier stages (ED9.5–10.5) where the single breakthrough originated exclusively from the primitive left ventricle, it was almost always present with the right-sided breakthrough (*Figure 3C* and *D*). We thus suggest that it represents activation through the emerging left bundle branch. The temporal difference between these two activation sides was minor, always below 2 ms, neither of them being consistently earlier than the other. The exception was at ED12.5, when the left breakthrough never preceded the right one in hearts showing dual activation.

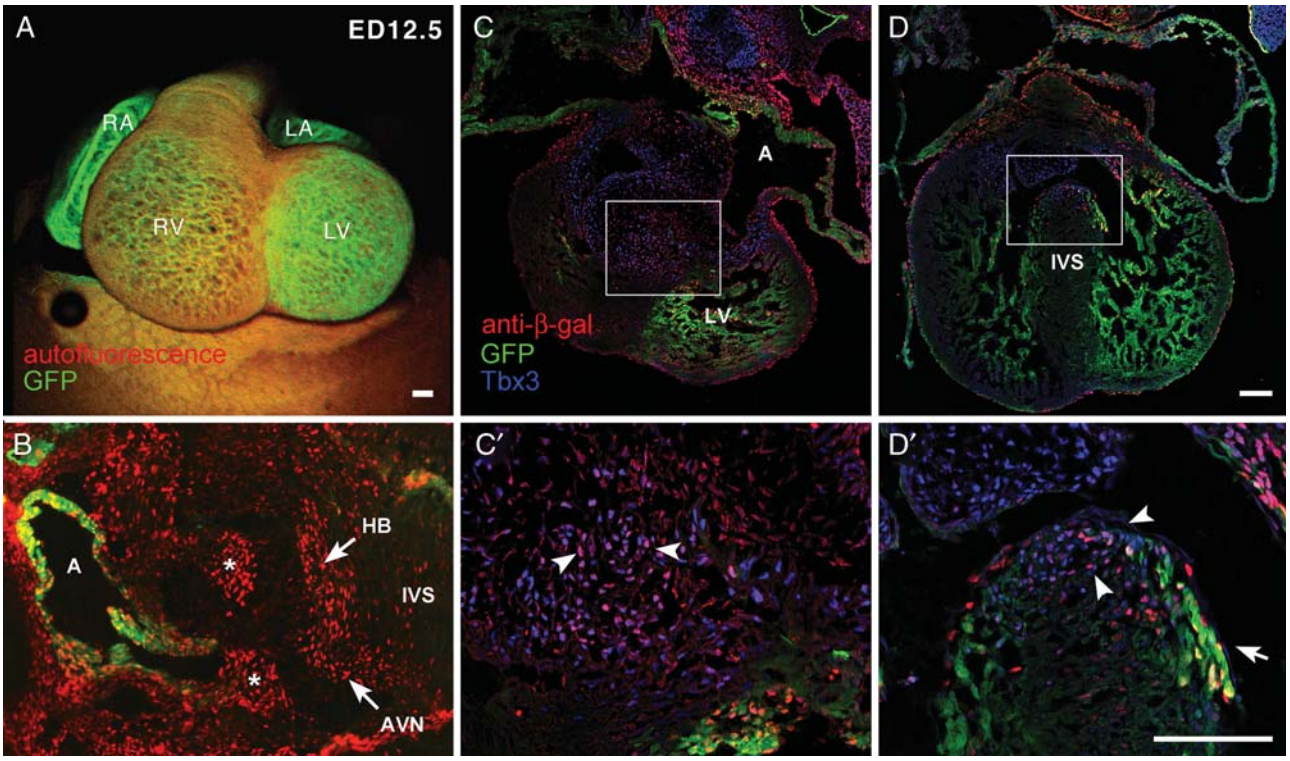

Figure 4 Heart structure and connection of the interventricular septum to atrioventricular node at ED12.5 in Cx40:GFP, T3-LacZ heterozygotes. (*A*) Whole-mount view depicts Cx40 expression in the heart; note stronger expression present in the left ventricle. Autofluorescence in red, GFP fluorescence in green. (*B*) Immunofluorescence staining on a sagittal section at the level of the interventricular septum (IVS). T3-lacZ detected in red is shown expressed at the level of the atrioventricular ring (*). It is also shown in a group of cells at the top of the interventricular septum (IVS) which corresponds to the His bundle (HB) connected to the dorsal atrioventricular node (AVN). (*C*, *C′*, *D*, *D′*) Immunofluorescence staining on transverse sections at the level of the atrioventricular node (*C*, *C′*) and His bundle (*D*, *D′*). In (*C*), Tbx3 immunostaining in blue highlights the AVN which cells also express the T3-lacZ transgene detected in red. (*C′*) corresponds to the high magnification of the AVN region boxed in (C) and showing Tbx3 and T3-LacZ both expressed in the same cells of the node (arrowheads). In (*D*), Cx40:GFP is detected in ventricular trabeculae of both ventricles while Tbx3 is detected in the mesenchymal cells of the cardiac cushion as wells as in the His bundle which covers the top of the IVS. Red cells expressing T3-lacZ transgene are also detected at the level of the His bundle. (*D′*) corresponds to the high magnification of this region boxed in (*D*) and showing Tbx3 and T3-LacZ both expressed in the same cells of the His bundle (arrowheads). The bundle branches express Cx40:GFP as well as Tbx3 and T3-LacZ (arrow). Scale bars 500 μm. LA, left atrium; LV, left ventricle; RA, right atrium; RV, right ventricle.

The ventricular activation pattern depends on the connection of the intraventricular conduction pathways to the atrioventricular node. The specificity of these connections as part of the atrioventricular conduction axis was verified by the Cx40:GFP marker (fast-conducting ventricular component, *Figure 4A*) and anti-β-galactosidase staining (T3-lacZ transgene labelling PIR tissues). At ED12.5, colocalization of these markers was observed at the proximal part of the bundle branches (*Figure 4D* and *D′*). The Tbx3 antibody labelled cells of the atrioventricular conduction system as well as the atrioventricular cushions (*Figure 4B–D*). Histological sectioning in the sagittal plane revealed the continuity of conduction markers between the atrial myocardium, atrioventricular canal, and the interventricular septum ventrally and dorsally (*Figure 4B*), consistent with the activation maps.

3.3 Calculation of left ventricular activation times

The left ventricular activation time showed a U-shaped relationship with development. It dropped to one-third between ED9.5–12.5, then stayed rather flat to increase slightly at later foetal stages (ED16.5 and ED18.5, *Figure 5A*). This suggests, however, continued increase in conduction velocity as the heart continues to increase in size (*Figure 3*). The shortest left ventricular activation time was recorded at ED13.5 (2.97 ± 0.83 ms) and was therefore used as a reference in statistical testing. No significant difference in activation time duration was observed between ED12.5–ED14.5, whereas it was significant ($P = 0.001$) at ED11.5 and highly significant ($P < 10^{-10}$) in the remaining embryonic days (ED9.5, 10.5, 16.5, 18.5, *Figure 5A*).

To discern whether the ventricular activation pattern has an influence on activation time and thus potential functional consequences, we performed a sub-analysis of ventricular activation times between ED9.5–ED11.5, where activation from the PIR was present. At all time points, activation from apical breakthrough resulted in shorter left ventricular activation time compared with activation through the PIR (*Figure 5B*). This difference reached statistical significance ($P = 0.005$) at ED10.5 and ED11.5.

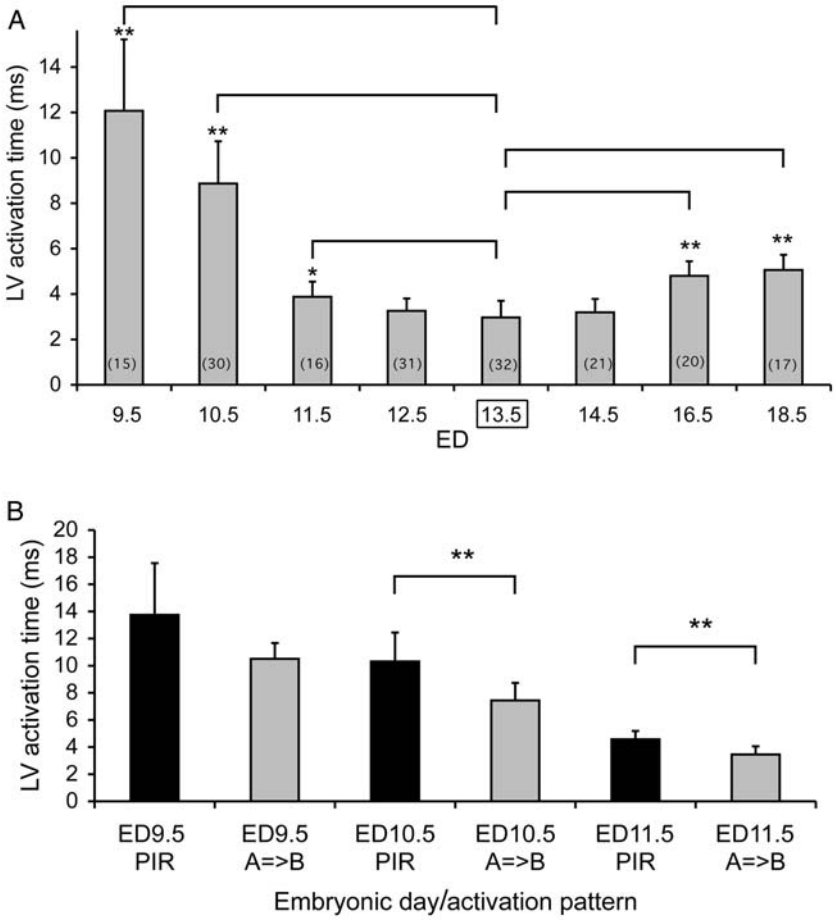

Figure 5 Quantification of ventricular conduction system maturation in *Cx40:GFP* heterozygotes. (*A*) Average time of left ventricular epicardial activation shows a U-shaped relationship with the development. The shortest activation time was found at ED13.5; against this stage were tested the remaining groups by unpaired two-tailed Student's *t*-test. The values are mean ± SD. $*P < 0.001$, $**P < 10^{-10}$. (*B*) The dependence of ventricular activation time duration on the activation pattern. Activation through the primary interventricular ring (PIR) is consistently slower than through the ventricular trabeculae (apex-to-base, A=>B). The *P*-value obtained with an unpaired two-tailed Student's *t*-test $**P < 0.005$. The values are mean ± SD.

3.4 Conduction changes in Cx40-deficient mice

There were no obvious differences in the frequency of the ventricular activation patterns between Cx40 null and control hearts at ED10.5 (data not shown) or ED12.5 (*Figure 6*). Interestingly, there was a notable decrease in the frequency of the left-sided apical breakthrough at ED12.5 and 14.5 in *Cx*40-deficient mice, with heterozygotes showing an intermediate phenotype. At these stages, however, the frequency of right-sided breakthrough was completely normal with no differences among genotypes (*Figure 6*). The resistance to right bundle branch block at ED14.5 could be correlated with *Cx*40 expression patterns in this region. Cx40 was initially expressed in a broad pattern (*Figure 7*), but during development became restricted to a thin strand of *Cx*40-positive tissue at ED18.5. The proportion of activation patterns began to reverse at ED16.5, where the left-sided breakthrough was present in nearly 100% in all genotypes (corresponding, at these stages, to functionality of the left bundle branch), while the frequency of the right-sided breakthrough began to decrease in the *Cx*40-deficient hearts, suggesting a developing right bundle branch dysfunction. These differences were even more prominent at ED18.5, where *Cx*40-deficient hearts presented only 33% of functional right bundle branches in contrast to 96% in heterozygotes and 94% in wild-type hearts (*Figure 6*). Quantitative analysis of left ventricle activation times performed at ED12.5–ED18.5 showed no differences between genotypes, including wild type vs. heterozygotes.

In a subset of hearts analysed at ED12.5, we observed a peculiar phenotype consisting of small ventricles with an elongated outflow tract, suggestive of abnormal morphogenesis described earlier[37] and consistent with a significantly less than 25% recovery rate for homozygous embryos in heterozygote crosses. The activation patterns of those morphologically abnormal hearts were not grossly disturbed (Supplementary material online, *Figure S1*), although the position of ventricular breakthroughs was slightly higher than in the control hearts.

4. Discussion

4.1 Conduction at early developmental stages

While a heartbeat was documented in mouse embryos as early as ED8.5 *in vivo* using ultrasound biomicroscopy,[38] we were able to

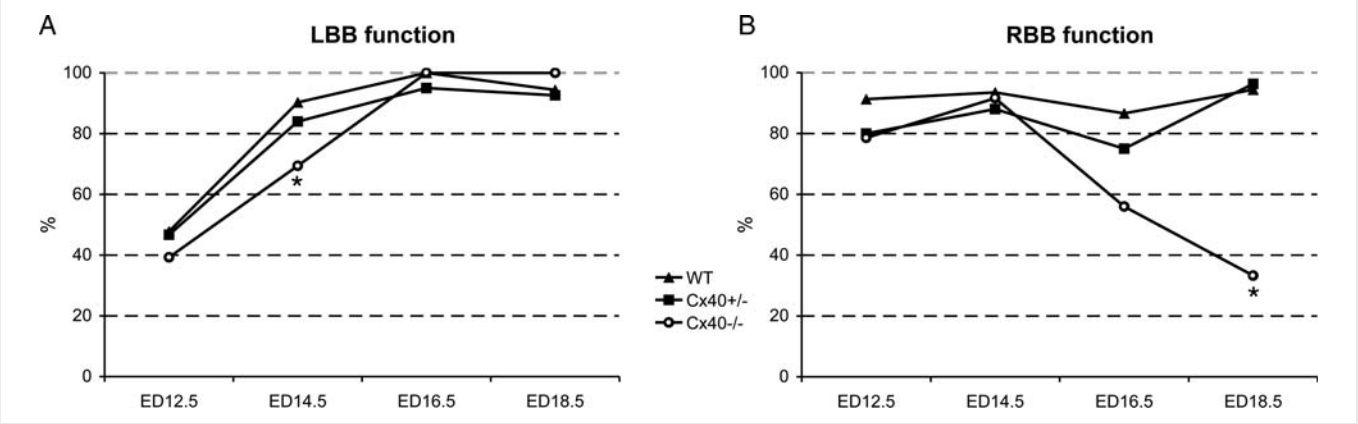

Figure 6 Conduction anomalies in *Cx*40-deficient embryonic ventricles. The frequency of the presence of left- and right-sided apical epicardial breakthroughs thought to correlate with the function of the left (LBB) and right bundle branch (RBB), respectively. Note that there is a left-sided deficiency initially (left panel) that is fully compensated by ED16.5, at which time point there is a clear decrease in the right-sided breakthrough frequency (right panel) corresponding to developing right bundle branch block. The heterozygotes show an intermediate phenotype. $*P < 0.05$ vs. wild type (as well as vs. heterozygotes for RBB at ED18.5); the difference between wild type and heterozygous animals was not significant.

obtain reproducible recordings only from ED9.5 onward using optical mapping. This could be due to the phototoxicity of the voltage sensitive dye, or generally higher sensitivity of mouse embryos compared with rats, in which similar recordings were obtained from the earliest stages of cardiac development by Hirota *et al.*[39] Their study described the location of the pacemaking tissue in the inflow region and its shift from the initially left side to the right side, but did not elaborate further on ventricular activation patterns. Our study extends previous reports on functionality of the developing mouse cardiac conduction system[7,8] by providing a quantification of the relative frequency of different activation patterns with appreciation of natural variability. Rentschler and associates quoted a small number of analysed hearts per group and concluded that only one activation pattern is typical at certain embryonic day. In the present study, we observed several activation patterns at each embryonic day, reflecting natural variability and consistent with the chick data.[2] Rentschler *et al.* described impulse propagation into the primitive ventricle along the dorsal wall only at ED9.5 (a pattern we interpret as an activation through the PIR), while our data show that the PIR can be recorded up to ED12.5. Moreover, activation from the apex of the primitive left ventricle towards the base in early embryonic development is a novel activation pattern at these stages.

A combination of functional recordings from a large number of hearts and both ventral and dorsal sides, together with our previous chick data,[3,5] changes our interpretation of the early activation patterns reported in the mouse by others[7,8] and in the rat by us.[10] Here, we show convincingly that the PIR, correlating with the forming interventricular groove,[6] is a specialized and preferred pathway used for ventricular activation. The PIR is composed of tissues around the interventricular foramen and part of the primary ring identified by Wessels *et al.*[6] Their description was based upon GlN2 expression in human samples: at stage 14 a ring around the interventricular foramen, but as the septation proceeded, GlN2 was expressed also in the right atrioventricular ring and the retroaortic root branch. In Aanhaanen *et al.*[40] as well as in *Figure 1*, the PIR is connected to the atrioventricular canal at two points, one ventral and one dorsal. The expansion of the atrioventricular canal towards right results in change in shape of the ring to a horseshoe, or U-shaped, structure. The ventral connection disappears later on, and only the dorsal node persists; otherwise, a dangerous arrhythmia (reciprocating tachycardia, as seen in Wolf–Parkinson–White syndrome) could result.

More discrete ring-shaped structures were described in the developing conduction system,[41] including the sinuatrial, atrioventricular, interventricular, and ventriculoarterial junctions using the minK-lacZ marker. While the expression of this marker changed with development, it provided developmental clues as to the possible origins of arrhythmias from regions outside the mature conduction system retaining expression of the marker. We believe that the PIR in our present work correlates well with the interventricular ring delineated by the minK-lacZ transgene at ED9.5. Multiple rings (3) were also described using the CCS-lacZ marker,[42] and again the connection between the atrioventricular canal and the 'primary ring' corresponds well with our observations (PIR, *Figure 1*). While the CCS-lacZ marker has the relative advantage of labelling the entire conduction system, further refinement is provided by using specific markers for slow (Tbx3, T3-lacZ transgene) and rapid (Cx40) conducting domains, allowing better appreciation of the connections between them.

Definitive connection between the atrial and ventricular myocardium through the atrioventricular node and His bundle occurs along the interatrial and ultimately fully fibrous atrioventricular septum. Hence, the atrial and ventricular septation process needs to be taken into consideration.[43] While the mature pattern of ventricular activation is present well before completion of ventricular septation, the role of atrial septum is less clear. It presents the shortest pathway between the sinoatrial and atrioventricular node, but it also forms a 'sink' slowing the propagation of the activation wave between the right and left atria.[44] Due to small size and delicacy of these structures during development, detailed analysis of conduction through this region would be challenging. While it is clearly part of the preferential atrioventricular conduction axis, experimental studies demonstrated functional pathways in the lateral region of the atrioventricular junction (Figure 5 in ref.[42]).

Conduction of electrical impulse through the PIR pathway is highly anisotropic (as can be appreciated from the shape of the isochrones)

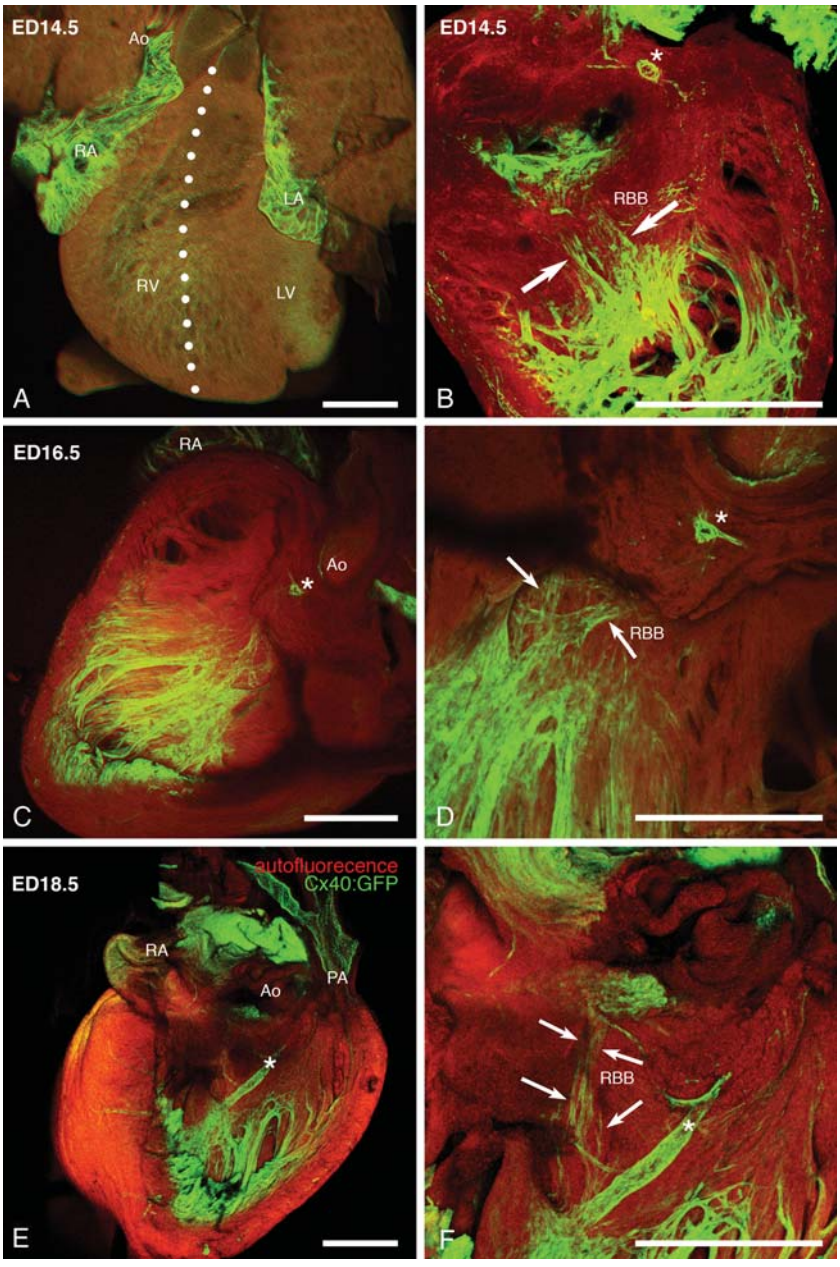

Figure 7 The development of the right bundle branch in *Cx40:GFP* heterozygotes. White dots indicate the line of right ventricle dissection to visualize the interventricular septum from the right side. The right bundle branch (RBB) is at ED14.5 a wide region of Cx40-positive fibres (marked laterally with arrows). *Cx*40 expression becomes restricted during later stages, resulting in the emergence of a thin strand of RBB at ED18.5. Asterisks indicate the septal artery, which is always near the RBB. Autofluorescence is in red and GFP fluorescence in green. Scale bars 500 μm. Ao, aorta; LA, left atrium; LV, left ventricle; PA, pulmonary artery; Pu, pulmonary trunk; RA, right atrium; RBB, right bundle branch; RV, right ventricle.

and slower than through the ventricular trabeculae forming the nascent definitive ventricular conduction system (*Figure 5B*). The differences in activation patterns between ED9.5 and 11.5 may potentially be due to ongoing cellular contribution from the second heart field, especially to the still forming right ventricle, which is complete at ED10.5. While the expression of *Cx*40 in right ventricular trabeculae is detectable already at ED10.5, activation from the right apical site was not observed until 1 day later, possibly because of the lack of connection of this expression domain with the preferential activation pathway utilizing the PIR and, much earlier, the left ventricular trabecular network.

*Cx*40-expressing trabeculae constitute the rapid conducting preferential pathway. In the left ventricle, Cx40 expression starts from ED9.5, and is always stronger than in the right ventricle. The functional consequence is demonstrated by sub-analysis of the activation time difference at stages where both conduction through the PIR and the more mature pathway utilizing the trabecular network, manifested as the apical breakthrough site, co-existed. In all cases, the activation through the trabecular network resulted in shorter ventricular activation time compared with the PIR (*Figure 5B*). A mature activation pattern from apex to base is connected with faster epicardial

activation time, which we consider, from the functional point of view, to be advantageous for efficient ventricular contraction. We postulate that such shorter epicardial activation time reflects a shorter ventricular activation time.

4.2 Conduction in later developmental stages and changes in Cx40-deficient mice

While the *Cx*40 is expressed in almost the entire trabecular network even at ED14.5 (*Figure* 7*A* and *B*) when the apical breakthrough sites suggest functionality of both bundle branches, not all trabeculae contribute to a definitive His-Purkinje network. Some will end up incorporated into the compact myocardium.[45] Pronounced left–right asymmetry, characteristic of the mature system[18] and resulting from gradual restriction of *Cx*40 expression, becomes apparent from ED18.5. This restriction, resulting in the emergence of a thin strand of *Cx*40-positive right bundle branch (*Figure* 7*E* and *F*), correlates with the time point at which right bundle branch block develops in Cx40-deficient embryos.

The data from Cx40 null mice suggest that while the function of the early ventricular conduction system is not strictly dependent upon the presence of *Cx*40 (as the PIR area is devoid of its expression), its later expression in the trabeculated chamber myocardium is important for the establishment of the preferential pathway through the trabecular network that will organize into the left and right bundle branches. The emergence of this pathway is manifested by the appearance of left and right apical epicardial breakthroughs in the spatiotemporal activation maps. We propose that tissue geometry is also of considerable importance for the function of the early conduction system. In the case of the developing right bundle branch in *Cx40*-deficient hearts, its function is initially normal and compensated by its relatively broad single-strand morphology until later stages, when increasing conduction velocity puts greater demands on the electrical coupling within specialized conduction fascicles. This correlates with the expression of *Cx*40 in right ventricular trabeculae starting 1 day before the appearance of the right apical breakthrough site. Indeed, conduction system morphology is normal in those hearts, and the right bundle branch block phenotype is fully penetrant only after birth.[22,23,25] Recently, right bundle branch block was reported in Irx3 null mice,[46] indicating higher sensitivity of this ventricular conduction system component to perturbations. On the other hand, high levels of expression of *Cx*40 in the left ventricular trabeculae seems to be more functionally relevant, as the diffuse conduction network, while providing a remarkable safety element, needs to be supplemented by appropriate electrical coupling for normal function. At this early stage, Cx43 is expressed in a similar pattern to Cx40, with a delay of 1 day. Cx40 is not expressed in the interventricular septum or the developing His bundle and its branches before ED14.5. The loss of Cx40 resulted in delayed left bundle branch functionality manifested initially as decreased frequency of the left-sided breakthrough, with tissue geometry (plus other conduction determinants, such as ion channel expression and other connexins) compensating only at later foetal stages (*Figure* 6).

4.3 Implications for future studies

Comparison of our wild-type data from different strains and background showed very little, if any, difference in frequency of ventricular activation patterns. Similarly, left ventricular activation times were not different between wild-type animals and Cx40 heterozygotes, suggesting that our data could be used as a baseline for analysis of other mutants. The variable that should be controlled is the crown rump length, as this varies among litters even with the same gestational age. Quantitative analysis of normal mouse embryonic ventricular conduction patterns will thus be useful for the interpretation of effects of mutations affecting the function of the cardiac conduction system. Additional topic worth of further investigation is the fate of the components of the atrioventricular ring as well as the interatrial septum in the final production of an atrioventricular node, and the details of its connections with the ventricular conduction system.

Supplementary material

Supplementary material is available at *Cardiovascular Research* online.

Acknowledgements

We would like to thank Ms Marie Jindrakova, Ms Jarmila Svatunkova, and Ms Eva Kluzakova for excellent technical assistance. The kind assistance of Dr Robert Kelly (IBDML, Marseille) with language revision is highly appreciated.

Conflict of interest: none declared.

Funding

This work was supported by the Ministry of Education VZ 0021620806, LC06044, and PRVOUK-P35/LF1/5; Academy of Sciences Purkinje Fellowship to D.S., and institutional AV0Z50110509 and RVO: 67985823. J.B. and B.S. were supported by the Graduate student training program of the First Faculty of Medicine, Charles University in Prague. Further support comes from the Grant Agency of the Czech Republic 304/08/0615, 204/09/H084, and P302/11/1308 to D.S. and the AFM (Association Française contre les Myopathies) to L.M.

References

1. Chuck ET, Freeman DM, Watanabe M, Rosenbaum DS. Changing activation sequence in the embryonic chick heart. Implications for the development of the His-Purkinje system. *Circ Res* 1997;**81**:470–476.
2. Reckova M, Rosengarten C, deAlmeida A, Stanley CP, Wessels A, Gourdie RG *et al.* Hemodynamics is a key epigenetic factor in development of the cardiac conduction system. *Circ Res* 2003;**93**:77–85.
3. Sedmera D, Reckova M, Bigelow MR, DeAlmeida A, Stanley CP, Mikawa T *et al.* Developmental transitions in electrical activation patterns in chick embryonic heart. *Anat Rec* 2004;**280A**:1001–1009.
4. Chuck ET, Meyers K, France D, Creazzo TL, Morley GE. Transitions in ventricular activation revealed by two-dimensional optical mapping. *Anat Rec* 2004;**280A**:990–1000.
5. Sankova B, Machalek J, Sedmera D. Effects of mechanical loading on early conduction system differentiation in the chick. *Am J Physiol Heart Circ Physiol* 2010;**298**:H1571–H1576.
6. Wessels A, Vermeulen JL, Verbeek FJ, Viragh S, Kalman F, Lamers WH *et al.* Spatial distribution of 'tissue-specific' antigens in the developing human heart and skeletal muscle. III. An immunohistochemical analysis of the distribution of the neural tissue antigen G1N2 in the embryonic heart; implications for the development of the atrioventricular conduction system. *Anat Rec* 1992;**232**:97–111.
7. Rentschler S, Vaidya DM, Tamaddon H, Degenhardt K, Sassoon D, Morley GE *et al.* Visualization and functional characterization of the developing murine cardiac conduction system. *Development* 2001;**128**:1785–1792.
8. Rentschler S, Zander J, Meyers K, France D, Levine R, Porter G *et al.* Neuregulin-1 promotes formation of the murine cardiac conduction system. *Proc Natl Acad Sci USA* 2002;**99**:10464–10469.
9. Rothenberg F, Nikolski V, Watanabe M, Efimov I. Electrophysiology and anatomy of embryonic rabbit hearts before and after septation. *Am J Physiol Heart Circ Physiol* 2005;**288**:H344–H351.
10. Sedmera D, Reckova M, Rosengarten C, Torres MI, Gourdie RG, Thompson RP. Optical mapping of electrical activation in developing heart. *Microscop Microanal* 2005;**11**:209–215.

11. Coppen SR, Severs NJ, Gourdie RG. Connexin45 (alpha 6) expression delineates an extended conduction system in the embryonic and mature rodent heart. *Dev Genet* 1999;**24**:82–90.
12. Kumai M, Nishii K, Nakamura K, Takeda N, Suzuki M, Shibata Y. Loss of connexin45 causes a cushion defect in early cardiogenesis. *Development* 2000;**127**:3501–3512.
13. Munshi NV, McAnally J, Bezprozvannaya S, Berry JM, Richardson JA, Hill JA *et al*. Cx30.2 enhancer analysis identifies Gata4 as a novel regulator of atrioventricular delay. *Development* 2009;**136**:2665–2674.
14. Gros D, Theveniau-Ruissy M, Bernard M, Calmels T, Kober F, Sohl G *et al*. Connexin 30 is expressed in the mouse sino-atrial node and modulates heart rate. *Cardiovasc Res* 2010;**85**:45–55.
15. Haugan K, Miyamoto T, Takeishi Y, Kubota I, Nakayama J, Shimojo H *et al*. Rotigaptide (ZP123) improves atrial conduction slowing in chronic volume overload-induced dilated atria. *Basic Clin Pharmacol Toxicol* 2006;**99**:71–79.
16. Severs NJ, Coppen SR, Dupont E, Yeh HI, Ko YS, Matsushita T. Gap junction alterations in human cardiac disease. *Cardiovasc Res* 2004;**62**:368–377.
17. Vaidya D, Tamaddon HS, Lo CW, Taffet SM, Delmar M, Morley GE *et al*. Null mutation of connexin43 causes slow propagation of ventricular activation in the late stages of mouse embryonic development. *Circ Res* 2001;**88**:1196–1202.
18. Miquerol L, Meysen S, Mangoni M, Bois P, van Rijen HV, Abran P *et al*. Architectural and functional asymmetry of the His-Purkinje system of the murine heart. *Cardiovasc Res* 2004;**63**:77–86.
19. Miquerol L, Moreno-Rascon N, Beyer S, Dupays L, Meilhac SM, Buckingham ME *et al*. Biphasic development of the Mammalian ventricular conduction system. *Circ Res* 2010; **107**:153–161.
20. van Kempen MJ, ten Velde I, Wessels A, Oosthoek PW, Gros D, Jongsma HJ *et al*. Differential connexin distribution accommodates cardiac function in different species. *Microsc Res Tech* 1995;**31**:420–436.
21. Leaf DE, Feig JE, Vasquez C, Riva PL, Yu C, Lader JM *et al*. Connexin40 imparts conduction heterogeneity to atrial tissue. *Circ Res* 2008;**103**:1001–1008.
22. Simon AM, Goodenough DA, Paul DL. Mice lacking connexin40 have cardiac conduction abnormalities characteristic of atrioventricular block and bundle branch block. *Curr Biol* 1998;**8**:295–298.
23. Tamaddon HS, Vaidya D, Simon AM, Paul DL, Jalife J, Morley GE. High-resolution optical mapping of the right bundle branch in connexin40 knockout mice reveals slow conduction in the specialized conduction system. *Circ Res* 2000;**87**:929–936.
24. Kirchhoff S, Nelles E, Hagendorff A, Kruger O, Traub O, Willecke K. Reduced cardiac conduction velocity and predisposition to arrhythmias in connexin40-deficient mice. *Curr Biol* 1998;**8**:299–302.
25. van Rijen HV, van Veen TA, van Kempen MJ, Wilms-Schopman FJ, Potse M, Krueger O *et al*. Impaired conduction in the bundle branches of mouse hearts lacking the gap junction protein connexin40. *Circulation* 2001;**103**:1591–1598.
26. Fedorov VV, Lozinsky IT, Sosunov EA, Anyukhovsky EP, Rosen MR, Balke CW *et al*. Application of blebbistatin as an excitation-contraction uncoupler for electrophysiologic study of rat and rabbit hearts. *Heart Rhythm* 2007;**4**:619–626.
27. Jou CJ, Spitzer KW, Tristani-Firouzi M. Blebbistatin effectively uncouples the excitation-contraction process in zebrafish embryonic heart. *Cell Physiol Biochem* 2011;**25**:419–424.
28. Sedmera D, Harris BS, Grant E, Zhang N, Jourdan J, Kurkova D *et al*. Cardiac expression patterns of endothelin-converting enzyme (ECE): implications for conduction system development. *Dev Dyn* 2008;**237**:1746–1753.
29. Nanka O, Krizova P, Fikrle M, Tuma M, Blaha M, Grim M *et al*. Abnormal myocardial and coronary vasculature development in experimental hypoxia. *Anat Rec (Hoboken)* 2008;**291**:1187–1199.
30. Viragh S, Challice CE. The development of the conduction system in the mouse embryo heart. I. The first embryonic A-V conduction pathway. *Dev Biol* 1977;**56**: 382–396.
31. Viragh S, Challice CE. The development of the conduction system in the mouse embryo heart. II. Histogenesis of the atrioventricular node and bundle. *Dev Biol* 1977;**56**:397–411.
32. Viragh S, Challice CE. The development of the conduction system in the mouse embryo heart. *Dev Biol* 1982;**89**:25–40.
33. Sedmera D, Reckova M, DeAlmeida A, Coppen SR, Kubalak SW, Gourdie RG *et al*. Spatiotemporal pattern of commitment to slowed proliferation in the embryonic mouse heart indicates progressive differentiation of the cardiac conduction system. *Anat Rec* 2003;**274A**:773–777.
34. Wessels A, Markman MW, Vermeulen JL, Anderson RH, Moorman AF, Lamers WH. The development of the atrioventricular junction in the human heart. *Circ Res* 1996; **78**:110–117.
35. Miquerol L, Dupays L, Theveniau-Ruissy M, Alcolea S, Jarry-Guichard T, Abran P *et al*. Gap junctional connexins in developing mouse cardiac conduction system. In: Goode J, eds. *Development of the Cardiac Conduction System*. Chichester: Wiley; 2003. p98–109.
36. Miller CE, Thompson RP, Bigelow MR, Gittinger G, Trusk TC, Sedmera D. Confocal imaging of the embryonic heart: How deep? *Microscop Microanal* 2005;**11**:216–223.
37. Kirchhoff S, Kim JS, Hagendorff A, Thonnissen E, Kruger O, Lamers WH *et al*. Abnormal cardiac conduction and morphogenesis in connexin40 and connexin43 double-deficient mice. *Circ Res* 2000;**87**:399–405.
38. Phoon CK. Imaging tools for the developmental biologist: ultrasound biomicroscopy of mouse embryonic development. *Pediatr Res* 2006;**60**:14–21.
39. Hirota A, Kamino K, Komuro H, Sakai T, Yada T. Early events in development of electrical activity and contraction in embryonic rat heart assessed by optical recording. *J Physiol* 1985;**369**:209–227.
40. Aanhaanen WT, Mommersteeg MT, Norden J, Wakker V, de Gier-de Vries C, Anderson RH *et al*. Developmental origin, growth, and three-dimensional architecture of the atrioventricular conduction axis of the mouse heart. *Circ Res* 2010;**107**:728–736.
41. Kondo RP, Anderson RH, Kupershmidt S, Roden DM, Evans SM. Development of the cardiac conduction system as delineated by minK-lacZ. *J Cardiovasc Electrophysiol* 2003; **14**:383–391.
42. Jongbloed MR, Wijffels MC, Schalij MJ, Blom NA, Poelmann RE, van der Laarse A *et al*. Development of the right ventricular inflow tract and moderator band: a possible morphological and functional explanation for Mahaim tachycardia. *Circ Res* 2005;**96**: 776–783.
43. Webb S, Brown NA, Anderson RH. Formation of the atrioventricular septal structures in the normal mouse. *Circ Res* 1998;**82**:645–656.
44. Sedmera D, Wessels A, Trusk TC, Thompson RP, Hewett KW, Gourdie RG. Changes in activation sequence of embryonic chick atria correlate with developing myocardial architecture. *Am J Physiol Heart Circ Physiol* 2006;**291**:H1646–H1652.
45. Sedmera D, Pexieder T, Vuillemin M, Thompson RP, Anderson RH. Developmental patterning of the myocardium. *Anat Rec* 2000;**258**:319–337.
46. Zhang SS, Kim KH, Rosen A, Smyth JW, Sakuma R, Delgado-Olguin P *et al*. Iroquois homeobox gene 3 establishes fast conduction in the cardiac His-Purkinje network. *Proc Natl Acad Sci USA* 2011;**108**:13576–13581.

The role of connexin40 in developing atrial conduction (under revision)

Jiri Benes Jr.1,2,4*, Grazia Ammirabile3, Barbora Sankova1,2, Marina Campione3, Eliska Krejci1,2, Alena Kvasilova2, David Sedmera1,2

1 Department of Cardiovascular Morphogenesis, Institute of Physiology, Academy of Sciences of the Czech Republic, Prague, Czech Republic

2 Charles University in Prague, First Faculty of Medicine, Institute of Anatomy, U Nemocnice 3, Prague, Czech Republic

3 CNR Institute of Neurosciences, Department of Biomedical Sciences, University of Padova, Italy

4 Charles University in Prague, First Faculty of Medicine, Department of Radiology of the First Faculty of Medicine and General Teaching Hospital, U Nemocnice 2, Prague, Czech Republic

*Correspondence to:

Jiri Benes, Institute of Anatomy, U Nemocnice 3, 12800, Prague 2

Phone +420-2-2496-5879, FAX +420-2-2496-5770, e-mail: jiri.benes2@lf1.cuni.cz

Abstract

Connexin40 (Cx40) is the main connexin expressed in the murine atria and ventricular conduction system. We assess here the developmental role of Cx40 in atrial conduction of the mouse. Cx40 deficiency significantly prolonged activation times in embryonic day 10.5, 12.5 and 14.5 atria during spontaneous activation; the severity decreased with increasing age. In a majority of Cx40 deficient mice the impulse originated from an ectopic focus in the right atrial appendage; in such a case the activation time was even longer. Cx40 has thus an important physiological role in the developing atria, which possess preferential conduction pathways.

Key words: heart development, arrhythmogenesis, sinoatrial node, optical mapping, mouse embryo

Introduction

Intercellular connections in the heart via gap junctions play an important role in impulse propagation in the myocardium (Kumar 1996). Cardiac gap junctions are composed of proteins called connexins (Cxs) that form low resistance channels, which enable electrical coupling of adjacent myocytes allowing intercellular electrical communication (Goodenough, 1996). Many studies have shown that alterations in the localization and expression of connexin proteins in the heart may cause abnormal activation spreading through the myocardium, thus leading to arrhythmias [1-3].

In mammalian hearts, mRNA for connexins 30.2, 40, 43 and 45 has been detected [4]. The expression of these connexins is dynamic in different parts of the heart, and the expression pattern is well conserved among species [5]. Each connexin forms a channel with unique electrophysiological properties [6]. The main connexin in murine atria is Cx40, but Cx43 and Cx45 are also expressed in smaller amounts [7]. Nevertheless, as a differentiation marker of the chamber myocardium [8], Cx40 is absent in the sinoatrial node.

The role of Cx40 in human arrhythmias was studied extensively [9,10]. The most common supraventricular arrhythmia in humans is atrial fibrillation. The studies investigating the relation between this arrhythmia and Cx40 have yielded rather conflicting results [11]. Simon et al. studied cardiac conduction abnormalities in mice lacking Cx40 and found no case of atrial fibrillation [3]. Verheule et al. described predisposition to tachyarrhythmias in adult Cx40 deficient mice after atrial burst pacing [12]. Recent studies in humans have discovered a polymorphism in the *Cx40* gene that is connected with a higher risk of developing atrial fibrillation [13]. Recently, Yang et al. [14] described a null mutation of Cx40 significantly associated with atrial fibrillation onset in humans.

Despite this fact, most of the studies performed in Cx40 deficient mice were focused on the ventricular conduction system, where several conduction pathologies such as right bundle branch block or slowed atrioventricular conduction were described [12,15]. In the adult mouse atria, prolongation of P wave and ectopic foci were reported [16]. Probably the most comprehensive study of the role of Cx40 deficiency on the developing atria was made by Greg Morley's group [17]. These authors described conduction velocity heterogeneity of the paced beat between the left and right atria in adult mice, which is lost in Cx40 deficiency. At the prenatal stages — embryonic day (ED)13.5 and ED15.5 — they found impaired SAN impulse initiation with ectopic sites of activation. The main objective of our study was to assess the role of Cx40 in impulse generation and spontaneous propagation in murine atria during early embryonic development.

Methods

Animals

Cx40:GFP knock-in mice developed by Lucile Miquerol [18] were used. As the knock-in of the *GFP* disrupts the endogenous *Cx40* gene, the homozygotes are functional nulls. *Cx40* null mice were maintained in homozygous state, as these animals are viable and fertile (albeit with a reduced life span, a smaller number of embryos per litter and a non-Mendelian ratio of nulls in heterozygous matings). Heterozygous embryos were obtained from timed matings of a Cx40-deficient male and a wild type (WT) female; for WT, mixed genetic background related to the Swiss strain and *Cx40:GFP* mice was used [19]. The experimental protocol was approved by the local animal committee and conforms to the Guiding Principles in the Care and Use of Vertebrate Animals in Research and Training.

Optical mapping of embryonic hearts

The animals were caged together overnight, and the noon of the day of vaginal plug detection was considered ED0.5. Pregnant females were killed by cervical dislocation on ED10.5, 12.5 and 14.5 and the embryos were rapidly dissected in ice-cold (to prevent ischemic damage to the heart) Tyrodes solution (composition: NaCl 145mmol/l, KCl 5.9mmol/l, $CaCl_2$ 1.1mmol/l, $MgCl_2$ 1.2mmol/l, glucose 11mmol/l, HEPES 5mmol/l; pH=7.4). These stages were selected to cover the early period of cardiac development prior to septation. The hearts with adjacent posterior body wall structures were isolated and stained in 2.5mmol/l di-4-ANEPPS (Invitrogen) for 10 minutes. Because of different focal planes for atria and ventricles (Figure 1), our standard imaging protocol had to be modified slightly as we were unable to use the recordings performed for the analysis of ventricular activation patterns in a separate study [19]. To avoid any perturbation of the pacemaking region, we chose the antero-superior view (Figure 1, 2). Despite the overall transparency of the heart, the outflow region obscured the central area, where the pacemaker is normally located; for this reason, we removed the outflow tract at the ventricular border and at its distal connection to pharyngeal arch arteries. Data acquisition and analysis were performed using the Ultima L high-speed camera and bundled software as described recently [20]. To better appreciate the dynamics of atrial activation, the percentile activation over time method, recently validated by the Gourdie lab [21], was used (Figure 2). Differences in quantitative parameters between genotypes were compared using a two-tailed Student's t-test, and $p<0.05$ was considered statistically significant.

Immunohistochemistry

To obtain a morphological view of the atrial myocardium and SAN position, six WT embryos and ten embryos of the *Cx40 -/-* line at ED12.5 were fixed in 4% paraformaldehyde in PBS

overnight at 4 °C, and transferred into OCT medium through ascending saccharose gradients. Ten-micron sections were cut on a cryomicrotome, and alternating sections were mounted on poly-lysine coated slides and alternatively stained with hematoxylin-eosin, anti-HCN4 (1:500, Alomone labs), and anti-Cx43/WGA/Hoechst (Sigma/Invitrogen). The specific antibody binding was visualized with goat-anti-rabbit antibody (Jackson Immuno) coupled with peroxidase with diaminobenzidine as a color substrate and hematoxylin nuclear counterstain, or by fluorescently labeled secondary antibody. Images were acquired on an upright Olympus BX51 microscope equipped with an Olympus DP71 CCD camera, and assembled and labeled in Adobe Photoshop. Confocal series of anti-Cx43 labeling were collected on an Olympus confocal microscope using 40x oil immersion lens, and quantified using ImageJ as described [22].

Results

The activation of the ED10.5 atria originated in an area right from the midline where the SA node is localized [23], and took on average 6 (n=8) ms (Figure 3). Same activation pattern, but almost doubled activation time, was observed in the heterozygotes (n=17). The homozygotes showed a wide range (11-92, n=13) of activation times, some within the range of the heterozygotes, but some extremely long close to 100 ms.

In ED12.5 mouse embryos, the atrial appendages were small and the atria were clearly visible in frontal view (Figure 1). We thus analyzed the spreading and the pattern of activation in the antero-superior view, after careful removal of the outflow tract.
The prototypical atrial activation patterns observed in our recordings are shown in Figure 2. In WT mice (n=19) the activation pattern was quite uniform among samples. The first epicardial breakthrough (the site of the first electrical activation) was located between the right and left atrium in the roof of the right atrium at the entrance of the superior caval vein,

in the place where the sinoatrial node is known to be located at these embryonic stages [24], [25,26]; the signal then spread to both atria, with the right atrium being activated sooner. The average time of total atrial activation was also evaluated (7 ms; see Figure 3).

In *Cx40* +/- mice (n=12) we saw an identical activation pattern. The first breakthrough was in the SAN area, but the average time of atrial activation was significantly prolonged compared to controls; it took on average 9 ms to activate both atria.

In the hearts deficient of Cx40 (*Cx40* -/-) we generally saw two patterns of activation. Only 6 of the 18 hearts analyzed at ED12.5 showed the typical pattern observed in WT hearts (i.e., activation from the SAN area); in the remaining 12 hearts an ectopic focus of the first electrical activation in the right atrial appendage was detected (Figure 2). Moreover, we found that the total atrial activation times differed depending on the site of activation. In the case of activation from the SAN area, the average time of activation was 19 ms vs. 28 ms necessary for atrial activation from the ectopic site. These differences were statistically significant (Figure 3). Analysis of atrial activation dynamics showed graphically that the prolongation of total activation time was due to a delay in activation between the left and right atrium (Figure 2). The frequency of this ectopic pacemaker was regular and did not migrate during the individual recordings.

We also tried to analyze the hearts at ED14.5 in the same way, but at this stage the atrial appendages protrude forward, making it difficult to get both them and the back of the atria into the same focal plane without mechanically deforming their shape (such a thing could affect the activation properties of the atria). Nevertheless, we can conclude from our data that the activation patterns remained the same: in WT hearts (n=5) the predominant pattern was still the activation from the SAN area, and in Cx40 -/- (n=11) there were the same two patterns of activation described above. The activation times were likewise prolonged in

the Cx40 deficient mice (Figure 3); there was no significant difference between the wild type and the heterozygotes (n=9).

We were also interested in the frequency of spontaneous atrial rhythm. The average rate of the WT atria at ED12.5 *in vitro* was 96 bpm (SD 27.5). When the activation originated in the SAN, the frequency was similar — in Cx40 +/- it was 92 bpm (SD 29), and in Cx40-/- 85 bpm (SD 25; p=NS). There was a big variation in frequencies in the ectopically activated atria — the average frequency was higher at 116 bpm, but with SD=53 the difference was not statistically significant.

Having observed all this, we hypothesized that this focus might have a morphological substrate (e.g., some kind of ectopic SA node). Therefore, we examined microscopically serial sections of the hearts of ten Cx40 -/- and six WT mice embryos at ED12.5 and ED14.5 stained with an anti-HCN4 antibody detecting an ion channel responsible for autonomic electrical activity in the cells, and found no evidence of HNC4-positive cells in the right appendage in Cx40 mutants (Supplemental Figure 1). HNC4 expression was detected in the posterior wall of the right atrium as well as around the orifice of the pulmonary vein, which corresponds with the whole mount in situ hybridization study by Garcia-Frigola et al. [23]. Lower levels of HNC4 signal were found throughout the atria and even lower signal, but clearly above background, was present in the ventricles (Supplemental Figure 1). Staining of sister sections with WGA did not reveal any significant increase of fibrosis, which was minimal in the atrial tissue (data not shown). Scanning electron microscopy was also performed to complement the morphological evaluation of the atria (data not shown) and revealed no significant changes in atrial morphology or arrangement of the pectinate muscles.

To study possible compensatory changes caused by expression of Cx43, we performed immunohistochemical reaction on sister sections from ED10.5, 12.5, and 14.5 hearts. No signal was present at ED10.5, in agreement with previous in situ hybridization

study by Delorme and associates [7]. There was an increase in immunoreactivity between ED12.5 and 14.5 (+96% WT, +36% Cx40 -/-), with increased localization of the particles to the cell membrane (Supplementary Figure 2). There was a trend towards lower Cx43 levels in the Cx40 -/- atria (-37%, p=0.047 at ED12.5 and -57%, p=0.097 at ED14.5).

Discussion

The role of Cx40 in cardiac arrhythmogenesis has been described earlier by a number of research groups [9,10,13]. Despite this, the functional role of this protein in development is still not fully understood. Our study contributes to this understanding with the following conclusions: 1) The lack of Cx40 in the embryonic atria directly influences the conduction properties of atrial myocardium (see Figure 3). This is consistent with the fact that Cx40 is the main gap junction protein in murine atria [6]. The function of missing Cx40 could be substituted by other connexins, especially Cx43. According to the study by Delorme et al., the expression of *Cx43* in mouse atria is detectable by *in situ hybridization* from ED12.5 onwards [7]. In our data, the prolongation of activation times in Cx40 deficient atria compared to WT is much higher at ED10.5 or 12.5 (more than 3 times longer) in contrast to ED14.5 (only about 30% more, see Figure 3), suggesting a mechanism of developmental compensation from the 43 isoform. Lower levels of Cx43 observed in Cx40 -/- are not likely biologically significant, as the amounts must be decreased by more than 90% to observe physiological phenotype. 2) In 2/3 of *Cx40* -/- embryonic hearts at ED12.5, the first breakthrough was located in an ectopic site in the right atrium without the presence of any morphological or molecular substrate that could explain these autorhythmic properties; this might reflect an abnormal exit [27] of the impulse from the SAN. However, study performed in the adult Cx40 -/- mice indicated that there are truly ectopic foci, since their ablation resulted in re-location of the pacemaker back to the SA node, although with much reduced

frequency [16]. Accordingly, we did not find any morphological changes in SA node formation in Cx40 deficient hearts (Supplemental Figure 1). The frequency of atrial pacing from ectopic foci was rather irregular, suggesting also a functional problem.
3) When the excitation was spreading from this ectopic place, the activation time of both atria was even more prolonged than in the rest of the CX40 -/-. We hypothesize that this could be a consequence of the presence of a preferential pathway (Bachmann's bundle) of signal spreading from the SAN to the left atrium, as described in the chick embryos [28] as well as other species [29] including humans [30]. This preferential pathway does not seem to be utilized during the ectopic activation, resulting in prolonged conduction through the working myocardium with the interatrial septum causing a further delay by acting like a sink.

Verheule et al. described several cardiac conduction abnormalities in adult mice lacking Cx40 [12]. They found a P wave prolongation on surface electrocardiographs (corresponding to the atrial activation time) and a 30% decrease in the conduction velocity in *Cx40* -/- mice compared with the WT. In addition, burst pacing was able to provoke atrial tachyarrhythmias in 50% of the mutants. This prolongation of atrial activation time is quantitatively very similar to our results at ED14.5, and such slowing of conduction velocity could be one of the arrhythmogenic factors in human cases of Cx40 disruption.

This is the first study that maps in detail the effect of CX40 deficiency on activation spreading and times of murine embryonic atria at ED12.5. Leaf et al. performed an extensive study about the effect of Cx40 on conduction heterogeneity in adult mice of a wide range of ages as well as in embryos (ED13.5 and ED15.5) [17]. In their study they detected the presence of more ectopic sites of activation at ED15.5, localized also in the left atrium, whereas at ED13.5 they described normal SA node activation both in *Cx40* +/+ and in *Cx40* -/- mice. This is in contrast with our data, as we found ectopic activation already at ED12.5 in two thirds of the hearts. Such a discrepancy can be due to a different method of gene deletion

(unlike Leaf et. al. we used GFP:Cx40 knock-in mouse line), and/or to the influence of different genetic background of the strains, and/or to slightly different methodological approaches (we did not use signal averaging and motion tracking in our optical recordings).

In conclusion, this study shows that a lack of Cx40 in atria during development influences the activation patterns of impulse propagation and significantly slows impulse propagation velocity (which directly correlates with the type of atrial activation). This study improves our understanding about the electrophysiological function of Cx40 during embryonic development and the relationship between the activation times of atria, the amount of Cx40 and the site of activation.

Acknowledgements

Our sincere thanks are due to Dr. Lucile Miquerol, IBDM, France, for supplying the *Cx40-/-* mice. We would like to thank Ms. Marie Jindrakova, Marketa Pleschnerova, Jarmila Svatunkova and Eva Kluzakova for their excellent technical assistance. Mr. Frantisek Alferi performed acquisition and quantification of the Cx43 and HCN4 immunostaining. Supported by the Ministry of Education PRVOUK-P35/LF1/5, and institutional RVO: 67985823. Further support comes from the Grant Agency of the Czech Republic 13-12412S, P302/11/1308, and 204/09/H084. J.B. and B.S. are supported by a training fellowship program of Charles University in Prague, First Faculty of Medicine.

Conflict of Interests

Neither author reports any conflict of interests.

References

[1] van der Velden, H.M., van Kempen, M.J., Wijffels, M.C., van Zijverden, M., Groenewegen, W.A., Allessie, M.A. and Jongsma, H.J. (1998) J Cardiovasc Electrophysiol 9, 596-607.

[2] Kirchhoff, S., Nelles, E., Hagendorff, A., Kruger, O., Traub, O. and Willecke, K. (1998) Curr Biol 8, 299-302.

[3] Simon, A.M., Goodenough, D.A. and Paul, D.L. (1998) Curr Biol 8, 295-8.

[4] Kanter, H.L., Saffitz, J.E. and Beyer, E.C. (1992) Circ Res 70, 438-44.

[5] Gros, D.B. and Jongsma, H.J. (1996) Bioessays 18, 719-30.

[6] Jalife, J., Morley, G.E. and Vaidya, D. (1999) J Cardiovasc Electrophysiol 10, 1649-63.

[7] Delorme, B., Dahl, E., Jarry-Guichard, T., Briand, J.P., Willecke, K., Gros, D. and Theveniau-Ruissy, M. (1997) Circ Res 81, 423-37.

[8] Moorman, A.F. and Christoffels, V.M. (2003) Physiol Rev 83, 1223-67.

[9] Dupont, E. et al. (2001) J Mol Cell Cardiol 33, 359-71.

[10] Polontchouk, L. et al. (2001) J Am Coll Cardiol 38, 883-91.

[11] Kanagaratnam, P. and Peters, N.S. (2004) Heart Rhythm 1, 746-9.

[12] Verheule, S., van Batenburg, C.A., Coenjaerts, F.E., Kirchhoff, S., Willecke, K. and Jongsma, H.J. (1999) J Cardiovasc Electrophysiol 10, 1380-9.

[13] Hauer, R.N., Groenewegen, W.A., Firouzi, M., Ramanna, H. and Jongsma, H.J. (2006) Adv Cardiol 42, 284-91.

[14] Yang, Y.Q., Zhang, X.L., Wang, X.H., Tan, H.W., Shi, H.F., Jiang, W.F., Fang, W.Y. and Liu, X. (2010) Int J Mol Med 26, 605-10.

[15] Tamaddon, H.S., Vaidya, D., Simon, A.M., Paul, D.L., Jalife, J. and Morley, G.E. (2000) Circ Res 87, 929-36.

[16] Bagwe, S., Berenfeld, O., Vaidya, D., Morley, G.E. and Jalife, J. (2005) Circulation 112, 2245-53.

[17] Leaf, D.E. et al. (2008) Circ Res 103, 1001-8.

[18] Miquerol, L. et al. (2004) Cardiovasc Res 63, 77-86.

[19] Sankova, B., Benes, J., Jr., Krejci, E., Dupays, L., Theveniau-Ruissy, M., Miquerol, L. and Sedmera, D. (2012) Cardiovasc Res.

[20] Sankova, B., Machalek, J. and Sedmera, D. (2010) Am J Physiol Heart Circ Physiol 298, H1571-6.

[21] O'Quinn, M.P., Palatinus, J.A., Harris, B.S., Hewett, K.W. and Gourdie, R.G. (2011) Circ Res 108, 704-15.

[22] Benes, J., Jr., Melenovsky, V., Skaroupkova, P., Pospisilova, J., Petrak, J., Cervenka, L. and Sedmera, D. (2011) Anat Rec (Hoboken) 294, 102-111.

[23] Garcia-Frigola, C., Shi, Y. and Evans, S.M. (2003) Gene Expr Patterns 3, 777-83.

[24] Liu, J., Dobrzynski, H., Yanni, J., Boyett, M.R. and Lei, M. (2007) Cardiovasc Res 73, 729-38.

[25] Mommersteeg, M.T. et al. (2007) Circ Res 100, 354-362.

[26] Viswanathan, S., Burch, J.B., Fishman, G.I., Moskowitz, I.P. and Benson, D.W. (2007) J Mol Cell Cardiol 42, 946-53.

[27] Verheijck, E.E., van Kempen, M.J., Veereschild, M., Lurvink, J., Jongsma, H.J. and Bouman, L.N. (2001) Cardiovasc Res 52, 40-50.

[28] Sedmera, D., Wessels, A., Trusk, T.C., Thompson, R.P., Hewett, K.W. and Gourdie, R.G. (2006) Am J Physiol Heart Circ Physiol 291, H1646-52.

[29] Dolber, P.C. and Spach, M.S. (1989) Am J Physiol 257, H1446-57.
[30] Ho, S.Y., Anderson, R.H. and Sanchez-Quintana, D. (2002) Cardiovasc Res 54, 325-36.

Figure legends

Figure 1. **Morphology of an ED12.5 mouse heart.** The heart of a *Cx40* +/- mouse embryo at ED12.5 in confocal projections (GFP fluorescence) in three complementary views. In the anterior view, it is evident how the outflow tract covers the central portion of the atria. In the posterior view, the same area is hidden by the veins entering the right atrium. In the superior view the extensive antero-posterior dimension of the atria is clearly visible, and a fine network of pectinate muscles in both atria can be appreciated. RA – right atrium; LA – left atrium; RV – right ventricle; LV – left ventricle; Ao – aorta; Pu – pulmonary trunk; asterisks mark the putative site of the SAN, distinguished from the surrounding GFP-positive atrial myocardium by its darkness.

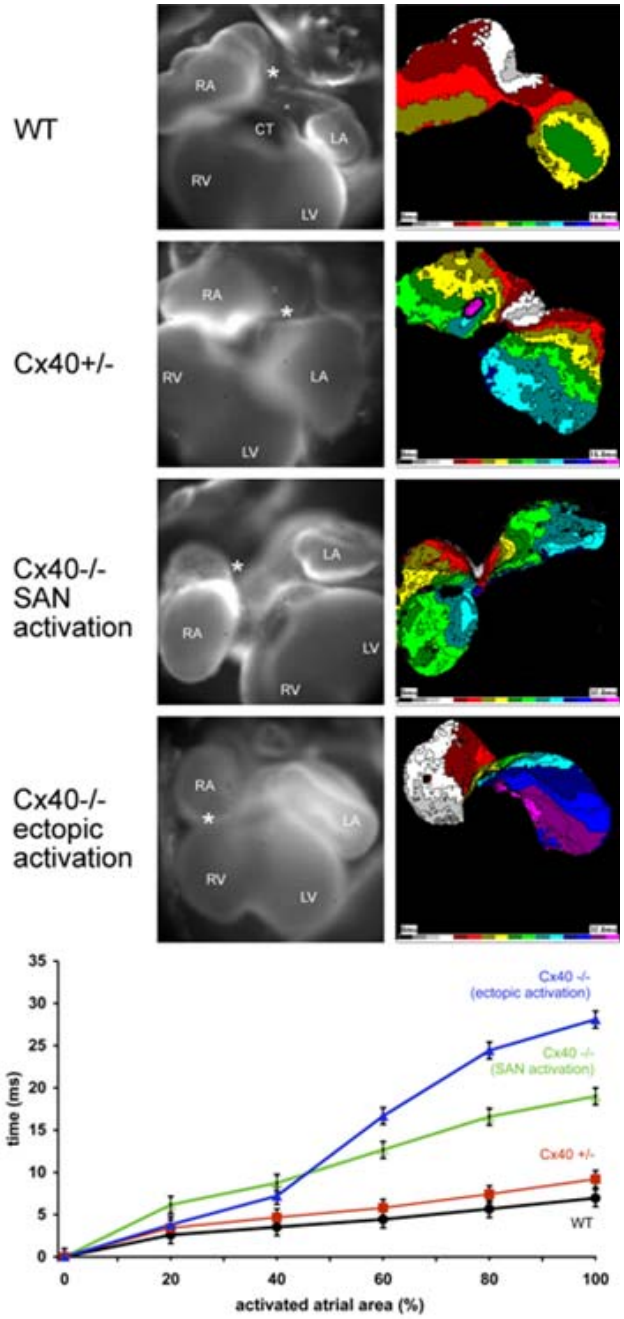

Figure 2. **Activation patterns of the atria at ED12.5** in WT, *Cx40* +/- and *Cx40* -/- hearts. In *Cx40* -/- hearts there are two main patterns of activation – normal SAN activation (third row) and ectopic activation (fourth row). In the first column are shown microscopical images of hearts with removed outflow tract (conotruncus - CT – labeled in the first image). In the second column are the corresponding activation maps. LA – left atrium; LV – left ventricle; RA – right atrium; RV – right ventricle; asterisk – site of first breakthrough (activation site). The chart below shows quantification of atrial activation times and dynamics. The time course of atrial activation demonstrates a significant delay between the left and right atrium in the right atrial ectopic activation.

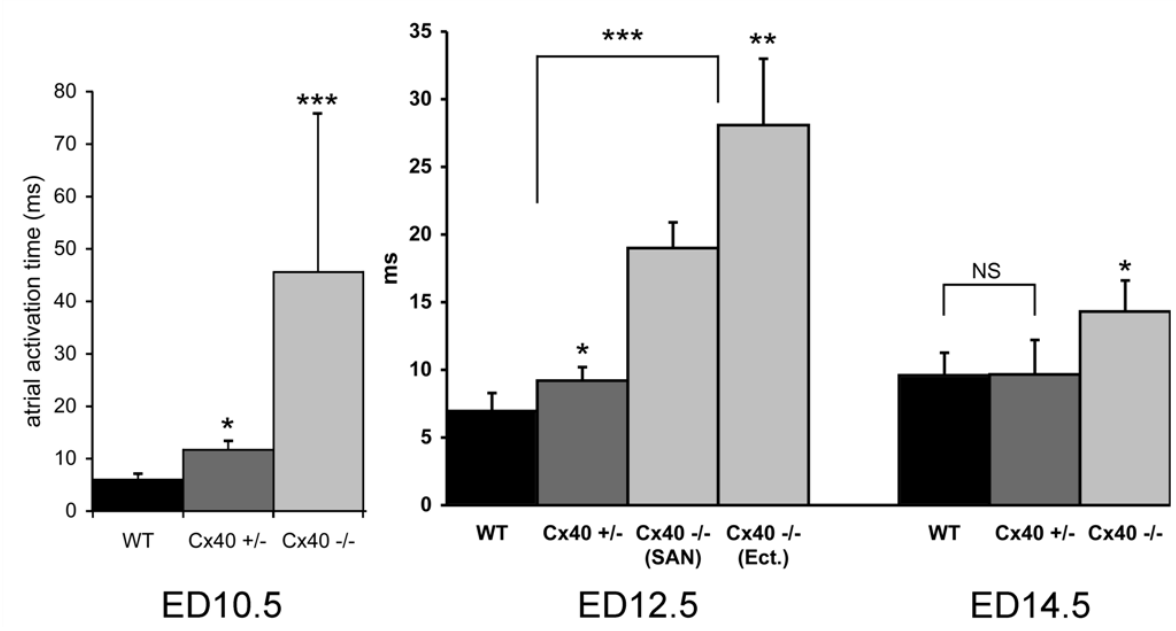

Figure 3. **Activation times of atria at ED10.5 to ED 14.5.** The values are means ± SD. ED10.5: * statistically significant vs. WT; *** statistically significant vs. both WT and heterozygotes. ED12.5: * statistically significant vs. WT; ** statistically significant vs. SAN activation; *** either Cx40 -/- group is significantly different vs. both WT and Cx40 +/- hearts. ED14.5: * significantly different vs. both WT and Cx40 +/- hearts. There is no difference between WT and Cx40 +/- hearts (NS).

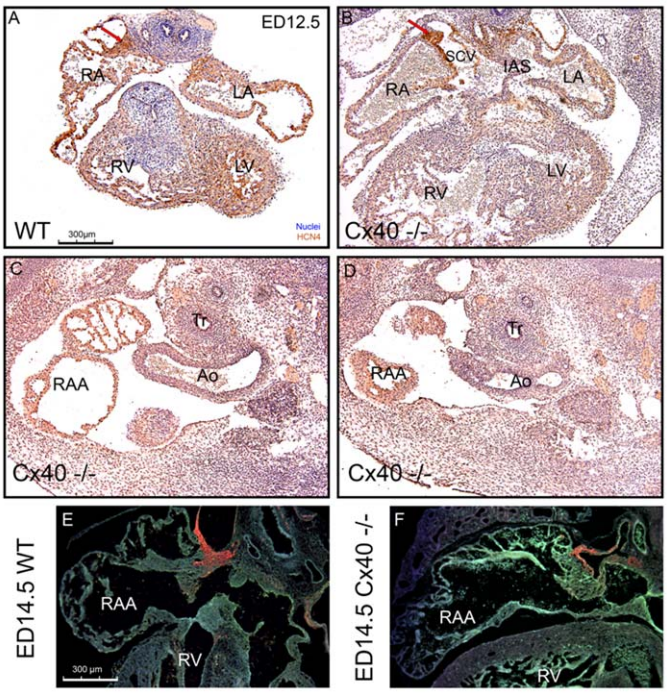

Supplemental Figure 1. **Immunohistochemical localization of the SAN in *Cx40*-/- mouse hearts at ED12.5.** Histological sections through the right atrial appendage. Panels A and B: Histological sections of mouse hearts stained with an anti-HCN4 antibody show the localization of positive cells in the SAN (red arrows) as well as around the remnants of the right sinus horn/forming pulmonary vein (red asterisks). Panels C and D: sections through the right atrial appendage showing no significant accumulation of HCN4 positive cells in the area from which the ectopic activation originated. Panels E and F show sections from ED14.5 heart visualized using fluorescence. There is no obvious difference in location or size of the SAN between the WT (E) and Cx40 -/- (F) heart. Ao – aortic arch; Eso, esophagus; IAS – intraatrial septum; LA – left atrium; LV – left ventricle; RA – right atrium; RAA – right atrial appendage; RV – right ventricle; RSCV – right superior caval vein; Tr – trachea. Nuclei are counterstained with hemotoxyllin; scale bar 300 µm.

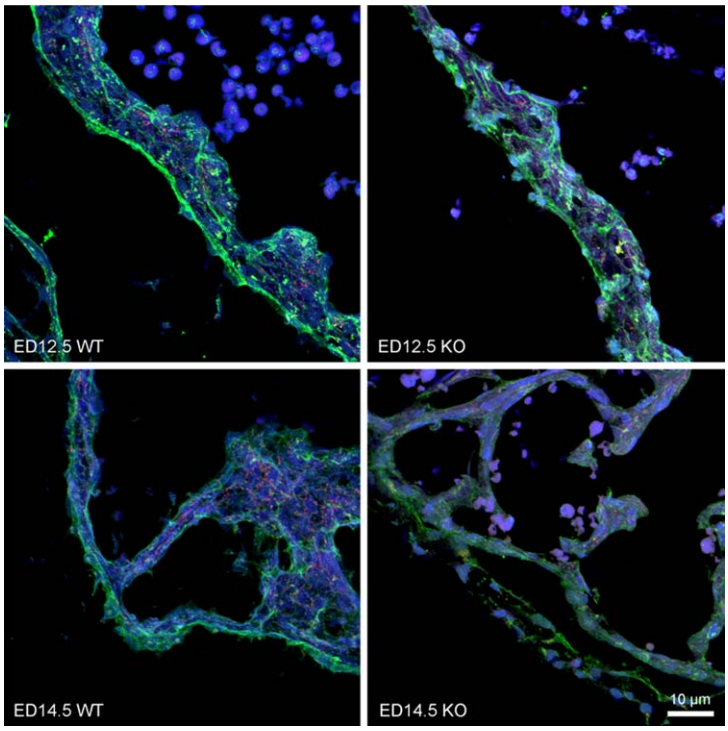

Supplemental Figure 2. **Immunohistochemical localization of Cx43 at ED12.5 and 14.5.** Maximum intensity confocal projections show the protein particles as red dots. There is a notable increase between ED12.5 and 14.5, with the mutant hearts showing less immunoreactivity. All pictures were taken from the lateral portion of right atrial appendage. Scale bar 10 µm.

Cardiovascular Research (2012) **93**, 291–301
doi:10.1093/cvr/cvr314

Pitx2 confers left morphological, molecular, and functional identity to the sinus venosus myocardium

Grazia Ammirabile[1], Alessandra Tessari[1], Viviana Pignataro[1], Dorota Szumska[2], Fabio Sutera Sardo[1], Jiri Benes Jr[3,4], Mariangela Balistreri[1], Shoumo Bhattacharya[2], David Sedmera[3,4], and Marina Campione[1]*

[1]CNR Institute of Neurosciences, Department of Biomedical Sciences, University of Padova, Viale G. Colombo 3, Padova 35121, Italy; [2]Department of Cardiovascular Medicine, Wellcome Trust Center for Human Genetics, Oxford, UK; [3]Institute of Physiology, Academy of Sciences of the Czech Republic, Prague, Czech Republic; and [4]Institute of Anatomy, First Faculty of Medicine, Charles University, Prague, Czech Republic

Received 6 June 2011; revised 16 November 2011; accepted 18 November 2011; online publish-ahead-of-print 23 November 2011

Time for primary review: 21 days

Aims The sinus venous myocardium, comprising the sinoatrial node (SAN) and sinus horns (SH), is a region subject to congenital malformations and cardiac arrhythmias. It differentiates from symmetric bilateral mesenchymal precursors, but morphological, molecular, and functional left/right differences are progressively established through development. The role of the laterality gene Pitx2 in this process is unknown. We aimed to elucidate the molecular events driving left/right patterning in the sinus venosus (SV) myocardium by using a myocardial Pitx2 knockout mouse.

Methods and results We generated a myocardial specific Pitx2 knockout model (cTP mice). cTP embryos present several features of Pitx2 null, including right atrial isomerism with bilateral SANs and symmetric atrial entrance of the systemic veins. By *in situ* hybridization and optical mapping analysis, we compared throughout development the molecular and functional properties of the SV myocardium in wt and mutant embryos. We observed that Pitx2 prevents the expansion of the left-SAN primordium at the onset of its differentiation into myocardium; Pitx2 promotes expansion of the left SH through development; Pitx2 dose-dependently represses the autorhythmic properties of the left SV myocardium at mid-gestation (E14.5); Pitx2 modulates late foetal gene expression at the left SH-derived superior caval vein.

Conclusion Pitx2 drives left/right patterning of the SV myocardium through multiple developmental steps. Overall, Pitx2 plays a crucial functional role by negatively modulating a nodal-type programme in the left SV myocardium.

Keywords Pitx2 • Sinus venosus myocardium • Optical mapping • Mouse cardiac development

1. Introduction

In human and mouse embryos, the sinus venosus (SV) myocardium includes the sinoatrial node (SAN) and the sinus horns (SH), from which the myocardial walls of the left superior caval vein (LSCV) and right superior caval vein (RSCV) will differentiate.[1,2] SV-derived structures generate great medical interest, since various congenital malformations[3] and arrhythmias[4,5] have their origin in this region. The molecular mechanisms underlying SV genetic origin and the molecular pathways driving its cellular differentiation have been extensively investigated.[6]

The SV myocardium is originated by a single genetic cell lineage, derived from Tbx18-positive/Nkx2.5-negative mesenchymal precursors, originally (E8.25 in mouse) located at the lateral rims of the splanchnic mesoderm.[7] The molecular mechanisms driving progressive reorganization from bilateral SV mesenchymal precursors into a lateralized SAN and an asymmetrically structured SH myocardium have not yet been clarified.

At early developmental stages, the entire SV region presents pacemaker properties.[8–11] Starting at mid-foetal stages, the SH myocardium, but not the SAN, progressively matures to obtain a molecular phenotype comparable to the atrial working myocardium.[7] Eventually,

* Corresponding author. Tel: +39 049 8276031; fax: +39 049 8276040, Email: campione@bio.unipd.it

in the adult heart, pacemaker activity is confined to the SAN. Mistakes in developmental modulation of this functional maturation programme may be the leading cause for adult SV-originated arrhythmias; however, the genetic mechanisms regulating this process are still not understood.

The homeobox transcription factor Pitx2 has been indicated as a susceptibility gene for atrial arrhythmias in humans[12] and in mice.[13–15] Pitx2 mediates early signalling events into left cardiac morphogenesis,[16] as Pitx2-null embryos present severe cardiac defects including right atrial isomerism (RAI).[17–20] This phenotype was recapitulated by conditional deletion of the gene in second heart field (SHF) progenitors,[21] but not in the developing myocardium;[22] therefore, left cardiac identity is due to Pitx2 action in cardiogenic precursors or at early cardiogenesis. To address this question, we have conditionally inactivated Pitx2 from the onset of cardiomyogenesis. We show here that Pitx2 is required from early cardiomyogenesis to confer left identity to the entire sinoatrial region, including the SV myocardium. Within the SV, left morphological, molecular, and functional identity is achieved through multiple developmental steps, corresponding to distinct actions of Pitx2 on SV cardiomyocytes. Our results highlight the myocardial role of Pitx2 in preventing the onset and maintenance of a nodal-type programme in left SV cardiomyocytes.

2. Methods

2.1 Mouse lines

Pitx2 floxed, Pitx2 constitutive mutant, cTnT Cre, and R26R transgenic mouse lines have previously been described;[17,22–24] mice were kept on a C57Bl6/J background. DNA for PCR screening was extracted with DNeasy Blood and Tissue Kit (Qiagen) from tails of anaesthetized mice (Zoletil, 30 mg/kg, ip) and from amniotic sac of embryos isolated after sacrifice of the anaesthetized mother by cervical dislocation. A PCR amplification protocol for Pitx2 and Cre has been described.[22]

This study was performed conforming to Guide for the Care and Use of Laboratory Animals described by Directive 2010/63/EU of the European Parliament. Animal work was approved by the Ethics Committee for Animal Experiments of the University of Padua, in compliance with NIH, and carried out in compliance with Italian government guidelines.

2.2 Histology

Stage E8.5, E10.5, and E14.5 embryos were fixed overnight with 4% paraformaldehyde, dehydrated through graded ethanol series, and embedded in paraffin. Sections were cut at 12 μm and processed for haematoxylin and eosin staining.

2.3 *In situ* hybridization

Non-radioactive *in situ* hybridization (ISH) on sections was performed as described previously.[22] RNA probes complementary to mouse Pitx2, Tbx3, Shox2, Hcn4, Tbx18, NKX2.5, Cx40, and the ATP-binding site of myosin heavy chain (MHC) were generated using standard protocols. Images were taken using a Leica DC300 digital camera.

2.4 Real-time PCR

E14.5 hearts were dissected from freshly isolated embryos and stored in liquid nitrogen. Total RNA was extracted using Trizol® (Invitrogen); then cDNA was synthesized using SuperScript III Reverse Transcriptase and random primers (Invitrogen). Amplifications were performed on three samples for each genotype using an iQ5 Real-time machine (Bio-Rad); Pitx2 expression values were normalized with the housekeeping genes GAPDH and β-actin. Primer sequences are reported in the Supplementary material online.

2.5 Magnetic resonance imaging analysis

Magnetic resonance imaging was performed on a horizontal 9.4 T/21 cm VNMRS Direct Drive MR system (Varian Inc., Palo Alto, CA, USA) on E14.5 embryos, as described previously.[25]

2.6 Optical mapping

E14.5 embryos were dissected on ice, their heart removed and stained for 10 min with di-4-ANEPPS (Invitrogen) at 4°C. Then, they were pinned, their dorsal part up, on the bottom of a silicone-lined copper dish filled with oxygenated Tyrode-HEPES solution (pH 7.4), with Blebbistatin added, positioned on a temperature-controlled stage (TH 60, 37°C) of an upright epifluorescence microscope (Leica DML-FS). To accommodate the entire heart, 4× and 10× water-dipping objectives and 0.63 photo tubes were used. Recordings were performed in the dorsal view, with the posterior atrial wall facing the optical apparatus. See also the Supplementary material online.

2.7 Statistical analysis

Atrial activation and propagation patterns could be grouped into three categories, each having a minimum of 10 hearts; differences between groups were analysed using Pearson's χ^2-test. Atrial activation times were calculated as an average between 4× and 10× recordings of each sample when these numbers did not differ more than 2 ms. Data are presented as mean ± standard deviations; comparisons between wt, cTP het, and cTP ko values were performed using a two-tailed Student's *t*-test; *P*-values <0.05 were considered significant.

3. Results

3.1 Characterization of the cTnT Cre-Pitx2 mouse line

We investigated the myocardial role of Pitx2 with a conditional ko approach by crossing Pitx2 floxed mice ($Pitx2^{loxP/loxP}$)[14] with Troponin T (TnT) Cre deletor mice, which are active from early cardiomyogenesis[23] (*Figure 1A*).

Myocardial deletion of one loxP allele (TnT Cre; $Pitx2^{loxP/wt}$ = $Pitx2\ het_{myo}$, from here onwards referred as cTP het) resulted in viable and fertile offspring. We then crossed cTP hets with $Pitx2^{loxP/loxP}$ mice to generate cTP ko mice. No cTP ko pups were identified at post-natal day (P)3; however, their embryonic distribution at E17.5 was according to the Mendelian ratio (data not shown); we concluded that the cTP ko phenotype is not viable.

Quantification of Pitx2 mRNA in E14.5 wt and mutant hearts indicated a dose-dependent reduction in Pitx2 transcript levels (see Supplementary material online, *Figure S1*). Histological and MRI analysis of E14.5 cTP embryos did not reveal obvious morphological defects in cTP hets (see Supplementary material online, *Figure S2A*; *Table 1*), whereas the ko hearts presented a complex phenotype (*Figure 1B* and *C*, and *Table 1*): the left auricle was identical in shape and orientation to the right one (*Figure 1B*, d–f) and the atrial septum was reduced or totally absent (ASD) (*Figure 1B*, e); additionally, we detected bilateral SAN and venous valves, bilateral caval vein (CV) entrance into the atria, and drainage of the inferior caval vein (ICV) and pulmonary vein (PV) into the medial part of the common atrium (*Figure 1B*, d–f). Overall, these are typical features of RAI; therefore, we concluded that early myocardial Pitx2 action is required to confer left atrial (LA) identity.

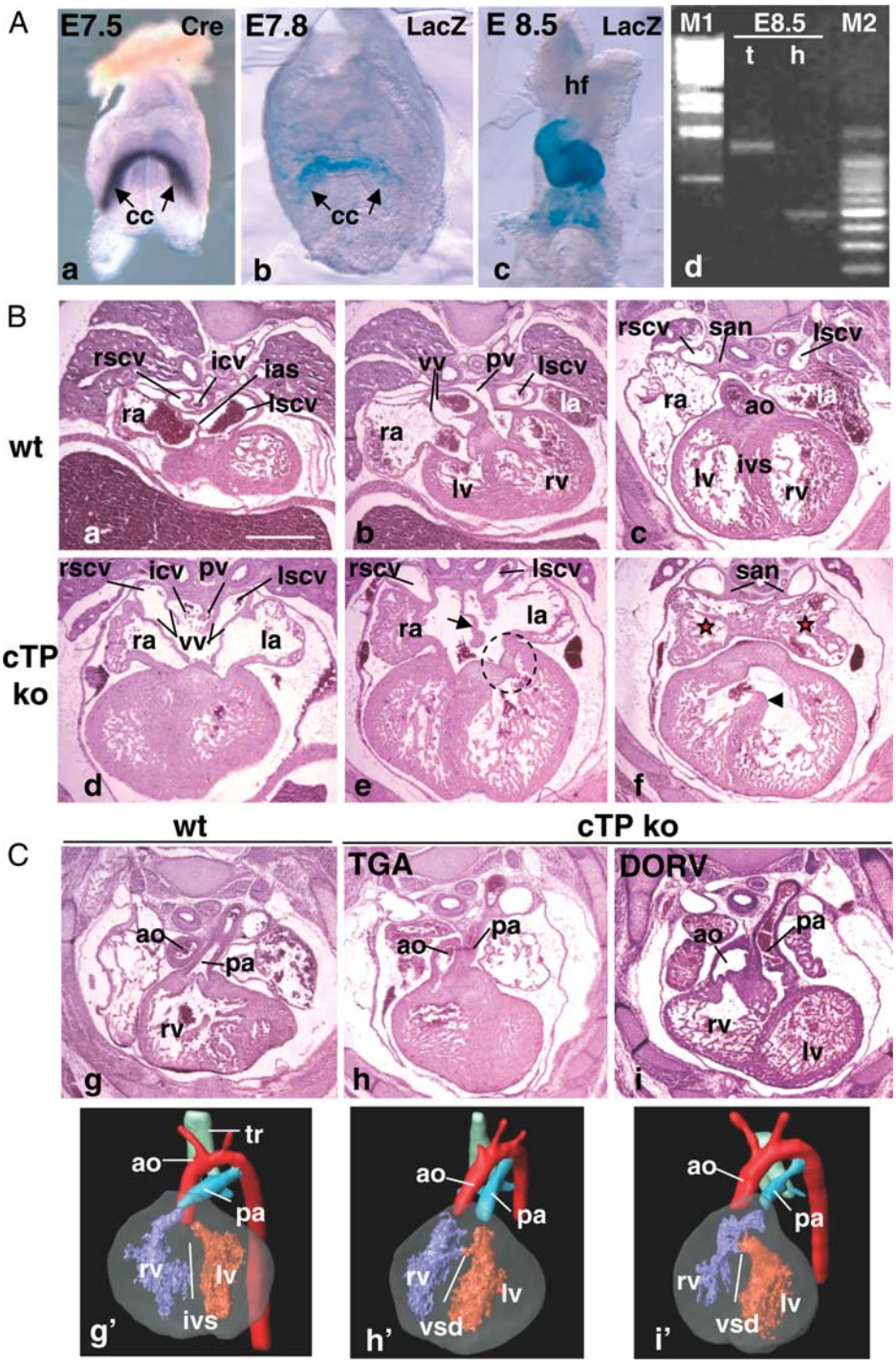

Figure 1 cTP mouse line characterization. (*A*) TnT Cre line characterization. Onset of Cre mRNA expression visualized by whole-mount ISH (Cre) (a) and onset of Cre activity (b), assessed by crossing TnT Cre with R26R mice (LacZ); (c) by E8.5 Cre activity is visible in the entire heart; (d) Pitx2 PCR on genomic DNA from trunk (t) and isolated heart (h) of a E8.5 cTP ko embryo to assess cardiac-specific recombination at the Pitx2 locus. M1: Lambda phage DNA, BstEII digested; M2: 100 bp ladder. From the embryonic trunk only the floxed allele is amplified (1232 bp band). In the corresponding heart only the 500 bp band is visible, indicating complete Cre-driven recombination.[22] (*B* and *C*) H/E staining and MRI analysis of E14.5 wt and cTP ko hearts. Note that the sinoatrial region of the ko hearts presents the morphological features of RAI. Red stars in (f) show symmetrical pectinate muscles arrangement in atria. (e) Arrow indicates ASD, dotted circle indicates abnormal shape of the left atrioventricular valve; (f) arrowhead indicates VSD. (*C*) (h and i) Ventriculo-arterial alignment defects in cTP ko and (h′ and i′) their corresponding 3D MRI reconstructions. Cc, cardiac crescent; hf, headfolds; ias, interatrial septum; la, ra, left and right atrium; ivs, interventricular septum; san, sinoatrial node; lscv, rscv, left and right superior caval veins; vv, venous valves; icv, inferior caval vein; pv, pulmonary veins; lv, rv, left and right ventricle; ao, aorta; pa, pulmonary artery; tr, trachea. Scale bar: 0.5 mm.

Table 1 Characterization of cardiac defects in wt and cTP mutants by MRI analysis

	wt ($n = 7$)	het ($n = 5$)	ko ($n = 5$)
Heart position			
Left-sided	6	5	0
Right-sided	0	0	5
Midline	1	0	0
Apex direction			
Left	6	0	0
Right	0	5	4
Down	1	0	1
Atrial shape			
No ASD, no RAI	7	5	0
ASD plus RAI	0	0	5
ICV drainage			
Into RA	7	5	0
Into common atrium	0	0	5
PV drainage			
Into LA	7	5	0
Into common atrium	0	0	5
AV junction			
Normal	7	5	0
Abnormal	0	0	5
Ao exit			
From LV	7	5	0
From RV	0	0	5
PA exit			
From RV	7	5	1
From LV	0	0	4
TGA	0	0	4
DORV	0	0	1

Additionally, in the cTP ko embryos, we detected abnormal atrioventricular junction with malformed left atrioventricular valves (*Figure 1B*, e), ventricular septal defects (VSD), and abnormal ventriculoarterial alignment, resulting in transposition of the great arteries (TGA) and double outlet right ventricle (DORV) (*Figure 1C* and *Table 1*).

To get insights into the myocardial role of the gene, we histologically compared Pitx2 constitutive mutants ($Pitx2^{wt/-}$ and $Pitx2^{-/-}$). E14.5 $Pitx2^{wt/-}$ embryos were normal, except one sample that presented mild VSD (see Supplementary material online, *Figure S2B* and *Table S1*). This indicates a differential sensitivity to Pitx2 gene dosage within the developing heart, the ventricles being more sensitive than the atria. In line with previous data,[18] E14.5 $Pitx2^{-/-}$ displayed RAI (see Supplementary material online, *Figure S2D*) and strong impairment in atrioventricular canal (AVC) and ventricular remodelling, resulting in common AVC (see Supplementary material online, *Figure S2E*), atrioventricular valve defects, severe VSD, and ventriculoarterial alignment defects (see Supplementary material online, *Figure S2F*). Additionally, the ventricular compact wall was thinner (see Supplementary material online, *Figure S2F*). Altogether, cTP and Pitx2 mutant hearts present some morphological differences outside the sinoatrial region (see Supplementary material online, *Table S1*); therefore, myocardial Pitx2 action is sufficient to confer the LA identity but not to drive complete cardiac morphogenesis.

3.2 Pitx2 prevents the expansion of left-SAN precursors cells as they differentiate in myocardium

ISH analysis (*Figure 2*) showed that in cTP ko embryos, both SANs were myocardialized and correctly expressed the nodal differentiation and functional markers Tbx18, Tbx3, Shox2, and Hcn4, but not the chamber myocardium markers Nkx2.5 and CX40.[7,26] Thus, we decided to investigate the role of Pitx2 in the earliest events of asymmetric right-SAN (R-SAN) formation.

SAN cardiomyocytes constitute a subpopulation of the SV myocardium derived from Tbx18 mesenchymal precursors, which at E8.5 are symmetrically located at the lateral rims of the splanchnic mesoderm,[26] flanking the proepicardial organ (*Figure 3A*, arrows). At the most lateral borders, SAN precursors can be identified by the co-expression of the SHF marker Isl1;[27] the left portion of the SV mesenchyme, including left-SAN (L-SAN) precursors, additionally co-expresses Pitx2 (*Figure 3A*). In E10.5 wt embryos, the embryonic SAN structure is right-sided and can be identified as a thickening of Isl1- and Tbx18-positive myocardial cells at the border between the RSCV and the RA[7] (*Figure 3B*), while the corresponding region on the left side is not myocardialized (*Figure 3B*). On the contrary, in E10.5 cTP ko embryos, the borders between the CVs and atria were both myocardialized and co-expressing Isl1 and Tbx18, thus indicating the presence of a second L-SAN, which presented a correct molecular pattern (data not shown).

The presence of an ectopic myocardial structure in the cTP ko embryos indicates that early left Isl1/Tbx18-positive SAN cardiomyocytes have expanded bilaterally. We conclude that Pitx2 prevents the expansion of the left Isl1/Tbx18-positive SAN precursors as they differentiate in cardiomyocytes.

3.3 Pitx2 modulates the developmental programme of the LSCV

We then investigated the role of Pitx2 in the left SH-derived CV myocardium. In E14.5 wt embryos, ICV entrance is positioned on the right (*Figure 1B*, a, and dotted circles in *Figure 4A*, b), at the site of RSCV confluence with the coronary sinus. Conversely, in the cTP ko, ICV enters medially into the common atrium (*Figure 1B*, d), the coronary sinus is absent, and CVs run symmetrically (*Figure 4A*, b and c); this has been highlighted by ISH with the hyperpolarization-activated channel Hcn4, which at this stage presents SV-wide expression. We conclude that symmetric organization of the CVs is due to the lack of Pitx2-dependent early left cardiomyocyte expansion into the coronary sinus,[2,28] which is missing in the cTP ko.

The SH myocardium will progressively expand and form the proximal myocardial cuff of CVs by E12.5;[1] we wondered if Pitx2 could affect LSCV cardiomyocyte expansion at later stages. In E14.5 wt embryos, LSCV myocardium is restricted to its most proximal portion; these SV cardiomyocytes are Pitx2-positive (*Figure 4B*, a–d), and at E17.5, they extend more distally (*Figure 4B*, e and f). This was not observed in the cTP ko (*Figure 4B*, g); therefore, we concluded that Pitx2 promotes LSCV cardiomyocyte expansion both at early and late developmental stages.

We then tested whether Pitx2 could modulate LSCV transcriptional properties. A progressive shift towards an atrial-type gene expression programme is started in the CV myocardium at E14.5 and is clearly visible by E17.5:[7] Nkx2.5 is up-regulated in the SAN and

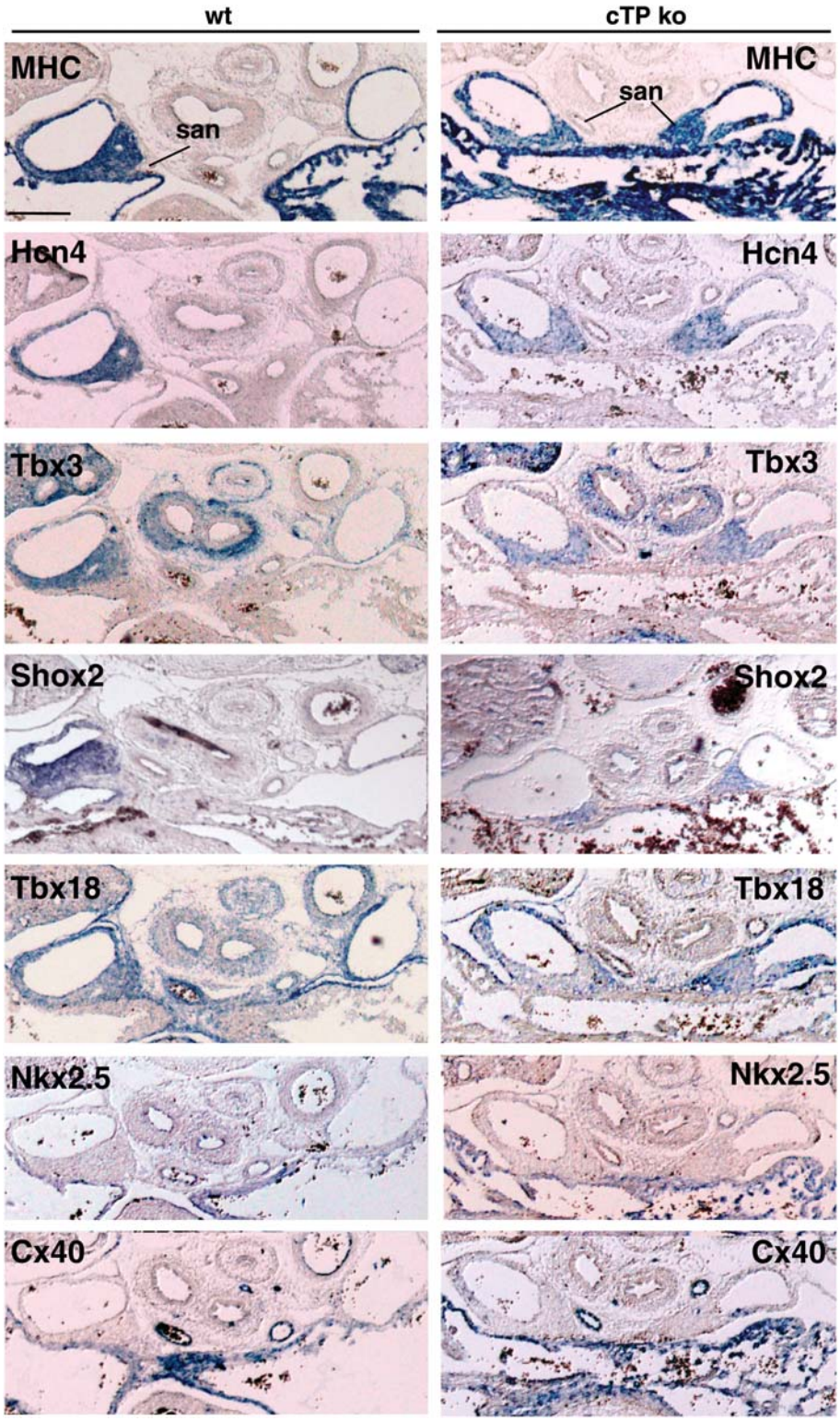

Figure 2 The L-SAN of the cTP ko presents correct molecular pattern. ISH analysis of E14.5 wt and cTP ko embryos to assess L-SAN molecular signature. Note SAN expression of MHC, Hcn4, Tbx3, Shox2, Tbx18, and the negative staining with Nkx2.5 and CX40 antisense probes. Scale bar: 0.2 mm.

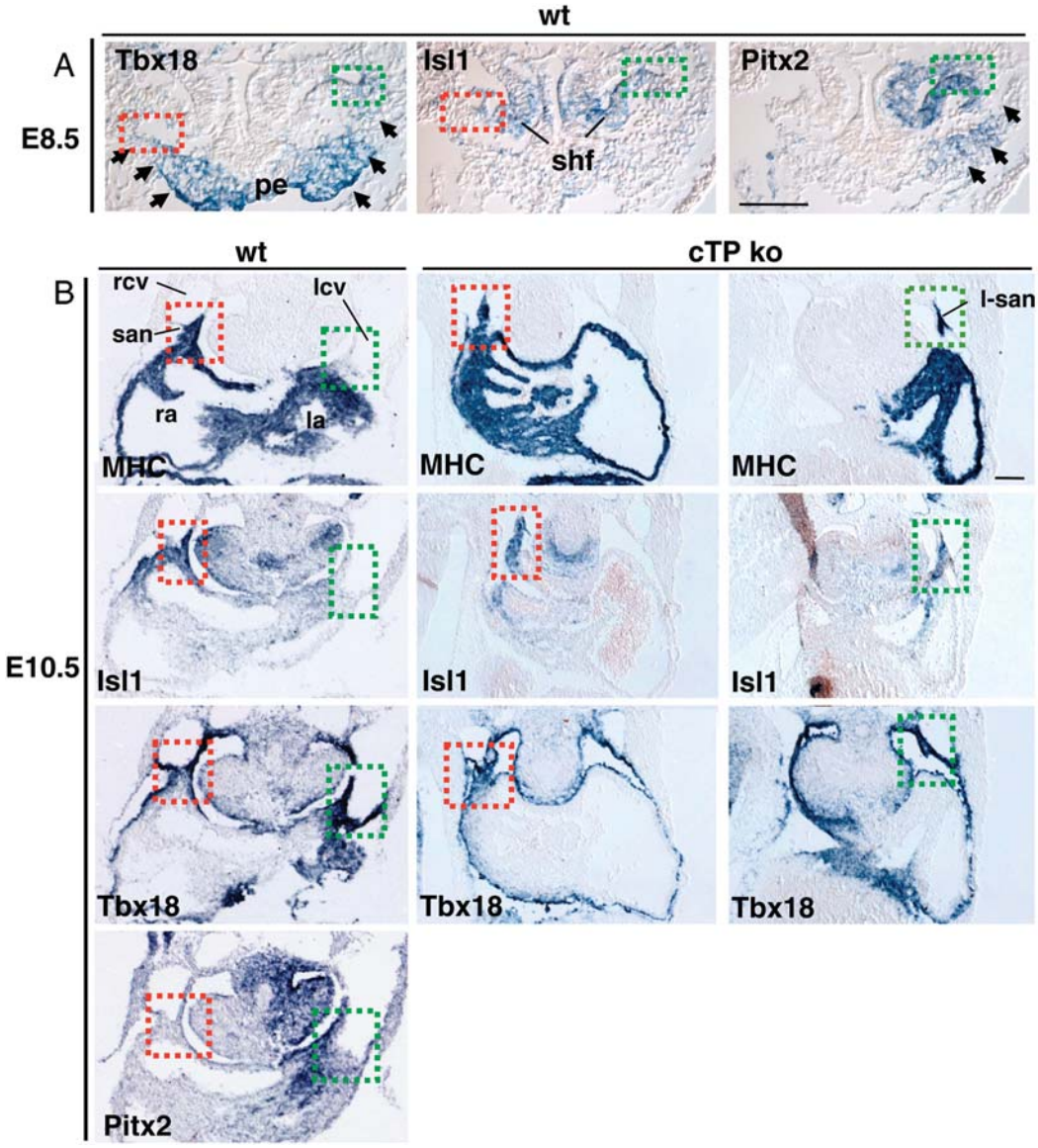

Figure 3 L-SAN mesenchymal precursors differentiate and expand into the left ectopic SAN of the cTP ko. (*A*) ISH of E8.5 wt embryos shows Tbx18 expression in SV mesenchymal precursors (arrows) and proepicardial organ (pe); Isl1 is bilaterally expressed in the second heart field (shf) overlapping Tbx18 at the SAN progenitors (dotted squares: green, right; red, left). Pitx2 expression delineates the left SV domain (arrows), including L-SAN progenitors (green dotted square). (*B*) At E10.5, cTP ko embryos present bilateral MHC, Isl1- and Tbx18-positive regions at the borders between left and right cardinal veins (lcv, rcv) and atria, identifying the early differentiated bilateral SAN. Scale bar: 0.1 mm.

CVs, whereas Cx40 is up-regulated exclusively in CVs, without obvious left–right differences (*Figure 4C*, a and c); concomitantly, Hcn4 expression is down-regulated exclusively in the LSCV (red arrows in *Figure 4C*, e). Since Hcn4 is responsible for the generation of pacemaker potentials,[29] this indicates that the late foetal RSCV myocardium retains a more nodal-type phenotype than the LSCV. In the cTP ko, the LSCV atrial gene programme was restricted to the most proximal, myocardialized region (red bars in *Figure 4C*, b, d, and f); moreover, it was incomplete since Nkx2.5 and Cx40 expression was unaffected, while Hcn4 expression was not down-regulated (*Figure 4*C, f). As a result, in the cTP ko, the nodal-type molecular profile was retained bilaterally.

3.4 Pitx2 represses left pacemaker activity in the SV-derived myocardium of E14.5 embryos

The functional properties of mid-foetal mouse hearts are as yet quite elusive. We approached this problem and investigated the atrial electrophysiology of E14.5 wt and cTP mutant hearts by optical mapping.

In wt hearts ($n = 36$), the site of first activated region was predominantly detected in the RA ($n = 29$; 80%) mainly around the R-SAN region; in a smaller group ($n = 6$; 17%), it mapped medially, in correspondence to the CVs, while in a single sample, impulse origin was left-sided ($n = 1$; 3%) (*Figure 5A*). The direction of action potential (AP)

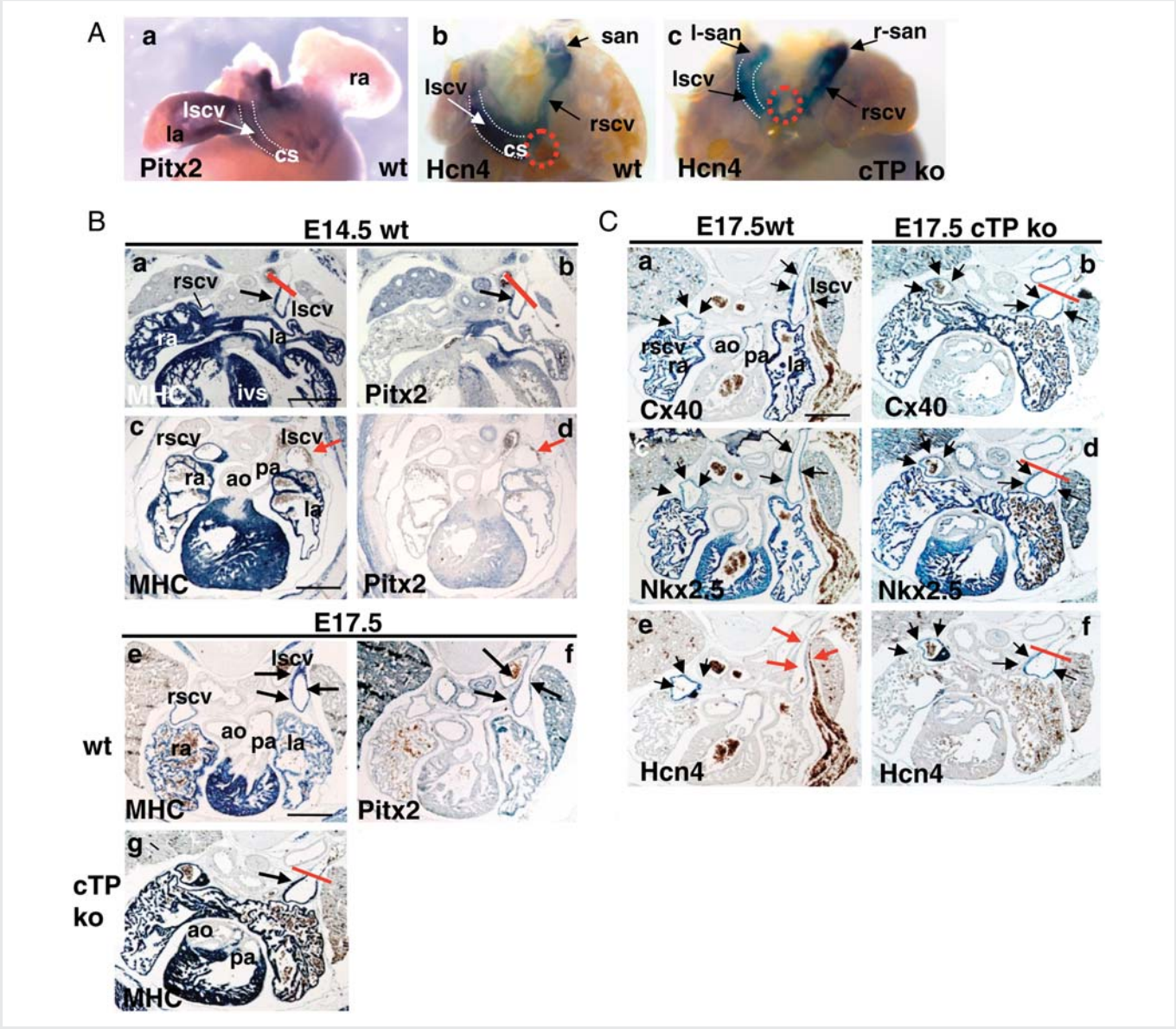

Figure 4 Pitx2 modulates the LSCV developmental programme. (*A*) Whole-mount ISH of E14.5 wt hearts (dorsal view) showing expression of Pitx2 in LA and LSCV (a) and of Hcn4 in the entire SV myocardium, including the SAN (b). Red dotted circles (b and c) indicate ICV entrance. Note the absence of coronary sinus (cs) and symmetric CVs arrangement in the cTP ko (c). (*B*) Correlation between Pitx2 expression and MHC extension in the LSCV. In E14.5 wt hearts, note Pitx2 and MHC co-expression in the LSCV in four-chamber view sections (a and b) but not more distally (c and d); red bar indicates the border of probe detection. In E17.5 wt, MHC and Pitx2 expression is visible more distally (e and f), but in the cTP ko distal MHC extension is impaired (red bar in g). (*C*) The atrialization programme is partially impaired in the cTP ko. E17.5 wt embryos bilaterally express Cx40 (a) and Nkx2.5 (c) in the CVs, while Hcn4 expression is strongly down-regulated only in the LSCV (red arrows, e). In the cTP ko, Cx40 and Nkx2.5 signals are still present (b and d) in the reduced LSCV myocardial domain. Note the absence of Hcn4 down-regulation in the LSCV (black arrows in f). Scale bar: 0.5 mm.

propagation was mostly sequential from RA to LA ($n = 28$; 78%), but synchronous bilateral propagation ($\approx$ 1–2 ms difference between LA and RA activation times) was also recorded ($n = 8$; 22%) (*Figure 5B*). Therefore, in wt embryos, both the site of first atrial breakthrough and the AP direction of propagation presented a variable distribution within the SV region with a pronounced right-sided dominance.

In the cTP ko hearts ($n = 10$), we found a reduced percentage of samples presenting right-sided ($n = 6$; 60%) or mid-dorsal ($n = 1$; 10%) impulse initiation, and higher incidence of left-originating breakthroughs ($n = 3$; 30%). Bilateral AP propagation was not detected, whereas a new left-to-right direction of impulse spread was present ($n = 4$; 40%). In a single ko sample, a double concomitant impulse firing was observed, with the two earliest activated sites located in the R- and L-SAN regions (*Figure 5C*), thus indicating that the L-SAN is functional. The cTP het samples ($n = 17$), although morphologically normal, presented an intermediate behaviour both in pacemaker location distribution and in the impulse propagation profile (*Figure 5A* and *B*). Heart rate did not significantly differ

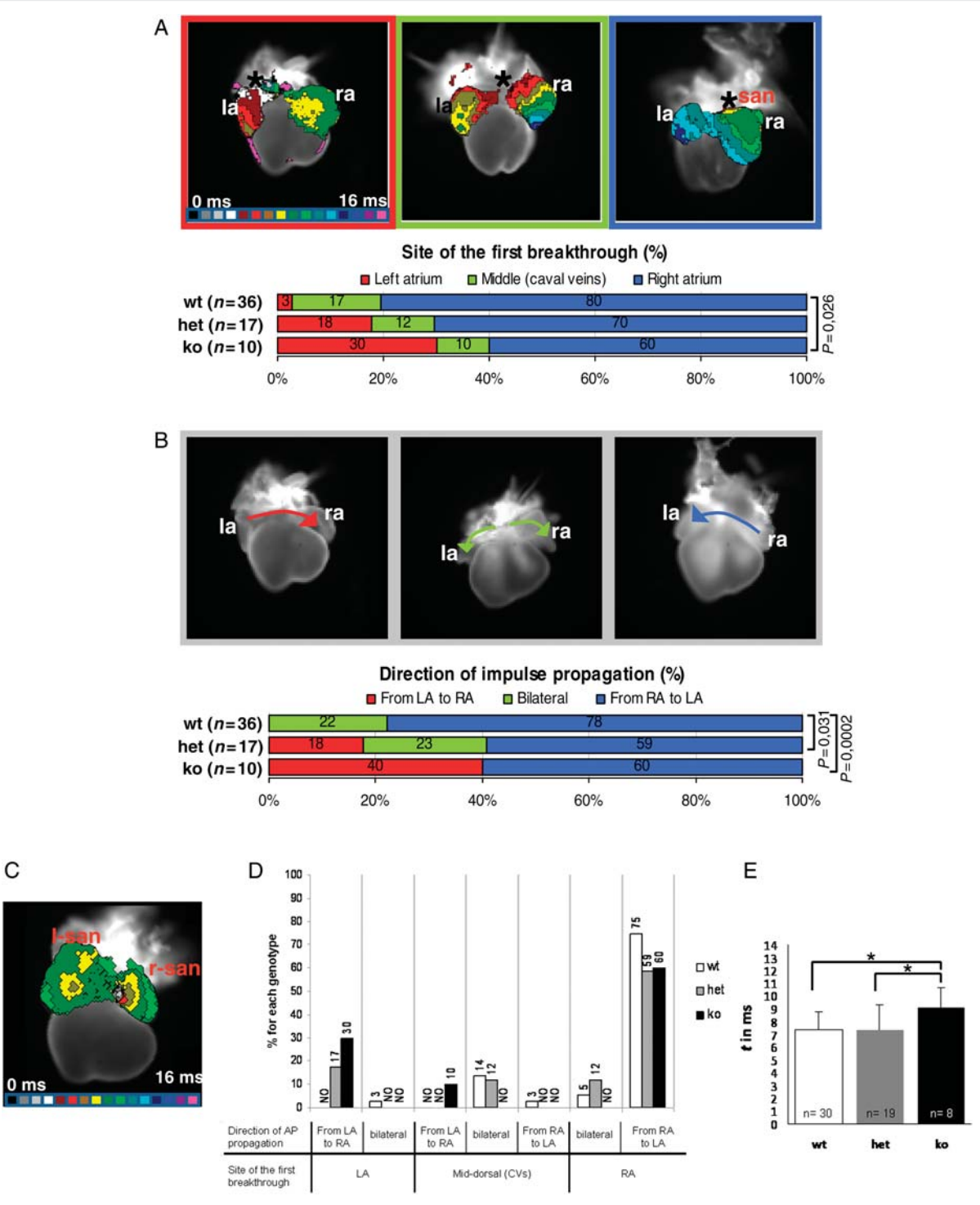

Figure 5 Pitx2 represses left pacemaker activity within the SV myocardium of E14.5 embryos. (*A*) Site of first breakthrough. Top: prototypical maps (dorsal view) showing the three main atrial activation patterns recorded in isolated E14.5 hearts by optical mapping. The earliest activated region is indicated with an asterisk. Isochronal lines, delimiting regions activated within the same time frame, are spaced at 1 ms intervals; colour progression visualizes the advancing activation wavefront. Below: diagram showing the distribution of the activation patterns in the three genotypes. *n* = classified samples. (*B*) Direction of impulse propagation. Top: three representative examples of observed impulse propagation patterns; arrows depict the direction of electrical activation spread. Below: diagram illustrating pattern distribution within the genotypes. *P*-values <0.05 are indicated. (*C*) The L-SAN is functional. Activation map of a cTP ko heart showing the almost synchronous activation of the two SANs. (*D* and *E*) Atrial conduction properties in E14.5 wt and cTP mutants. (*D*) Correlation between the site of first atrial breakthrough and direction of impulse propagation. Columns indicate the combined distribution of atrial activation and propagation patterns within genotypes. Data are expressed as percentages; NO, never observed. (*E*) Atrial activation times. Data are presented as averages ± standard deviations; $*P < 0.05$.

among genotypes (wt: 102 ± 24, het: 91 ± 36, ko: 104 ± 42; $P > 0.05$). Movies of representative activation and propagation patterns are presented as Supplementary material online.

In conclusion, our optical mapping analyses have revealed some functional plasticity in E14.5 hearts, which display pacemaker activity at both the R-SAN and CVs. In wt hearts, SV-wide capacity to generate the first electrical activity is mainly restricted to the right side where the SAN is located; when Pitx2 gene dosage is reduced (cTP het) or its action is lacking (cTP ko), a left pacemaker potential is progressively uncovered. Therefore, Pitx2 prevents the occurrence of left pacemaker activity in the SV myocardium in a dose-dependent way, thus restricting impulse generation to its right side.

Moreover, correlation between pacemaker location and AP spread direction (*Figure 5D*) demonstrated that given a site of impulse initiation, atrial propagation patterns are different in the three genotypes, indicating differences in their conduction properties. In line with this observation, we found that time of atrial impulse propagation (*Figure 5E*) is significantly higher in cTP ko hearts compared with wt and het (wt: 7.3 ms; het: 7.3 ms; ko: 9.0 ms).

4. Discussion

4.1 The myocardial role of Pitx2

Here, we have presented the outcome of Pitx2 deletion from the onset of cardiomyogenesis. At the morphological level, we found that the cTP ko partially recapitulates the cardiac phenotype of Pitx2 constitutive nulls. In particular, RAI was detected in both models, thus indicating that Pitx2 action within the myocardium is sufficient to confer LA identity.

Additionally, the comparative analysis of cTP and constitutive mutant embryos has shown that unlike the sinoatrial region, the AVC and ventricles are more severely affected in Pitx2 constitutive mutants, indicating that morphogenesis of these regions is extremely sensitive to Pitx2 dosage. Moreover, it has uncovered that Pitx2 function is additionally required in precardiac cells of the venous and arterial poles contributing to those regions and/or in early cardiomyocytes before E8.5, when cTnT Cre-driven recombination is complete (*Figure 1A*).

We have also shown that the SV myocardium is molecularly left/right patterned through multiple developmental steps. A later myocardial deletion of Pitx2 with α-MHC Cre driver mice had resulted in molecular atrial isomerism in the absence of any morphological alterations;[22] at the light of this previous result, we propose that the molecular features of the cTP hearts are not the indirect consequence of the earlier Pitx2 deletion, but correspond to a specific and distinct action of Pitx2 on SV cardiomyocytes.

4.2 Opposite effects of Pitx2 within the left SV myocardium: a regional-specific differential transcriptional modulation?

We have shown here that myocardial loss of Pitx2 leads to symmetrical morphological organization of the CVs, absence of the coronary sinus, and reduced expansion of LSCV myocardium. These results suggest that Pitx2 promotes the higher proliferation and/or migration rate in Tbx18-derived cardiomyocytes of the left SH from early to late foetal stages (*Figure 6*). On the other hand, myocardial loss of Pitx2 leads to the presence of a novel L-SAN, visible from its onset; therefore, we conclude that Pitx2 prevents the expansion of the left Isl1/Tbx18 + SAN precursors at the onset of their differentiation into nodal cells. Thus, Pitx2 seems to exert an opposite role on SH and SAN cardiomyocytes (*Figure 6*).

SH differentiate through progressive recruitment of Tbx18-positive mesenchymal precursors, their myocardial differentiation, and subsequent proliferation.[1] SAN mesenchymal precursors additionally co-express Isl1,[27] thus having features of both SHF (Isl1+) and SV (Tbx18+) progenitors. Isl1 promotes the proliferation of cardiogenic precursors;[30] since its expression is selectively retained in the SAN[7,31] through early development, it might exert a similar function also in nodal cardiomyocytes. It is possible that Pitx2 could differentially modulate Tbx18 and Isl1 transcriptional action in the left SV-derived cardiomyocytes; however, the characterization of its molecular mechanisms of action still requires additional analysis.

4.3 Pitx2 restricts nodal conductive properties to the right SV region: implications for adult heart disease

In the adult heart, pacemaker activity is restricted to the SAN as shown by Hcn4 expression,[32] crucial for this function.[29] Conversely, broader Hcn4 expression in the embryo[7] suggests the existence of wider areas with pacemaker potential, in line with several functional studies performed in chick[8,10,11] and in mouse pre-early somite embryos.[9] Functional characterization of mid-foetal mouse hearts has so far been elusive.

Our optical mapping analyses have shown that mid-foetal hearts present a heterogeneous profile of pacemaker activity originating within the SV, thereby revealing some functional plasticity, which can be modulated by Pitx2. In this respect, the intermediate functional properties of the cTP hets, morphologically normal, must be solely due to a Pitx2 dose-dependent modulation of SV molecular properties (*Figure 6*). The capacity of Pitx2 to inhibit the expression of transcripts crucial for the SAN programme in developing and adult atria has been shown previously.[13] Our results additionally highlight the importance of a correct Pitx2 gene dosage for repressing the LSCV autorhythmic potential, in order to restrict pacemaker activity to the SAN.

Critical for confinement of pacemaker activity to the adult SAN is the onset, at mid-foetal stages, of a novel genetic programme in CV myocardium, which progressively acquires a molecular phenotype comparable to the atrial working myocardium.[7] Crucial for this developmental programme is the transcriptional left down-regulation of pacemaker channel Hcn4 which, as we have shown here, is Pitx2-dependent.

Atrial arrhythmias are devastating diseases of the adult heart caused by ageing, acquired diseases, or genetic defects. Arrhythmogenic foci are mostly located at the PVs[33] or in left SV-derived structures, such as the coronary sinus or LSCV.[4,5] Ectopic pacemaker foci in the left SV myocardium might occur if the developmental programme repressing nodal properties of the left SV structures does not occur completely, or alternatively, if an embryonic 'left' programme is reinitiated there. Our results suggest that proper regulation of Pitx2 dosage in the left SV is crucial to prevent this process. An additional role of Pitx2 in other left arrhythmogenic areas, such as the PV, cannot be ruled out and is currently being explored.

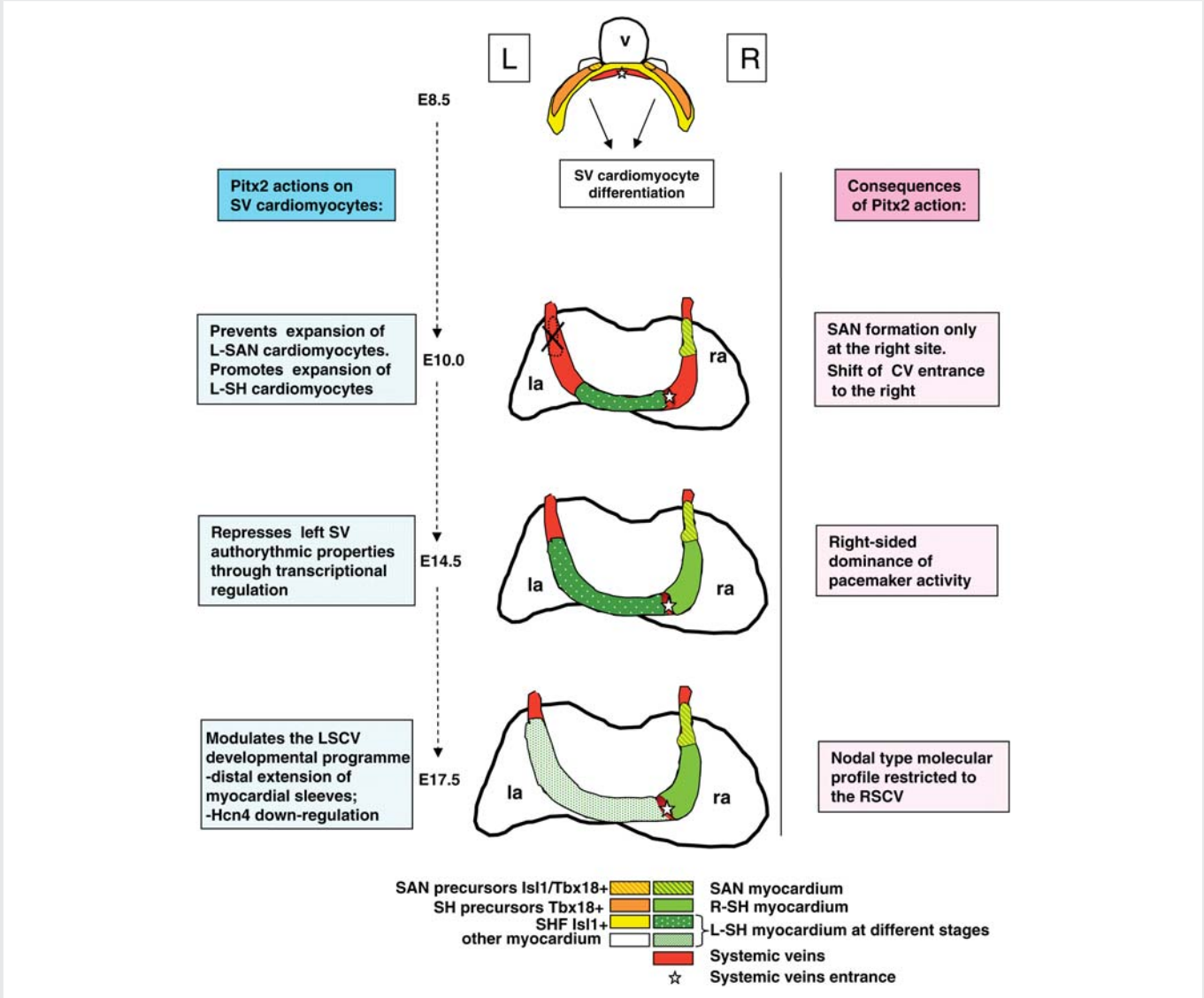

Figure 6 Proposed model for Pitx2 action in left SV cardiomyocytes; hearts are shown in the dorsal view. Left columns summarize the temporal actions of Pitx2 in the developing SV region; right columns summarize the resulting morphogenetic and functional effects; v, embryonic ventricle; la, ra, left and right atrium.

Genome-wide study populations in humans[12] have indicated PITX2 as a candidate susceptibility gene for atrial arrhythmias, later confirmed by functional studies in adult Pitx2 heterozygous mice.[13–15] Parallel microarray analysis has additionally identified a wide range of Pitx2 transcriptionally modulated left targets, possibly mediating its action.[13,14] Future studies will be required to precisely refine their sites of expression and effective role, thereby delineating a Pitx2-dependent anti-arrhythmogenic road map.

Supplementary material

Supplementary material is available at *Cardiovascular Research* online.

Acknowledgements

We thank Kai Jiao for providing cTnT Cre mice, Marta Martin and Giulia Rainato for initial contribution with experiments, and Anne Picard and Sandra Furlan for support with real-time PCR analysis.

Conflict of interest: none declared.

Funding

This work was supported by grants from European Community's Sixth Framework Programme (I.P Project 'Heart repair', n. LSHM-CT-2005-018630) and Telethon Grant n. GGP08112 to M.C.; by Purkinje Fellowship and AV0Z50110509 of the Academy of Sciences of the Czech Republic, Ministry of Education VZ 0021620806 and Grant Agency of the Czech Republic 304/08/0615 to D.S. (David Sedmera). Funding to pay the Open Access publication charges for this article was provided by Telethon.

References

1. Christoffels VM, Mommersteeg MT, Trowe MO, Prall OW, de Gier-de Vries C, Soufan AT *et al.* Formation of the venous pole of the heart from an Nkx2-5-negative precursor population requires Tbx18. *Circ Res* 2006;**98**:1555–1563.
2. Sizarov A, Anderson RH, Christoffels VM, Moorman AF. Three-dimensional and molecular analysis of the venous pole of the developing human heart. *Circulation* 2010; **122**:798–807.

3. Attenhofer Jost CH, Connolly HM, Danielson GK, Bailey KR, Schaff HV, Shen WK *et al*. Sinus venosus atrial septal defect: long-term postoperative outcome for 115 patients. *Circulation* 2005;**112**:1953–1958.
4. Lin WS, Tai CT, Hsieh MH, Tsai CF, Lin YK, Tsao HM *et al*. Catheter ablation of paroxysmal atrial fibrillation initiated by non-pulmonary vein ectopy. *Circulation* 2003;**107**:3176–3183.
5. Katritsis DG, Giazitzoglou E, Korovesis S, Karvouni E, Anagnostopoulos CE, Camm AJ. Conduction patterns in the cardiac veins: electrophysiologic characteristics of the connections between left atrial and coronary sinus musculature. *J Interv Card Electrophysiol* 2004;**10**:51–58.
6. Christoffels VM, Smits GJ, Kispert A, Moorman AF. Development of the pacemaker tissues of the heart. *Circ Res* 2010;**106**:240–254.
7. Mommersteeg MT, Hoogaars WM, Prall OW, de Gier-de Vries C, Wiese C, Clout DE *et al*. Molecular pathway for the localized formation of the sinoatrial node. *Circ Res* 2007;**100**:354–362.
8. Van Mierop LH. Location of pacemaker in chick embryo heart at the time of initiation of heartbeat. *Am J Physiol* 1967;**212**:407–415.
9. Kamino K, Hirota A, Fujii S. Localization of pacemaking activity in early embryonic heart monitored using voltage-sensitive dye. *Nature* 1981;**290**:595–597.
10. Sedmera D, Wessels A, Trusk TC, Thompson RP, Hewett KW, Gourdie RG. Changes in activation sequence of embryonic chick atria correlate with developing myocardial architecture. *Am J Physiol Heart Circ Physiol* 2006;**291**:H1646–H1652.
11. Vicente-Steijn R, Kolditz DP, Mahtab EA, Askar SF, Bax NA, Van Der Graaf LM *et al*. Electrical activation of sinus venosus myocardium and expression patterns of RhoA and Isl-1 in the chick embryo. *J Cardiovasc Electrophysiol* 2010;**21**:1284–1292.
12. Gudbjartsson DF, Arnar DO, Helgadottir A, Gretarsdottir S, Holm H, Sigurdsson A *et al*. Variants conferring risk of atrial fibrillation on chromosome 4q25. *Nature* 2007;**448**:353–357.
13. Wang J, Klysik E, Sood S, Johnson RL, Wehrens XH, Martin JF. Pitx2 prevents susceptibility to atrial arrhythmias by inhibiting left-sided pacemaker specification. *Proc Natl Acad Sci USA* 2010;**107**:9753–9758.
14. Kirchhof P, Kahr PC, Kaese S, Piccini I, Vokshi I, Scheld HH *et al*. PITX2c is expressed in the adult left atrium, and reducing Pitx2c expression promotes atrial fibrillation inducibility and complex changes in gene expression. *Circ Cardiovasc Genet* 2011;**4**:123–133.
15. Chinchilla A, Daimi H, Lozano-Velasco E, Dominguez JN, Caballero R, Delpón E *et al*. PITX2 insufficiency leads to atrial electrical and structural remodeling linked to arrhythmogenesis. *Circ Cardiovasc Genet* 2011;**4**:269–279.
16. Campione M, Steinbeisser H, Schweichert A, Deissler K, van Bebber F, Lowe LA *et al*. The homeobox gene Pitx2: mediator of asymmetric left-right signaling in vertebrate heart and gut looping. *Development* 1999;**126**:1225–1234.
17. Gage PJ, Suh H, Camper SA. Dosage requirement of Pitx2 for development of multiple organs. *Development* 1999;**126**:4643–4651.
18. Liu C, Liu W, Lu MF, Brown NA, Martin JF. Regulation of left-right asymmetry by thresholds of Pitx2c activity. *Development* 2001;**128**:2039–2048.
19. Liu C, Liu W, Palie J, Lu MF, Brown NA, Martin JF. Pitx2c patterns anterior myocardium and aortic arch vessels and is required for local cell movement into atrioventricular cushions. *Development* 2002;**129**:5081–5091.
20. Lu MF, Pressman C, Dyer R, Johnson RL, Martin JF. Function of Rieger syndrome gene in left-right asymmetry and craniofacial development. *Nature* 1999;**401**:276–278.
21. Ai D, Liu W, Ma L, Dong F, Lu MF, Wang D *et al*. Pitx2 regulates cardiac left-right asymmetry by patterning second cardiac lineage-derived myocardium. *Dev Biol* 2006;**296**:437–449.
22. Tessari A, Pietrobon M, Notte A, Cifelli G, Gage PJ, Schneider MD *et al*. Myocardial Pitx2 differentially regulates the left atrial identity and ventricular asymmetric remodeling programs. *Circ Res* 2008;**102**:813–822.
23. Jiao K, Kulessa H, Tompkins K, Zhou Y, Batts L, Baldwin HS *et al*. An essential role of Bmp4 in the atrioventricular septation of the mouse heart. *Genes Dev* 2003;**17**:2362–2367.
24. Soriano P. Generalized lacZ expression with the ROSA26 Cre reporter strain. *Nat Genet* 1999;**21**:532–537.
25. Schneider JE, Böse J, Bamforth SD, Gruber AD, Broadbent C, Clarke K *et al*. Identification of cardiac malformations in mice lacking Ptdsr using a novel high-throughput magnetic resonance imaging technique. *BMC Dev Biol* 2004;**22**:4–16.
26. Blaschke RJ, Hahurij ND, Kuijper S, Just S, Wisse LJ, Deissler K *et al*. Targeted mutation reveals essential functions of the homeodomain transcription factor Shox2 in sinoatrial and pacemaking development. *Circulation* 2007;**115**:1830–1838.
27. Mommersteeg MT, Domínguez JN, Wiese C, Norden J, de Gier-de Vries C, Burch JB *et al*. The sinus venosus progenitors separate and diversify from the first and second heart fields early in development. *Cardiovasc Res* 2010;**87**:92–101.
28. Soufan AT, van den Hoff MJ, Ruijter JM, de Boer PA, Hagoort J, Webb S *et al*. Reconstruction of the patterns of gene expression in the developing mouse heart reveals an architectural arrangement that facilitates the understanding of atrial malformations and arrhythmias. *Circ Res* 2004;**95**:1207–1215.
29. Stieber J, Herrmann S, Feil S, Löster J, Feil R, Biel M *et al*. The hyperpolarization-activated channel HCN4 is required for the generation of pacemaker action potentials in the embryonic heart. *Proc Natl Acad Sci USA* 2003;**100**:15235–15240.
30. Cai CL, Liang X, Shi Y, Chu PH, Pfaff SL, Chen J *et al*. Isl1 identifies a cardiac progenitor population that proliferates prior to differentiation and contributes a majority of cells to the heart. *Dev Cell* 2003;**5**:877–889.
31. Sun Y, Liang X, Najafi N, Cass M, Lin L, Cai CL *et al*. Islet 1 is expressed in distinct cardiovascular lineages, including pacemaker and coronary vascular cells. *Dev Biol* 2007;**304**:286–296.
32. Liu J, Dobrzynski H, Yanni J, Boyett MR, Lei M. Organisation of the mouse sinoatrial node: structure and expression of HCN channels. *Cardiovasc Res* 2007;**73**:729–738.
33. Haïssaguerre M, Jaïs P, Shah DC, Takahashi A, Hocini M, Quiniou G *et al*. Spontaneous initiation of atrial fibrillation by ectopic beats originating in the pulmonary veins. *N Engl J Med* 1998;**339**:659–666.

Mol Cell Biochem (2011) 354:83–96
DOI 10.1007/s11010-011-0808-3

Metabolic characterization of volume overload heart failure due to aorto-caval fistula in rats

Vojtech Melenovsky · Jan Benes · Petra Skaroupkova · David Sedmera · Hynek Strnad · Michal Kolar · Cestmir Vlcek · Jiri Petrak · Jiri Benes Jr · Frantisek Papousek · Olena Oliyarnyk · Ludmila Kazdova · Ludek Cervenka

Received: 19 October 2010 / Accepted: 24 March 2011 / Published online: 5 April 2011

Abstract Metabolic interactions between adipose tissue and the heart may play an active role in progression of heart failure (HF). The aim of the study was to examine changes in myocardial and adipose tissue metabolism and gene expression in a rat HF model induced by chronic volume overload. HF was induced by volume overload from aorto-caval fistula (ACF) in 3-month-old male Wistar rats and animals were studied in the phase of decompensated HF (22nd week). HF rats showed marked eccentric cardiac hypertrophy, pulmonary congestion, increased LV end-diastolic pressure, and intraabdominal fat depletion. HF rats had preserved glucose tolerance, but increased circulating free fatty acids (FFA) and attenuated insulin response during oral glucose challenge. Isolated organ studies showed preserved responsiveness of adipose tissue lipolysis and lipogenesis to epinephrine and insulin in ACF. The heart of HF animals had markedly reduced triglyceride content (almost to half of controls), attenuated anti-oxidative reserve (GSH/GSSG), upregulated HF markers (ANP, periostin, thrombospondin-4), specific signaling pathways (Wnt, TGF-β), and downregulated enzymes of mitochondrial fatty acid oxidation, citric acid cycle, and respiratory chain. Adipose tissue transcription profiling showed upregulated receptor for gastric inhibitory polypeptide. In conclusion, ACF-induced HF model

Electronic supplementary material The online version of this article (doi:10.1007/s11010-011-0808-3) contains supplementary material, which is available to authorized users.

J. Benes
Department of Cardiology and Center for Cardiovascular Research, Institute for Clinical and Experimental Medicine—IKEM, Prague, Czech Republic

P. Skaroupkova · L. Cervenka
Center for Cardiovascular Research, Institute for Clinical and Experimental Medicine—IKEM, Prague, Czech Republic

O. Oliyarnyk · L. Kazdova
Department of Experimental Medicine, Institute for Clinical and Experimental Medicine—IKEM, Prague, Czech Republic

D. Sedmera · F. Papousek
Institute of Physiology, Academy of Sciences of the Czech Republic, Prague, Czech Republic

H. Strnad · M. Kolar · C. Vlcek
Institute of Molecular Genetics, Academy of Sciences of the Czech Republic, Prague, Czech Republic

J. Petrak
First Faculty of Medicine, Institute of Pathological Physiology, Charles University, Prague, Czech Republic

D. Sedmera · J. Benes Jr
First Faculty of Medicine, Institute of Anatomy, Charles University, Prague, Czech Republic

L. Cervenka
Second Faculty of Medicine, Department of Physiology, Division of Physiology, Charles University, Prague, Czech Republic

V. Melenovsky (✉)
Department of Cardiology and Center for Cardiovascular Research, Institute for Clinical and Experimental Medicine—IKEM, Videnska 1958/9, Prague 4 140 21, Czech Republic
e-mail: vojtech.melenovsky@ikem.cz

displays several deregulations of systemic metabolism. Despite elevation of systemic FFAs, myocardial triglycerides are low and insulin levels are attenuated, arguing against a role of lipotoxicity or insulin resistance in this model. Attenuated postprandial insulin response and relative lack of its antilipolytic effects may facilitate intraabdominal fat depletion observed in ACF-HF animals.

Keywords Heart failure · Lipid metabolism · Insulin · Triglycerides · Body composition · Free fatty acids

Introduction

Heart failure is often associated with derangements of systemic and myocardial fat metabolism that may have a role in the disease progression [1–5]. Fatty acids (FA) represent the predominant energetic substrate for the heart, covering 50–70% of myocardial ATP need [2]. The majority of FA supplied to the heart originates from adipose tissue. FA are released from adipocytes by lipolysis and transported in the bloodstream as free FA (FFA). After the entry into a cardiomyocyte, FA is either imported into mitochondria and oxidized or re-esterified into triglycerides (TG) and stored [6].

In chronic HF, excessive fat mobilization and weight loss is associated with poor prognosis [7]. Characteristics of adipose tissue in HF and the mechanisms of adverse effects of fat mobilization on cardiac function remain poorly understood. Circulating FFA are often elevated [8, 9] due to increased levels of prolipolytic hormones (catecholamines, TNF-α, and angiotensin-II) [10] that dominate over of antilipolytic factors, primarily insulin. Elevated circulating FFA can also contribute to insulin resistance [11] that is independently associated with adverse prognosis in HF [12].

Myocardial metabolism in HF is characterized by downregulation of enzymes of β-oxidation of FA and of other mitochondrial enzymes [3, 13, 14]. It has been suggested that imbalance between myocardial FFA delivery and utilization may lead to myocardial FA overload, TG over-accumulation, altered gene transcription due to lipid-responsive regulatory elements [3], and to deposition of toxic lipid intermediates [15] that can promote cardiac dysfunction. Evidence for cardiac "lipotoxicity" was found in obese rats [16], in transgenic animals [17] and in diabetic or obese end-stage HF patients [15]. The extent of myocardial lipid accumulation in HF due to hemodynamic overload, without concomitant diabetes or obesity, has never been addressed even in animal models.

Despite volume overload is clinically common cause or contributing factor of HF, it is far less studied than pressure overload or chronic myocardial infarction. Importantly, mechanisms and consequences of cardiac adaptation may differ according to type of overload [18]. Chronic volume overload due to aorto-caval fistula (ACF) in rats is an established model of chronic HF [19–22]. The creation of ACF leads rapidly to development of compensatory cardiac hypertrophy to maintain elevated, but largely ineffective cardiac output. After long asymptomatic stage, HF signs gradually develop and overt HF is present in 80% of animals at 21st week post-fistula [22]. The ACF-HF model recapitulates many features of human advanced HF, including gradual onset, elevated cardiac filling pressures [21, 23–25], diminished "effective" cardiac output with splanchnic hypoperfusion [21], neurohumoral activation [23], and altered calcium handling with diminished cardiac energetic efficiency [26]. Moravec et al. [14, 27] had documented that myocardial long-chain FA oxidation is impaired in ACF rats [2], but substrate metabolism at the whole body level has not yet been further studied in this model. The aim of the study was to examine changes in myocardial and adipose tissue metabolism and gene expression in a rat HF model induced by chronic volume overload.

Materials and methods (for details see online Suppl. 1)

Chronic heart failure model

Volume overload HF was induced in male Wistar rats (300-350 g) by creating ACF using 1.2 mm needle from laparotomy in general anesthesia, as described previously [19, 22, 28]. The animals were kept on a 12/12-h light/dark cycle, fed normal salt/protein diet (0.45% NaCl, 19–21% protein, SEMED, and CR) and were weighted weekly until the end of the experiment in the 22nd week. The investigation conformed to the NIH Guide for the care and use of laboratory animals (NIH Publication No. 85-23, 1996), Animal protection laws of the Czech Republic (311/1997) and was approved by the ethics committee of IKEM.

Echocardiography and hemodynamics

Echocardiography was performed in general anesthesia with 10 MHz probe (Vivid System 5, GE, USA) 10th week post-ACF. End-systolic and end-diastolic LV volumes were derived by cubic equation [20] and stroke volume as their difference. Relative wall thickness was defined as sum of end-diastolic anterior wall + posterior wall LV thickness, divided by end-diastolic LV diameter. Hemodynamics was measured at the study end (22th week) with 2F micro-manometer catheter (Millar Instruments) inserted into the aorta and LV via carotid artery in general

anesthesia. The presence of ACF was verified from laparotomy and the animals were exsanguinated. The coronary tree of the excised heart was rapidly flushed with cardioplegic solution. The organs were weighted and normalized to body weight or tibial length.

Myocardial morphology and fat staining

Basal portions of the left ventricle were fixed in 4% paraformaldehyde, embedded into TissuTek, cut and stained with Sudan Black for lipids. Staining with anti-α actinin antibody together with Alexa488-conjugated wheat germ agglutinin (WGA) was performed to evaluate myocyte size and proportion of fibrosis. Images were acquired from Olympus BX51 microscope and Leica SPE confocal system and quantitatively analyzed using ImageJ (NIH) software.

Gene expression and GSEA pathway analysis in the myocardial and adipose tissue

Samples of LV tissue and epididymal fat ($n \geq 6$ in each group) were immediately harvested into RNA preserving solution (RNA-Later, Ambiogen, USA). Total RNA was isolated (RNeasy-MicroKit, Qiagen, USA), checked for integrity, amplified, and hybridized on Illumina RatRef-12v1 Expression BeadChip (Illumina, USA). The raw data were analyzed and processed using *beadarray* package of the *Bioconductor*, as described before [29]. Analysis of differential expression was performed with the *Limma* package [30] and annotated against RatRef_12_V1_0_R3_11222119_A.bgx maniphest (Illumina, USA). Cut-off level for differential regulation was set to fold change >2 or <0.5, with Storey $q < 0.01$. The data are MIAME-compliant and are deposited in the ArrayExpress database (accession #: E-MTAB-190). Gene set enrichment analysis (GSEA) was performed on the samples from LV tissue on gene pathways defined by the KEGG database (release 57.0) [31]. Only the pathways with false discovery rate < 0.05 are reported.

Quantitative real-time PCR

Reverse transcription was performed by QuantiTect® Reverse Transcription Kit (QIAGEN Inc., USA). The qRT-PCR was performed on LightCycler 2.0 System using LightCycler® 480 DNA SYBR Green I Master kit (Roche Diagnostics, Germany) and results were analyzed by LightCycler software. Crossing point values were further determined using the *R environment* (R Development Core Team 2007). Detailed description of the analysis and the list of amplicons/primers of target and housekeeping genes are provided in Supplementary file 1 and 3, respectively.

Biochemical analyses

Oral glucose tolerance tests (OGTT, 300 mg glucose/100 g BW after overnight fasting) were performed at the 21st week by sampling tail vein at 0, 30, 60, and 120 min. Serum glucose was measured by enzymatic assay (Pliva-Lachema, CR), FFA with colorimetry (Roche Diagnostics, Germany), and insulin with rat-specific ELISA (Mercodia, Sweden). Tissue TG were measured after N_2 pulverization, and chloroform/methanol extraction with enzymatic assay (Pliva-Lachema, CR) was also used for serum TG. The activity of SOD was analyzed by the reaction of nitrotethrazolium blue reduction and nitrophormasane formation [32]. The reduced (GSH) and oxidized form of glutathione (GSSG) was determined by high performance liquid chromatography with fluorescent detection (Chromsystems, Germany). The level of thiobarbituric acid-reactive substances (TBARS) was determined by the reaction with thiobarbituric acid [33].

Metabolic assessment of isolated adipose tissue

Basal and epinephrine-stimulated epididymal adipose tissue lipolysis was examined during a 2-h in vitro fat tissue incubation in Krebs–Ringer buffer with or without epinephrine (0.25 mg ml^{-1}) as described previously [34]. Lipolysis was quantified as FFA release into the medium. Basal and insulin-stimulated lipogenesis was quantified by incorporation of ^{14}C-U-glucose into neutral, chlorophorm-extracted lipids during 2 h incubation in Krebs–Ringer bicarbonate buffer with or without insulin (250 μU ml^{-1}) as described previously [34].

Statistics

Animals that died during the experiment (18% total mortality including ACF operation) were excluded from the analyses. Sample size for echocardiography was 12–14/group, for other methods 5–8/group. Data are expressed as means ± SD, in graphs as means ± SE. Student's t test statistics was used for comparisons, and P value < 0.05 was considered significant. Gene expression differences were compared with false discovery rate (FDR) and described with Storey's q value.

Results

Echocardiography, hemodynamics, and organ weights

ACF animals had similar growth rate and final body size as controls (Fig. 1). Echocardiography (Table 1) confirmed cardiac enlargement, reduced relative wall thickness (0.33 ± 0.05 vs. 0.45 ± 0.05, $P < 0.001$), mildly reduced

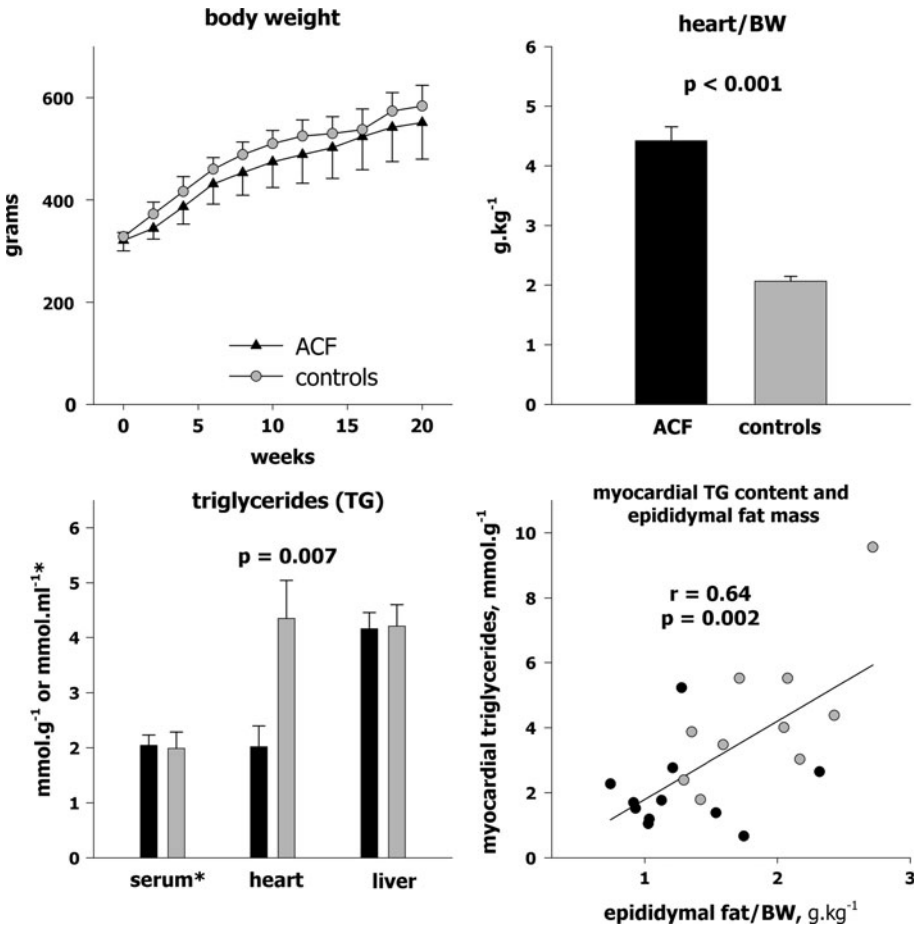

Fig. 1 *Upper panel* Body weight during the course of experiment, and the weight of the whole heart normalized to body weight. *Lower panel* Concentration of triglycerides (*TG*) in heart, or liver tissue and in serum, correlation between myocardial TG content and epididymal fat. *Gray* controls, *black* aorto-caval fistula (*ACF*)

fractional shortening, and markedly increased stroke volume and cardiac output (+196%) in ACF. By the end of experiment (22th week), 65% of ACF animals showed clinical HF signs (lethargy, jagged fur, and labored breathing). Hemodynamics (Table 1) showed similar systemic arterial pressure, LV dP/dt_{max} and maximal LV pressures, but markedly elevated LV end-diastolic pressure (+263%), longer systolic duration (+21%), or LV relaxation time constant τ (+33%), and slower relaxation rate dP/dt_{min} (+24%, $P = 0.07$) in ACF. ACF animals had a marked increase in heart (+148%), lung (+72%), and liver weights (+17%) (Table 2). Despite similar body weights, the ACF group had surprisingly lower epididymal fat pad weight (−29%) (Fig. 6). Subcutaneous (inguinal) fat pad and kidney weights were similar in both groups.

Myocardial morphology and biochemistry

LV mid-wall histology (Fig. 2) showed biventricular myocyte hypertrophy due to myocyte elongation [5], with no increase in morphologic measure of fibrosis (WGA-positive area: ACF: 25 ± 0.8%, sham: 30 ± 4%, $P = 0.39$). Sudan Black staining for lipids, performed to examine possible lipid overload, showed no visible fat vacuoles and no difference in stain intensity (ACF: 205 ± 22, sham 208 ± 23 intensity units, $P = 0.13$). Myocardial TG concentration was by 53% lower in ACF (2.2 ± 1.2 vs. 4.3 ± 2.2 μmol g^{-1}, $P = 0.006$, Fig. 1), but the liver TG content was similar (ACF: 4.2 ± 0.8 vs. 4.2 ± 0.8 μmol g^{-1}, $P = 0.9$). Myocardial TG correlated ($r = 0.64$, $P = 0.002$) with epididymal fat pad weight (Fig. 1). Parameters of redox state and oxidative stress were also analyzed in the myocardium. ACF group had a similar myocardial level of reduced glutathione (GSH: 4.4 ± 1.4 vs. 4.3 ± 0.3 μmol g^{-1}, $P = 0.8$), a trend toward more of oxidized glutathione (GSSG: 0.39 ± 0.11 vs. 0.32 ± 0.03 μmol g^{-1}, $P = 0.12$), and significantly lower redox reserve (GSH/GSSG ratio, Fig. 3) than controls. Superoxide dismutase (SOD) tended to be lower in ACF hearts ($P = 0.07$), and there was no difference in myocardial TBARS concentration ($P = 0.44$) as a marker of oxidative stress.

Myocardial gene expression

Exploratory principal component analysis (PCA) and hierarchical clustering (HC) revealed pronounced

Table 1 Echocardiography and invasive hemodynamics

	Sham	ACF	*P* value
Echocardiography			
Heart rate, s^{-1}	368 ± 39	350 ± 32	0.2
Body weight, g	422 ± 30	427 ± 24	0.6
LV diastolic diameter, mm	7.3 ± 0.4	10.9 ± 0.9	<0.001
LV systolic diameter, mm	4.3 ± 0.5	6.9 ± 0.8	<0.001
Fractional shortening, %	41 ± 2.9	36 ± 3.5	0.002
LV anterior wall thickness in diastole, mm	1.6 ± 0.1	1.8 ± 0.2	0.05
LV posterior wall thickness in diastole, mm	1.6 ± 0.2	1.8 ± 0.2	0.03
RV diastolic diameter, mm	4.0 ± 0.9	5.8 ± 1	<0.001
LV end-diastolic volume, ml	0.38 ± 0.1	1.31 ± 0.3	<0.001
Stroke volume, ml	0.30 ± 0.1	0.96 ± 0.2	<0.001
Cardiac output, ml	110 ± 16	326 ± 64	<0.001
Invasive hemodynamics			
Aortic mean pressure, mmHg	99 ± 25	89 ± 22	0.5
Aortic pulse pressure, mmHg	45 ± 19	46 ± 10	0.9
Maximal LV pressure, mmHg	114 ± 21	120 ± 22	0.6
End-diastolic LV pressure, mmHg	4.1 ± 2.3	14.9 ± 4.6	0.0003
Heart rate, s^{-1}	351 ± 53	338 ± 88	0.8
Systolic time of total cycle, %	48 ± 4	58 ± 7	0.009
dP/dt_{max}, mmHg s^{-1}	7412 ± 2919	8170 ± 3568	0.7
dP/dt_{max}/IP, s^{-1}	112 ± 27	122 ± 35	0.6
dP/dt_{min}, mmHg s^{-1}	−7987 ± 2009	−6053 ± 1550	0.07
LV relaxation constant τ, ms	12 ± 2	16 ± 3	0.006

Values are means ± SD. Echocardiography performed 10th week after ACF, N = 12–14/group. *LV* left ventricle, *RV* right ventricle, *ACF* aorto-caval fistula group. Hemodynamics performed at the end of study. N = 6–8/group, dP/dt_{max} maximal rate of LV pressure increase, *IP* instantaneous pressure, dP/dt_{min} maximal rate of LV pressure decrease

differences in gene expression between groups. Although the variation among ACF animals was large, the samples formed a well-defined and separated cluster. Of 23401 transcripts analyzed, 249 were differentially regulated (fold change >2 or <0.5, $q < 0.01$), 186 upregulated and 63 downregulated in ACF (heat maps in Supplementary file 2). GSEA analysis using KEGG database [31] was used to identify systematic changes of transcription in pathways (Table 4). The list of the most differentially expressed genes ($q < 0.01$, fold change > 3.8 or <0.38) in those pathways are presented in the Table 3. Fatty acid metabolism, oxidative phosphorylation, glycolysis, citric acid cycle, branched amino-acid degradation, and PPAR signaling pathway were the most downregulated pathways. In contrast, pathways of complement cascade, extracellular matrix–receptor interaction, cell adhesion, phagosome/lysosome, and antigen presentation and cell adhesion molecules were the most upregulated. Quantitative RT-PCR confirmed upregulation of heart failure markers (natriuretic peptide precursor A), EC-matrix components (periostin, thrombospondin-4) and components of regulatory WNT1 pathway (WISP2), along with downregulation of enzymes of glycolysis (enolase 3) and FA oxidation (hydroxyacyl-CoA dehydrogenase) (Fig. 4).

Adipose tissue gene expression

Gene expression analysis was also performed in epididymal adipose tissue to identify changes induced by the presence of HF. PCA and HC revealed well-separated clusters of control and ACF rats. As ACF animals showed larger variation, only eight genes were differentially regulated at fold-change level > 2 or <0.5, $q < 0.01$ (all downregulated in ACF). The differences between groups were less pronounced than in myocardial tissue, so a GSEA was not performed. The list of the most differentially expressed genes ($q < 0.01$, fold change >1.5 or <0.5) is presented in Table 5. Full lists of differentially expressed genes and pathways (q or FDR < 0.05) are provided in online (Suppl. 2 and 3).

Oral glucose tolerance test

To assess the dynamics of metabolic substrates in the blood and its coordination by insulin, oral glucose tolerance test

Table 2 Organ weights

	Sham	ACF	*P* value
Body weight, g	487 ± 42	510 ± 37	0.3
Tibia length, mm	42 ± 2	43 ± 0.4	0.4
Heart weight, g	1.05 ± 0.08	2.61 ± 0.25	<0.0001
Heart weight/TL, mg mm^{-1}	2.50 ± 0.11	6.14 ± 0.57	<0.0001
Lung weight, g	1.68 ± 0.27	2.88 ± 0.34	<0.0001
Lung weight/BW, g kg^{-1}	3.44 ± 0.47	5.68 ± 0.88	0.0003
Liver weight, g	14.2 ± 1.1	16.6 ± 2.0	0.03
Liver weight/BW, g kg^{-1}	29.3 ± 1.7	32.4 ± 2.2	0.02
Left kidney weight, g	1.26 ± 0.1	1.26 ± 0.08	0.9
Left kidney weight/BW, g kg^{-1}	2.60 ± 0.2	2.48 ± 0.25	0.4
Right kidney weight, g	1.28 ± 0.1	1.29 ± 0.06	0.9
Right kidney weight/BW, g kg^{-1}	2.63 ± 0.2	2.54 ± 0.23	0.4
Fat compartments			
Epididymal fat pad, g	9.75 ± 1.85	6.90 ± 2.72	0.01
Inguinal subcutaneous fat pad, g	1.05 ± 0.06	0.96 ± 0.69	0.8

Values are means ± SD. 22nd week after ACF-the end of the study. $N = 6$–8/group. *LV* left ventricle, *RV* right ventricle, *TL* tibial length, *BW* body weight

was performed. ACF and controls had similar baseline serum glucose (4.5 ± 0.6 vs. 4.6 ± 0.7 mmol l^{-1}, $P = 0.5$) and insulin (26 ± 20 vs. 37 ± 30 pmol ml^{-1}, $P = 0.25$), but increased serum FFA (1.57 ± 0.3 vs. 1.15 ± 0.2 mmol l^{-1}, $P = 0.001$, Fig. 5). Glycaemia at 30′, 60′, and 120′ ($P = 0.12$; 0.11; and 0.40) and its AUC area (819 ± 101 vs. 761 ± 63 mmol s l^{-1}, $P = 0.2$) were similar between groups. Interestingly, serum insulin response during OGTT was markedly attenuated in HF animals—insulin at 60′and 120′ were significantly lower in ACF (43 ± 27 vs. 105 ± 91, $P = 0.007$; 58 ± 44 vs. 185 ± 151 pmol ml^{-1}, $P = 0.001$). FFA at 60′ OGTT remained elevated in ACF by 63% ($P = 0.0007$).

Adipose tissue metabolism

To understand the mechanism for ACF-associated intraabdominal fat depletion and to assess responsiveness of fat tissue to humoral stimuli, epididymal adipose tissue was examined in vitro. Basal and epinephrine-stimulated of lipolysis was intact in ACF animals. Similarly, the lipogenesis was normal both at baseline and after insulin stimulation (Fig. 6), indicating preserved responsiveness of adipocytes.

Discussion

Presented study revealed several specific, previously not described metabolic abnormalities in rats with HF due to ACF. The heart of HF animals had diminished redox reserve (GSH/GSSG ratio), upregulated HF markers, and downregulated mitochondrial metabolic pathways, including β-oxidation of FA. Despite circulating FFA were elevated, myocardial TG content was reduced in ACF group compared to sham. Body fat distribution was also affected by the presence of HF-ACF animals demonstrated selective depletion of intraabdominal adipose tissue, probably due to enhanced fat mobilization. The latter finding might be linked to abnormally attenuated insulin response to glucose challenge in ACF rats. The results argue against the role of myocardial lipid overload in this particular HF model and indicate that hypoinsulinaemia can contribute to intraabdominal fat tissue depletion observed in HF. The results of the study help to understand mechanisms leading to cardiac cachexia and suggest possible targets for an intervention.

Cardiac remodeling due to ACF

Creation of aorto-caval fistula led to volume overload with an increase of cardiac output by ~200% and to marked eccentric biventricular hypertrophy. Increased LV end-diastolic filling pressures and lung weights confirmed decompensated HF by the end of the study (22nd week post-ACF). Invasive hemodynamics showed relatively preserved LV contractility (dP/dt_{max}), although to fully exclude latent contractile dysfunction we would have to use truly load-independent contractile measures [35]. Diastolic function was already impaired, probably due to combined effect of eccentric chamber remodeling, increased myocardial mass, and upregulation of ECM proteins that may increase passive ventricular stiffness (lysyl oxidase, fibronectin, collagen VIII, and thrombospondin-4). The findings are in line with previous reports from ACF-HF model indicating that intense neurohumoral activation precedes the gross decline of myocardial performance [36]. Myocardial gene expression analysis did confirm robust changes typical for HF phenotype, with more than 1% of targeted transcripts being differentially expressed. The highest overexpression in ACF hearts (Table 3) was found for natriuretic peptide precursors, thrombospondin-4 [37], Wnt-pathway [18], TGF-β pathway components, periostin [38], and thyrotropin-releasing hormone [39] that were already identified as markers of stress-induced myocardial remodeling. Gene set enrichment analysis (GSEA) that detects concordant changes in transcription in functional pathways [31], indicated widespread upregulation of genes of extracellular matrix–receptor interaction, cell adhesion molecules (Table 4). This probably reflects increased matrix turnover due to stretch-activated transcription in ACF hearts, although the histology did not show excessive ventricular fibrosis, confirming previous reports [5, 18, 23, 24, 28]. The upregulation of complement cascade components, phagosome/

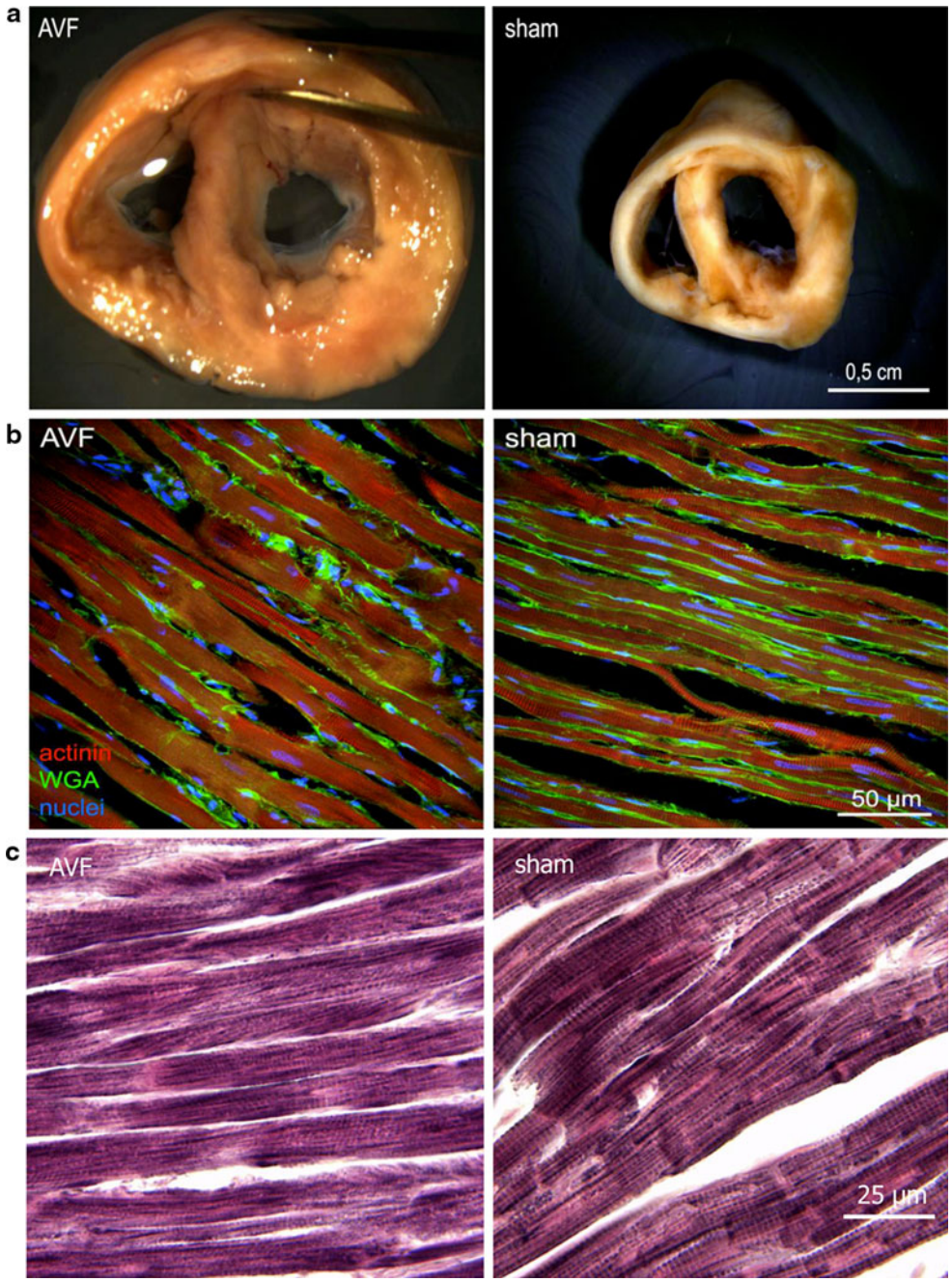

Fig. 2 Myocardial morphology. **a** Transversal section of the heart illustrates marked biventricular enlargement in the ACF animal (*left*) compared to control (*right*). **b** Confocal microscopic image of mid-section of the left ventricle. *Red* myocytes stained with α-actinin Ab, *Green* tissue fibrosis stained with Alexa488-conjugated wheat germ agglutinin, *Blue* Hoechst nuclear counterstaining. Note wider and longer myocytes in ACF, but similar extent of fibrosis. **c** Sudan Black staining for fat. Note similar density of staining and absence of lipid inclusions in both groups. Figure in color is available in online version

lysosome, and cytokine–cytokine interaction pathways may reflect inflammatory cell infiltration, yet active synthesis of complement components in stressed cardiomyocytes is also possible [40]. The most significant change detected by GSEA was downregulation of pathways for FA oxidation, citric acid cycle, respiratory electron chain, and branched amino-acid catabolism (Table 4). Similar broad downregulation of mRNAs of metabolic enzymes had been described also in other models of advanced HF [3] and it results from attenuated activity of PPARα/RXRα/PGC-1α regulatory complex [2]. Despite the functional impact of diminished transcription of these important genes is attenuated by redundancy in enzymatic activities [41], ACF hearts do show altered substrate use with selective decrease

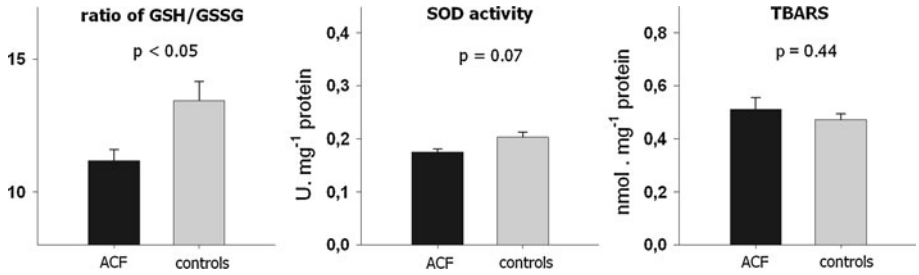

Fig. 3 Markers of myocardial oxidative stress. *Left* The ratio of reduced to oxidized glutathione (*GSH/GSSG*), *middle* superoxide dismutase activity (*SOD*), *right* thiobarbituric acid-reactive substances (*TBARS*). *Gray* controls, *black* aorto-caval fistula (*ACF*)

in oxidation of long-chain FA [14, 27, 42] and the critical limit apparently is intramitochondrial import of fatty acyls [14].

Decreased intramyocardial TG content in ACF hearts

In ACF group, myocardial TG content was reduced almost to a half compared to control despite circulating FFA levels were elevated. This important finding suggest that myocardial TG content does not merely reflect prevailing serum FFA concentration as suggested [3, 43], but it is also affected by the presence of heart failure or perhaps by the cause of heart hypertrophy. Similarly to the study, 30% reduction in myocardial TG pool was described by Lewandowski's group in pressure-overloaded rat hearts [44]. The reduction of myocardial TG content was explained by an increase of "anaplerotic" influx of carbons into the citric acid cycle via malic enzyme [45] that competes with other NADPH-consuming reactions, like TG synthesis or glutathione reduction. This may occur in ACF as well, since we noticed a parallel reduction of GSH/GSSG ratio and TG content in ACF hearts. Low TG content might also be explained by limited intracellular FFA import, because several transport genes were downregulated in ACF hearts (CD36/FAT, FABP3, and FATP3, fold change: 0.7–0.8, $q = 0.02$–0.004). On the other side, physiologic, exercise-induced cardiac hypertrophy is associated with an increase of myocardial TG content [46]. Myocardial TG content in rodents might have implications for cardiac reserve [4], as 10–30% of ATP production in heart comes from oxidation of intramyocardial TG [47]. Conversely, excessive myocardial TG accumulation is linked to "lipotoxicity" [15, 48]. Recent evidence suggests that not TG itself, but rather diacylglycerols, ceramides, or acylcarnitines are responsible for these toxic effects [49]. The observation of diminished myocardial TG content in pathological heart hypertrophy speaks against causal involvement of lipotoxicity in non-diabetic, non-obese HF.

Attenuated response of insulin to oral glucose challenge in ACF animals

Insulin has a key role in coordination of substrate metabolism [50], but whether ACF-induced HF has an impact on insulin levels has never been addressed. Against the expectations, HF animals showed normal basal serum insulin, but attenuated increase of insulin after oral glucose loading. The reasons for attenuated postprandial dynamics of insulin in ACF are not clear. Diminished glucose absorption is ruled out, because post-load glycaemia was even higher in ACF. A steal effect of ACF is also improbable because the shunt is distal to the pancreas. Plausible explanation could be in insufficient insulin release due to HF-induced splanchnic vasoconstriction [21, 51] and/or due to protracted exposure of pancreatic β-cells to increased FFA that impairs insulin secretion [52]. Despite of postprandial hypoinsulinaemia, the whole body glucose tolerance (glucose-time AUC area) was maintained in ACF rats by an unknown mechanism. Extrapancreatic effects of incretins or increased insulin sensitivity of peripheral tissues could be involved and need further investigation. The findings suggest that drugs aiming to improve cardiac metabolism by improving insulin sensitivity may not be effective in ACF-induced volume overload HF. Because secretion of insulin after a meal suppresses adipose tissue lipolysis [53], relative postprandial *hypoinsulinaemia* in ACF may contribute to increased FFA release from adipose tissue and to body fat loss.

Depletion of intraabdominal adipose tissue in ACF

Animals with ACF had significantly reduced epididymal fat weight, although total body weight was similar, probably due to more pronounced fluid retention. Epididymal fat is highly vascularized and dynamic fat pool and represents 30–50% of confined intraabdominal depots in rats. Depletion of intraabdominal (retroperitoneal) fat was also reported in rat model of cardiac volume overload from aortic regurgitation [54]. In the study, adipose tissue of ACF animals showed several differentially expressed genes (Table 5), but the changes were less pronounced than in cardiac tissue. Interestingly, the most upregulated gene in HF adipose tissue was a receptor for gastric inhibitory polypeptide (GIP), a gut-produced hormone (incretin) with insulin-releasing and extrapancreatic glucoregulatory actions that also regulates fat deposition in adipocytes [55]. Recent genome-wide association study found that genetic

Table 3 Most differentially regulated genes in the heart (assigned to KEGG pathways)

Gene description, name of pathway	Fold change	Adjusted *P*	Gene symbol	RefSeq ID
Phagosome (rno04145)				
Similar to Fcγ-(IgG) receptor II, α (predicted)	4.5	<0.00001	LOC498276	XM_573502.1
Complement and coagulation cascades (rno04610)				
Complement component 4, gene 2	5.6	0.00014	C4-2	NM_001002805.1
Complement component 1, qβ subcomponent	5	<0.00001	C1qb	NM_019262.1
Complement component 1, qC subcomponent	4.4	<0.00001	C1qc	NM_001008524.1
Lysosome (rno04142)				
CD68 antigen (predicted)	4.5	<0.00001	Cd68	XM_001079491.1
ECM–receptor interaction (rno04512)				
Thrombospondin 4	12.9	0.00001	Thbs4	XM_342172.3
Latent TGF-β binding protein 2	10.5	0.00001	Ltbp2	NM_021586.1
Secreted phosphoprotein 1	8.5	0.00015	Spp1	NM_012881.1
Procollagen, type VIII, α1 (predicted)	5	0.00014	Col8a1_pred.	XM_221536.4
Fibronectin 1	4.5	0.00032	Fn1	NM_019143.1
Lectin, galactose binding, soluble 3	4.4	0.00001	Lgals3	NM_031832.1
Connective tissue growth factor	3.9	0.00009	Ctgf	NM_022266.2
Cytokine–cytokine receptor interaction (rno04060)				
TGF β2	5.1	0.00001	Tgfb2	NM_031131.1
Platelet factor 4	4	<0.00001	Pf4	NM_001007729.1
TNF receptor superfamily, 11b (osteoprotegerin)	3.9	0.00009	Tnfrsf11b	NM_012870.2
Cell adhesion molecules (rno04514)				
Periostin (pred.)	16	0.00002	Postn_pred.	XM_342245.3
WNT1 inducible signaling pathway protein 2	4.5	0.00002	Wisp2	NM_031590.1
Limbic system-associated membrane protein	0.32	0.00017	Lsamp	NM_017242.1
Metabolic pathways (rno01100)				
Chitinase 3-like 1	5.5	0.00004	Chi3l1	NM_053560.1
Lysyl oxidase-like 1	4.2	0.00008	Loxl1	NM_001012125.1
Glutamic pyruvic transaminase 1, soluble	0.38	0.00002	Gpt1	NM_031039.1
Dehydrogenase/reductase member 7C (pred.)	0.25	0.00148	Dhrs7c_pred.	XM_001078936.1
Fatty acid metabolism (rno00071)				
Hydroxyacyl-Coenzyme A dehydrogenase	0.37	0.00079	Hadh	NM_057186.1
Peroxisome (rno04146)				
Epoxide hydrolase 2, cytoplasmic	0.3	0.001	Ephx2	NM_022936.1
Glycolysis/Gluconeogenesis (rno00010)				
Enolase 3	0.23	0.00003	Eno3	NM_012949.1
Other—membrane transport				
FXYD domain-containing ion transport regulator 3	0.38	0.00004	Fxyd3	NM_172317.1
Plasma membrane proteolipid	0.34	0.00001	Pllp	NM_022533.1
Solute carrier family 22, member 3	0.31	0.00001	Slc22a3	NM_019230.1
ATPase, Na+/K+ transporting, α2 polypeptide	0.29	0.00001	Atp1a2	NM_012505.1
Potassium channel, subfamily K, member 2	0.26	0.00008	Kcnk2	NM_172041.1
Other—regulatory				
Natriuretic peptide precursor type A	11.4	0.00225	Nppa	NM_012612.1
Thyrotropin-releasing hormone	7.2	0.0001	Trh	NM_013046.2
Nuclear protein 1	5.8	0.00001	Nupr1	NM_053611.1
TGF α	5.4	<0.00001	Tgfa	NM_012671.1
Hepcidin	4.6	0.00105	Hamp	NM_053469.1
Histone deacetylase 2	0.38	0.00005	Hdac2	XM_342149.3

Table 3 continued

Gene description, name of pathway	Fold change	Adjusted *P*	Gene symbol	RefSeq ID
Iroquois related homeobox 2	0.37	0.0045	Irx2	XM_001053004.1
Thyroid hormone receptor β	0.35	0.00385	Thrb	NM_012672.1
DNA-damage-inducible transcript 4-like	0.29	0.00004	Ddit4 l	NM_080399.1
Protein disulfide isomerase associated 2 (pred.)	0.23	0.00002	Pdia2_pred.	XM_213263.4
Other				
Tissue inhibitor of metalloproteinase 1	7.9	0.00001	Timp1	NM_053819.1
Protease inhibitor 16 (predicted)	4.7	0.00002	Pi16_pred.	XM_215351.4
Regenerating islet-derived 3β	4.5	0.00337	Reg3b	NM_053289.1
Suprabasin (pred.)	4	0.00089	Sbsn_pred.	XM_214902.4
Membrane-spanning 4-domains, subfamily A	3.8	<0.00001	Ms4a4a_pred.	XM_001075321.1
Similar to RIKEN cDNA 1700028P14 (pred.)	3.8	0.00116	RGD1560242_pred.	XM_001078678.1
Tropomodulin 4 (predicted)	0.36	0.00008	Tmod4_pred.	XM_001054854.1
Ataxin 2 binding protein 1	0.33	0.00068	A2bp1	XM_001076609.1
Similar to microsomal glutathione S-transferase 3	0.31	0.00033	RGD1561381_pred.	XM_001073485.1

Presented are only transcripts with FC >3.8 or <0.33 and FDR <0.001, full list of differentially regulated transcripts is in online supplement 2 and 3. *KEGG* Kyoto Encyclopedia of Genes and Genomes [31]

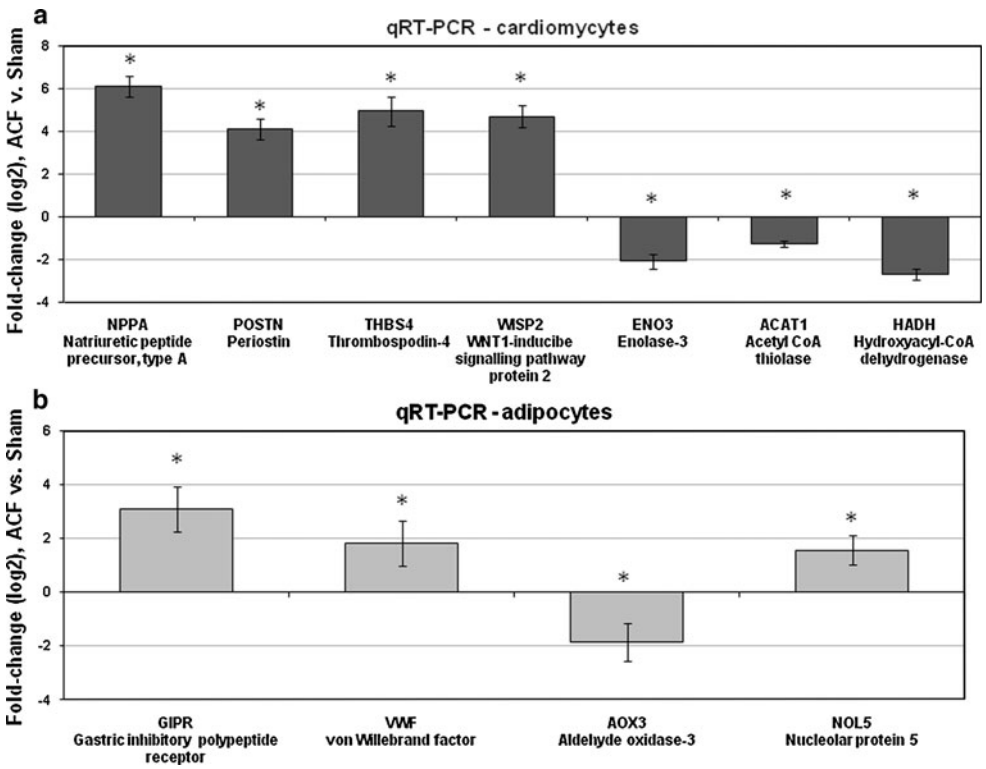

Fig. 4 Validation of gene expression changes in cardiomyocytes (**a**) and adipocytes (**b**) using quantitative real-time polymerase chains reaction (qRT-PCR). Results are normalized to housekeeping genes (see methods in supplementary file 1) and expressed as fold change in ACF versus Sham animals. $^*P < 0.01$

variation GIP receptor significantly influences insulin and glucose responses to an oral glucose challenge in humans [56]. An involvement of GIP receptor in HF-induced changes of adipose tissue metabolism has never been reported and it requires further investigation. In vitro studies of adipose tissue metabolism showed preserved lipolysis and lipogenesis in ACF hearts, with normal responsiveness to epinephrine or insulin stimulation. Increased catecholamines or angiotensin-II [10] can explain increased FFA release in ACF. Previously, it has

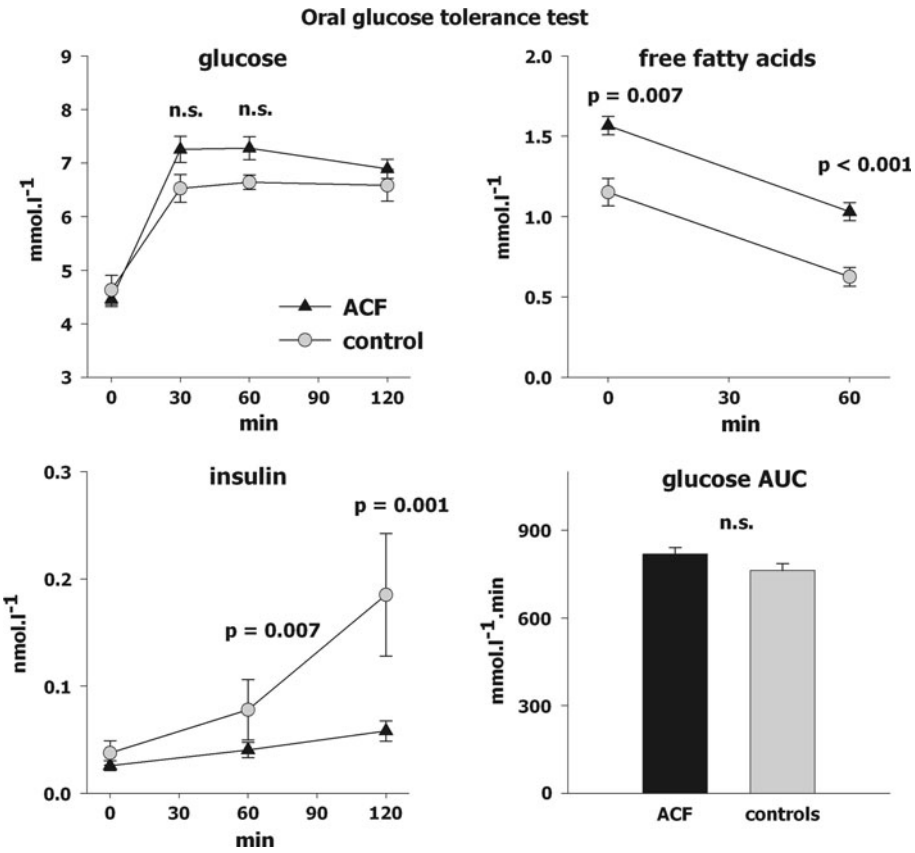

Fig. 5 Oral glucose tolerance test. *Upper panel* serum glucose and FFA. *Lower panel* insulin and area under the curve (*AUC*) of glucose–time plot. 0 min = administration of glucose. Note attenuated increase of insulin after glucose challenge in ACF group

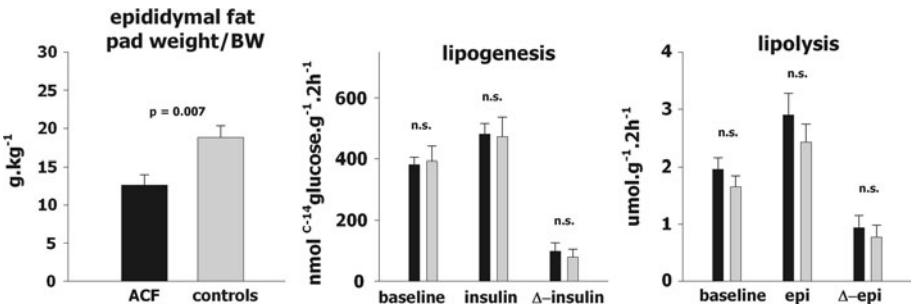

Fig. 6 Epididymal adipose tissue weight and metabolism. Epididymal fat weight, lipogenesis, and lipolysis in basal and epinephrine-stimulated state. Note intraabdominal–epididymal fat tissue depletion and preserved responsiveness of adipocytes to stimuli

been shown in rats that chronic angiotensin-II infusion leads to adipose tissue lipolysis and to weight loss and these effects are attenuated by angiotensin or β-adrenergic receptor blockade [10]. Postprandial hypoinsulinemia and attenuated antilipolytic effects can also contribute to excessive intraabdominal fat mobilization in HF due to ACF. Although HF in general is associated with elevated insulin levels and impaired whole body insulin sensitivity [9, 12], attenuated insulin secretion has been described in patients with decompensated advanced HF [51]. The study raises the question whether correction of hypoinsulinemia might favorably modulate fat depletion, or whether long-term inhibition of lipolysis could be beneficial in HF. Lipolysis in adipose tissue can be inhibited by GPR109A receptor agonists (nicotinic acid and acipimox) [57]. Acute administration of acipimox acutely reduced cardiac work and oxygen efficiency [58], but long-term effects on cardiac function of in advanced HF have not yet been tested. Lipolysis can also be inhibited by angiotensin receptor antagonists or β-adrenergic receptor blockers [10] and their antilypolytic effects might contribute to favorable effects of these drugs on weight loss and prognosis of patients with HF.

The study has several limitations. First, we performed metabolic characterization of ACF state only in male rats. It has been shown previously that sex and estrogen status are important determinants of cardiac adaptation to volume overload, with less eccentric hypertrophy in females than in males [59, 60], but no study examined yet sex-related differences in myocardial metabolism in ACF. Second, cardiac and metabolic remodeling of the heart is

Table 4 Most differentially regulated pathways in the heart (KEGG pathway analysis)

Pathway description	KEGG ID	*P* value	FDR	Count	Size
Upregulated in ACF					
Phagosome	rno04145	<0.00001	<0.00001	26	113
Complement and coagulation cascades	rno04610	<0.00001	0.00003	13	39
Lysosome	rno04142	<0.00001	0.00008	17	72
ECM–receptor interaction	rno04512	0.00011	0.00194	10	37
Cytokine–cytokine receptor interaction	rno04060	0.00013	0.00204	17	94
Antigen processing and presentation	rno04612	0.00018	0.00252	12	54
Cell adhesion molecules (CAMs)	rno04514	0.00028	0.00353	14	73
Downregulated in ACF					
Metabolic pathways	rno01100	<0.00001	<0.00001	74	614
Fatty acid metabolism	rno00071	<0.00001	<0.00001	13	27
Citrate cycle (TCA cycle)	rno00020	<0.00001	<0.00001	11	20
Peroxisome	rno04146	<0.00001	<0.00001	15	50
Valine, leucine, and isoleucine degradation	rno00280	<0.00001	<0.00001	11	28
Oxidative phosphorylation	rno00190	0.00001	0.00014	13	65
Pyruvate metabolism	rno00620	0.00010	0.00091	7	24
Glycolysis/Gluconeogenesis	rno00010	0.00030	0.00247	9	46
PPAR signaling pathway	rno03320	0.00039	0.00277	8	38

ACF aorto-caval fistula, *FDR* false discovery rate, *KEGG* Kyoto Encyclopedia of Genes and Genomes [31]

Full list of pathways and elements (including heat maps) is in online supplement 2 and 3. $N = 6$/group

Table 5 Most differentially regulated genes in ACF adipose tissue

Gene description	Fold change	*q* value	Gene symbol	RefSeq_ID
Upregulated in ACF				
Gastric inhibitory polypeptide receptor	1.95	0.00501	Gipr	NM_012714.1
Similar to very large G-protein coupled receptor 1	1.90	0.00571	LOC362068	XM_001056150.1
Similar to CG8841-PA (predicted)	1.84	0.00354	RGD1311422_predicted	XM_001081678.1
Hypothetical protein RDA279	1.78	0.00332	Rda279	XM_001070821.1
Pleckstrin homology domain containing, F2 (pred.)	1.75	0.00401	Plekhf2_predicted	XM_342803.3
von Willebrand factor (Vwf) (predicted)	1.73	0.00665	Vwf	XM_001066203.1
Cyclin L2 (predicted)	1.66	0.00393	Ccnl2_predicted	XM_216597.3
Interferon regulatory factor 3	1.55	0.00401	Irf3	NM_001006969.1
Nucleolar protein 5	1.54	0.00921	Nol5	NM_021754.1
RT1 class I, CE7	1.53	0.00498	RT1-CE7	NM_001008845.1
Camello-like 1	1.52	0.00836	Cml1	NM_133558.1
Armadillo repeat containing 5	1.50	0.00772	Armc5	NM_001009455.1
Laminin, beta 1 (predicted)	1.50	0.00424	Lamb1_predicted	XM_216679.4
Downregulated in ACF				
Aldehyde oxidase 3	0.33	0.00077	Aox3	NM_001008527.1
Similar to microsom. glutathione S-transferase 3 (pred.)	0.42	0.00958	RGD1561381_predicted	XM_001073485.1
Complement component 6	0.42	0.00401	C6	NM_176074.2
Cystatin E/M	0.42	0.00304	Cst6	NM_133566.1
RT1 class II, locus Db1	0.43	0.00077	RT1-Db1	NM_001008884.1
RT1 class II, locus Da	0.45	0.00681	RT1-Da	NM_001008847.1
Nephrosis 1 homolog (nephrin)	0.46	0.00536	Nphs1	NM_022628.1
Similar to hypothetical protein D630003M21	0.48	0.00698	RGD1563354_predicted	XM_001068317.1

Ranked by fold change. Full list of differentially regulated transcripts is in online supplement 3. $N = 6$–8/group

time-dependent, dynamic process, but we studied just one time-point—advanced HF stage. Further studies in different stages of HF development are warranted. Third, statistical methods that we used for gene expression analysis may not discern modest, but still potentially relevant changes in transcriptional regulation bellow the pre-specified cut-off of gene expression. Fourth, to fully quantify the impact of ACF on intrinsic LV contractility, we would have to subject animals to simultaneous invasive pressure–volume analysis of the heart and its lack is a limitation of the study.

In conclusion, animals with HF due to ACF displayed several specific alterations of FA metabolism and fat distribution. Circulating FFA were higher but cardiac TG content was reduced in HF group, arguing against the role of lipid overload. The observation of intraabdominal fat depletion and attenuated postprandial insulin dynamics may help to understand mechanisms of HF-induced fat loss and cachexia.

Acknowledgments This study was supported by Ministry of Heath [MZO-00023001 to V.M. and L.C., IGA MZCR NS-10300-3 to J.P., NS10497-3/2009 to V.M.]; Ministry of Education [MSMT-1MO510 to V.M., J.B. and L.C., VZ 0021620806 to D.S., 0021620806 to J.P., 1M6837805002 to H.S. and M.K.]; the Grant agency [305/09/1390 to V.M.]; and the Academy of sciences [AV0Z50520514 to H.S. and M.K, AV0Z50110509 to D.S.] of the Czech Republic.

References

1. Opie LH, Knuuti J (2009) The adrenergic-fatty acid load in heart failure. J Am Coll Cardiol 54:1637–1646
2. Lopaschuk GD, Ussher JR, Folmes CD, Jaswal JS, Stanley WC (2010) Myocardial fatty acid metabolism in health and disease. Physiol Rev 90:207–258
3. Stanley WC, Recchia FA, Lopaschuk GD (2005) Myocardial substrate metabolism in the normal and failing heart. Physiol Rev 85:1093–1129
4. van Bilsen M, van Nieuwenhoven FA, van der Vusse GJ (2009) Metabolic remodelling of the failing heart: beneficial or detrimental? Cardiovasc Res 81:420–428
5. Benes J Jr, Melenovsky V, Skaroupkova P, Pospisilova J, Petrak J, Cervenka L, Sedmera D (2011) Myocardial morphological characteristics and proarrhythmic substrate in the rat model of heart failure due to chronic volume overload. Anat Rec (Hoboken) 294:102–111
6. Sorokina N, O'Donnell JM, McKinney RD, Pound KM, Woldegiorgis G, LaNoue KF, Ballal K et al (2007) Recruitment of compensatory pathways to sustain oxidative flux with reduced carnitine palmitoyltransferase I activity characterizes inefficiency in energy metabolism in hypertrophied hearts. Circulation 115:2033–2041
7. Anker SD, Ponikowski P, Varney S, Chua TP, Clark AL, Webb-Peploe KM, Harrington D et al (1997) Wasting as independent risk factor for mortality in chronic heart failure. Lancet 349:1050–1053
8. Lommi J, Kupari M, Yki-Jarvinen H (1998) Free fatty acid kinetics and oxidation in congestive heart failure. Am J Cardiol 81:45–50
9. Paolisso G, De Riu S, Marrazzo G, Verza M, Varricchio M, D'Onofrio F (1991) Insulin resistance and hyperinsulinemia in patients with chronic congestive heart failure. Metabolism 40:972–977
10. Cabassi A, Coghi P, Govoni P, Barouhiel E, Speroni E, Cavazzini S, Cantoni AM et al (2005) Sympathetic modulation by carvedilol and losartan reduces angiotensin II-mediated lipolysis in subcutaneous and visceral fat. J Clin Endocrinol Metab 90: 2888–2897
11. Shulman GI (2000) Cellular mechanisms of insulin resistance. J Clin Invest 106:171–176
12. Doehner W, Rauchhaus M, Ponikowski P, Godsland IF, von Haehling S, Okonko DO et al (2005) Impaired insulin sensitivity as an independent risk factor for mortality in patients with stable chronic heart failure. J Am Coll Cardiol 46:1019–1026
13. Razeghi P, Young ME, Alcorn JL, Moravec CS, Frazier OH, Taegtmeyer H (2001) Metabolic gene expression in fetal and failing human heart. Circulation 104:2923–2931
14. Christian B, Alaoui-Talibi Z, Moravec M, Moravec J (1998) Palmitate oxidation by the mitochondria from volume-overloaded rat hearts. Mol Cell Biochem 180:117–128
15. Sharma S, Adrogue JV, Golfman L, Uray I, Lemm J, Youker K, Noon GP, Frazier OH, Taegtmeyer H (2004) Intramyocardial lipid accumulation in the failing human heart resembles the lipotoxic rat heart. FASEB J 18:1692–1700
16. Zhou YT, Grayburn P, Karim A, Shimabukuro M, Higa M, Baetens D, Orci L, Unger RH (2000) Lipotoxic heart disease in obese rats: implications for human obesity. Proc Natl Acad Sci USA 97:1784–1789
17. Listenberger LL, Schaffer JE (2002) Mechanisms of lipoapoptosis: implications for human heart disease. Trends Cardiovasc Med 12:134–138
18. Toischer K, Rokita AG, Unsold B, Zhu W, Kararigas G, Sossalla S, Reuter SP, Becker A et al (2010) Differential cardiac remodeling in preload versus afterload. Circulation 122:993–1003
19. Garcia R, Diebold S (1990) Simple, rapid, and effective method of producing aortocaval shunts in the rat. Cardiovasc Res 24:430–432
20. Cantor EJ, Babick AP, Vasanji Z, Dhalla NS, Netticadan T (2005) A comparative serial echocardiographic analysis of cardiac structure and function in rats subjected to pressure or volume overload. J Mol Cell Cardiol 38:777–786
21. Flaim SF, Minteer WJ, Nellis SH, Clark DP (1979) Chronic arteriovenous shunt: evaluation of a model for heart failure in rat. Am J Physiol 236:H698–H704
22. Brower GL, Janicki JS (2001) Contribution of ventricular remodeling to pathogenesis of heart failure in rats. Am J Physiol Heart Circ Physiol 280:H674–H683
23. Ruzicka M, Yuan B, Leenen FH (1994) Effects of enalapril versus losartan on regression of volume overload-induced cardiac hypertrophy in rats. Circulation 90:484–491
24. Ryan TD, Rothstein EC, Aban I, Tallaj JA, Husain A, Lucchesi PA, Dell'Italia LJ (2007) Left ventricular eccentric remodeling and matrix loss are mediated by bradykinin and precede cardiomyocyte elongation in rats with volume overload. J Am Coll Cardiol 49:811–821
25. Brower GL, Henegar JR, Janicki JS (1996) Temporal evaluation of left ventricular remodeling and function in rats with chronic volume overload. Am J Physiol 271:H2071–H2078
26. Takewa Y, Chemaly ER, Takaki M, Liang LF, Jin H, Karakikes I, Morel C, Taenaka Y, Tatsumi E, Hajjar RJ (2009) Mechanical work and energetic analysis of eccentric cardiac remodeling in a volume overload heart failure in rats. Am J Physiol Heart Circ Physiol 296:H1117–H1124
27. Alaoui-Talibi Z, Landormy S, Loireau A, Moravec J (1992) Fatty acid oxidation and mechanical performance of volume-overloaded rat hearts. Am J Physiol 262:H1068–H1074

28. Ruzicka M, Yuan B, Harmsen E, Leenen FH (1993) The renin-angiotensin system and volume overload-induced cardiac hypertrophy in rats. Effects of angiotensin converting enzyme inhibitor versus angiotensin II receptor blocker. Circulation 87:921–930
29. Strnad H, Lacina L, Kolar M, Cada Z, Vlcek C, Dvorankova B, Betka J, Plzak J, Chovanec M et al (2010) Head and neck squamous cancer stromal fibroblasts produce growth factors influencing phenotype of normal human keratinocytes. Histochem Cell Biol 133:201–211
30. Smyth GK (2005) Limma: linear models for microarray data. In: Gentleman V, Careyand S, Dudoid S, Irizarry R, Huber W (eds) Bioinformatics and computational biology solutions using R and Bioconductor. Springer, New York, pp 397–420
31. Kanehisa M, Goto S (2000) KEGG: Kyoto encyclopedia of genes and genomes. Nucleic Acids Res 28:27–30
32. Concetti A, Massei P, Rotilio G, Brunori M, Rachmilewitz EA (1976) Superoxide dismutase in red blood cells: method of assay and enzyme content in normal subjects and in patients with beta-thalassemia (major and intermedia). J Lab Clin Med 87:1057–1064
33. Yokode M, Kita T, Kikawa Y, Ogorochi T, Narumiya S, Kawai C (1988) Stimulated arachidonate metabolism during foam cell transformation of mouse peritoneal macrophages with oxidized low density lipoprotein. J Clin Invest 81:720–729
34. Pravenec M, Kazdova L, Maxova M, Zidek V, Mlejnek P, Simakova M, Kurtz TW (2008) Long-term pioglitazone treatment enhances lipolysis in rat adipose tissue. Int J Obes (Lond) 32: 1848–1853
35. Carabello BA (2002) Evolution of the study of left ventricular function: everything old is new again. Circulation 105: 2701–2703
36. Lee L, Campbell R, Scheuermann-Freestone M, Taylor R, Gunaruwan P, Williams L et al (2005) Metabolic modulation with perhexiline in chronic heart failure: a randomized, controlled trial of short-term use of a novel treatment. Circulation 112:3280–3288
37. Schellings MW, van Almen GC, Sage EH, Heymans S (2009) Thrombospondins in the heart: potential functions in cardiac remodeling. J Cell Commun Signal 3(3–4):201–213
38. Stansfield WE, Andersen NM, Tang RH, Selzman CH (2009) Periostin is a novel factor in cardiac remodeling after experimental and clinical unloading of the failing heart. Ann Thorac Surg 88:1916–1921
39. Jin H, Fedorowicz G, Yang R, Ogasawara A, Peale F, Pham T, Paoni NF (2004) Thyrotropin-releasing hormone is induced in the left ventricle of rats with heart failure and can provide inotropic support to the failing heart. Circulation 109:2240–2245
40. Singh MV, Kapoun A, Higgins L, Kutschke W, Thurman JM, Zhang R, Singh M, Yang J et al (2009) Ca2+/calmodulin-dependent kinase II triggers cell membrane injury by inducing complement factor B gene expression in the mouse heart. J Clin Invest 119:986–996
41. Morgan EE, Chandler MP, Young ME, McElfresh TA, Kung TA, Rennison JH, Tserng KY, Hoit BD, Stanley WC (2006) Dissociation between gene and protein expression of metabolic enzymes in a rodent model of heart failure. Eur J Heart Fail 8:687–693
42. Benes J, Kazdova L, Drahota Z, Houstek J, Medrikova D, Kopecky J, Kovarova N et al (2011) The effect of metformin therapy on cardiac function and survival in volume-overload model of heart failure in rats. Clin Sci (Lond) 121:29–41
43. Hammer S, van der Meer RW, Lamb HJ, Schar M, de RA, Smit JW, Romijn JA (2008) Progressive caloric restriction induces dose-dependent changes in myocardial triglyceride content and diastolic function in healthy men. J Clin Endocrinol Metab 93:497–503
44. O'Donnell JM, Fields AD, Sorokina N, Lewandowski ED (2008) The absence of endogenous lipid oxidation in early stage heart failure exposes limits in lipid storage and turnover. J Mol Cell Cardiol 44:315–322
45. Pound KM, Sorokina N, Ballal K, Berkich DA, Fasano M, La Noue KF, Taegtmeyer H, O'Donnell JM, Lewandowski ED (2009) Substrate-enzyme competition attenuates upregulated anaplerotic flux through malic enzyme in hypertrophied rat heart and restores triacylglyceride content: attenuating upregulated anaplerosis in hypertrophy. Circ Res 104:805–812
46. Liu L, Shi X, Bharadwaj KG, Ikeda S, Yamashita H, Yagyu H, Schaffer JE, Yu YH, Goldberg IJ (2009) DGAT1 expression increases heart triglyceride content but ameliorates lipotoxicity. J Biol Chem 284:36312–36323
47. Saddik M, Lopaschuk GD (1991) Myocardial triglyceride turnover and contribution to energy substrate utilization in isolated working rat hearts. J Biol Chem 266:8162–8170
48. Wende AR, Abel ED (2010) Lipotoxicity in the heart. Biochim Biophys Acta 1801:311–319
49. Son NH, Yu S, Tuinei J, Arai K, Hamai H, Homma S, Shulman GI, Abel ED, Goldberg IJ (2010) PPARgamma-induced cardiolipotoxicity in mice is ameliorated by PPARα deficiency despite increases in fatty acid oxidation. J Clin Invest 120:3443–3454
50. Cahova M, Vavrinkova H, Kazdova L (2007) Glucose–fatty acid interaction in skeletal muscle and adipose tissue in insulin resistance. Physiol Res 56:1–15
51. Sharma B, Majid PA, Pakrashi BC, Dykes JR, Taylor SH (1970) Insulin secretion in heart failure. Br Med J 2:396–398
52. Grill V, Bjorklund A (2000) Dysfunctional insulin secretion in type 2 diabetes: role of metabolic abnormalities. Cell Mol Life Sci 57:429–440
53. Groop LC, Bonadonna RC, DelPrato S, Ratheiser K, Zyck K, Ferrannini E, De Fronzo RA (1989) Glucose and free fatty acid metabolism in non-insulin-dependent diabetes mellitus. Evidence for multiple sites of insulin resistance. J Clin Invest 84:205–213
54. Bouchard-Thomassin AA, Lachance D, Drolet MC, Couet J, Arsenault M (2011) A high-fructose diet worsens eccentric left ventricular hypertrophy in experimental volume overload. Am J Physiol Heart Circ Physiol 300:H125–H134
55. Irwin N, Flatt PR (2009) Therapeutic potential for GIP receptor agonists and antagonists. Best Pract Res Clin Endocrinol Metab 23:499–512
56. Saxena R, Hivert MF, Langenberg C, Tanaka T, Pankow JS, Vollenweider P, Lyssenko V et al (2010) Genetic variation in GIPR influences the glucose and insulin responses to an oral glucose challenge. Nat Genet 42:142–148
57. Tunaru S, Kero J, Schaub A, Wufka C, Blaukat A, Pfeffer K, Offermanns S (2003) PUMA-G and HM74 are receptors for nicotinic acid and mediate its anti-lipolytic effect. Nat Med 9:352–355
58. Tuunanen H, Engblom E, Naum A, Nagren K, Hesse B, Airaksinen KE, Nuutila P, Iozzo P, Ukkonen H, Opie LH, Knuuti J (2006) Free fatty acid depletion acutely decreases cardiac work and efficiency in cardiomyopathic heart failure. Circulation 114:2130–2137
59. Brower GL, Gardner JD, Janicki JS (2003) Gender mediated cardiac protection from adverse ventricular remodeling is abolished by ovariectomy. Mol Cell Biochem 251:89–95
60. Gardner JD, Murray DB, Voloshenyuk TG, Brower GL, Bradley JM, Janicki JS (2010) Estrogen attenuates chronic volume overload induced structural and functional remodeling in male rat hearts. Am J Physiol Heart Circ Physiol 298:H497–H504